Influence des profils verticaux d'humidité et de température sur l'émission micro-onde d'un sol nu : conséquence sur l'estimation de la teneur en eau du sol

S. Raju

UNIVERSITE PARIS VII
PARIS

INRA
Unité de Science du Sol
AVIGNON
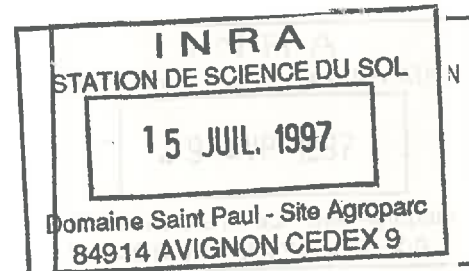
THESE

Présentée par : **Suresh Raju**

Pour l'obtention du titre de

DOCTEUR DE L'UNIVERSITE DE PARIS VII

Spécialité : Méthodes physiques en télédétection

INFLUENCE DES PROFILS VERTICAUX D'HUMIDITE ET DE TEMPERATURE SUR L'EMISSION MICRO-ONDE D'UN SOL NU : CONSEQUENCE SUR L'ESTIMATION DE LA TENEUR EN EAU DU SOL

Soutenue le 17 Marche 1997 à INRA, Avignon

Membres du Jury :

M.M.

G. De Rosny	Professeur à l'Université Paris VII	**Président**
Y.Kerr	Ingénier CNES, Toulouse, France	**Rapporteur**
A. Royer	Professeur CARTEL, Uni. Sherbrooke, Canada	**Rapporteur**
L. Bruckler	Directeur de thèse, Directeur de Recherches INRA	**Examinateur**
A. Chanzy	Charge de Recherches, INRA	**Examinateur**
J. Lemorton	Ingénier CERT, Toulouse, France	**Examinateur**

Finally I express my thanks to all other staff and thésards as it is difficult to name everybody. I am sure that I had a very smooth and pleasant life in the laboratory only due to their cooperation and help.

I should not forget to thank **André's family** from whom we tasted the French food in the first time.

And finally I remember **Thara** at this occasion since she who was with me throughout my stay in France and adjusted herself a lot to help me in my work. And at last I thanks to **Arvind Raju** who associated more with his mother to allow his father to finish the Ph.D.

CONTENTS

Appendix A :   Models for soil dielectric constant

1.   Dielectric models

    1.1.   Wang and Schmugge model

    1.2.   Dobson's dielectric models

        1.2.1.   Dobson's physical model

        1.2.2.   Dobson's semi-empirical model

        1.2.3.   Dielectric constant of water

Appendix B :   Njoku and Kong model presentation

LIST OF SYMBOLS

Symbol	Description	Units
A	: area	(m^2)
a	: absorptivity	(no dim.)
B	: brightness	$(W\ m^{-2}sr^{-1})$
B_b	: brightness of Blackbody	$(W\ m^{-2}Sr^{-1}Hz^{-1})$
C	: clay fraction	(no dim.)
c	: velocity of EM radiation in vacuum	$(m\ s^{-2})$
dz	: layer thickness	(m)
$d\Omega$	: solid angle	(sr)
E	: value of electric field at p	$(V\ m^{-1})$
E_0	: initial value electric field	$(V\ m^{-1})$
e	: emissivity of smooth soil surface	(no dim.)
f	: frequency	(Hz)
H	: Magnetic field	$(A\ m^{-1})$
h	: Plank's constant	$(6.63 \cdot 10^{34}\ J)$
h_r	surface height parameter	(m)
I	: intensity of the radiation	$(W\ m^{-2}\ sr^{-1}Hz)$
J_α	absorption source function	$(W\ m^{-2}\ sr^{-1})$
j	: layer number	(no dim.)
k	: wave number	(m^{-1})
k_B	: Boltzmann's constant	$(1.38 \times 10^{-23}\ J\ K^{-1})$
l	: surface correlation length	(m)
P	: average power of a wave	$(W\ m^{-2})$
P_a	: average power of a wave	$(W\ m^{-2})$
p	: polarization H or V	(no dim.)
P_i	: incident power	(W)
P_s	: transmitted power	(W)
p_r	: porosity of soil medium	(no dim.)
Q	: polarization mixing parameter	(no dim.)
R_H or R_V	: Fresnel reflection coefficient	(no dim.)
S_l	: salinity	(parts per 1000)
S%	: percentage of sand fraction	(no dimension)
T	temperature	(K)
T_B	brightness temperature	(K)
T_i	contribution by cosmic radiation	(K)

T_d	: deeper depth soil temperature	(K)
T_e	: effective Temperature	(K)
T_s	: effective Temperature	(K)
T_H or T_V	: transmission coefficient	(no dim.)
T_S	: surface soil temperature	(K)
T_V	: vegetation temperature	(K)
$T(z)$	: soil temperature at a depth z (m)	(K)
v	: phase velocity of radiation	(m s^{-2})
W_C	: plant water content	(Kg m^{-1})
$\alpha(z)$	: attenuation coefficient at the depth z	(Npm^{-1})
κ_a	power absorption coefficient	(Npm^{-1})
Γ	: reflectivity	(no dim.)
γ	: fitted parameter in Wang dielectric model	(no dimension)
δp	: penetration depth	(m)
ε	: dielectric constant	(farad.m^{-1})
ε_r	: relative dielectric constant	(no dim.)
ε' and ε''	: real and imaginary part of ε	(farad.m^{-1})
ε_0	: permittivity of vacuum	(farad.m^{-1})
ε_a	: permittivity of air	(farad.m^{-1})
ε_{fw}	dielectric constant of water	(no dimension)
ε_{w0}	: static dielectric constant of water	(no dimension)
$\varepsilon_{w\infty}$	: dielectric constant of water at high frequency limit	(no dimension)
η	: refractive index	(Ω)
Θ	: incidence angle	(degree)
θ	: soil moisture	(cm^3.cm^{-3})
θ_p	: welting point	(cm^3.cm^{-3})
θ_t	: transition point	(cm^3.cm^{-3})
λ	: wavelength of the radiation	(m)
λ_0	: wavelength in vacuum	(m)
μ	: magnetic permeability	(henry m^{-1})
μ_0	: magnetic permeability of vacuum ($4\pi \cdot 10^{-7}$)	(henry m^{-1})
μ_r	: relative magnetic permeability	(henry m^{-1})
ρ	: standard deviation of vertical height variation	(m)
ρ_b	: soil dry bulk density	(kgm^{-3})
ρ_s	: density of solid rock	(kgm^{-3})

σ_s	: scattering cross section	(m^2)
σ_i	: electric conductivity	$(S\ m^{-1})$
τ_w	: relaxation time of water	(s)
χ	: transmissivity	(no dim.)
ω	: angular frequency	$(rad.s^{-1})$

Summary of thesis in French

Résumé détaillé du Thèse

MOTIVATIONS ET OBJECTIFS DE L'ETUDE

L'émission par un sol nu du rayonnement électromagnétique dans le domaine spectral des micro-ondes dépend de plusieurs facteurs dont les principaux sont la rugosité de surface ainsi que l'humidité et la température dans les couches superficielles (quelques centimètres). Les gradients hydriques et thermiques au voisinage de la surface sont très marqués et varient en fonction de l'heure de la journée, des conditions climatiques et des propriétés physiques du sol. L'influence des gradients hydrique et thermique sur l'émission micro-onde du sol est encore mal connue. Il est par exemple difficile de prévoir à l'heure actuelle quelles seront les variations diurnes de la température de brillance micro-onde qui seront à la fois reliées au cycle diurne de température, mais également aux séquences de dessiccation le jour et de réhumectation la nuit. Dans la perspective d'utilisation de la radiométrie micro-onde pour estimer l'humidité ou la température de surface du sol il est donc nécessaire d'appréhender finement l'influence des gradients de température et d'humidité dans le sol sur son émission micro-onde.

Dans notre étude, nous visons donc les objectifs suivants :

 * mettre en oeuvre et valider des modèles physiques d'émission micro-onde permettant de prendre en compte les profils d'humidité et de température au voisinage de la surface.

 * déterminer la profondeur de pénétration en fonction de l'humidité et de la configuration de mesure micro-onde. Cette étude sur la profondeur de pénétration devrait permettre d'optimiser l'épaisseur de la couche dans laquelle l'humidité du sol est déterminée. On essayera notamment d'évaluer quelles sont les conséquences du choix d'une profondeur fixée d'échantillonnage de la teneur en eau sur les relations entre la teneur en eau et la température de brillance.

 * l'effet de la température sur l'émission micro-onde d'un sol est généralement exprimé par la température effective micro-onde qui prend en compte les gradients thermiques et une pondération liée à la contribution de chaque couche à l'émission micro-onde. Pour l'estimation de l'humidité des sols, il est important de pouvoir connaître avec une bonne précision la température effective. Nous chercherons donc à évaluer si en combinant des mesures micro-ondes effectuées à différentes fréquences il serait possible d'avoir une estimation fiable de la température effective.

RESUME DES CONCLUSIONS DE L'ETUDE

Ce travail a permis de mettre en place une importante base de données dont la richesse repose sur l'utilisation d'un radiomètre multifréquence et le suivi de sols soumis à une grande gamme de conditions d'humidité, de rugosité et de végétation. Les mesures ont été acquises à différentes échelles de temps allant de la minute à la décade.

Les modèles d'émission micro-onde sur des sols lisses représentés par un milieu stratifié donnent les résultats suivants :

      * confirmation de la similitude entre les modèles cohérents (Wilheit (1978)et Njoku(1977));

      * confirmation des différences entre le modèle incohérent de Burke (Burke et. al 1979) et les modèles cohérents. La confrontation avec les données expérimentales donne un net avantage aux modèles cohérents. La couche de surface influence très fortement les calculs avec le modèle de Burke. L'épaisseur de cette couche doit être calée pour obtenir des valeurs de température de brillance (T_B) raisonnables. Ceci est contradictoire avec l'objectif même de ces modèles qui doivent pouvoir s'affranchir de tout calage. Par conséquent nous avons retenu pour la suite le modèle cohérent de Wilheit qui est combiné à un modèle mécaniste de transferts couplés d'eau et de chaleur dans le sol. Ce couplage permet de simuler l'évolution diurne de T_B et ceci selon différentes contraintes climatiques, tout en prenant en compte les propriétés hydriques du sol considéré. Un tel outil est particulièrement bien adapté pour étudier :

      * l'influence des profils hydrique et thermique du sol sur l'émission micro-onde d'un sol;

      * l'influence des conditions climatiques sur les relations T_B-humidité de surface avec notamment la prise en compte des variations diurnes et saisonnières de la demande climatique.

      * l'influence des propriétés hydriques et diélectriques des sols sur cette même relation.

Pour la simulation des données, l'intérêt d'utiliser un modèle d'émission d'un milieu stratifié par rapport à des modèles plus simples représentant le sol comme un milieu monocouche (modèle de Fresnel par exemple) n'est significatif qu'à 1.4 GHz. A cette fréquence on obtient avec le modèle de Wilheit des résultats meilleurs qu'avec le modèle de Fresnel. De plus, les évolutions diurnes présentent des variations différentes entre ces modèles. Ces différences affectent l'amplitude de variation diurne de T_B ainsi que l'heure d'obtention des maximums journaliers de T_B. On voit par ce résultat que des caractéristiques de l'évolution de la température de brillance telles que des amplitudes ou des déphasages pourraient constituer des critères pertinents pour comparer les performances de plusieurs modèles. En effet, les comparaisons modèle-expérience sont entachées de telles erreurs dans le cas des modèles d'émission micro-onde qu'il est difficile de valider ou d'invalider un modèle sur la base d'une simple comparaison modèle-expérience.

On montre dans cette étude que l'influence de la forme des profils hydrique est considérable (environ 30K). On montre par exemple que l'erreur d'estimation sur l'humidité d'une couche donnée peut atteindre 0.06 m^3/m^3, si la température du sol et la forme du profil d'humidité ne sont pas prises en compte. Cette erreur est fortement réduite lorsque la température effective du sol est connue. Une des conséquences de l'influence de la forme du profil hydrique sur la relation entre l'humidité de surface et T_B se traduit par une limitation du domaine de validité de l'épaisseur de la couche dans laquelle on caractérise l'humidité (profondeur d'échantillonnage) pour mettre en oeuvre un modèle d'émission micro-onde monocouche. La profondeur d'échantillonnage est généralement calée. Nous montrons que la plage horaire pendant laquelle on effectue les mesures radiométriques peut se répercuter sur la valeur de cette profondeur. Il est probable que le passage d'une période climatique à une autre, ou d'un sol à un autre, se répercuterait de manière similaire sur la profondeur d'échantillonnage. Une

des suites logiques de ce travail consisterait à modéliser les variations de cette profondeur d'échantillonnage en s'appuyant sur des données radiométriques multifréquences.

De manière plus pratique, nous proposons un nouveau modèle semi-empirique pour estimer la température effective en bandes L et C. Ce modèle est fondé sur l'utilisation de la température de l'air, de la température de brillance en bande X et polarisation verticale, de la température du sol en profondeur (50 cm) et de la température de surface lorsqu'elle est disponible. Ce modèle présente l'avantage par rapport aux modèles existants (modèle de Choudhury) de pouvoir s'affranchir de la mesure de la température de surface, lorsque sa mesure est rendue impossible par la présence d'une couverture nuageuse. On montre que le domaine de validité de ce modèle est étendu aux cas des sols nus lisses ou rugueux, et dans une certaine mesure, aux couverts peu denses tels que ceux rencontrés en zones arides et semi-arides.

INTRODUCTION

Soil moisture is an environmental parameter that integrates much of the land surface hydrology and plays a crucial role in the interface between the earth and the atmosphere. The topographic factors, land use and vegetation cover contribute to the large fluctuations of the soil moisture over small spatial scales and the land - atmospheric interaction causes large temporal variations in the surface soil moisture. Such variations make a regular monitoring of soil moisture over large areas difficult. A regular monitoring is however necessary for environmental studies, and hydrological and/or climatic models.

There has been significant research efforts invested in developing the capability of monitoring the soil moisture by microwave remote sensing techniques (Newton et al. 1982; T. J. Schmugge 1983; T. J. Jackson 1988; Jackson and Schmugge 1989). The microwave remote sensing at the low frequencies (1.4 - 10 GHz) got much attention to soil moisture studies. The results of these studies have encouraged an increase in the capability of observing the earth surface with microwave sensors. Concerning the passive techniques, several airborne microwave radiometers are now operational in different countries. Moreover, in the near future, Multifrequency Imaging Microwave Radiometer (MIMR), and Adavnced Microwave Scanning Radiometer (AMSR), with a C band channel, will be installed on a satellite platform. If the poor ground resolution of the microwave radiometers remains the major drawback for the future applications, progress is expected with the use of interferometric method. In this way, the development of ESTAR (Le Vine et al. 1990) is a step towards the future space-borne L band radiometer. Therefore, an L-band radiometer which allows a daily coverage of the world with a ground resolution of about 10 km seems to be technically possible in the future.

The microwave emission (or microwave brightness temperature hereafter referred to as T_B) from land surface is basically governed by the soil surface moisture, the surface roughness, the vegetation cover through its water content and structure, and the temperature of the surface. With the aim of estimating soil surface moisture, variations in T_B due to soil moisture variations must be isolated from those attributed to the other factors of influence. Several studies were carried out to understand the vegetation and soil surface roughness influences (Choudhury et al., 1979, Jackson et al. 1982, Wang, 1983, Wigneron et al., 1993, Chanzy et al. 1995) and inversion methods are proposed to infer the soil moisture from microwave observations. If encouraging results were obtained, these methods can not be yet implemented operationally. From these studies, there is however a general agreement on the interest of the low frequencies (<10 GHz).

At low frequencies the microwave radiations penetrate the soil within a layer of several centimeters. This soil layer is characterized by strong gradients of both soil moisture and soil temperature. Moreover, it is well known that the moisture and temperature profiles are influenced by the time of the day, the climatic demand and the soil hydrodynamic properties (Chanzy and Bruckler. 1993). At the present time. only a few studies were devoted to the

influence of the soil moisture and temperature profiles profile on microwave emission (Njoku and Kong, 1977, Wilheit, 1978). In most studies, the soil penetration of the low frequency microwave radiations is accounted for by fitting a moisture sampling depth which allows the best relationship between the soil moisture and T_B (Newton et al. 1982, Wang, 1987, Chanzy and Kustas, 1994). The sampling depth is generally established on limited sets of data and we don't know exactly how the diurnal and seasonal variations in soil moisture and temperature vertical profiles affect the validity of the sampling depth. To prepare the future applications based on frequent microwave observations, we must be able to infer the temporal evolution of the soil moisture through both the day and the year. The goal of the presented study was then to analyze 1) the influence of the soil moisture and temperature profiles on the soil microwave emission, and 2) the resulting consequences on the soil moisture accuracy.

We focus our work on the L, C and X band. The study is limited to the smooth bare field condition not only to maximize the effect of moisture and temperature profiles but also to use a theoretical background which is more suited to bare soil. We have considered both experimental and simulation approach in this study. We used the radiometric data collected in 1991 and 1993 from the test site of INRA, Avignon, France. The radiative transfer model developed in stratified soil is used to study the soil moisture and temperature profiles effect on microwave emission. To study the diurnal and textural effect on microwave emission and moisture estimation we coupled the microwave emission model to mechanistic model of mass and heat flow in unsaturated soils.

In the first part we present the physics involved in the thermal microwave emission and define the basic radiometric parameters. A brief bibliography on passive microwave radiometry is then presented. In chapter1 we present the different microwave emission models used in the study and a summary of the mechanistic model of soil heat and water flows is given. We present in chapter 3 the experiments. Results are given in chapter 4 and 5. In chapter 4, a comparison between different models of smooth bare soil microwave emission is done. From this comparison we select an emission model which is then combined to a mechanistic model of soil heat and mass flow. The mechanistic model simulates the evolution of soil temperature and moisture profiles which are then taken as input in the soil emission model. This combination of models is then used in the two papers (chapter 5) as a data simulator. In the first article, we discuss the soil moisture and temperature profile effect on moisture estimation. In the second article we propose a new semi empirical model to estimate the effective temperature.

CHAPTER 1

Microwave radiometry for estimating soil moisture: Theory and Bibliography.
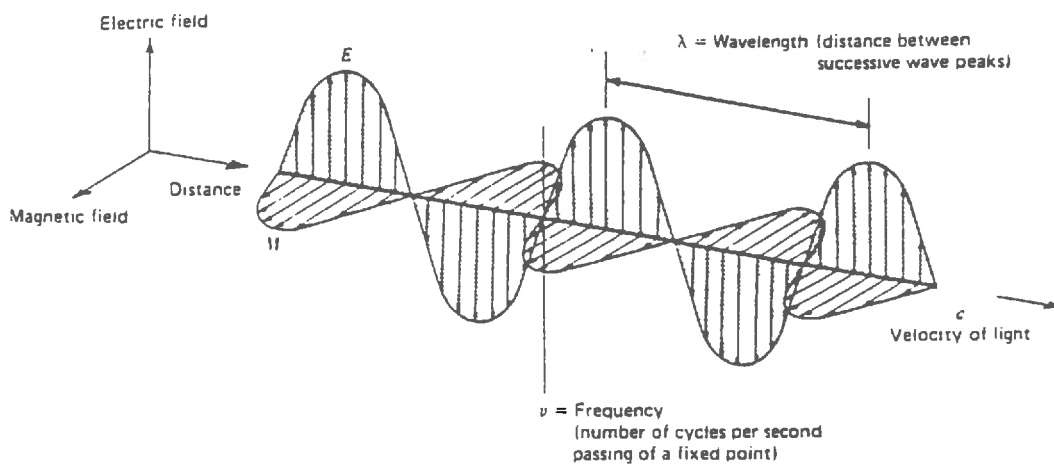
Figure 1.1: Schematic presentation of electromagnetic wave propagation.

1   Introduction

In passive microwave remote sensing the microwave radiation emitted from the earth surface is measured. The physical properties of the emitting media such as soil, vegetation canopy and the atmosphere influence the wave propagation and the intensity of the measured radiation. In this chapter, we introduce the basic elements of wave propagation and different physical phenomena involved in the microwave emission and propagation. Then we discuss the link between the soil microwave emission and the soil parameters. Then, a brief discussion on the development of microwave emission models for bare soil is presented.

1.1   Electromagnetic waves

In remote sensing the electromagnetic radiation of different spectral bands are being used as a mean to collect the information of the interested area or medium. Here, we present an introduction of electromagnetic waves and their propagation.

1.1.1   Wave equation

An electromagnetic wave consists of a sinusoidal electric field $\vec{E}$ and a sinusoidal magnetic field $\vec{H}$, both are being perpendicular to each other and to the direction of propagation (figure 1.1). The electric and magnetic waves could be described by solving the Maxwell's equations.   The magnetic field could be derived from the electric field by :

$$\frac{|\vec{E}|}{|\vec{H}|} = \sqrt{\frac{\mu}{\varepsilon}}$$ (1.1)

where
- ε is the pemittivity (farad m^{-1})
- μ is the magnetic permeability (henry m^{-1})

Therefore, we focus our presentation on the electric field. Assuming that an electromagnetic wave propagating in the positive direction along the z axis, the wave equation for the electric field is given by:

$$\vec{E} = \vec{E}_0 e^{i(\omega t - kz)}$$ (1.2)
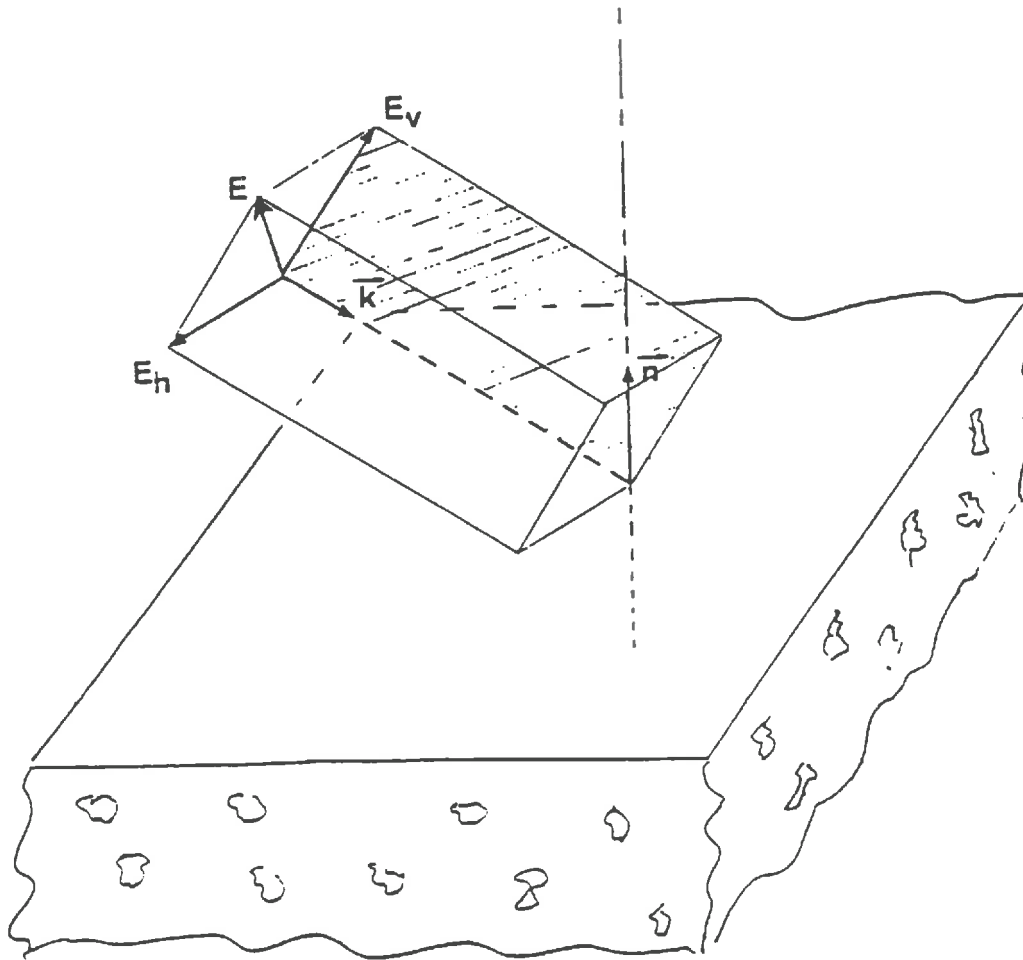
Figure 1.2: Description of the wave polarization.

where

- $\vec{E}$ is the electric field, (V m^{-1})
- $\vec{E}_0$ is the amplitude of electric field vector, (V m^{-1})
- ω is the angular frequency, (rad. s^{-1})
- k is the wave number (m^{-1})

The temporal and spatial properties of the wave are described by ω and k. If f is the wave frequency :

$$\omega = 2\pi f \quad (rad.s^{-1}) \tag{1.3}$$

and

$$k = \frac{2\pi}{\lambda} \ (m^{-1}) \tag{1.4}$$

where

- λ is the wavelength (m).

1.1.2   Concept of polarization

In an electromagnetic wave, the electric and magnetic fields are always oriented in a plane perpendicular to the direction of wave propagation.   The polarization describes the directions of these fields.   Let us take the case of an electromagnetic wave propagating toward a plane surface as shown in figure (1.2).   In a two dimensional plane the incident electric field vector ($\vec{E}$) can be resolved into two mutually orthogonal polarization components.   The horizontal polarization ($\vec{E}_H$) is defined by the electric field component parallel to the surface. The vertically polarized ($\vec{E}_V$) is defined by the electric field component in the plane determined by the propagation vector $\vec{k}$ and the normal vector ($\bar{n}$) to the surface as shown in figure (1.2).   Thus the incident electric field vector:

$$\vec{E} = \vec{E}_H + \vec{E}_V \tag{1.5}$$

1.2   Medium properties and wave propagation

1.2.1   Permitivitty and permeability

When an electromagnetic wave propagates through natural medium, the medium particles undergo polarization, magnetization and conduction. These processes cause the storage and dissipation of the electric and magnetic energy.   The real and imaginary part of complex dielectric constant (Permitivitty, ε) describe the storage and dissipation of electric

energy. Similarly the complex parameter, permeability (μ) describes the variation of magnetic energy.

The complex dielectric constant is represented as:

$$\varepsilon = \varepsilon' - j\varepsilon'' \quad \text{(farad m}^{-1}\text{)} \tag{1.6}$$

where ε' and ε'' is the imaginary part of ε. The relative dielectric constant is defined by $\varepsilon_r = \varepsilon/\varepsilon_0$ where ε_0 is the Permitivitty of vacuum ($8.85 \cdot 10^{-12}$ farad m^{-1}). The complex permeability μ is represented as

$$\mu = \mu' - j\mu'' \quad \text{(henry m}^{-1}\text{)} \tag{1.7}$$

For most natural media the magnetization is very weak and its permeability (μ) can be replaced by permeability of vacuum (μ_0). To understand the influence of the complex quantity in the wave propagation, we consider the wave equation presented in (1.2), where the wavenumber k is

$$k = \frac{2\pi}{\lambda} = \omega\sqrt{\mu_0\varepsilon_0}\sqrt{\varepsilon_r' - i\varepsilon_r''} \tag{1.8}$$

$$k = k' - ik'' \tag{1.9}$$

By combining expressions 1.2 and 1.3 we obtain :

$$\vec{E} = \vec{E}_0 e^{-k''z} e^{i(\omega t - k'z)} \tag{1.10}$$

The expression (1.10) describes that during the propagation along the **z** direction, the wave amplitude is attenuated by a factor of ($e^{-k''z}$).

1.2.2 Energy of the electromagnetic wave

The energy of an electromagnetic wave is a vector quantity given by the vector product of the electric and magnetic field strength. This quantity called poynting vector which flows in the direction perpendicular to both electric and magnetic fields and in the same direction of propagation vector. The poynting vector $\vec{P}$:

$$\vec{P} = \frac{1}{2}\vec{E} \times \vec{H} \quad \text{(W m}^{-2}\text{)} \tag{1.11}$$

where * denotes the complex conjugate. In a sinusoidal wave, both $\vec{E}$ and $\vec{H}$ changes with time and the same with power density also. The average power density for a time interval t:

$$\langle \vec{P} \rangle = \frac{1}{t} \int_0^t \vec{P} dt = \vec{P}_a \qquad (1.12)$$

where $\langle\ \rangle$ denotes the averaging operation. Applying the equations (1.9) and (1.10) in (1.11) we have:

$$\left| \vec{P}_a \right| = \sqrt{\frac{\mu_0}{\varepsilon_0}} \exp(-2k''z) \frac{\mathrm{Re}(\vec{E}.\vec{E})}{2} \qquad (1.13)$$

or

$$\left| \vec{P}_a \right| = \sqrt{\frac{\mu_0}{\varepsilon_0}} \exp(-2k''z) \frac{E_0^2}{2} \qquad (1.13a)$$

where "Re" denotes the real part of complex number. The above equation shows that as the wave propagates through a lossy media, its power is attenuated as a function of $e^{-2k''z}$.

1.2.3 Absorption of electromagnetic waves

In order to study the absorption of electromagnetic waves we consider the above equation (1.13) where the power is attenuated as function of exp($-2k''z$). The factor $-2k''$ may be termed as the power attenuation coefficient. From expressions (1.8 and 1.9) we can express k" as a function of the dielectric properties of the media :

$$\vec{k}^2 = \omega^2 \varepsilon \mu \qquad (1.14)$$

or

$$(\vec{k}' - i\vec{k}'')(\vec{k}' - i\vec{k}'') = \omega^2 \mu \varepsilon \qquad (1.15)$$

From equation 1.15, k" is given by :
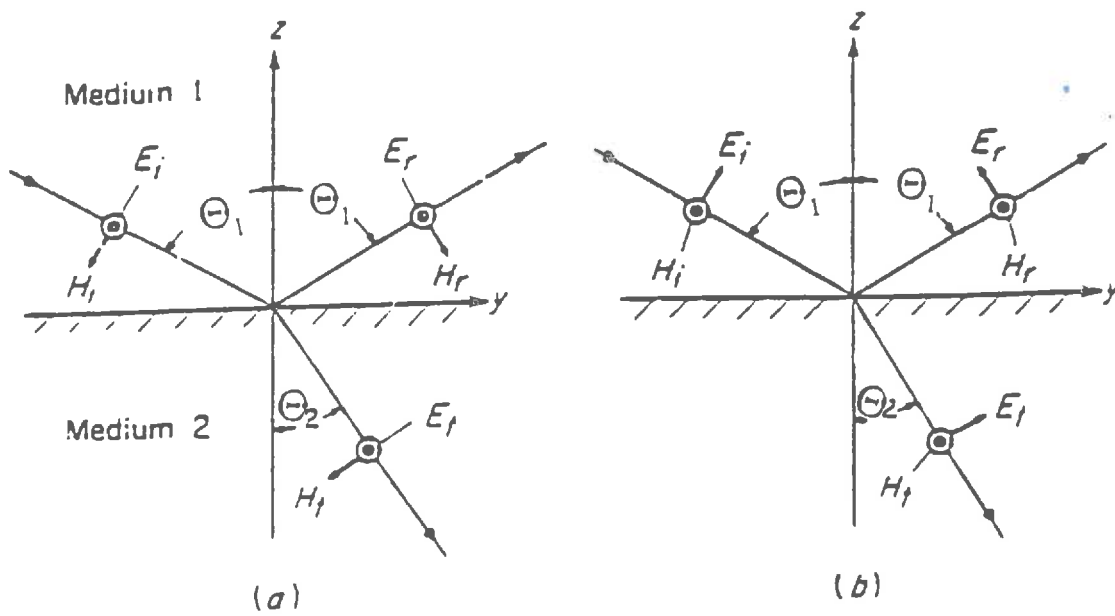
Figure 1.3: Reflection and refraction of waves having (a) horizontal polarization; and (b) vertical polarization.

$$k'' = \frac{1}{\sqrt{2}} \omega(\mu_0 \varepsilon_0) \sqrt{\varepsilon_r' \left[\sqrt{1 + \frac{\varepsilon_r''^2}{\varepsilon_r'^2}} - 1 \right]} \qquad (1.16)$$

In case of soils, $\varepsilon_r''/\varepsilon_r' \ll 1$; then:

$$\sqrt{\left(1 + (\varepsilon_r''/\varepsilon_r')^2\right)} \cong 1 + \frac{1}{2}(\varepsilon_r''/\varepsilon_r')^2 \qquad (1.17)$$

and

$$k'' \cong \frac{2\pi}{\lambda_0} \cdot \frac{\varepsilon_r''}{(2 \cdot \sqrt{\varepsilon_r'})} \qquad (1.18)$$

1.2.4 Propagation of electromagnetic waves through heterogeneous media

1.2.4.1 Reflection and transmission

At the interface between two media which differ by their dielectric properties, an incident electromagnetic wave is partly reflected and partly transmitted as shown in the figure (1.3). The propagation directions of the reflected and transmitted waves are described by the Snell's law. The law can be written by :

$$\eta_1 \sin(\Theta_1) = \eta_2 \sin(\Theta_2) \qquad (1.20)$$

where
- Θ_1 is the angle of incidence
- Θ_2 is the angle of refraction

η_1 and η_2 are the refractive index of medium 1 and medium 2.

The refractive index is related to dielectric constant of soil:

$$\eta = \sqrt{\varepsilon}, \text{ (unit less)}. \qquad (1.21)$$

The reflection and transmission of vertically and horizontally polarized fields are treated separately. The reflection coefficient (R_H or R_V) is the amplitude ratio of the reflected field to the incident field. The expressions for the reflection coefficient are :

$$R_H = \frac{\sqrt{\varepsilon_1}\cos(\Theta_1) - \sqrt{\varepsilon_2 - \varepsilon_1 \sin^2(\Theta_1)}}{\sqrt{\varepsilon_1}\cos(\Theta_1) + \sqrt{\varepsilon_2 - \varepsilon_1 \sin^2(\Theta_1)}} \qquad (1.22)$$

$$R_V = \frac{\left(\dfrac{\varepsilon_2}{\varepsilon_1}\right)\cos(\Theta_1) - \sqrt{\dfrac{\varepsilon_2}{\varepsilon_1} - \sin^2(\Theta_1)}}{\left(\dfrac{\varepsilon_2}{\varepsilon_1}\right)\cos(\Theta_1) + \sqrt{\dfrac{\varepsilon_2}{\varepsilon_1} - \sin^2(\Theta_1)}} \qquad (1.23)$$

The expressions for transmission coefficients are:

$$T_H = \frac{2\sqrt{\varepsilon_1}\cos(\Theta_1)}{\sqrt{\varepsilon_1}\cos(\Theta_1) + \sqrt{\varepsilon_2 - \varepsilon_1 \sin^2(\Theta_1)}} \qquad (1.24)$$

$$T_V = \frac{2\left(\dfrac{\varepsilon_2}{\varepsilon_1}\right)\cos(\Theta_1)}{\left(\dfrac{\varepsilon_2}{\varepsilon_1}\right)\cos(\Theta_1) + \sqrt{\dfrac{\varepsilon_2}{\varepsilon_1} - \sin^2(\Theta_1)}} \qquad (1.25)$$

The above equations (1.22 - 1.25) represent the field amplitude coefficients and subscripts H and V represent for the horizontal and vertical polarization, respectively. The corresponding power coefficients are the reflectivity $\left(\Gamma_p\right)$ and the transmissivity $\left(\chi_p\right)$ which are related to Fresnel coefficient by :

$$\Gamma_P = |R_P|^2 \qquad (1.26)$$

$$\chi_P = |T_P|^2 \qquad (1.27)$$

Here p represents either the polarization **H** or **V**.

1.2.4.2 Scattering of electromagnetic waves

An object scatters an incident wave into all directions. The scattering patterns defined as the energy distribution into the different directions of space vary according to :
  - the wavelength of the radiations and the incident direction of the wave;
  - the size and dielectric properties of the particles that interact with the electromagnetic wave.

Incident wave

(a) smooth;

Incident wave

(b) medium rough;

Incident wave
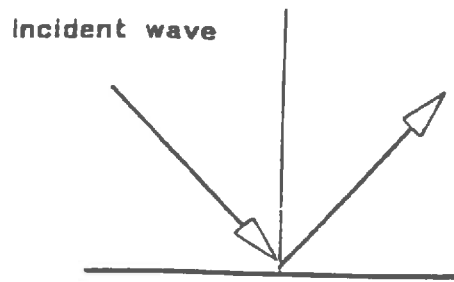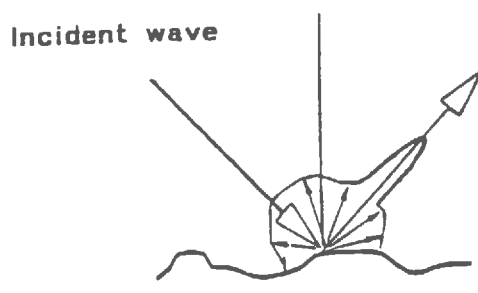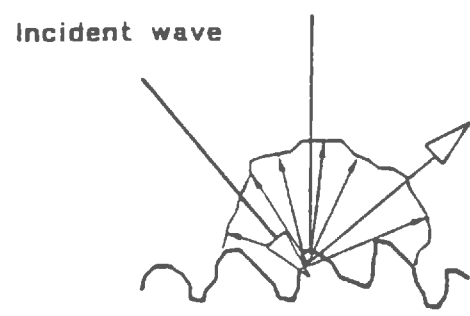
(c) very rough.

Figure 1.4: Example of surface scattering pattern from (a) smooth surface; (b) medium rough surface. and (c) very rough surface.

The scattering properties of an illuminated target is quantified by the bistatic cross section (σ_{PQ}^0 $(\theta_i \phi_i \theta_s \phi_s)$) defined as the ratio of the total power scattered by an equivalent isotropic scatterer to the incident power density on the target. $(\theta_i \phi_i)$ and $(\theta_s \phi_s)$ describe the direction of the incident and scattered waves. P and Q represent the polarization of the incident and scattered wave, respectively. In case of a surface target like sea or earth surfaces, the radiation pattern of the scattered radiation is a function of the surface roughness. Figure (1.4) shows the surface scattering pattern of surface with different roughness. We can consider two extreme cases: 1) specular reflection from a very smooth surface and 2) lambertian scattering very rough surface. But the scattering from most of the natural surfaces have the intermediate roughness condition.

The surface is generally describe by the standard deviation of the surface height (ρ), the surface correlation length (l) and the autocorrelation function. The degree of surface roughness is decided based on the asperity height with respect to λ. Assuming that ρ determines the asperity height, criteria as Fraunhofer criterion ($\rho < \lambda/(32 \cos\Theta)$) or Rayleigh criterion ($\rho < \lambda/(8 \cos\Theta)$ allow the distinction between smooth and rough surfaces (Ulaby et al. 1982).

The determination of σ_{PQ}^0 $(\theta_i \phi_i \theta_s \phi_s)$ of soil surface is difficult to determine theoretically because of the soil structure and surface roughness complexity. However, several analytical models of σ_{PQ}^0 $(\theta_i \phi_i \theta_s \phi_s)$ are now available (Kirchhoff approximations, small perturbations models (Ulaby et al. 1982), IEM (Fung, 1994). These models compute σ_{PQ}^0 $(\theta_i \phi_i \theta_s \phi_s)$ from the dielectric properties of the soil surface and the roughness statistical parameters mentioned above. These models are limited to the surface scattering. They can not be used for representing the volume scattering and they are therefore not suitable for studying the effect of moisture and temperature profiles.

1.3   Thermal emission

In accordance with quantum theory, every material above zero absolute temperature radiates energy in the form of electromagnetic waves (Kraus, 1966). The energy emitted by the body per unit area per solid angle is called the brightness temperature of the body. The brightness is a function of body temperature, dielectric property of the body and the direction of emission. To understand how the brightness of an object is related to its physical temperature, the concept of black body is used. Under thermal equilibrium, the physical temperature of an object is a constant. Thus to keep the temperature constant, the

object must absorbs and emits the energy at the same rate. A black body is an idealized object which absorbs all the radiation and radiates them uniformly in all direction.

1.3.1 Blackbody radiation - Plank's law

The Plank's blackbody radiation law describes the energy radiation by the blackbody at any frequency. According to Plank's law the brightness of the blackbody (B_b) at a temperature T and frequency f :

$$B_b = \frac{2hf^3}{c^2}\left(\frac{1}{e^{hf/K_BT} - 1}\right) \quad (W\ m^{-2}sr^{-1}Hz^{-1}) \tag{1.31}$$

where
 - K_B is the Boltzmann's constant ($1.38 \cdot 10^{-23}$ Ws K^{-1})
 - h is the Plank's constant ($6.63 \cdot 10^{-34}$ Ws)

The Rayleigh-Jean's law is a low frequency approximation $\left(hf/kT \ll 1\right)$ to Plank's law. Thus for low frequencies the brightness is formulated as:

$$B_b = 2KT/\lambda^2 \quad (Wsr^{-1}m^{-2}Hz^{-1}) \tag{1.32}$$

$$B_b = CT \quad (Wsr^{-1}m^{-2}H z^{-1}) \tag{1.33}$$

where
$$C = 2K/\lambda^2$$

The Rayleigh-Jeans approximation is valid for the frequencies below 10^{12} Hz. In passive microwave remote sensing, Equation 1.33 relates the brightness (radiometric measurements) to temperature of the object. At 300 K the Rayleigh-Jeans law holds up to a frequency of 117 GHz with less than 1% of deviation form Plank's law (Ulaby et al. 1982).

1.3.2 Brightness temperature

The radiometer measures the brightness of the land surface. The land surface is gray body which does not emit all the radiation as the case of blackbody whose emissivity is one. So often we express the radiometric data in terms of blackbody brightness temperatures

$$T_B(\Theta, \phi) = e(\Theta, \phi) \cdot T \quad (K) \tag{1.34}$$

Where:

    T is the physical temperature

    e is the emissivity of the land surface which is always less than one for all natural materials. The emissivity of the land surface is related to the dielectric properties of soil, and vegetation, surface roughness and vegetation layer.

1.3.3 Relation between emissivity and reflectivity - Kirchhoff law

The Kirchhoff law relates the emissivity and reflectivity. This relationship is being used often in passive microwave remote sensing to calculate the emissivity. When an electromagnetic wave interacts with the surface of the soil medium, the medium reflects, transmits and absorbs the incident radiation. If the medium is opaque or having infinite thickness, as the soil media, the transmission could be neglected. If the incident radiation has unit power, according to the law of conservation;

$$a + \Gamma = 1 \tag{1.35}$$

where a is the absorptivity and Γ is the global reflectivity of the surface (it integrates all the scattering in all directions). The absorption of the energy radiation increases the temperature of the medium and this provokes the atomic and molecular agitation of the medium. The result is the emission of energy radiation by the medium. If the medium and the surroundings are in thermal equilibrium state, then according to Kirchhoff law, the medium emits the same radiation as it absorbs. This means that the emissivity (e) of the medium is equal to the absorptivity (a). Then, we can write :

$$e = 1 - \Gamma \tag{1.36}$$

This relationship is used for the theoretical calculation of emissivity. Peake(1959) relates the emissivity to the bistatic scattering coefficient by:

$$e_P(\Theta_s, \phi_s) = 1 - \int_0^{2\pi} \int_0^{\pi/2} \left(\sigma_{HP}^0(\Theta_s, \phi_s, \Theta_s, \phi_s) + \sigma_{VP}^0(\Theta_s, \phi_s, \Theta_s, \phi_s) \right) \cdot \frac{1}{4\pi \cos\Theta_s} \sin\Theta_s \, d\Theta_s \, d\phi_s \tag{.37}$$

The equation (1.37) relates the passive and active microwave remote sensing. The equation enables us to calculate the emissivity of rough surface from surface scattering coefficient. When the soil is smooth, the only possible scattering direction is the specular one. Therefore the integral in equation (1.37) is equal to the Fresnel reflectivity Γ_P (Equation (1.26)).
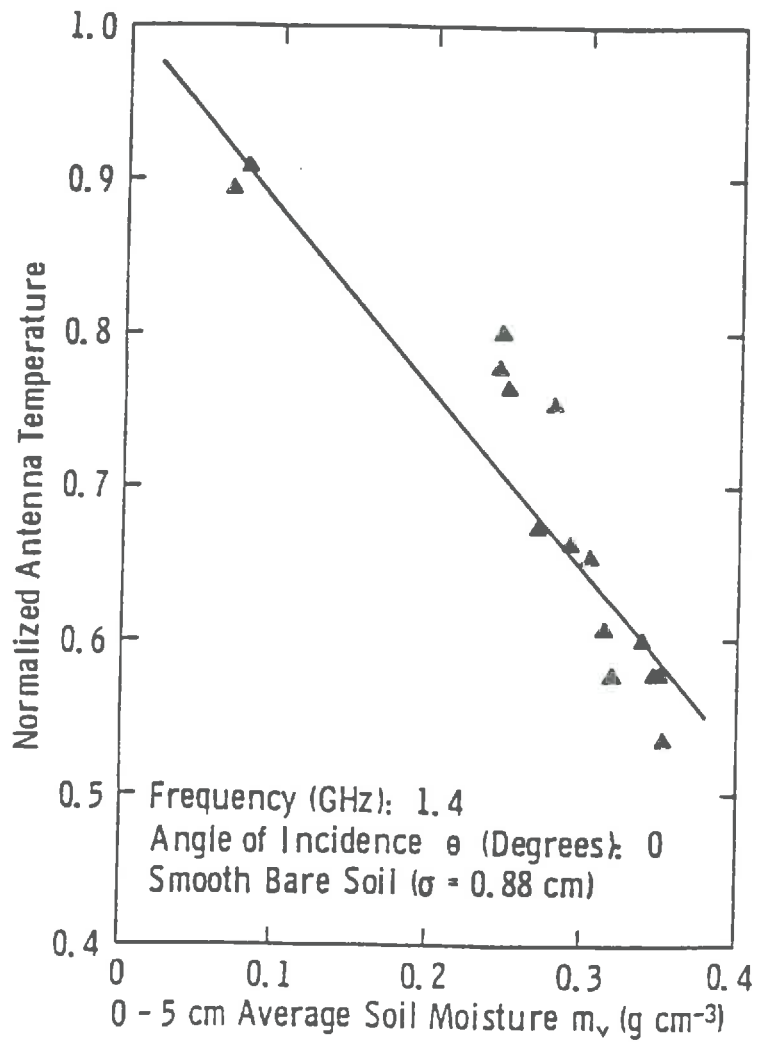
Figure 1.5: Relation between the soil moisture and normalized antenna temperature (from Newton and Rouse, 1980).

1.3.4   Influence of the soil parameters on microwave emission

The surface parameters; soil moisture, surface roughness and vegetation cover affect the intensity of the microwave radiation emitted from the earth surface. The potentiality of microwave remote sensing for soil moisture studies has been established from a series of experimental and theoretical studies. (Njoku and Kong 1977; Wilheit 1978; Burke et al. 1979; Wang and Schmugge 1980; Schmugge and Choudhury 1981; and Choudhury et al. 1982; Njoku and O'Neill 1982; Newton et al. 1982; Schmugge 1983; Wang 1983; Wang et al. 1983; Hallikainen et al. 1985; Dobson et al. 1985; Schmugge et al. 1986; Jackson and O'Neill 1986; Wang et al. 1987; Wang 1987; Hallikainen et al. 1985; Dobson et al. 1985; Jackson and Schmugge 1989; and Reutov and Shutko 1992).   Both theoretical and experimental studies were aimed to understand the microwave emission from the soil medium with non-uniform moisture and temperature profiles.   Here we make a quick review on the studies carried out to understand the influences of the ground surface parameters on microwave emission from earth surface.

1.3.4.1   Soil moisture effect

The microwave emission from bare soil is related to the surface soil moisture. This is due to the large contrast between the dielectric properties of liquid water ($\cong 80$) and that of dry soil ($\cong 3 - 4$). The relationship between soil moisture and microwave emission is shown in the figure (1.5). In this Figure, the effect of the temperature is removed by normalizing T_B with soil temperature. This figure exhibits the microwave emission sensitivity to the soil moisture which is high enough to perform soil moisture measurements.

The wet soil medium is a mixture of soil particles, air voids and liquid water. The water contained in the soil is usually divided into bound water and free water. The bound water refers to the water molecules contained in the first few molecular layers surrounding the soil particle. These water molecules are tightly held to the solid particle due to the electric forces (Wang and Schmugge (1980). The free water refers the water molecules that are loosely attached to soil matrix. The free water molecule are free to align along the electric field direction. The soil texture determines the partition of soil water into bound and free water. One difficulty in modeling the soil dielectric permitivitty is to divide the soil water into bound and free fractions.

Most of the soil dielectric models available today are developed based on the mixing of the dielectric constituents. Laboratory measurements of soil dielectric constant for different
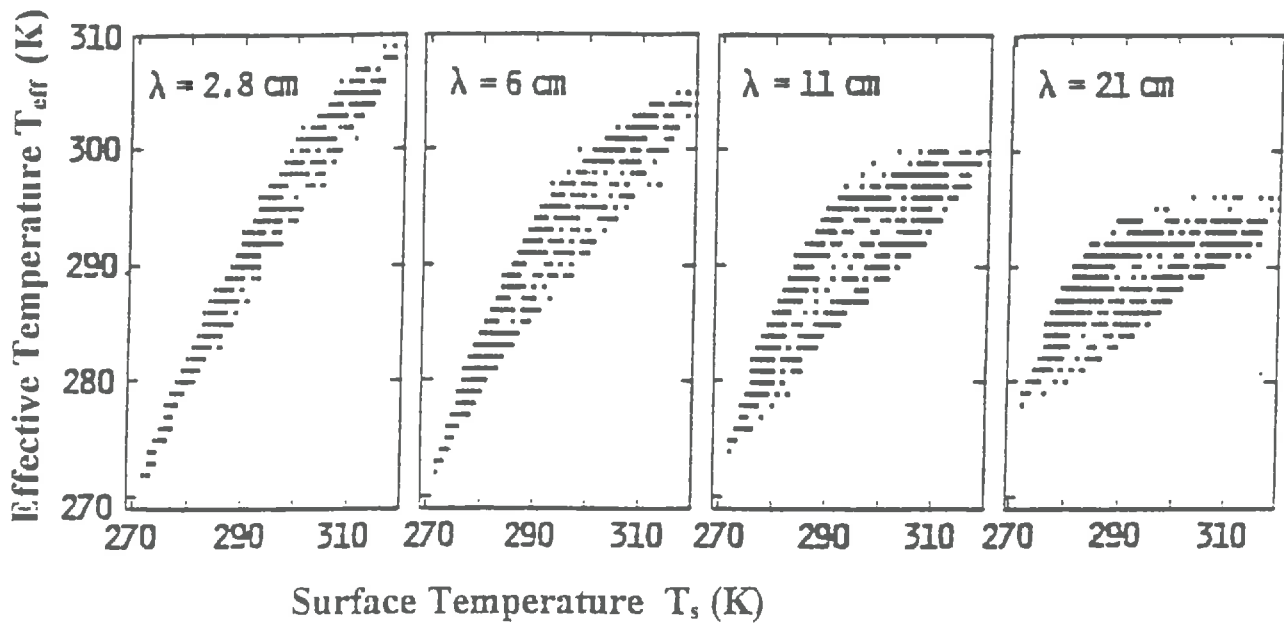
Figure 1.6: Scatter plots of effective temperature for different wavelength versus surface temperature (from Choudhury et al. 1982).

soil texture (Lundien 1971; Newton 1977; Wang et al. 1978; Hallikainen et al. 1985) were used to develop and verify the models. Among these models, those developed by Wang and Schmugge (1980) and Dobson et al. (1985) are widely used. These two models are detailed in the appendix A. Conceptually both models are similar, but they differ each other in the treatment of the bound water and the free water. Wang and Schmugge (1980) considered a soil texture (via wilting point) dependent parameter called transition point to separate the bound water and free water. Dobson et al. (1985) directly related the specific surface area of soil particle to the bound water.

The dielectric behavior of moist soils at the microwave frequencies up to 18 GHz is studied on experimentally and theoretically (Hallikainen et al. 1985; Wang and Schmugge 1980, Dobson et al. 1985). However, very limited work has been reported to calculate the soil dielectric constant for higher frequencies. England et al. (1992) proposed a simple expression of soil dielectric constant at 37 and 85.5 GHz frequencies. Based on the analysis of PORTOS data over a smooth silty loam soil, Calvet et al.(1995) proposed an adaptation of Wang and Schmugge model for the frequencies at 23.8, 36.5 and 90.0 GHz.

1.3.4.2 Temperature effect

The brightness measured by the radiometer is the resultant of the thermal emission taking place at different parts in the soil medium. A parameter called effective temperature (T_e) is defined to account for the soil temperature profile and soil moisture profile contribution in the microwave emission from the soil. Figure (1.6) represents the relation between T_e for different frequencies and surface soil temperature (T_s). Except for 17 GHz (λ = 2.8 cm), T_e is poorly correlated to T_s.

Many theoretical models based on radiative transfer equation are available to calculate T_e (Njoku and Kong 1977; Wilheit 1978; Burke et al. 1979 and Schmugge and Choudhury, 1981). These models are developed in the second paper in part V. To summarize, there are, on one hand, the models based on a radiative transfer approach. These models need a complete description of the soil moisture and temperature profiles. These profile information is seldom available at the scale of remote sensing studies. On the other hand, a semi-empirical model to characterize T_e was proposed by Choudhury et al. (1982):

$$T_e = T_d + (T_s - T_d) \cdot C_c \qquad (1.38)$$

where
- T_s is the surface temperature (K)
- T_d is the deeper depth (above 100 cm) soil temperature (K)
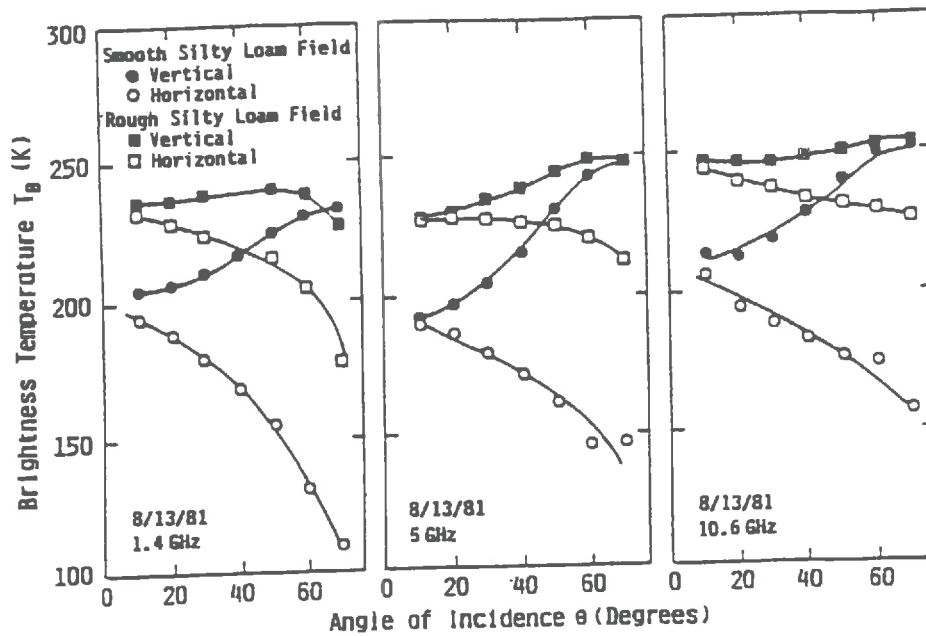
Figure 1.7: Roughness effect on the angular dependence of T_B at 1.4 GHz; 5.0 GHz and 10.65 GHz frequencies. The volumetric soil moisture content for the smooth field was about 0.250 $cm^3.cm^3$ and for rough field was about 0.259 $cm^3.cm^3$, in the top 10 cm layer (from Wang et al. 1983).
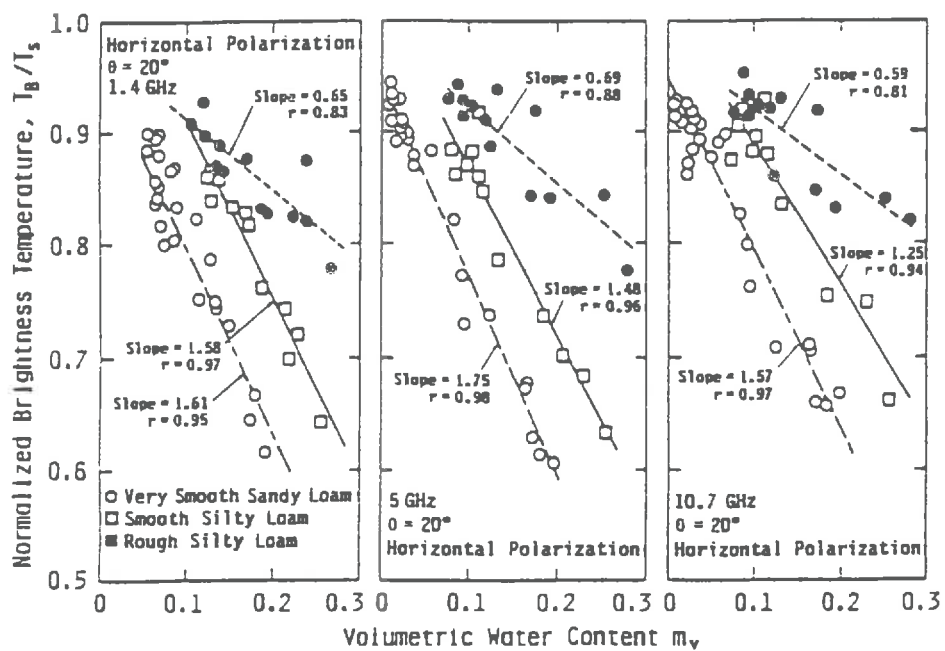
Figure 1.8: The roughness effect on the radiometric sensitivity to soil moisture variations at 1.4 GHz, 5.0 GHz and 10.65 GHz. The data is from three fields having different soil texture and surface roughness (from Wang et al. 1983).

- C_t is a fitted parameter (2.46, 0.48, and 0.667 for L, C and X band frequencies.

The T_s can obtain from satellite-borne infrared radiometry and an approximate value of T_d can be either simulated or taken from local meteorological center. The Choudhury's model requires, however, the knowledge of the surface temperature which may not be always available, since the clouds prevent thermal infra-red observations from satellites.

1.3.4.3 Surface roughness effect

The surface roughness affects the microwave T_B in different ways. The roughness reduces the polarization difference and angular variations of the microwave emission as demonstrated in figure (1.7) for different frequencies. The two sets of curves shown in the figure (1.7) are representing the T_B observed from two fields having different roughness but having almost same soil moisture and temperature conditions. The figure also demonstrates the frequency dependence of roughness effect. The roughness has an effect on soil moisture sensitivity also. The loss of radiometric sensitivity to soil moisture variation due to the surface roughness is demonstrated in the figure (1.8). The roughness influence on the "soil microwave emission-soil moisture" relationship is one of the major difficulties to infer operationally the soil moisture from microwave observations.

1.3.4.4 Vegetation effect

The presence of vegetation reduces the sensitivity of radiometric measurements to surface soil moisture, (Basharinov and Shutko 1975; Jackson et al. 1982; Ulaby et al. 1983; Pampaloni and Paloscia (1986); Jackson and Schmugge 1991; Kerr and Wigneron 1993; and Wigneron et al. 1994a and b). The vegetation attenuates the microwave emission from the soil and adds its own contribution to total emission. The attenuation by vegetation is a function of the water content (W_c) in the vegetation, the vegetation density and its structure. The brightness temperature observed over vegetation covered soil consists of three components as shown in the figure (1.9):

T_{B1} - the direct emission by the vegetation
T_{B2} - the emission by vegetation reflected by soil surface and attenuated by the vegetation
T_{B3} - emission by the soil attenuated by the vegetation

$$T_B = T_{B1} + T_{B2} + T_{B3} \qquad (1.39)$$

Jackson (1982); Pampaloni and Paloscia (1986) reported small angular dependence and small polarization difference of T_B measured from the vegetated fields. This reduction in polarization difference could be used to estimate the vegetation water content (Schmugge

$$T_B = T_B1 \quad + \quad T_B2 \quad + \quad T_B3$$

air medium

emission from
vegetation

vegetation layer

soil medium   emission from soil
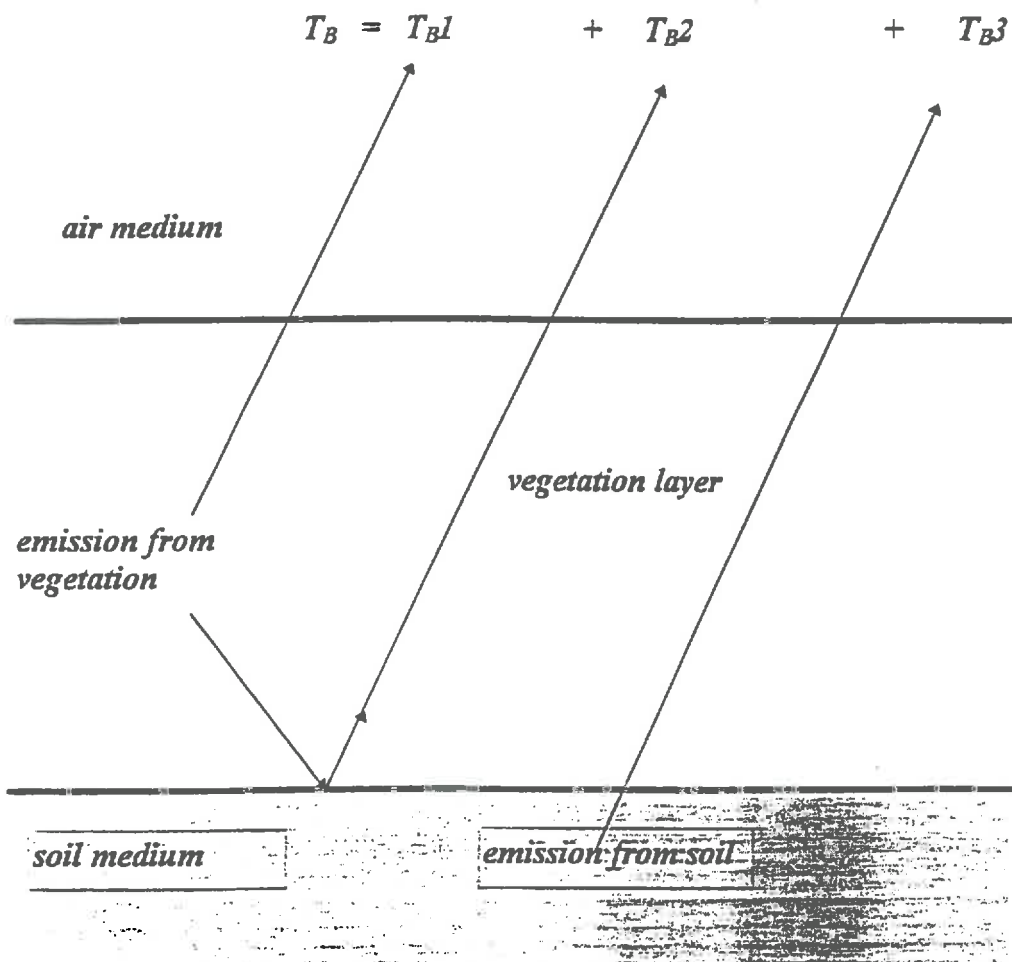
Figure 1.9: Schematic presentation of microwave emission from vegetation covered soil.

and Jackson, (1994)). Besides the change in emissivity with vegetation water content, attenuation is also a function of wavelength. Kirdiashev et al. (1979); and Wang et al. (1980) evaluated the effect of vegetation on soil moisture study by using a parameter called slope reduction factor (ratio of slope of emissivity- soil moisture of the vegetated field to emissivity - soil moisture of bare soil). Large values of slope reduction factor were observed at higher wavelength. Radiation penetration in the vegetation explain the variations in the slope reduction factor. It increases when the vegetation attenuation increases. As an extreme case, very thick vegetation or forest can completely mask the moisture information (Wang et al. (1980)) and therefore the slope reduction factor tends the infinity.

1.3.5 Modeling of microwave emission from soil medium

The modeling activities of microwave emission are important because they provide a physical frame work for understanding the microwave emission and improving the soil moisture retrieval algorithms derived from remotely sensed data. In the following parts the modeling of microwave emission from bare soil is briefly discussed.

We can distinguish the surface models, which only accounts for the wave scattering at the surface, and the emission models from layered media which accounts for the emission from the soil volume.

Surface scattering models :
A physical approach is based on the Kirchhoff formula (1.39), where the bistatic scattering coefficients are computed using the Small Perturbation Model (SPM), the Physical Optics Model (PO) and Geometric Optics model (GO). These models were tested by Tsang and Newton (1982), Mo and Schmugge (1987), Saatchi et al., 1994 and Laguerre (1995). They have shown a good agreement between the observations and the simulations. However, the high sensitivity of the models to the soil roughness parameters and the restricted fields of validity make these models difficult to be used for inversion.

When the surface is smooth, there is only a specular reflection and the soil reflectivity can therefore be computed by the Fresnel reflectivity. The calculation of the soil microwave emission is then easy to run and suitable for inversion. To extend the approach to the rough soils, Choudhury et al. (1978) and Wang and Choudhury (1981) proposed semi-empirical models which correct the Fresnel reflectivity to account for the influence of the surface roughness. The roughness is parameterized by empirical parameters which are difficult to

link to the surface roughness parameter. Therefore, these parameters must be determined by inversion or set to prescribed values.

In all these model, the volume contribution of the soil microwave emission is implicitly involved in the determination of the soil sampling depth, which is the depth of the soil layer used to characterize the soil dielectric permitivitty. The soil sampling depth will be further developed.

Emission from layered media :

The microwave emission models based on radiative transfer principle in the layered media are capable of accounting for moisture and temperature profiles in the emissivity calculation. These models are all limited to smooth soils. The models are classified into coherent models (Njoku and Kong model 1977 and Wilheit model 1978) and incoherent model (Burke et al. 1979). The details of the emission models are presented in the chapter II.

The presentation of the models shows that it is not possible to investigate simultaneously the roughness and the volume effects on the soil microwave emission in an existing theoretical framework. The simulation of T_B is a key tool to evaluate profile influence on microwave emission in a wide range of climatic and soil conditions. Considering a smooth land surface in the experimental study, we bring experimental data more near to the reality of the theoretical frame. The layered emission models are developed for the smooth surface condition. And also we vegetation influence to maximize the effect of the profiles. This supports our choice to limit the study in the smooth land surface condition in order to study the influence of soil moisture and temperature profiles on microwave radiometric measurements.

1.4   Soil moisture estimation from microwave radiometry

Different methodologies have been developed to retrieve the radiometric quantity which represents the surface soil moisture from the radiometric measurements. In the following part we discuss about the different parameters that define the retrieved soil moisture quantity.
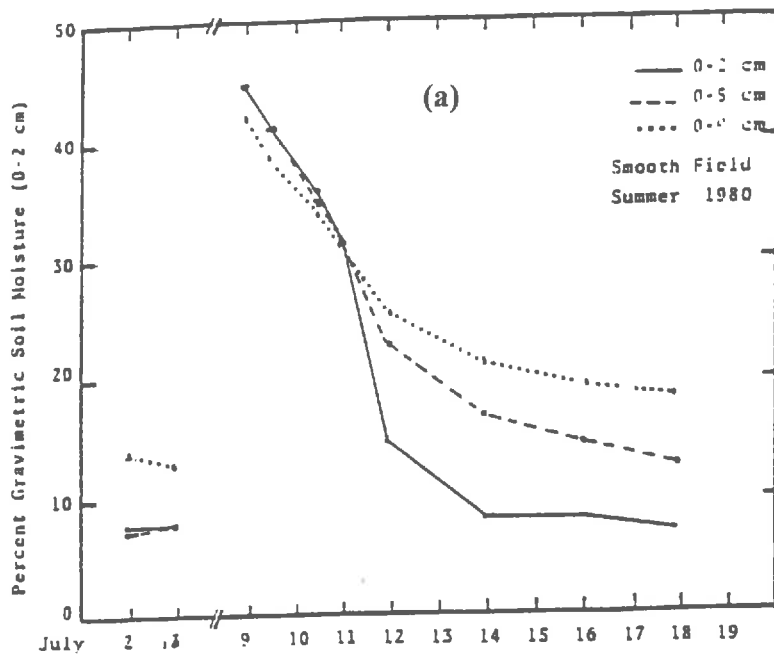
Fig. 2. Dry-down curves for three soil layers in the smooth field.
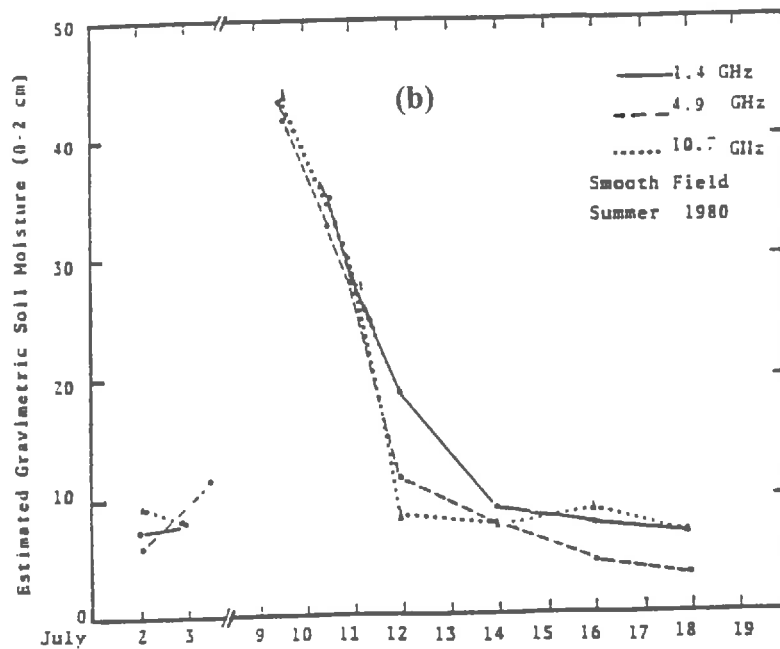
Fig. 3. Percent soil moisture versus time estimated from 1.4-, 5.0-, and 10.7-GHz measurements of the smooth field.

Figure 1.10: The soil moisture variation in a smooth bare field; (a) measured; (b) retrieved from radiometric data (from Newton et al. 1982).

1.4.1 Soil moisture quantity

In soil science, several quantities exist to characterize the soil moisture such as :

1) Gravimetric water content ($Kg.Kg^{-1}$) (Ulaby et al. 1978; Kobayashi and Hirosawa, 1985);

2) Volumetric water content ($cm^3.cm^{-3}$), (Dobson and Ulaby, 1981; Bernard et al. 1982; Bruckler et al,. 1988)

3) Percent of field capacity (% by weight), Ulaby et al. 1978; Schmugge 1980 and Bernard et al. 1982)

4) Productive water content (total water content minus permanent wiltering water content, $cm^3.cm^3$) (Zotova and Geller 1985)

An ideal characterization of the soil moisture should be the volumetric free water content weighted by the contribution of each layer to the microwave emission (Chanzy, 1993). Obviously, a practical measurements of this parameter is not feasible. Among the moisture quantities presented above, the volumetric water content is preferred to the gravimetric water content, since the relationship "soil moisture-microwave measurements" is sensitive to the soil dry bulk density. The choice of the percent of field of capacity or the productive water content leads to less textural effect on soil dielectric constant (Dobson et al. 1984; J. W. Rouse 1983) but requires more information on the soil (field capacity, water retention curve). In fact the latter moisture quantities were used for establishing direct relationships between the soil moisture and the microwave observations. In this study we apply the Wang and Schmugge (1980) and the Dobson et al. (1985) semi-empirical models to compute the soil dielectric constant and therefore, we take the volumetric water content to characterize the soil moisture.

1.4.2 Sampling depth of microwave radiometry

Many investigators have attempted to provide a quantitative definition for the sampling depth based on both theoretical and experimental studies (Schmugge et al. 1974; Newton 1977; Wilheit 1978; Ulaby et al. 1978; Burke et al. 1979; Newton and Rouse, 1980; Shutko 1982; Newton et al. 1982; Njoku and O'Neill 1982; Wang 1987, and Chanzy and Kustas 1994).   In a theoretical analysis, Wilheit (1978) estimated the sampling approximately equal to one tenth of the wavelength. He noticed that the sampling depth is also a function of moisture. Burke et al. (1979) used a incoherent model and arrived to similar conclusions.
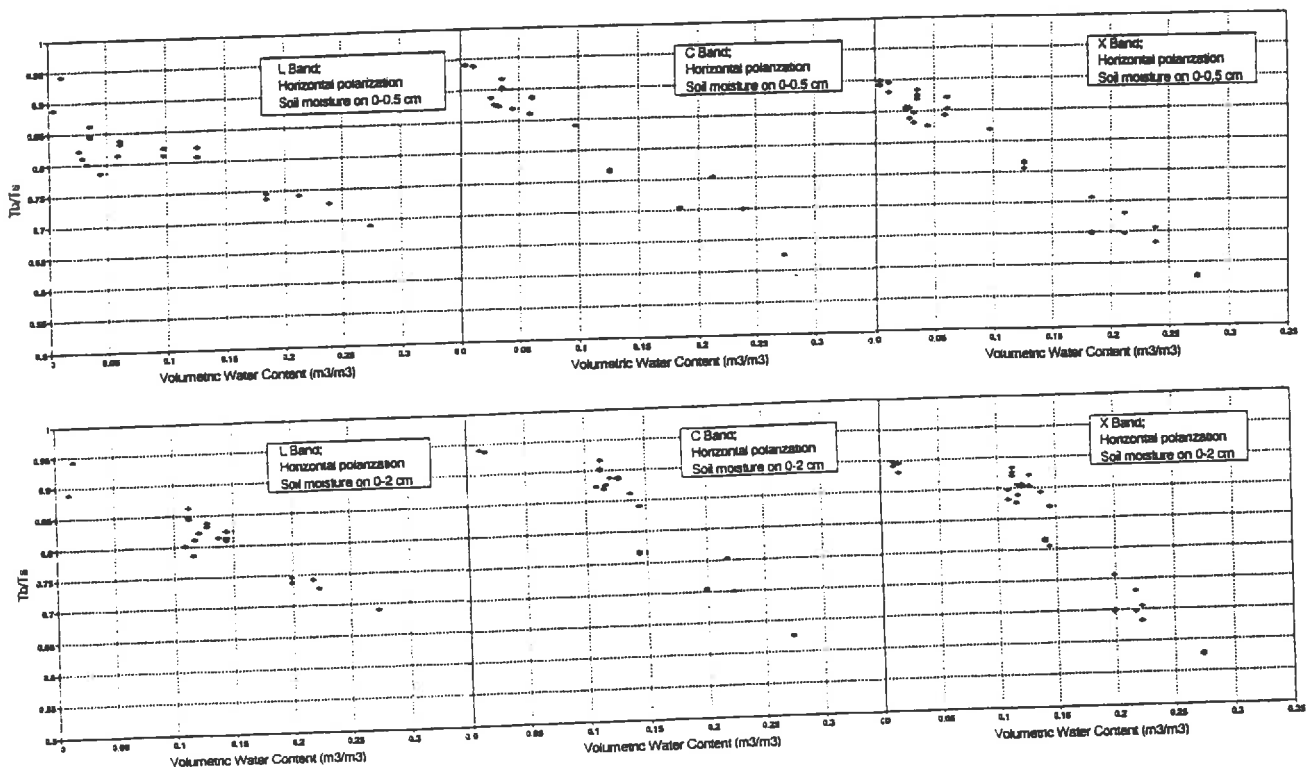
Figure 1.11: The relationship between soil moisture and normalized radiometric data (T_B/T_S) at (a) 1.4; (b) 5.05 and 10.65 GHz (from Chanzy and Kustas, 1994).

Many experimental investigation were done on the sampling depth. They were performed by analyzing the microwave measurement together with soil moisture sampled in different soil layers. In a preliminary study, Newton (1977) claimed a deep sampling depth of the order of 20 cm at 1.4 GHz based on his experimental observation. In fact, he used a parameter called equivalent soil moisture (EQSM which is the product of soil moisture and thermal microwave emission profile) to correlate the radiometric data. In a later study, Newton et al. (1982) compared the soil moisture variations measured at different depth during a drying down period (figure 1.10a) against the T_B collected at different frequencies (Figure1.10b). At L-band, the best similarity between the T_B variations and the soil moisture was obtained when the soil moisture was sampled in the 0-2 cm layer. This leads to the conclusion that for L band radiation the sampling depth may be near to 2 cm for that soil condition.

A more detailed investigation in this aspect was reported by Wang (1987). In his study he used both experimental and theoretical data. His results were in agreement with Wilheit (1978) and Schmugge (1974). Wang (1987) suggested that for inverting soil moisture from radiometric data, the sampling depth information can be used to calibrate the Fresnel model provided the knowledge of the soil texture. In a recent study, Chanzy and Kustas (1994) observed a constant sensitivity of T_B/T_s to the soil moisture in the top 0.5 cm layer ($\theta_{0-0.5}$) for a wide range of soil moisture conditions at X and C-bands (figure 1.11). On the contrary, T_B/T_s at these frequencies is no longer sensitive to soil moisture variation in the top 2.0 cm layer (θ_{0-2}) when $\theta_{0-2} < 0.1$ ($cm^3.cm^3$). In case of L band, the T_B/T_s is more sensitive to θ_{0-2} than $\theta_{0-0.5}$. The common conclusion made from the above studies is that sampling depth is a frequency dependent parameter which is approximately of the order of one tenth of the wavelength. In fact higher values of sampling was reported by Jackson (Jackson et al 1996) based on the data collected from sandy soil. Practically, the sampling depth falls within the following range of values 0.5, [0.5-2] and [2-5] cm at X, C and L bands, respectively.

1.4.2.1 Influence of soil and climatic conditions on soil moisture profile

The soil hydrodynamic properties and diurnal changes of climatic conditions are the two factors that strongly affect the soil moisture and temperature vertical profiles. As a result, the water content in the soil surface layer changes spatially and temporarily. Here we make a survey on the studies carried out to understand the influence of hydrodynamic properties and climatic changes on the diurnal evolution of soil moisture quantity within the sampling depth soil layer.
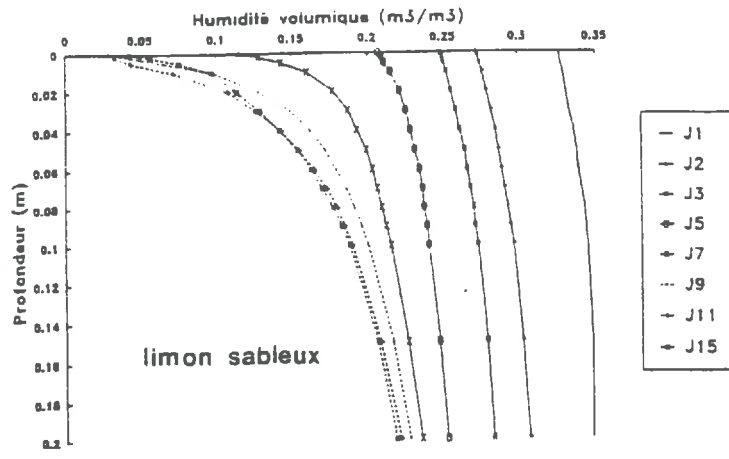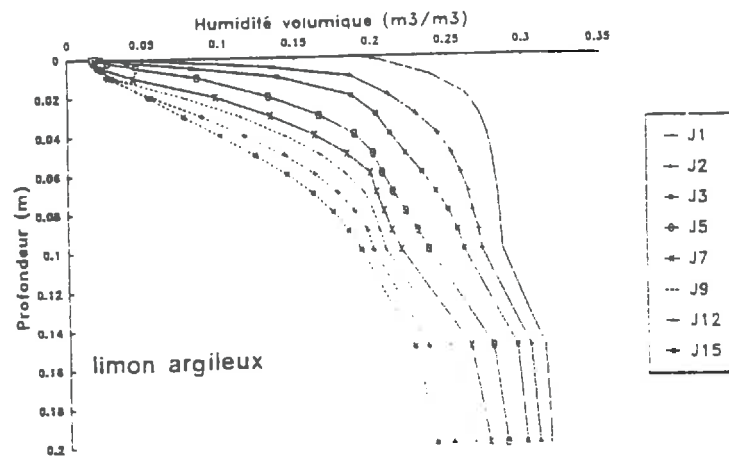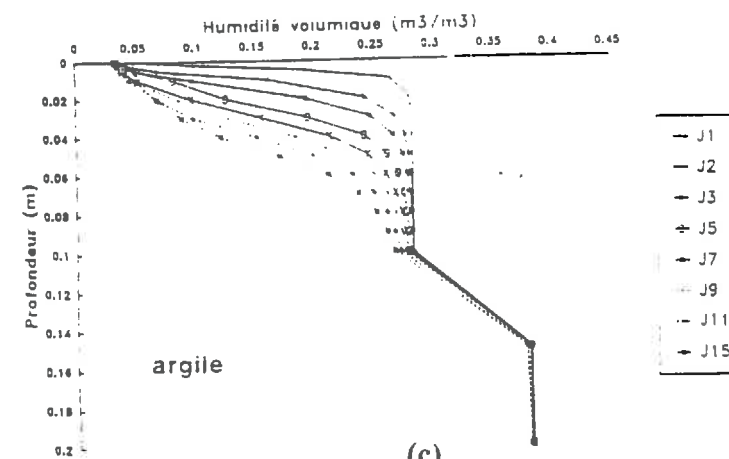
Figure 1.12: Evolution of soil moisture profiles during the dry down period of 15 days in (a) Sandy soil; (b) Silty clay loam soil and (c) Clay soil (A. Chanzy 1991).

The hydrodynamic properties, which are influenced by the soil texture and porosity, have an effect on the evolution of soil moisture vertical profile (A. Chanzy (1991)) The figures (1.12 (a), (b) and (c)) support the above statement. The figures(1.12 (a) - (c) present the evolution of soil moisture vertical profiles in three types of soils, which are a sandy, a silty clay loam and a clay soils during a continuous drying down period of 15 days. The profiles were simulated using a mechanistic model of heat and mass flow in non-saturated soils (Chanzy and Bruckler (1993) ran with summer climatic conditions. The evolution of soil moisture profile in each soil type is different and this may indicate the soil texture effect on the soil hydrodynamic properties. In the clay and silty clay loam soils, the surface soil layers dry very fast. Therefore, in these soils, the moisture profiles are characterized by steep gradients that are entirely different from what we observed in the loamy soil.

The soil moisture quantity in the near surface layer undergoes large variations according to the day - night cycle and climatic demands. The range of soil moisture variations is larger under warm conditions than under cold climatic conditions. The influence of climatic demand on the water content gradient in the 0-5 cm surface soil layer is shown in the figure (1.13) (Chanzy and Bruckler 1993). In the figure (1.13) the difference of the soil moisture between 1 and 5 cm depth levels as a function of soil moisture in 0 - 5 cm layer in case of silty clay loam soil is plotted. The data for the figure is derived from the simulated data by the mechanistic model of heat and mass flows. The water content gradients are lower at the wet and dry ends. The data in the figure is grouped into three classes according to the potential of evaporation. When the potential evaporation was less the 3 mm/day, the water content gradient are significantly lower in the medium region of water in the 0 - 5 cm than those obtained for the higher climatic demand. This analysis shows there is not a single relationship for a soil between the soil moisture in 0 - 5 cm layer and the soil moisture near the surface. This indicates that for a given value of soil moisture in the 0 - 5 cm layer, the vertical water distribution depends on the climatic demand.

Thus, from the above results we make the conclusion that the evolution of soil moisture vertical profiles near the soil surface is strongly influenced by soil texture, and seasonal climatic conditions. As a result, for a given average moisture in the sampling layer, we can have a variety of soil moisture profiles that differ from one profile to another by the soil moisture gradients near the surface. This variability in moisture profiles can alter the accuracy of soil moisture retrieval when a fixed sampling depth is used for the inversion. The impact of such variability on the soil microwave emission and on the accuracy of the inverted soil moisture were not investigated until now.
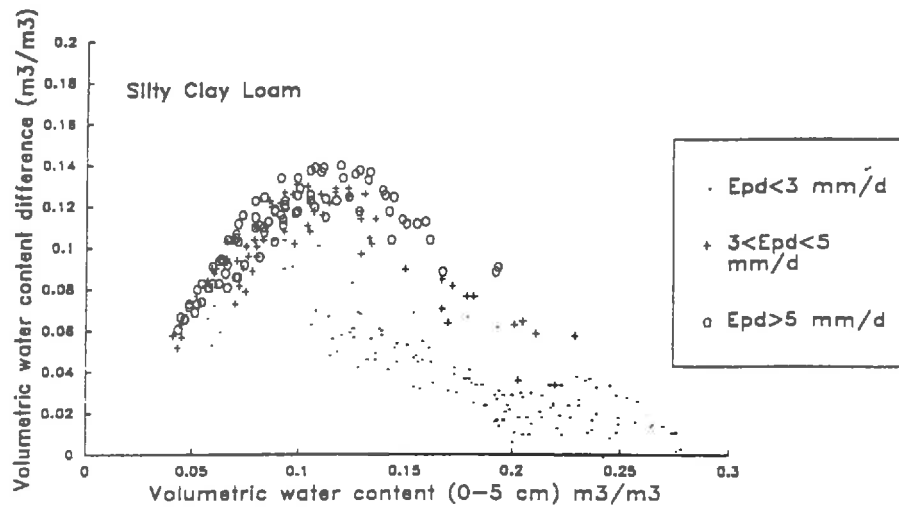
Figure 1.13: Volumetric water content difference between 5 and 1 cm depth in relation to soil moisture of 0 - 5 cm layer of Silty clay loam soil. The data were simulated by mechanistic model (Chanzy and Bruckler 1993)

1.4.2.2 The diurnal evolution of soil temperature

The soil temperature of the surface soil layer undergoes large variation during the day time. In the clay soil, the surface temperature shows the variations above 30 K during the day and night cycle (A. Chanzy 1991). The temperature variation in sandy soil is small compared to that observed in the silty clay loam soil and sandy loam soil. The range of variation of soil temperature and its variability between soils and soil moisture condition highlights the need of characterizing T_e.

1.4.3 Inversion of soil moisture on bare soil from radiometric data.

For the accurate estimate of soil moisture from radiometric data, one has to take into account the influence of the other parameters which influence the microwave emission. Numerous inversion methods have been developed to the retrieve surface parameters including soil moisture (Ishimaru et al. 1992 and Wigneron et al. 1994(a), Chouhan et al. 1994). They are based on either statistical techniques or forward model inversion approach. The forward model approach is based on the physical models that relate the microwave emission to the ground parameters. Once this model is developed and tested, it could be inverted using optimization algorithms to retrieve the surface parameters.

1.5 Conclusions

The microwave radiometry is being used as a tool for the mapping of spatial and temporal surface soil moisture over large area. There are many theoretical models available to account for the influences of surface roughness and vegetation cover. These models are developed and verified on the basis of ground controlled experiments. Recently many airborne campaign were conducted to test the applicability of these models and the capability of radiometer system to map the surface soil moisture over large area with heterogeneous land cover (Jackson et al. 1993; Chanzy et al. 1995; and Ijjas and Rao, 1992). The comparison between the model predicted and observed "emissivity - soil moisture relationship" showed a close agreement which indicates the reliability of these models in data interpretation and a validation for extending them to very large area. However, many basic questions still remain open. They are:

sampling depth definition: The sampling depth is key parameter to infer soil moisture from microwave observations. The variation of soil moisture and temperature profile driven by the climatic condition and soil hydrodynamic properties must be addressed to determine the

field of validity (in time and between soils) of a sampling depth and/or to evaluate the accuracy obtained on the retrieved soil moisture when a fixed sampling depth is used.

<u>effective radiating temperature</u>: The soil temperature undergoes large variation during the daily and seasonal cycles. We have to establish the impact of the effective temperature (T_e) on the accuracy in soil moisture. We will see the importance of T_e and therefore, there is a need to develop a model that estimates T_e based on data that are available whatever the weather conditions.

<u>roughness effect</u>: at present we do not have the direct method for inferring the radiometric observation to surface roughness parameter which changes both spatially and temporally. These parameters are represented by some fitted values. The utility of the cross polarization as an indicator of roughness parameter is accompanied by vegetation soil roughness ambiguity.

In this work we address the first two problems mentioned above. In order to study the soil texture and diurnal changes in the climatic conditions, one needs to have a large set of experimental radiometric data that would be very difficult to obtain. To overcome this situation we have used both simulation and experimental studies. The experimental data is used for the validation of the microwave emission models and to compare the simulated data (both radiometric and ground measurements). Once the models are tested and validated, the experimental results can be extended to other climatic conditions by using simulated data. These are obtained by applying radiative transfer models developed in stratified soil medium to the outputs of a mechanistic model of heat and mass flow. The mechanistic model is capable of providing the continuous soil moisture and temperature profiles in stratified soil layer according to the requirements of radiative transfer models. Thus, by coupling both mechanistic model to radiative transfer model we are able to study the diurnal evolution of soil moisture profile effect, soil texture influence, and climatic conditions of microwave emission. The radiative transfer models and the mechanistic model of heat and mass flows are presented in next section.

CHAPTER 2

MODELS
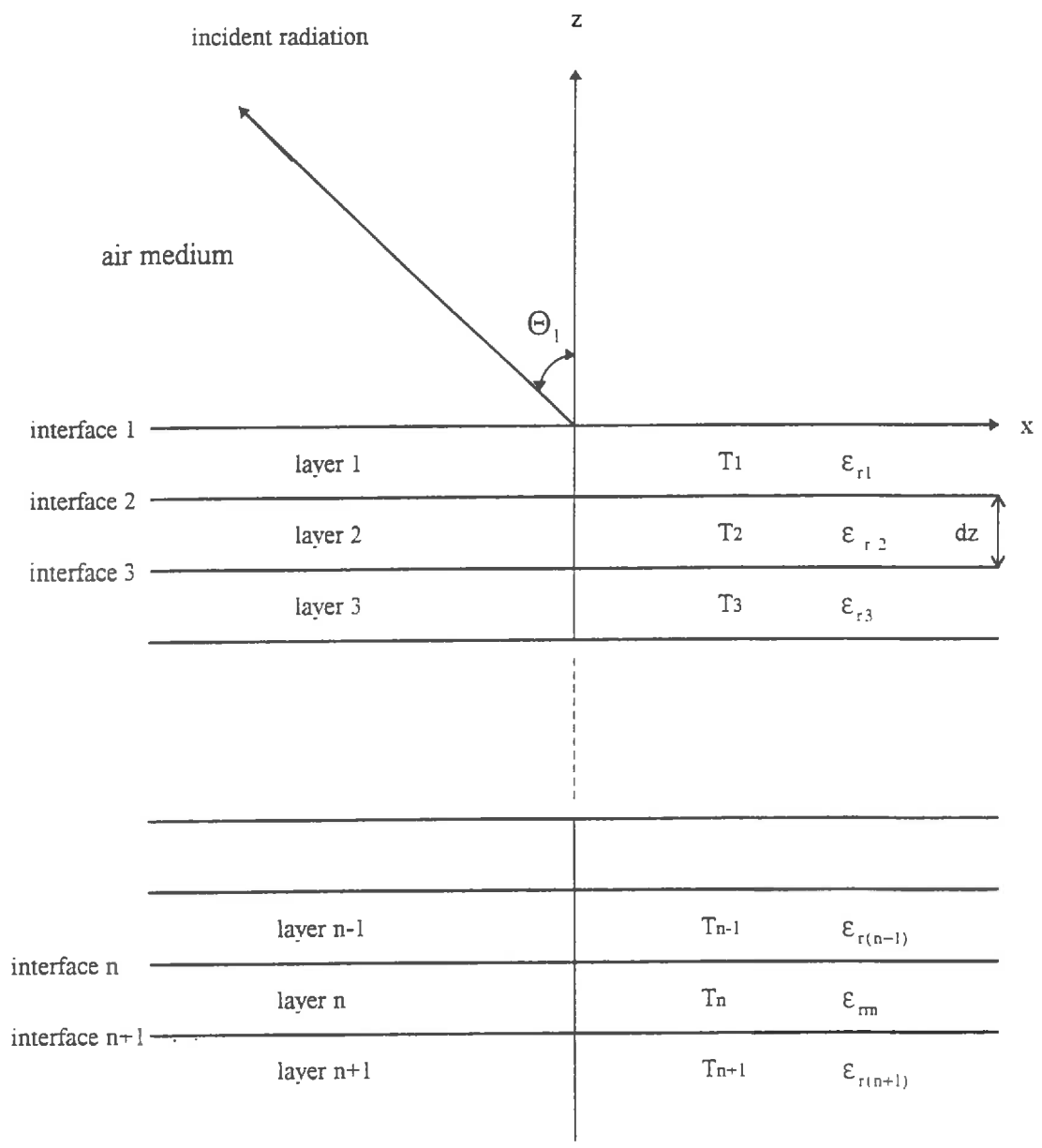
Figure 2.1: A cross section of stratified soil medium

2.0 Introduction

This chapter is devoted to the presentation of microwave emission models based on radiative transfer equation. To apply the radiative transfer equation more easily and preserve the moisture and temperature profiles, the stratification of the soil medium is considered. Then the energy contribution by each layer and their propagation towards the surface layer are calculated.

2.1 Microwave Emission Models from layered media

In the following parts, the soil is considered as a layered media as shown in figure 2.1. The following assumptions are considered in the development of radiative transfer models:
1) the soil medium is stratified into thin horizontal layers;
2) each layer has uniform dielectric and temperature;
3) moisture and temperature are function of depth;
4) the interface between layers are horizontal and plane;
5) there is no scattering in the layers;
6) except for Njoku and Kong model, the soil layers are considered as in thermal equilibrium state.

Basis of the radiative transfer formulation

When a radiation passes through a stratified soil medium, each layer absorbs a fraction of the incident radiation. If the layer is in thermal equilibrium state, it emits the same radiation as it absorbs. According to the Rayleigh Jeans approximation (Equation 1.32) the intensity of the radiation emitted by a layer is linearly related to its temperature. Since radiations intensity emitted by each layer is independent of the temperature of the other layers, the total emission can be obtained by adding the contribution of every layers.

Two alternative approaches are used in this study. The coherent approach (Njoku and Kong model and Wilheit model) and incoherent approach (Burke model) are considered to calculate propagation of these radiation towards the surface layer and the total emission from the soil medium

2.1.1 Incoherent approach : Burke model

The Burke model (Burke et. al 1979) is based on the radiative transfer equation formulated by Chandrasekhar (1960). The radiative transfer equation governs the variation in intensity of an incident radiation in a medium due to absorption, scattering and emission. As in every multilayer emission model, here also is assumed that long enough wavelength to consider the soil as a scatter free medium.

Let us consider the equation of the radiative transfer. We assume that the radiations have an intensity I. The change in intensity of the radiation dI while propagating through a medium is due to the absorption loss ($-\alpha . I . dz$) and the thermal emission ($\alpha . j_e . dz$) where

- j_e is the emission source function ($Wm^{-2}sr^{-1}Hz^{-1}$)

- α is the absorption coefficient (Npm^{-1}); here volume absorption coefficient, $N \langle \sigma_{av} \rangle$ is taken. and N is the number density of the absorbing particles and $\langle \sigma_{av} \rangle$ is the mean absorption coefficient of the absorbing particles

The equation of the radiative transfer for an absorbing medium is given by :

$$\frac{dI}{dz} = -\alpha . I + \alpha . J_e \qquad (2.1)$$

In equation (2.1), J_e is Plank' emission function which is proportional to the medium temperature T (Equation 1.32) . Adopting a similar scalar rule, the intensity (I) in the equation (2.1) can be replaced by T_B since the brightness temperature is directly related to the intensity of the radiations. The modified form of the equation (2.1) for j^{th} layer of the stratified soil medium:

$$\frac{dT_B}{d(\alpha_j z_j)} = -T_{Bj} + T_j \qquad (2.2)$$

The equation (2.2) can be integrated from a point just below the upper boundary of the jth layer to the bottom boundary of the jth layer. If the dielectric properties are constant across the layer we can easily demonstrate that

$$T_{Bj}^- = T_j[1 - exp(-\alpha_j . dz_j)] + T_{B(j+1)}^+ exp(-\alpha_j . dz_j) \qquad (2.3)$$

29

Air medium

$$T_B^{1+} = T_{Bp}^{1-}(1-\Gamma_1)$$

Air-soil interface ———————————————————— Γ_1

$$T_{Bp}^{1-} = T_1(1-e^{(-\alpha_1 dz_1)}) \quad + \quad T_1(1-e^{(-\alpha_1 dz_1)})\Gamma_2 e^{(-\alpha_1 dz_1)} \quad + \quad T_{Bp}^{2-}(1-\Gamma_2)e^{(-\alpha_1 dz_1)}$$

upward emission
by the layer

Layer 1   Reflected dz_1

down ward emission
by the layer

Interface 2 ———————————————————————— Γ_2

Emission from T_{Bp}^{2-}
second layer
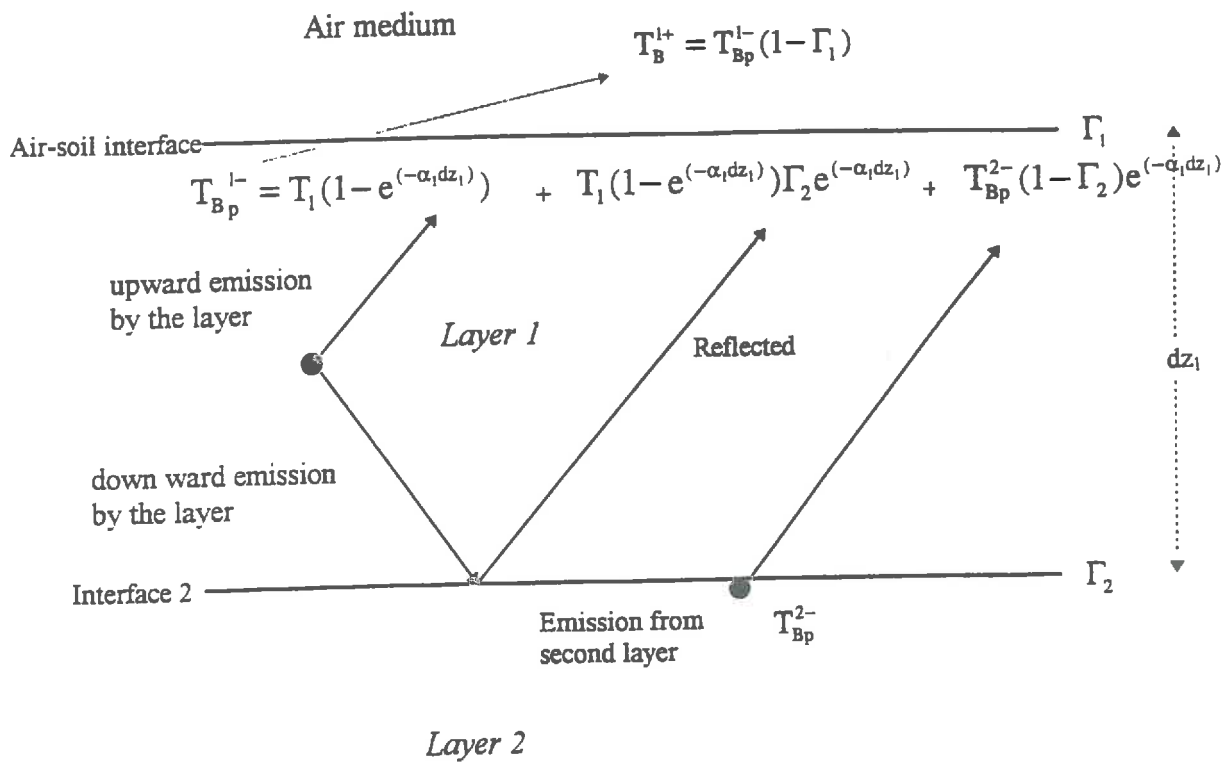
Layer 2

Figure 2.2: Schematic presentation of thermal microwave emission from the first layer of a stratified soil medium.

where the signs - and + represent the location just below or just above a boundary between two layers. In equation (2.3) the first term in the right hand side represents the emission by the jth layer and the second term represents the brightness from the $(j+1)^{th}$ layer. This equation is used to compute the brightness contribution by each layer. Now let consider the propagation of the radiation between the layers. The Burke model is a first order model which describes the radiations that come out of a considered layer by the sum of three components :

* the upward emission by the considered layer,

* the downward emission by the considered layer which is reflected at the bottom of the layer and then attenuated during the travel from the bottom to the top of the layer.

* the transmitted radiation coming from the layer just below the considered layer.

These three components are detailed in Figure (2.2) which represent the case of the first layer ($T_B{}^1$). More generally, we can write that the radiations which comes out of the jth ($T_B{}^{j-}$) is given by :

$$T_B^{j-} = T_j(1 - \exp(-\alpha_j.dz_j)).(1 + \Gamma_{j+1}.\exp(-\alpha_j.dz_j)) + T_B^{(j+1)-}(1 - \Gamma_{j+1}).\exp(-\alpha_j.dz_j) \quad (2.4)$$

Starting from the top we can notice from Figure (2.2) and Equation (2.4) that $T_B{}^{2-}$ is related to the third layer contribution T_B^{3-}, which is itself is related to T_B^{4-} and so on. We can then express $T_B{}^{1-}$ by a recurrent sum involving all the $T_B{}^j$ terms of every layers. The total radiation emitted from first layer into air depends on the reflectivity of the air soil-interface :

$$T_B = (1 - \Gamma_1).T_B^{1-} \quad (2.5)$$

The final expression of the Burke model applied to a media with n layers is :

$$T_{Bp}^{1+}(\Theta) = \sum_{j=1}^{n} T_j.\left(1 - \exp(-\alpha(\Theta)dz_j\right).(1 + \Gamma_{j+1}^{p}(\Theta).\exp(-\alpha(\Theta)_j dz_j)).$$

$$\prod_{i=1}^{j} \left[1 - \Gamma_i^{p}(\Theta)\right]e^{-\left(\sum_i \alpha_{i-1} dz_{i-1}\right)} \quad (2.6)$$

In the final stage, we have included the polarization and incidence angle in the equation (2.6). The two parameters (polarization and angle) are introduced in the equation through the reflectivity which is evaluated by Fresnel model. The attenuation coefficient α in the above equation is:

$$\alpha_j = \frac{\varepsilon_j''}{2\beta_j} \tag{2.7}$$

and

$$\beta_j = \left\{ \frac{1}{2} \cdot (\varepsilon_j' - \sin^2(\Theta)) \cdot \left[1 + \left(1 + \frac{\varepsilon_j''^2}{(\varepsilon_j' \sin^2(\Theta))} \right)^{1/2} \right]^{1/2} \right\} \tag{2.8}$$

The Burke model (Equation 2.6) is suitable for a deep soil medium with very large number of soil layer, where the contribution from the last layer is insignificant. If we want to apply this model in the experimental data which is collected within 0 - 10 cm soil layer, we have to assume that the soil moisture of the soil column below 10 cm has the same soil moisture as it for 10th cm soil layer. In order to do this theoretically in more efficient way, we made some modification to the final equation presented in (2.8).

$$T_n \cong T_n(1 - \exp(-\alpha_n dz_n)) \tag{2.9}$$

The modified form of the model is:

$$T_{Bp}^{1+}(\Theta) = \sum_{j=1}^{n} T_j \cdot \left(1 - \exp(-\alpha(\Theta)dz_j) \right) \cdot (1 + \Gamma_{j+1}^p(\Theta)\exp(-\alpha(\Theta)dz_j)).$$

$$\prod_{i=1}^{j} \left[1 - \Gamma_i^p(\Theta) \right] e^{-\left(\sum_{i=2}^{j} \alpha_{i-1} dz_{i-1} \right)} +$$

$$T_n \cdot \prod_{i=1}^{j} \left[1 - \Gamma_j^p(\Theta) \right] e^{-\left(\sum_{j=2}^{n} \alpha_{i-1} dz_{i-1} \right)} \tag{2.10}$$

This form of the equation is applicable to our experimental conditions. Indeed, the soil moisture was only sampled within the top 10 cm layer. Beyond this depth, the soil layer is considered as a single layer. We will see the justification of this statement in the chapter IV.

2.1.2 Coherent approach - Wilheit model

We recall that a layer in thermal equilibrium emits same energy as it absorbs. In the Wilheit model, (Wilheit (1978)) the electric and magnetic fields of a coherent wave propagating through a layer media is used to compute the attenuation by the layers. Indeed, the propagation of an electromagnetic wave through a layered media can be determined by well known electromagnetic theory. In the Wilheit model, each layer absorbs a fraction of the incident radiation (F_j). The brightness of each layer (T_{Bj}) is then the product of T_j and F_j. The total T_B^p of the soil medium is then obtained numerically by adding the brightness contribution by each layer ($\sum T_B^p = \sum T_j . F_j$).

Let consider an incident electromagnetic propagating through a layered media. The propagation of the electric field in the jth layer can be written by

$$\vec{E} = \vec{E}_{0j}.exp(i\vec{k}_j \vec{r}) \tag{2.11}$$

where $\vec{r}$ is the position vector. Assuming that the z direction is normal to the layer interfaces and that z=0 corresponds to the boundary between the first and the second layers (typically the air-soil boundary, we can write the propagator function of the electromagnetic wave in the layered media by :

$$P^{\pm}(z) = e^{\pm(2\pi i/\lambda)\int_0^z \eta(z')cos(\theta(z'))dz'} \tag{2.12}$$

The + and - sign represent the forward and the backward directions of propagation, respectively. The value of the angle between the direction and of propagation and the z direction is governed at each layer interface by the Snell's law :

$$\eta_1.sin(\Theta_j) = cons\tan t \tag{2.13}$$

The propagator function $P_j^{\pm}$ at the interface between the j and $j+1^{th}$ layers is given by the following equation:

$$P_j^{\pm} = exp(\pm(2\pi i/\lambda_0)\eta_j cos\Theta_j dz_j).P_{j-1}^{\pm}$$
$$P_1^{\pm} = 1 \tag{2.14}$$
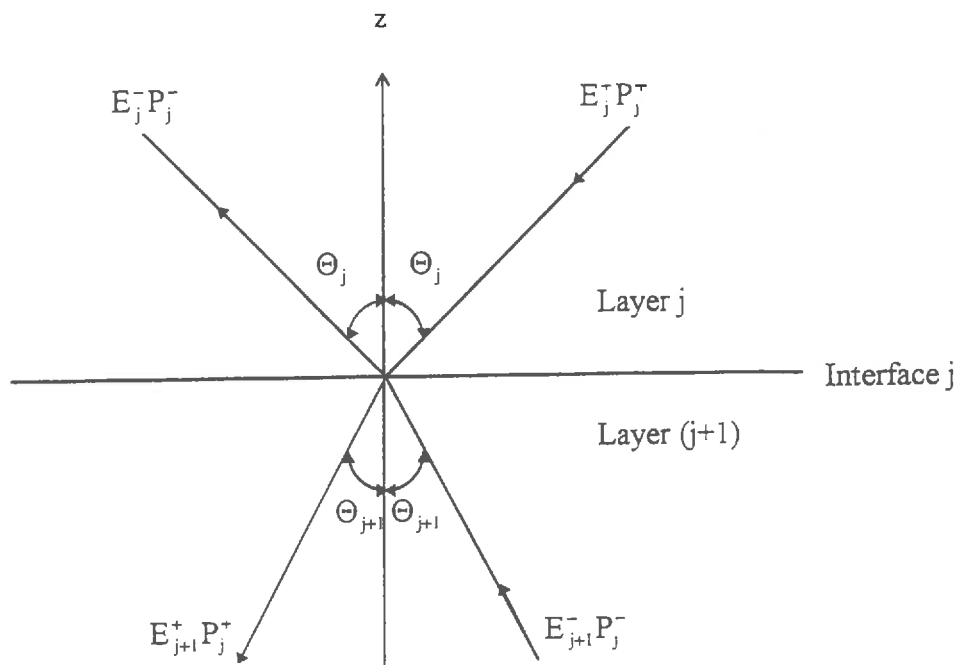
Figure 2.3:   Presentation of reflected and transmitted waves at the interface between the $j^{,th}$ layer and $(j+1)^{th}$ layer.

Estimation of electric field at every interface

The figure (2.3) presents the electric field at j^{th} interface. In each layer, there are two waves propagating in positive (E_j^+) and negative (E_j^-) direction according to the z-axis. To estimate the electric field at every interface, we apply the continuity of the tangential component of the electric and magnetic fields. Thus we will have a set of equations for $\vec{E}$ and $\vec{H}$ fields at the interface between the j and j+1th layers.

$$\vec{z} \times (P_j^+ \vec{E}_j^+ + P_j^- \vec{E}_j^-) = \vec{z} \times (P_j^+ \vec{E}_{j+1}^+ + P_j^- \vec{E}_{j+1}^-) \tag{2.15}$$

and

$$\vec{z} \times (P_j^+ \vec{k}_j^+ \times \vec{E}_j^+ + P_j^- \vec{k}_j^- \times \vec{E}_j^-) = \vec{z} \times (P_j^+ \vec{k}_{j+1}^+ \times \vec{E}_{j+1}^+ + P_j^- \vec{k}_{j+1}^- \times \vec{E}_{j+1}^-) \tag{2.16}$$

Using the Snell's law, we can demonstrate that :

1) for horizontal polarization

$$(P_j^+ E_j^+ + P_j^- E_j^-) = (P_j^+ E_{j+1}^+ + P_j^- E_{j+1}^-) \tag{2.17}$$

and

$$\eta_j \cos(\Theta_j)(P_j^+ E_j^+ - P_j^- E_j^-) = \eta_{j+1} \cos(\Theta_{j+1})(P_j^+ E_{j+1}^+ - P_j^- E_{j+1}^-) \tag{2.18}$$

2) for vertical polarization

$$\cos(\Theta_j)(P_j^+ E_j^+ + P_j^- E_j^-) = \cos(\Theta_{j+1})(P_j^+ E_{j+1}^+ + P_j^- E_{j+1}^-) \tag{2.19}$$

$$\eta_j (P_j^+ E_j^+ - P_j^- E_j^-) = \eta_{j+1}(P_j^+ E_{j+1}^+ - P_j^- E_{j+1}^-) \tag{2.20}$$

where E^- or E^- represent the electric field vector norm. By using the property of the propagator function $P_j^+ = \dfrac{1}{P_j^-}$ the above four equations can be further simplified into:

$$((P_j^+)^2 E_j^+ + E_j^-) = ((P_j^-)^2 E_{j+1}^+ + E_{j+1}^-) \tag{2.21}$$

33

$$\eta_j \cos(\Theta_j)\left((P^+_j)^2 E^+_j - E^-_j\right) = \eta_{j+1} \cos(\Theta_{j+1})\left((P^+_j)^2 E^+_{j+1} - E^-_{j+1}\right) \qquad (2.22)$$

2) for vertical polarization

$$\cos(\Theta_j)\left((P^+_j)^2 E^+_j + E^-_j\right) = \cos(\Theta_{j+1})\left((P^+_j)^2 E^+_{j+1} + E^-_{j+1}\right) \qquad (2.23)$$

$$\eta_j\left((P^+_j)^2 E^+_j - E^-_j\right) = \eta_{j+1}\left((P^+_j)^2 E^+_{j+1} - E^-_{j+1}\right) \qquad (2.24)$$

For n layers, we have (2n - 2) equations to compute 2n unknowns which are the electric fields. The resolution of these system of equations is possible by adding the limit conditions that are : $E_1^+ = 1$, and $E_n^+ = 0$ and $E_n^- = 0$. We are then able to calculate E^+_{n-1} and E^-_{n-1} using the boundary conditions for the last interface and continuing for each of the interface in turn.

Estimation of the Fj coefficients:

The poynting vector of the electromagnetic radiation provides the energy of the wave at any point in the medium. This enables us to estimate the energy of the incident wave before entering and after passing through each layer and hence the energy absorbed by the layer. The poynting vector P_j for j^{th} layer:

$$\vec{P}_j = Re(\vec{E}_j \times \vec{H}_j^*) \qquad (2.25)$$

Using this relationship we can show that:

$$P_j = \frac{2\pi}{\lambda_0 \mu \omega}\left(Re(\eta_j \cos(\Theta_j)).\left|E^+_j P_j\right|^2 + Re(\eta_j \cos(\Theta_j))\left|\frac{E^-_j}{P_j}\right|^2 + \right.$$

$$\left. 2 Im(\eta_i \cos(\Theta_j)) Im(E^+_j (E^-_j)^* \frac{P_j}{P_j^*})\right) \qquad (2.26)$$

and

$$P_{j-1} = \frac{2\pi}{\lambda_0 \mu \omega} \left(Re(\eta_j \cos(\Theta_j)) . \left| E_j^+ P_{j-1} \right|^2 + Re(\eta_j \cos(\Theta_j)) \left| \frac{E_j^-}{P_{j-1}} \right|^2 + \right.$$

$$\left. 2 Im(\eta_j \cos(\Theta_j)) Im(E_j^+ (E_j^-)^* \frac{P_{j-1}}{P_{j-1}^*}) \right) \quad (2.27)$$

$$P_1 = \frac{2\pi \cos(\Theta_1)}{\lambda_1 \mu \omega} \quad (2.28)$$

If the first layer is the air $\lambda_1 = \lambda_0$. P_1 is the initial energy of the radiation incident at the first surface whereas P_{j-1} and P_j are the energy of the incident wave at the upper $((j-1)^{th})$ and lower (j^{th}) interface of the jth layer. F_j is defined by :

$$F_j = \frac{P_{j-1} - P_j}{P_1} \quad (2.29)$$

The fraction of energy absorbed by the jth layer (F_j) is obtained by substituting the equations (2.26), (2.27) and (2.28) in (2.29) :

$$F_j = \frac{1}{\cos(\Theta_1)} \left\{ Re(\eta_j \cos(\Theta_j)) . \left| E_j^+ \right|^2 \left(\left| P_{j-1} \right|^2 - \left| P_j \right|^2 \right) + \right.$$

$$Re(\eta_j \cos(\Theta_j)) \left| E_j^- \right|^2 \left(\left| \frac{1}{P_j} \right|^2 - \left| \frac{1}{P_{j-1}} \right|^2 \right) +$$

$$\left. 2 Im(\eta_j \cos(\Theta_j)) Im(E_j^+ (E_j^-)^* \left(\frac{P_{j-1}}{P_{j-1}^*} - \frac{P_j}{P_j^*} \right)) \right\} \quad (2.30)$$

Now, we have the information on the fraction of energy (F_j) absorbed by j^{th} layer. According to Rayleigh Jeans approximation to Plank's law (equation 1.29), the brightness

Figure 2.4: Presentation of Mechanistic model of heat and mass flow in unsaturated soil medium (Chanzy and Bruckler, 1993).

of the jth layer in thermal equilibrium state at a temperature T_j is $F_j.T_j$. Because of the emission by each layer is independent of the temperature of the other layers, the brightness observed by a radiometer in the first medium (air) can be written as:

$$T_{B(\Theta)}^p = \sum_{j=2}^{n} F_i^p . T_j + \Gamma_{(\Theta)}^p T_{Binc}^p \qquad (2.31)$$

where T_{Binc} is the incident radiation with polarization H or V and $\Gamma_{(\Theta)}$ is the Fresnel reflectivity of the first interface (air - soil interface)

The second term in (2.31) represents for the radiation incident radiation reflected by the air soil interface. At the lower frequencies $\Gamma_{(\Theta)}^p T_{Binc}^p$ is very small compared to soil emission and can be neglected.

By conservation of energy :

$$\sum_{j=1}^{n} F_j^p + \Gamma_{(\Theta)}^p \equiv 1 \qquad (2.32)$$

In case of microwave radiometry, the radiometer receives the microwave emission given in the equation (2.31).

2.1.3 Coherent approach - Njoku and Kong Model

Njoku and Kong model (Njoku and Kong (1977)) is the adaptation of the formula developed by Stogryn (1970) for the determination of the intensity of thermal radiation from a medium. In this model, every soil layer is assumed to radiate the electromagnetic radiation due to thermal agitation. The flow of electromagnetic radiation produces a source current $J(r,\omega)$ in the medium. The fluctuation and dissipation theorem and solutions of Maxwell's equations are used to calculate the source current and the electric field ($E(r,\omega)$) at every layer. The intensity (I_p) of the thermal radiation is then estimated using $E(r,\omega)$ values. The brightness contribution by each layer is thus calculated and added to obtain the total emission by the soil medium. A brief presentation of this model is given in Appendix B.

Inputs to

Mechanistic model ; shown in figure(2.3)

Emission model:
System parameter:
Frequency, polarization, incidence angle
Medium property: Total depth, layer thickness, dielectric constant, Soil temperature

Dielectric model.
θ (z), T(z) : output of mechanistic model
Soil property: sand, clay, bulk density, sp. density, salinity, Frequency

Mechanistic model

θ z(t), Tz(t)

Dielectric model
(Wang model, Dobson model)

ε z(t), Tz(t)

Emission model
(Wilheit model, Burke model)

Brightness temperature and emissivity

Figure(2.5): The scheme of the coupling of mechanistic model and emission model.

2.2 Mechanistic model for heat and mass flow in unsaturated soils

The Mechanistic model is derived from the theory of heat and water flow in the unsaturated non - isothermal soils. The flowchart of the mechanistic model is presented in figure (2.4). The model is based on the Philip and De Vries (1975) partial differential equations reduced to the case of vertical flow. The nonlinear partial differential equations of the soil model are solved by Galerkin finite element method. At the soil - atmosphere interface, the boundary conditions are obtained by solving the energy balance with an iterative procedure.

The Mechanistic model requires, as input, the knowledge of the surface properties : the albedo, the emissivity and the surface roughness. For the soil description, the model need the dry bulk density, the "water potential-water content" relationship, the hydraulic conductivity, the gazeous diffusivity, the thermal conductivity and the heat capacity. Initial water potential and temperature profiles are necessary to start the simulations. The model is then driven by the climatic conditions characterized by the global radiation, wind velocity, air temperature and the air vapor pressure. The outputs of the model are the evolution of water potential and temperature profiles, the energy fluxes at the soil surface and the potential evaporation. More details about this model are presented by Witono and Bruckler, (1989) and Chanzy and Bruckler, (1993).

The microwave emission models in layered media require the stratification of soil medium into very thin horizontal layer to preserve the continuity of the soil moisture and temperature profile gradients. The mechanistic model of heat and mass flows is also based on a stratification of soil medium. According to the requirement of the emission model soil moisture and temperature values for very thin soil layer of thickness less than 0.1cm could be simulated by the mechanistic model. The figure (2.5) shows the presentation of the coupling of the two models. Since details of the mechanistic model are given in Figure (2.4), the inputs of the mechanistic model are not detailed in the figure (2.5).

To summarize the coupling procedure, the soil moisture and temperature profiles simulated by mechanistic model are used to compute the soil dielectric constant vertical profile with a dielectric model. The brightness temperature and emissivity for a given frequency and polarization is then computed by the microwave emission model. Since the mechanistic model is a dynamic model, we obtain the evolution of the brightness temperature across the diurnal and/or climatic cycles as presented in Chapter 4.

CHAPTER 3

EXPERIMENTAL DATA COLLECTION

E

N

←······ 20 m ·····→

↕ 40 m

Calibration plot

rough field

smooth field

sorghum - field

sorghum - field

pool

Orthogonal observation

RAIL

Crane

Parallel observation

PORTOS

↕ 40 m

Wheat field

←························ 60 m ························→
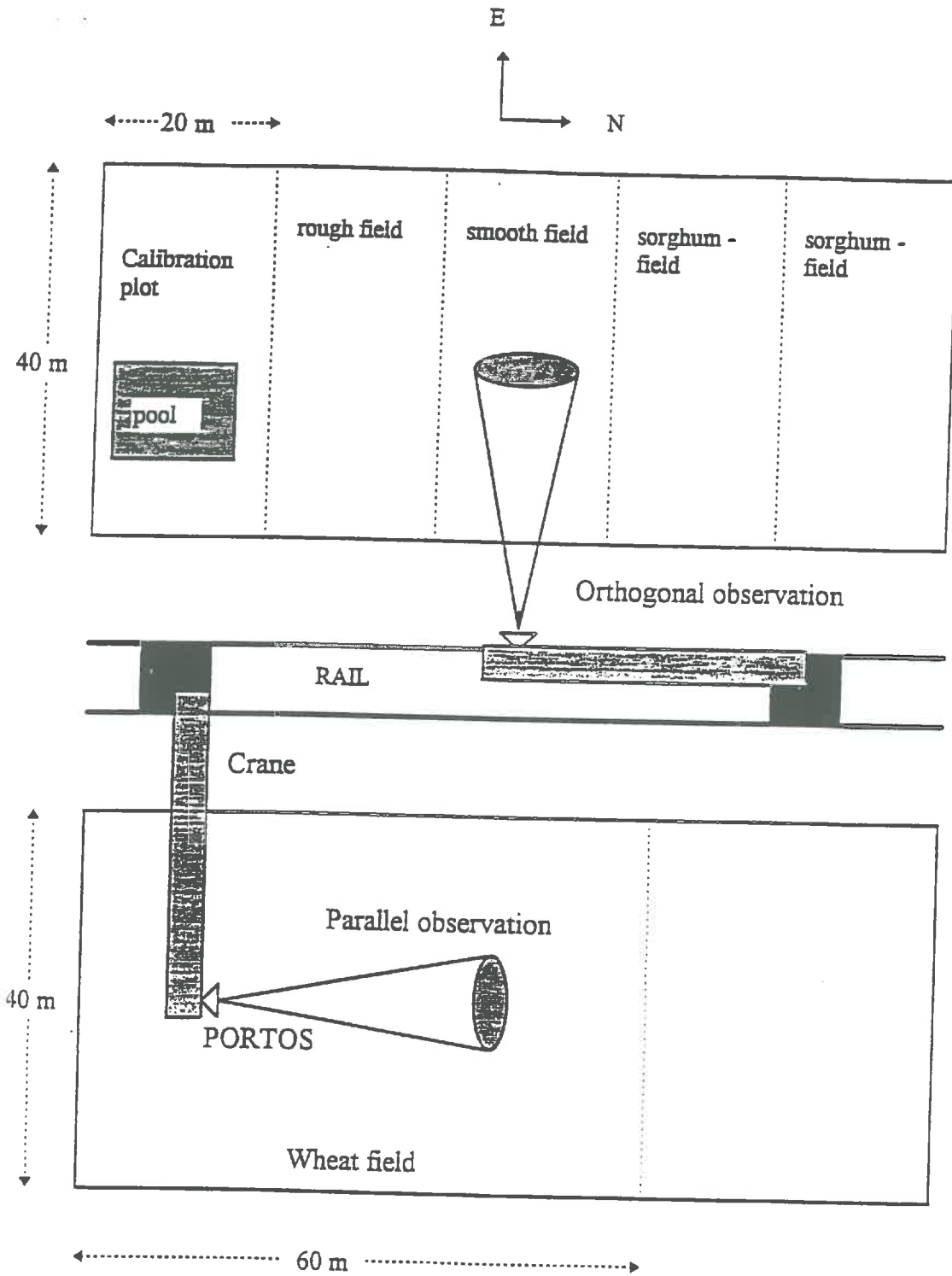
Figure 3.1:   Field description of Avignon test site.

3.1 PORTOS 93 experimentation

The experimental data were collected during two field campaigns which held in 1991 and 1993. Both experiments were carried out at the test site of INRA, AVIGNON, France. The 1991 experiment covered a period of two month in August and September. The 1993 experiment started the 15th April and covered a period of three months till the 10th of July. The experimental set up was designed to study the influence of the ground parameters (vegetation, surface roughness and soil moisture and temperature profiles) on the microwave emission. Therefore, in this campaign, the radiometric data were collected from

- bare fields with different roughness conditions to study the roughness effect on microwave emission
- bare fields with very smooth surface condition to study the influence of soil moisture and temperature profiles on microwave emission.
- vegetated field (Wheat and Sorghum in homogeneous and heterogeneous nature in cultivation) to study the influence of the vegetation.

However, our study is limited to the bare soil condition and to the smoother roughness conditions. Most of the data used in this study were collected during the 1993 experiment since it covers a wider range of ground conditions and the quality of the radiometric data was better.

3.1.1 Field description

The AVIGNON test site is described in figure (3.1). The test site consisted of 7 plots located on the two sides of a rail of 100 m long. The site was equipped with a crane which can move along the rail. Remote sensing sensors were attached under the crane boom at a height of 20 m. Bare fields were located on the eastern side of the rail which was divided into five plots having the area of 40×20 m^2 for each plot.

The data used in this study were collected under five surface conditions. All the fields were prepared by one pass with a rotary harrow tiller followed by a pass with a rotary digging machine. The cloud size distribution was made different according to the speed of the rotator digging machine. Two surface conditions (SR and SRb) presented a roughness which corresponded to a seed bed. The surface conditions SMb was smoother. The soil presented a very fine structure and the surface was covered by slaking crusts. To obtain the smoothest surface condition in the field named (SM), we used a small roller (road roller) to
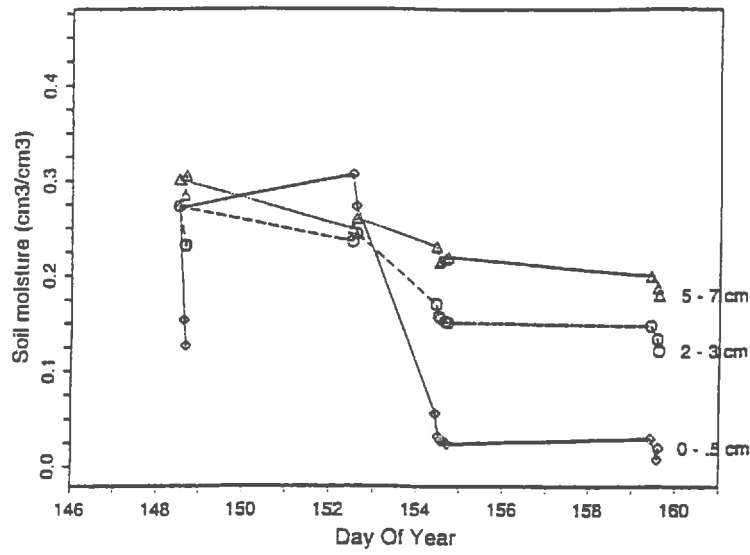
Figure 3.2 : The soil moisture variations observed with the SR surface condition.
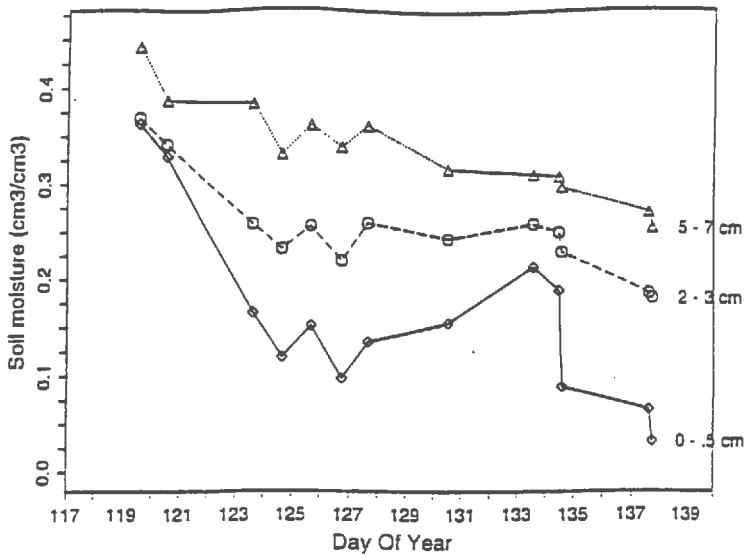
Figure 3.3 : The soil moisture variations observed with the SRb surface condition.
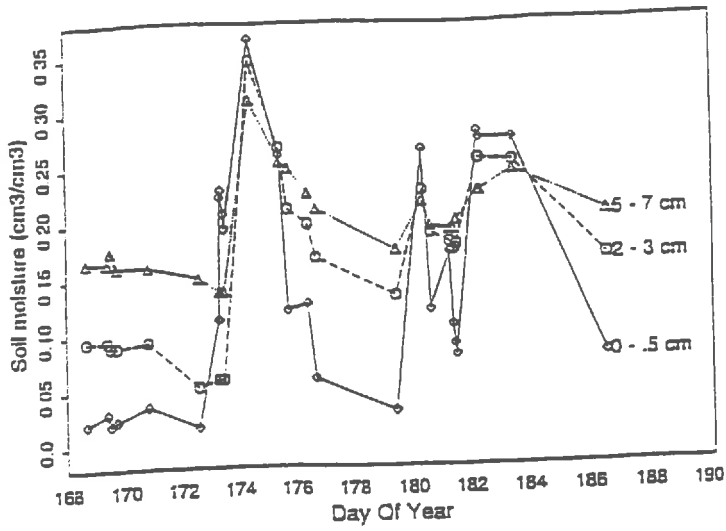
Figure 3.4 : The soil moisture variations observed with the SM surface condition,
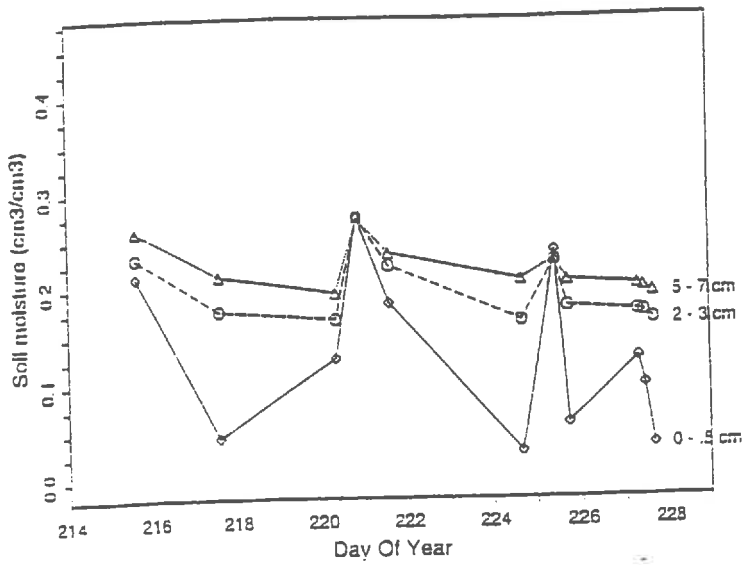
Figure 3.5 : The soil moisture variations observed with the SMb surface condition.

make the surface more compact, smooth and plane. In addition to above bare fields, we prepared three bare fields that are characterized with rough surface condition.

3.1.2   Ground data collection

3.1.2.1   Soil moisture measurements

The soil of the experimental site is a silty clay loam soil with 11% sand, 61.7% silt and 27.2% clay. Concurrent to every radiometric data measurement, soil moisture profiles were sampled by measuring the gravimetric soil moisture in the layers 0 -0.5, 0 - 1, 1 - 2, 2 - 3, 3 - 4, 4 - 5, 5 - 7 and 7 - 10 cm with five replications. The profiles were then averaged to account for the spatial variation of soil moisture. The soil dry bulk density in the soil layer of 0 - 3, 3 - 5, 5 - 7, and 7 - 10 cm were measured by a transmission gamma ray probe (Bertuzzi et al. 1987). Then the bulk density values were combined to gravimetric soil moisture to derive the volumetric soil moisture profiles. The table 3.1 presents bulk density of the all experimental fields.

Table 3.1   Dry bulk density profile of the fields

Field	Dry bulk density (g/cm^3) in the soil layer			
	0 - 3 cm	3 - 5 cm	5 - 7 cm	7 - 10 cm
SM	1.437	1.376	1.36	1.347
SMb	1.37	1.37	1.37	1.37
SR	1.293	1.331	1.339	1.334
SRb	1.438	1.511	1.541	1.523

The figures (3.2, 3.3, 3.4 and 3.5) show the soil moisture variation in the surface layers of 0 - 0.5 cm, 2 - 3 cm and 5 - 7 cm, in the in the SR, SRb, SM and SMb fields respectively. From the above figures, we can notice that:

• For all surface condition, a wide range of moisture condition was covered

• for all surface condition, significant moisture gradients were established especially during the soil drying period (the gradients can be evaluated in the figures (3.2 - 3.5) by the magnitude of the difference in the soil moisture between the two adjacent layers)
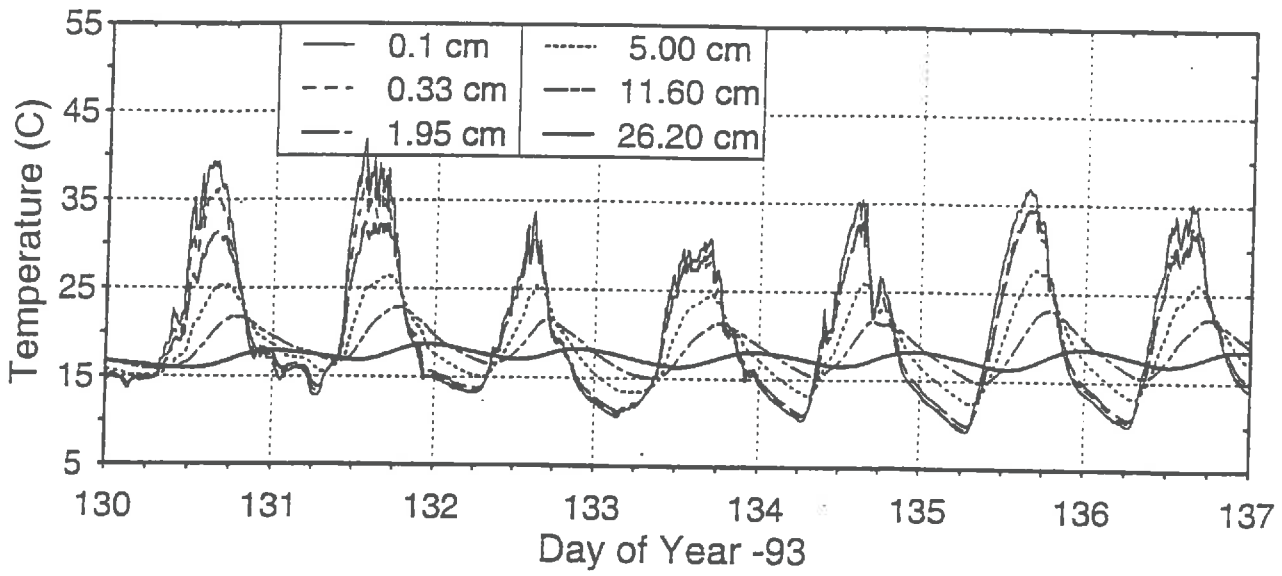
Figure 3.6 : The soil temperature measured (SRb surface condition).
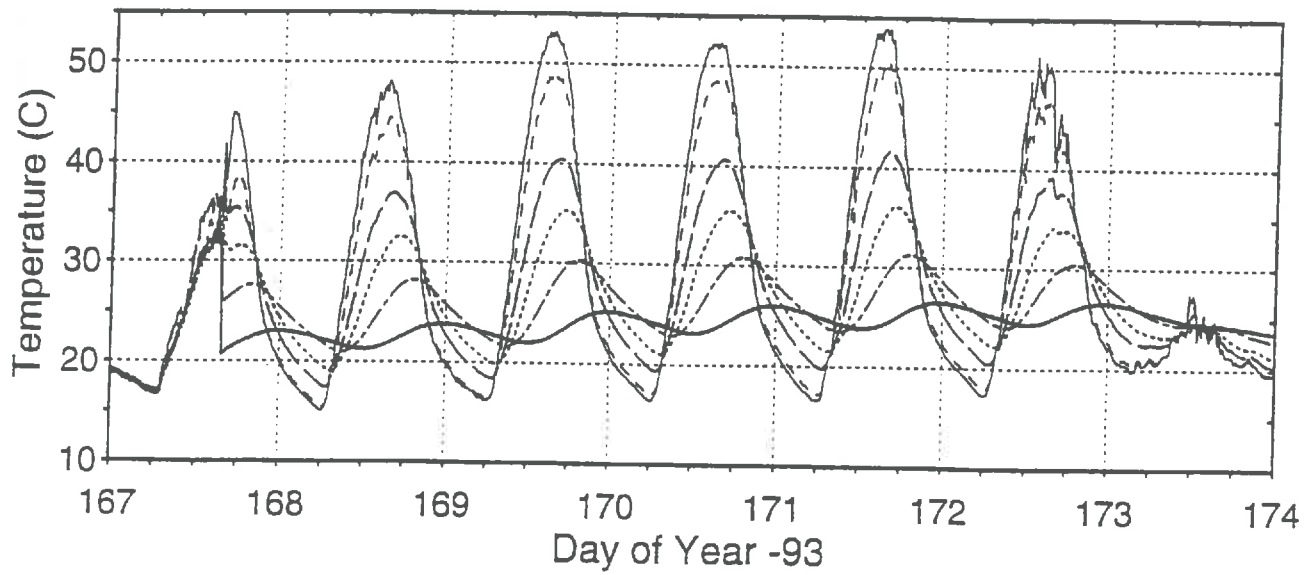
Figure 3.7 : The soil temperature measured (SM surface condition).

- the soil moisture gradients are affected by the soil structure. The SM field presents a higher hydraulic conductivity, thanks to the better contact between the clods resulting from the field compact by the roller. As a consequence, the soil moisture gradients are smaller with the SM field.

The experimental analysis of the soil moisture data confirms the variability in the soil moisture profiles. This variability seems to be driven by different factors as the climatic demand, the time of the day and/or the soil structure.

3.1.2.2 Soil temperature measurements

Platinum resistance temperature probes were used to measure the soil temperature profiles. Ten probes were installed in the soil at different depths from very near surface to a depth of 25 cm. All the probes were connected to a data logger. The probes measured the temperature every 10 seconds. The data acquisition system recorded the average temperature for every 10 minute interval. This automatic data collection enabled us to measure the soil temperature profile continuously throughout the experimental period. The soil temperature measured at different depths in SRb and SM fields are shown in the figures (3.6) and (3.7). The soil temperature in SM field shows the large variations (about 35 C) of the diurnal cycle. In dry soil condition, the surface soil temperature increases beyond 50 C in the afternoon. The figure (3.8) shows the examples of the reconstruction of the continuous soil temperature profiles from the probe data measured at different depths. We used an exponential fitting

$$T(z) = T_d + (T_s - T_d) \cdot \exp(C.z) \tag{3.1}$$

where
- T_s is the surface temperature
- $T(z)$ is the temperature at the depth z
- T_d is the temperature measured at the deepest depth (25 cm)
- C is a fitted parameter.

This model is not adapted to the case where an extreme of temperature is found between the surface and the deepest considered depth (see Figure 3.8). Such temperature profiles are obtained for instance in the evening when the soil cools more quickly at the surface than at a depth of several cm. The temperature profile thus present both positive and negative
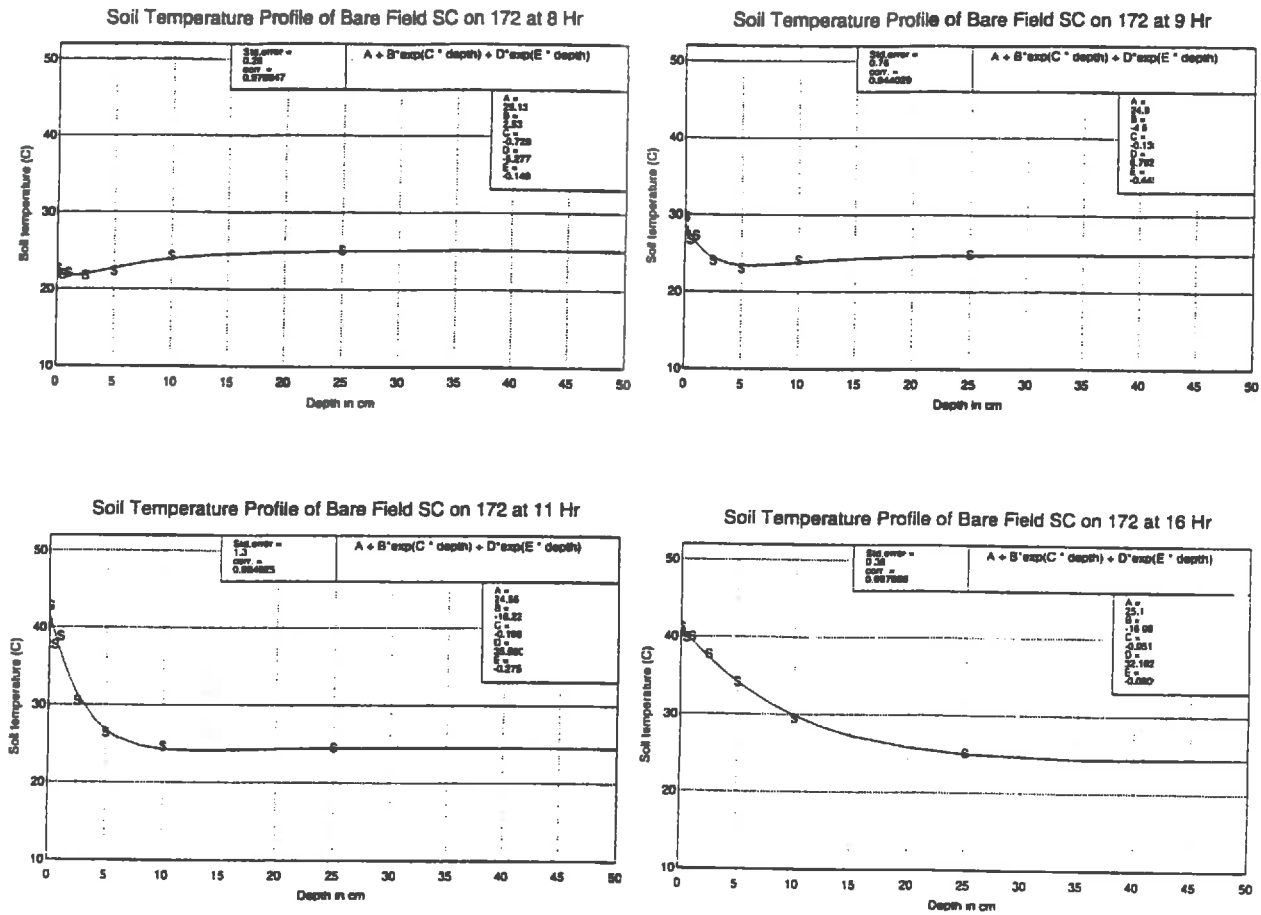
Figure 3.8 : The soil temperature profile reconstruction from the temperature probe data.
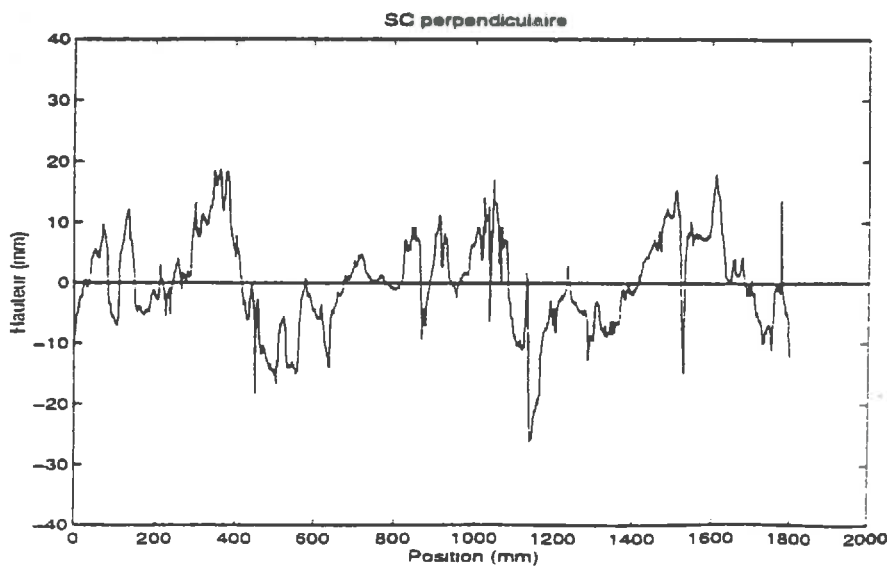
Figure 3.9: Examples of the surface roughness profiles measured from the bare fields in the PORTOS 93 campaign.

gradients which cannot be accounted for by Equation (3.1). To represent such a case, we used an exponential relationship with more parameters:

$$T(z) = T_d + (T_s - T_d) \cdot \exp(C.z) + D \cdot \exp(E.z) \tag{3.2}$$

Where D and E are fitted parameters.

3.1.2.3 Surface roughness measurements

Surface roughness profiles were measured using a noncontact laser profilometer (Bertuzzi et al. 1990). The roughness measurements were made along a transect of 2 m in the direction perpendicular and parallel to the tillage direction. An example of a measured

Table 3.2 Surface roughness characteristics

Field iden-tification	R.M.S Height ρ(cm)	Correlation lengthl l(cm)
SM	0.237	16.021
SMb	0.30	10.9
SR	0.769	2.347
SRb	0.84	3.15

roughness profile is given in Figure (3.9). The roughness parameters ρ and l for each profiles were calculated. The mean values of ρ and l obtained after taking the mean of all profile values. Average values of ρ and l measured for the different surface conditions are presented in Table 3.2. The SM, and SMb surface conditions satisfied the Rayleigh criterion for the lower frequencies (L and C bands) and can therefore be considered as smooth surfaces

3.2 Radiometric measurements

3.2.1 The PORTOS radiometer

Microwave radiometric measurements were performed by the PORTOS radiometer. It is a six frequency microwave radiometer which has been used in many ground and air borne field campaign (Grosjean and Sand, 1994). The system was built by Matra-Marconi Espace

for CNES (Centre National d'Etudes Spatiales). This radiometer is based on the principle of Dicke. PORTOS measures the microwave radiation in nine channels at 1.4 H or V, 5.05 H and V, 10.65 H and V, 23.8 H or V, 36.5 H or V and 90 GHz H and V. The Table 3.3 presents the PORTOS characteristics.

TABLE 3.3 PORTOS characteristics

Frequency GHz	channel 1 1.4135	channel 2, 3 5.05	channel 4, 5(1) 10.65	channel 6 23.8	channel 7 36.5	channel 8, 9 90.0
Band width (MHz)	+/-13.5	+/-50	+/-50	+/- 200	+/- 200	+/-200
Polarization	H or V	H and V	H and V	H or V	H or V	H and V
-3dB beamwidth	12.5°(1)	12.3°(1)	13.0°	10.3°	9.6°	11.3°
-20 dB beamwidth	30.0°(1)	30.1(1)	39.2°	31.8°	31.5°	32.8°
Beam efficiency %	84.0 (1)	81.0(1) 79.4	96.0	97.0	97.0	98.0
XPO maximum %	2.0	5.0	4.0	1.6	0.7	0.3

(1)　＊ the characteristics are given for the 1993 experiment. During the 1991 experiment horn antenna were used at 1.4 and 5.05 GHz.

　　＊ H polarization was not available in 1991

PORTOS can receive the radiation in both horizontal and vertical polarization simultaneously at the frequencies of 5.05, 10.65 and 90.0 GHz. At 23.8 and 36.5 GHz the polarization was switched by a remote commutation. At 1.4 GHz, a manual rotation of the antenna was necessary. This induced a time delay of 10' to two hours between H and V polarization measurements. The PORTOS radiometer has several antennas for the different frequencies. The Table 3.3 presents the characteristics of these antennas. The 1.4 GHz antenna was mounted outside of the radiometer system without any temperature regulation, whereas the other antennas were thermally controlled. As a result, the temperature of the antenna and transmission line of 1.4 GHz channel had a fluctuating temperature which induced an additional error to the measurement at this frequency.

The radiometer was coupled to a mechanical system for varying the angle of incidence from 0 to 60 degree. By moving the crane along the rail, the T_B measurements were centered on
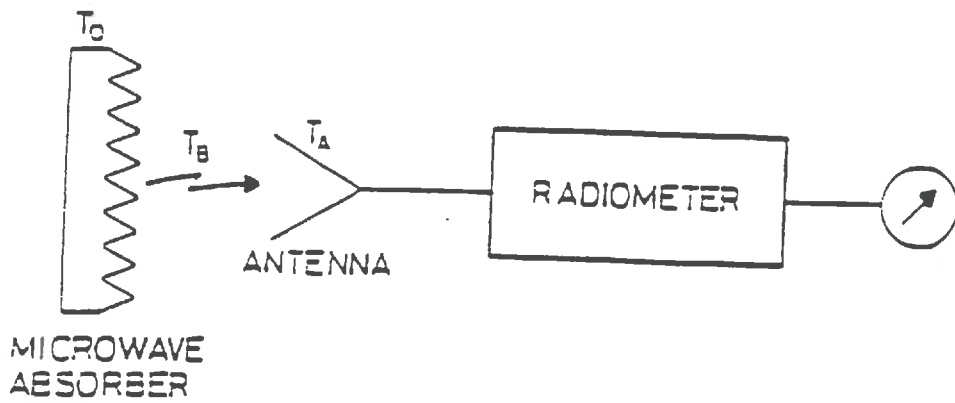
Figure 3.10: Schematic presentation of high temperature point calibration.

5.05 GHz

H pol
O = 1.115 , S= 11.11
r2 = 0.999

V pol

O = 1.761 , S= -156.9
r2 = 0.997
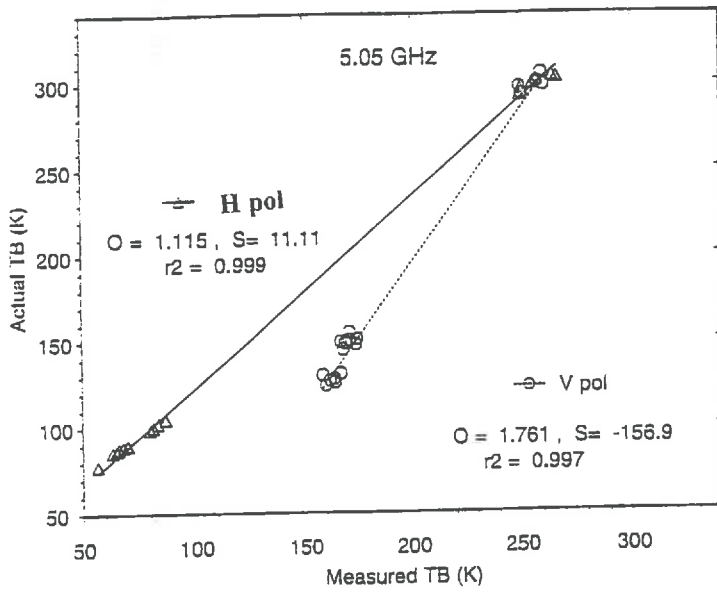
Figure 3.11:

General calibration of 5.05 GHz channels.

10.65 GHz

H pol
O = 1.106 , S= -22.62
r2 = 0.999

V pol

O = 2.071 , S= -323.4
r2 = 0.998
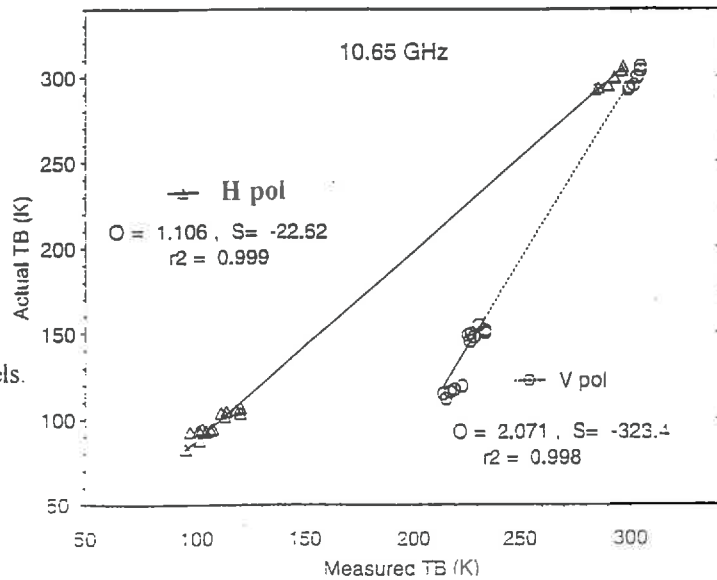
Figure 3.12:
General calibration of 10.65 GHz channels.

the same target for all incidence angle. Unfortunately, the size of the fields was too small to make measurements at angles of incidence higher than 40°.

3.2.2 External calibration of Radiometer

The radiometer calibration consisted in establishing the relationship between the output of the system and the T_B of an object whose T_B is known. The targets used for the calibration were an ecosorb plate, whose emissivity is close to one, a pool of water and an end termination placed on the coaxial cable, between the receiver and the antenna.

The calibration with ecosorb at the ambient temperature : Hot point
Since the ecosorb emissivity is close to one, its T_B is equal to its thermodynamic temperature. In the hot point calibration, the ecosorb was left in thermal equilibrium with the air and its brightness was measured by the antenna which was placed in front of the ecosorb plate as shown in the figure (3.10). The temperature of the ecosorb was measured by platinum temperature probe inserting in the ecosorb plate near its surface.

However, this method has some limitations as:
- the size of the 1.4 GHz antenna was too large in comparison to the ecosorb plate dimension, which made the hot point acquisition at this frequency impossible.
- under windy conditions, we met problems to stabilize the ecosorb temperature.

The calibration with ecosorb - cold point:
The ecosorb plate was dipped in liquid nitrogen which temperature is +77 K. However, the obtained results were not satisfactory. Several explanations can be advanced :
- a reflection occurred at the air-liquid nitrogen interface which induced a coupling with the antennas,
- vapor condensation appeared at the antenna surface
- the Nitrogen container was too small for the 5.05 GHz antenna and therefore, the container contributes to the energy received by the radiometer.

Calibration over calm water:
The calibration over water provided the points between the hot and cold points observations.

In our study, we measured the T_B at 35 and 45° incidence angle to minimize the reception of the reflected radiation emitted by the antenna. The temperature of the water surface was measured by the IR thermal radiometer which was kept along with the PORTOS radiometer. The T_B of the water was then calculated as:

$$T_{BP} = (1 - \Gamma_{P(\Theta)})T_s + \Gamma_{P(\Theta)} \cdot T_{atm(\Theta)}) \tag{3.3}$$

where T_{atm} is the descending atmospheric microwave brightness temperature (K). It was estimated using the radiative transfer equation of Chandrashekar (1960) which used the air temperature profile, atmospheric water content and atmospheric pressure simulated by the meteorological model PERIDOT of Meteo-France. The method is more detailed in Calvet et al. (1995). The dielectric constant of the water for the calculation of $\Gamma_{P(\Theta)}$ was obtained using the Debye's equation (Ulaby et al. (1986)).

Calibration with an end terminator: L band channel
At 1.4 GHz, the antenna was replaced by an end terminator. The end terminator produces a thermal noise equivalent to its thermodynamic temperature. The end terminator was either kept at the air temperature or dipped in liquid nitrogen.

Since the water point were easy to collect, they were made daily, at least before and after the radiometric measurements and sometimes in between the measurements. The high temperature calibration points were also taken often during the experiment. On the contrary, there were only a few measurements over the ecosorb placed in liquid nitrogen.

Since the antenna were involved in the calibration of 5.05 and 10.65 GHz channels and the radiometers were thermally regulated, we could directly relate the scene T_B ($T_{B\ actual}$) and the measured T_B (T_{rec}) through a linear relationship:

$$T_{Bactual} = 1.115 * T_{Brec} + 11.11 \quad \text{(5.05 GHz H)}$$
$$T_{Bactual} = 1.761 * T_{Brec} - 156.9 \quad \text{(5.05 GHz V)}$$
$$T_{Bactual} = 1.106 * T_{Brec} - 22.62 \quad \text{(10.65 GHz H)}$$
$$T_{Bactual} = 2.071 * T_{Brec} - 323.4 \quad \text{(10.65 GHz V)} \tag{3.4}$$

The calibration lines drawn for 5.05 and 10.65 GHz frequencies are shown in the figure (3.11) and figure (3.12) respectively. These relationships were established by gathering all the calibration data collected with a given channel.
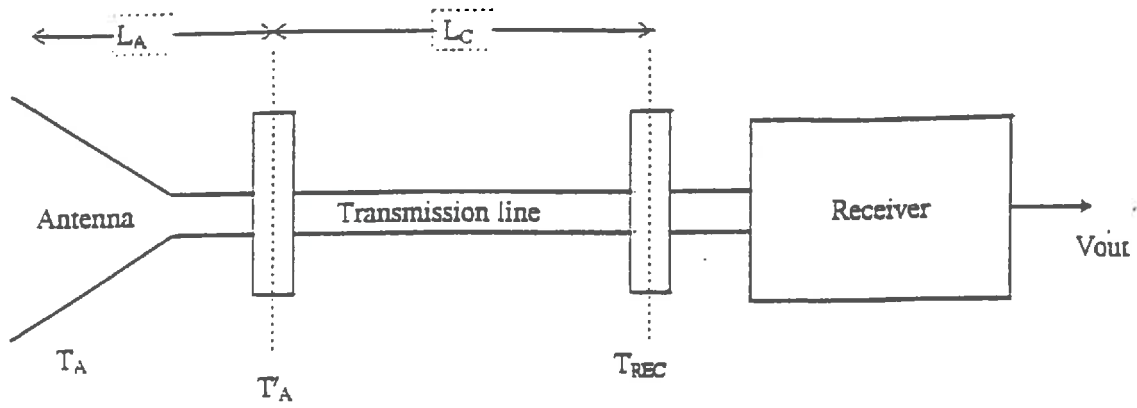
Figure 3.13: Schematic presentation of antenna and constituent elements of the L band radiometer.
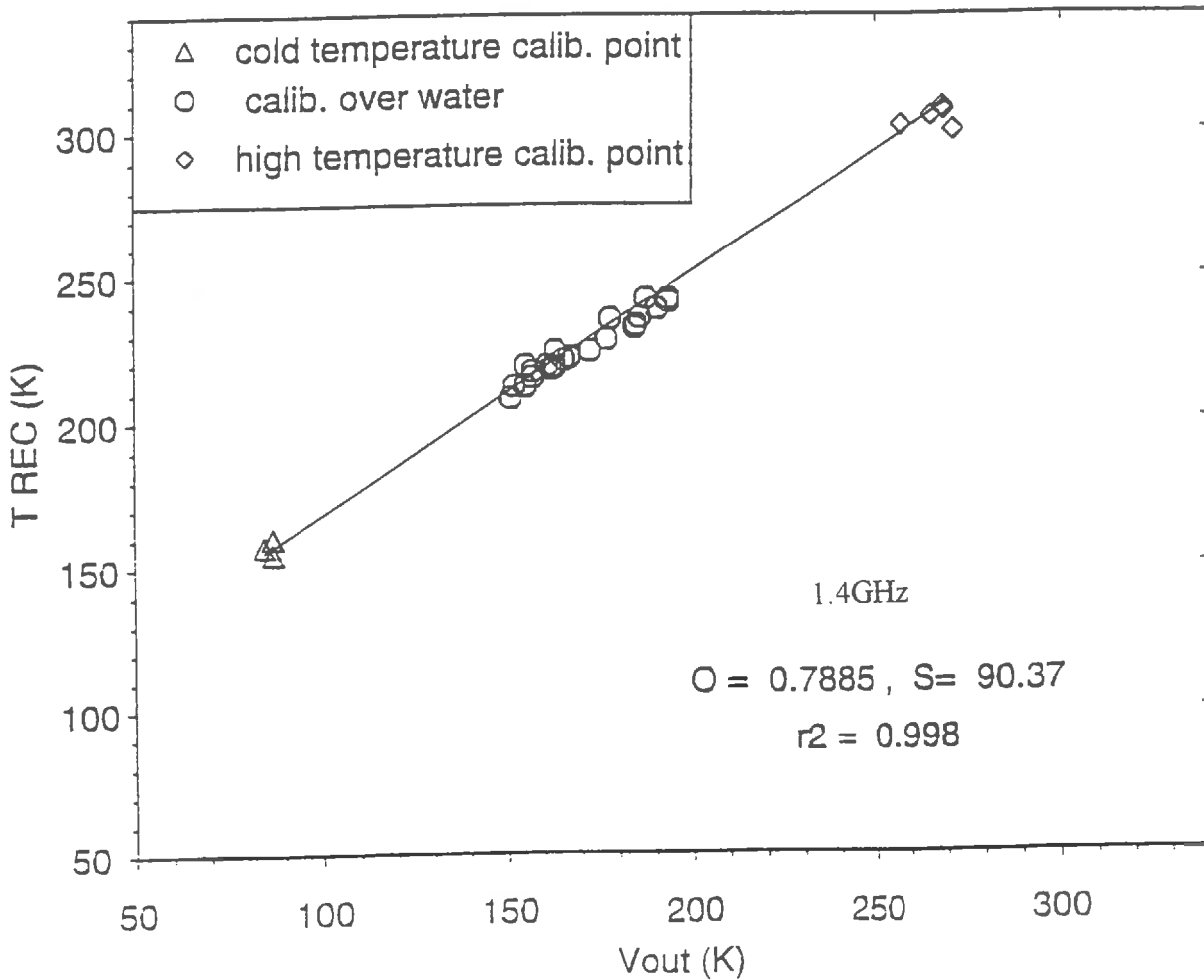
Figure 3.14: The relationship between T_{REC} and V_{out}

At 1.4 GHz, the calibration was complicated, since the antenna and transmission lines were kept in the air and not thermally regulated. The schematic presentation of the 1.4 radiometer is shown in the figure (3.13). The antenna is connected to the radiometer through a transmission cable. In the calibration process, we have to account for the antenna loss factor L_A and the cable loss factor L_C.

The term T'_A in the figure(3.13) represents the energy delivered by the antenna. It is equal to the antenna temperature T_A attenuated by the antenna loss factor L_A and the thermal contribution by the antenna itself. Thus, T'_A is given by :

$$T'_A = \frac{T_A}{L_A} + \left(1 - \frac{1}{L_A}\right).T_{PA} \qquad (3.5)$$

where T_{PA} is the thermodynamic temperature of the antenna. The temperature at the receiver (T_{REC}) is the sum the temperature T'_A attenuated by the loss factor of the cable L_C and the self contribution by the cable at the thermodynamic temperature T_{PC} :

$$T_{REC} = \frac{T'_A}{L_C} + \left(1 - \frac{1}{L_C}\right).T_{PC} \qquad (3.6)$$

By combining the above two equations (3.5 and 3.6), we can relate T_A to T_{REC} by:

$$T_A = L_A L_C T_{REC} + (1 - L_C)L_A T_{PC} + (1 - L_A)T_{PA} \qquad (3.7)$$

In the above equation the physical temperature of the antenna; T_{PA} and T_{PC} were measured by platinum resistance thermometer during the data acquisition. L_C was measured in laboratory, while L_A is fitted to the calibration results. It was the value of L_A which allows to obtain a single relationship between T_{REC} and the output of the receiver (V_{out})(Figure 3.14) for all the calibration points. The loss factors were equal to :
$L_A = 1.9118$ dB $= 1.5530$
$L_C = 2.0$ dB $= 1.5849$ $\qquad (3.8)$

The output of the receiver (V_{out}) and the radiometric temperature at the receiver were related to a simple linear equation as shown in the figure (3.14):
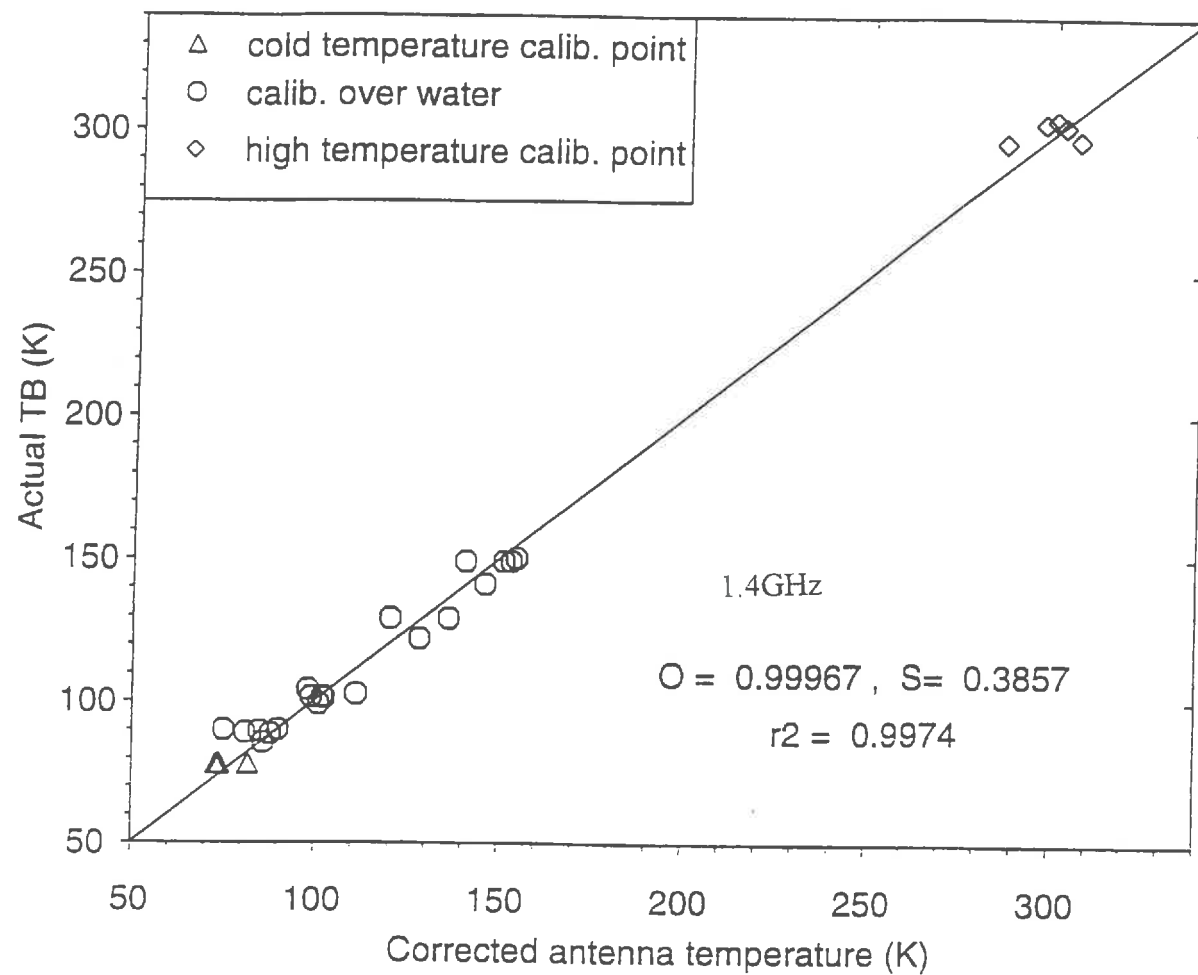
Figure 3.15: The relation between the corrected antenna temperature T_A and the T_B of the calibration targets.

$$T_{REC} = a.V_{out} + b \qquad (3.9)$$

where a and b are fitted parameter (a= 0.788, b=90.370). Thus final expression for T_A is:

$$T_A = a.V_{out.}L_A L_C + b.L_A L_C + (1-L_C)L_A T_{PC} + (1-L_A)T_{PA} \qquad (3.10)$$

The relationship between the actual T_B and the corrected T_B (T_A) is presented in the figure (3.15)

3.2.3 Study on the stability of PORTOS.

An analysis on the PORTOS stability was done in order to examine the behavior of the radiometer at different time scale (the whole experiment, the day or within the day). One question behind this analysis was the choice of the calibration relationship which can be either the average relationship given in Equations 3.6 to 3.10 or the individual calibration lines. The latter were established every day and for some days, several times per day. This analysis is limited to the C and X bands. At 1.4 GHz, the calibration involved too many sources of errors, and therefore it was difficult to perform a stability analysis that accounts for the whole radiometric chain.

As a first step, we plotted the calibration data collected at different times during the radiometric data collection.   The figure (3.16) presents the calibration data drawn for a selected day. The figure (3.16) shows the variations of the radiometric calibration within the day and also by comparing the plot of different days, we have the idea about the stability of the system between the days also. At 5.05 and 10.65 GHz, the calibrations lines were less variable for the H polarization than for the V polarization. To evaluate the importance of such variations we quantify their impact as follow. For each calibration relationship, the T_B was computed by increasing V_{out} across the range of measured values with a step which corresponds roughly to 10°K. Then differences between the T_B obtained from two calibration lines were computed for every V_{out}. In Table 3.4, every individual calibration line were compared to the average calibration line. The standard deviation of the difference between the T_B was computed and the minimum, maximum and mean standard deviation are reported in the Table.
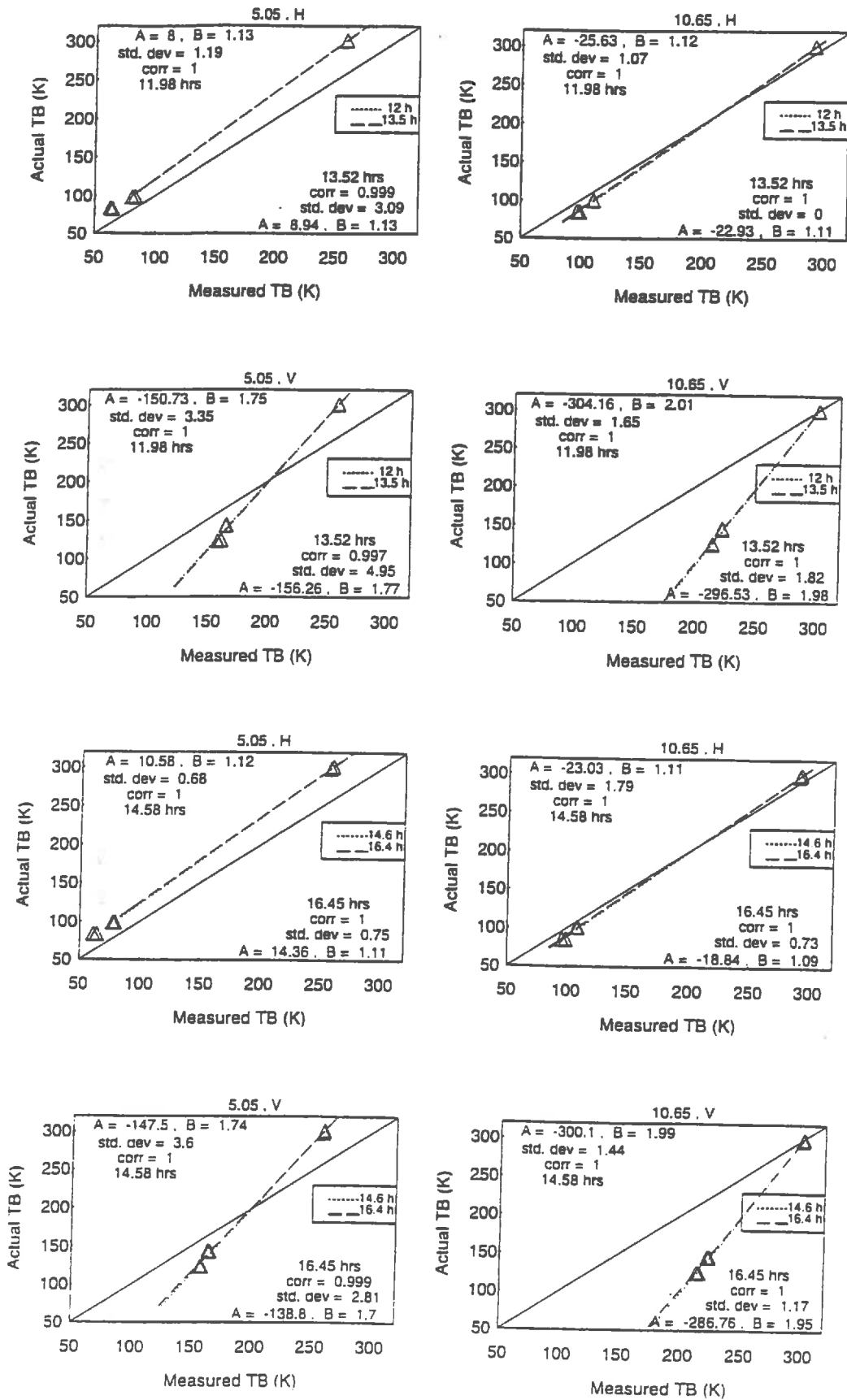
Figure 3.16: Comparison of the radiometric calibration lines of the DOY 153 for 5.05 and 10.65 GHz channels.

The maximum error associated with the calibration of the H polarization of 5.05 and 10.65 GHz channels was lower than 1.5 K. This indicates that these channels remained stable throughout the measurement campaign. In case of vertical polarization, the error reached 5 K. However, the extreme values were obtained in the early morning, when the thermal regulation of the radiometer was not optimal. The mean value of the standard deviation was 1.5 K which is more representative of the radiometer stability during the measurements. From the results displayed in Table 3.4, we considered that the radiometer remains stable through the 1993 experiment, and therefore we retained the average calibration line.

Table 3.4   Statistical results on the PORTOS stability during the 1993 campaign

Channel	Standard deviation max/min (K)	Mean standard deviation (K)
5.05 - h	0.99 / 0.00	0.356
5.05 - v	5.04 / 0.13	1.04
10.65 - h	1.49 /0.03	0.47
10.65 - v	4.54/0.10	1.48

3.2.4.   Radiometric data collection

The field description and mode of radiometric measurements are presented in the figure (3.1). PORTOS system was mounted on crane at a height of 20 m. By rotating the boom of the crane, the look direction (axis of the beam) can be directed either parallel to the rail (parallel observation) or orthogonal to rail (orthogonal observation) as indicated in figure (3.1). In case of parallel observation the incidence angle was varying from 0 to 40 with 10 degree increment and for perpendicular observation the incidence one can have the incidence angle between 20 to 50 degree. In the parallel observation, the same area of the soil surface could be observed by moving the crane along the rail for different incident angles.

The radiometric data were collected in two modes :

Instantaneous data collection: Here we measured the microwave emission for a short period of time (few seconds) in different incidence angles and dual polarization. This mode

of data collection was aimed to track drying property of soil. We collected the soil moisture in this case with in two hour of the radiometric data collection.

Continuous data collection: The brightness temperature was collected continuously for long period of time (3 - 4 hours). The duration of the observation was based on the computer storage capacity. In this case, the incidence angle and polarization of L band were kept fixed. This data collection was aimed to study the continuous evolution of surface soil moisture and temperature profiles effect the on microwave emission. The soil moisture profile was measured every two hours during the radiometric data collection.

CHAPTER 4

RESULTS
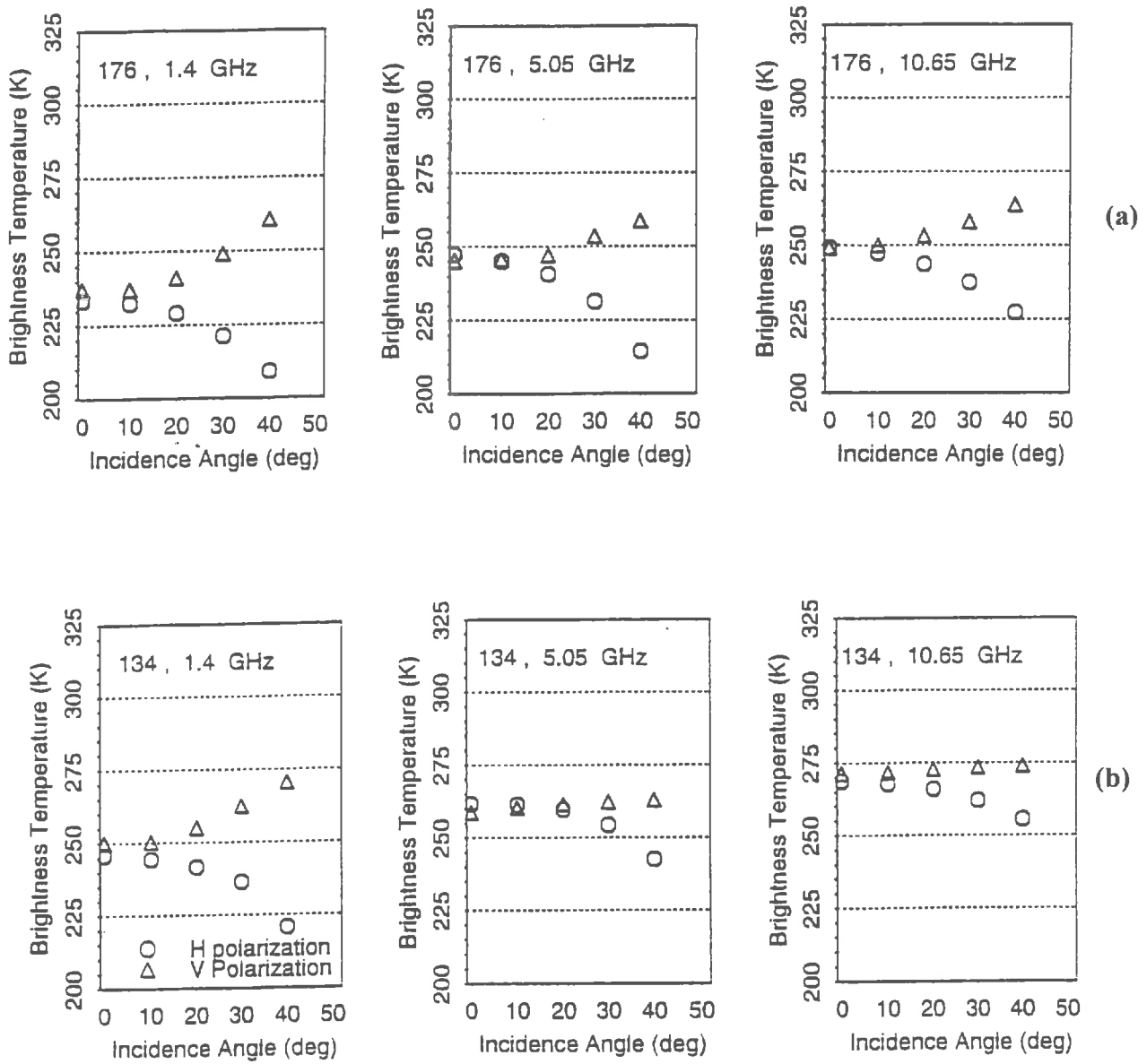
Figure 4.1: Radiometric data measured from (a) SM and (b) SRb fields.

4.0   Introduction

In this chapter we present the results of the study. Most of them are presented in two papers, which are given at the end of the chapter. However, to propose a coherent presentation of the whole study, we chose to present the results in a frame, which include the both published and unpublished results. As far as the published data are concerned, a brief summary of the prominent conclusions is given and a reference is proposed to get more details. In the following sections, the papers are referred to as Paper I and II for "Soil moisture and temperature profile effects on microwave emission at low frequency" and "Estimation of soil microwave temperature at L and C bands", respectively.

The goals of this chapter are :
- to study the quality of the radiometric data;
-   to optimize the emission model parameters and evaluate the error expected in the comparison between theoretical and experimental results;
- to evaluate the microwave emission models against the experimental data;
- to analyze the effect of soil moisture and temperature profiles on microwave emission and their implications in the soil moisture retrieval form radiometric data
- to estimate the microwave effective temperature, which appeared as an important factor in the inversion procedure to retrieve the soil moisture.

4.1   PORTOS data analysis

The microwave data collected from SM and SRb surface conditions are shown in the figure (4.1 (a) and (b)), respectively. We recall that SRb corresponded to a medium rough surface condition, whereas SM was the smoothest surface. In these Figures, the angular variations of the T_B are very similar between the two fields at L band, whereas the angular variations are significantly lower at C and X bands in the case of SRb Field. It is a consequence of the surface roughness, which influences the soil microwave emission at C and X band. Therefore, results from the SRb surface conditions can not be used for the validation of microwave emission model by layered media. The analysis of the other fields have shown that SM and SMb are the only surface conditions suitable for the validation of the emission models used in the study.

The figures (4.2) and (4.3) show the relationship between the soil moisture and the T_B obtained with the SM and SMb surface conditions, respectively. In spite of the use of two
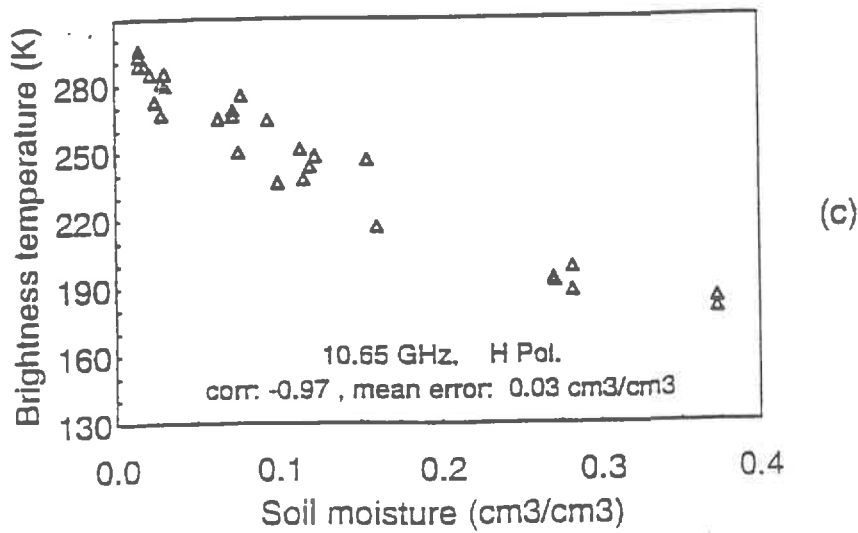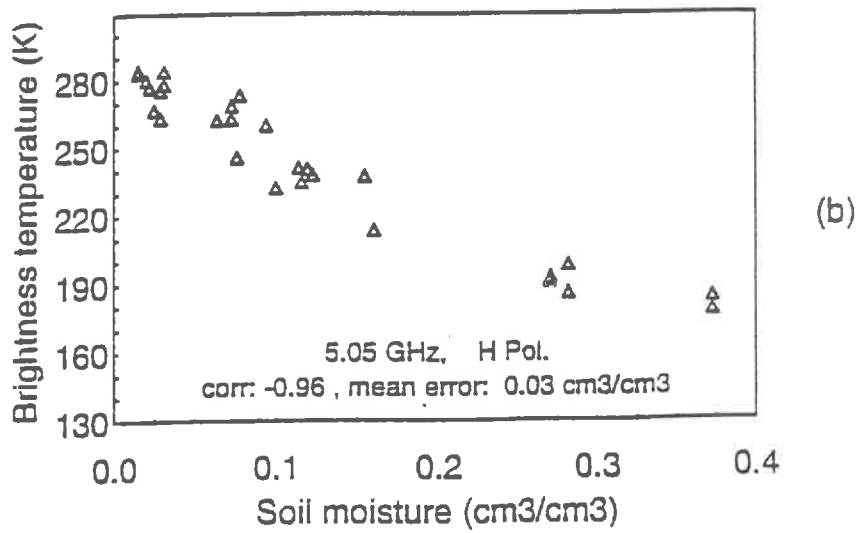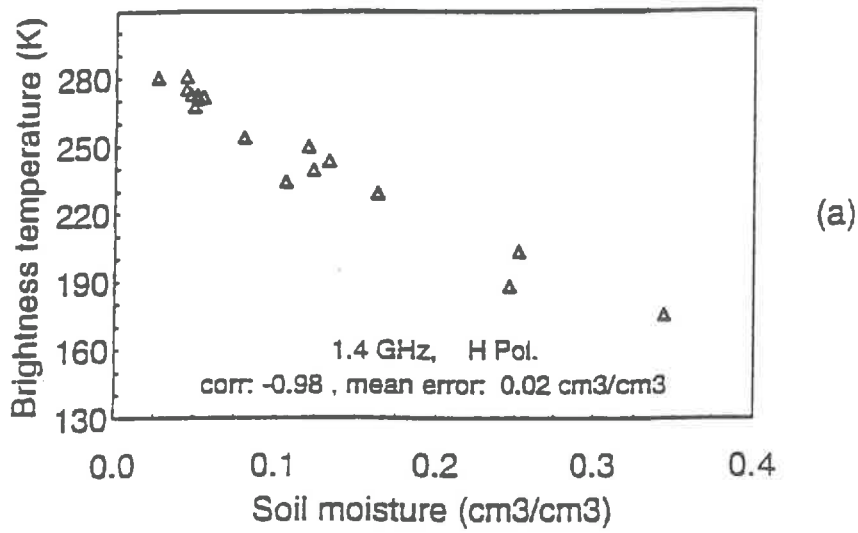
Figure 4.2: Soil moisture - T_B relationship observed in the SM field. The soil moisture in the layer of 2.5, 0.5 and 0.5 cm are considered for (a) 1.4, (b) 5.05 and (c) 10.65 GHz respectively.
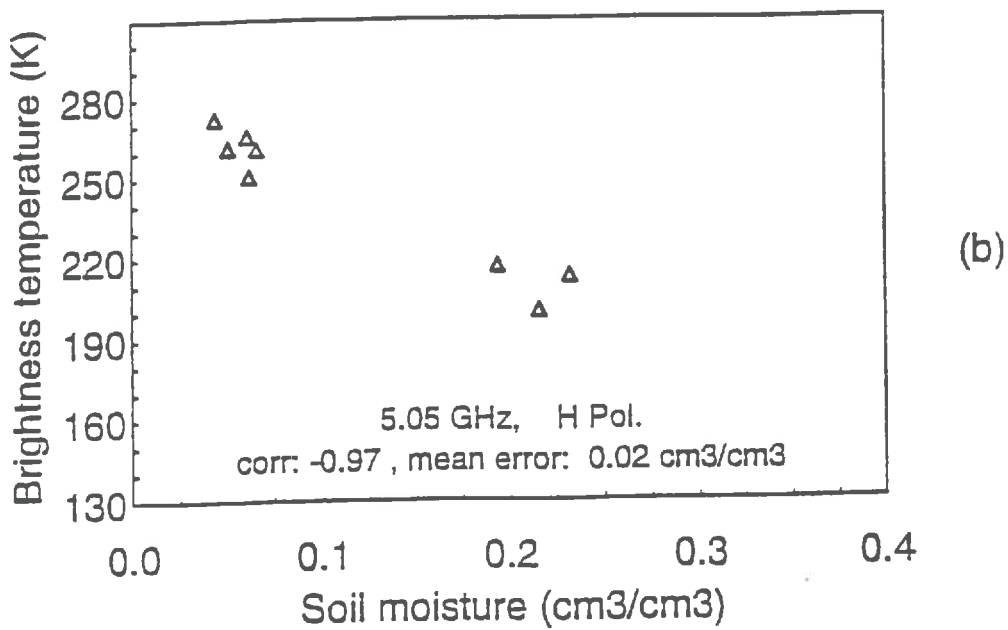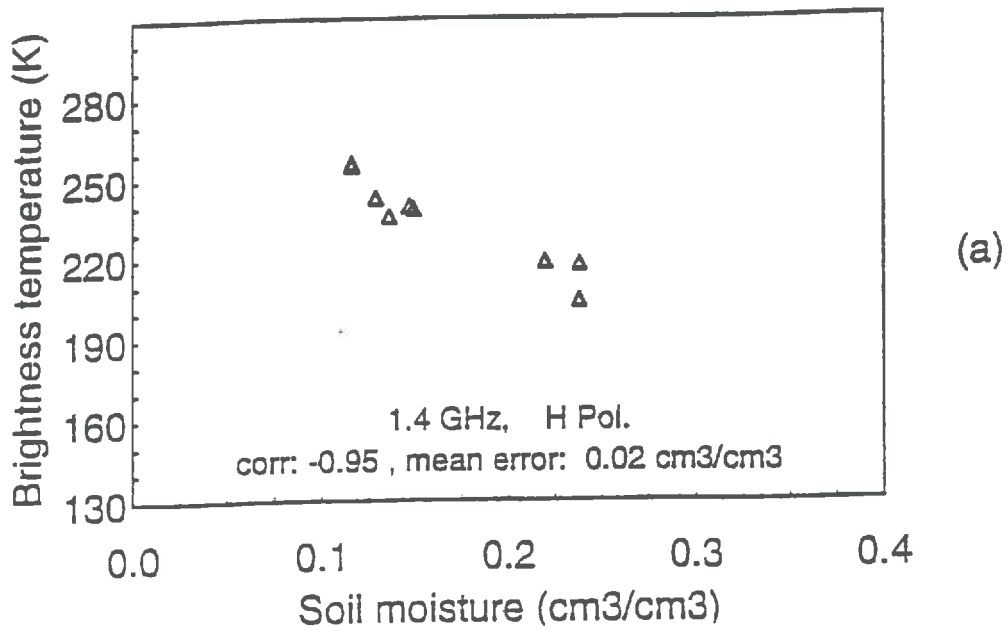
Figure 4.3: Soil moisture - T$_B$ relationship observed in the SMb field. The soil moisture in the layer of 2.5, and 0.5 cm are considered for (a) 1.4, and (b) 5.05 GHz respectively.
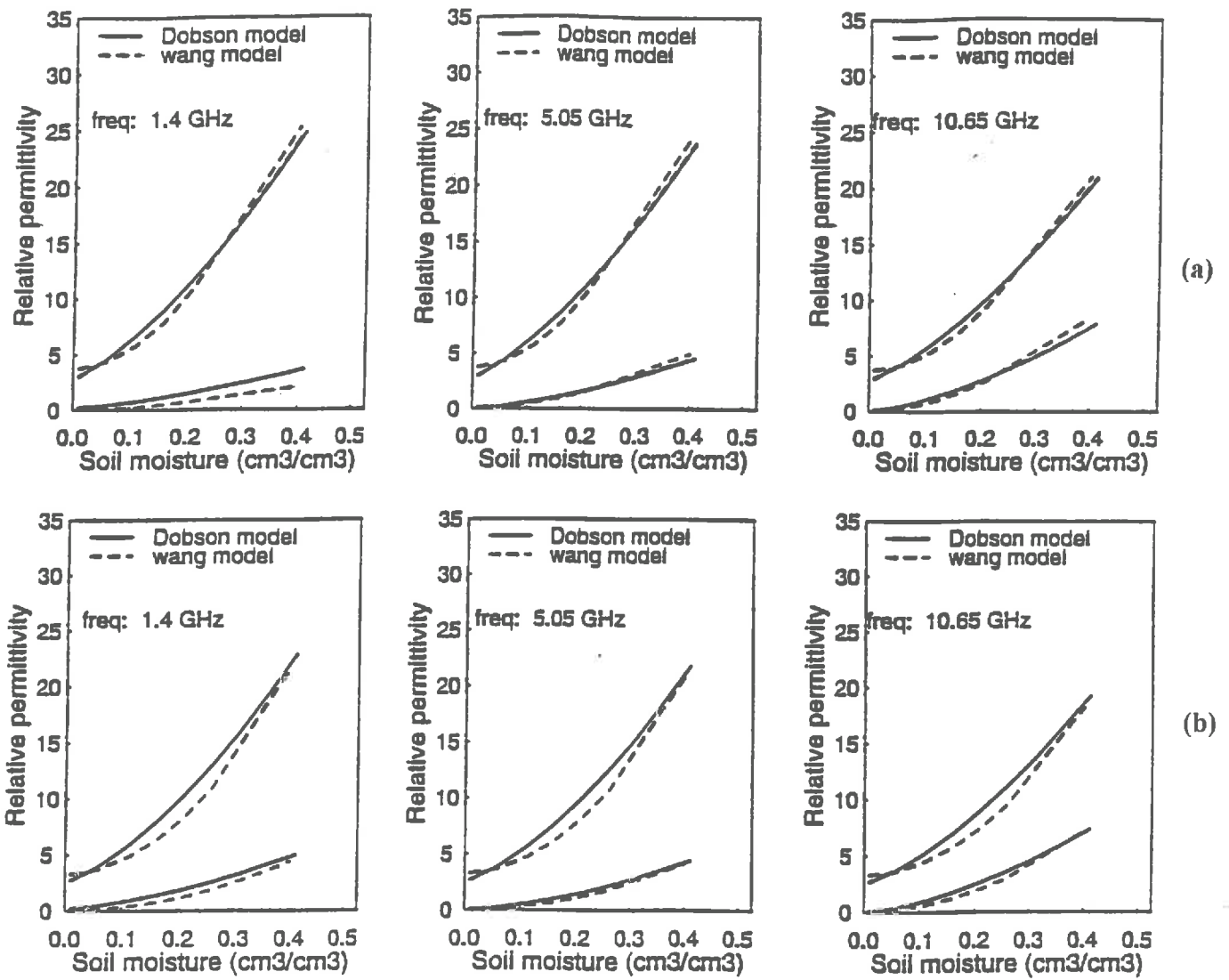
Figure 4.4: Dielectric constant calculated using Wang and Schmugge model and Dobson semi-empirical model; (a) for sandy soil and (b) silty clay loam soil.
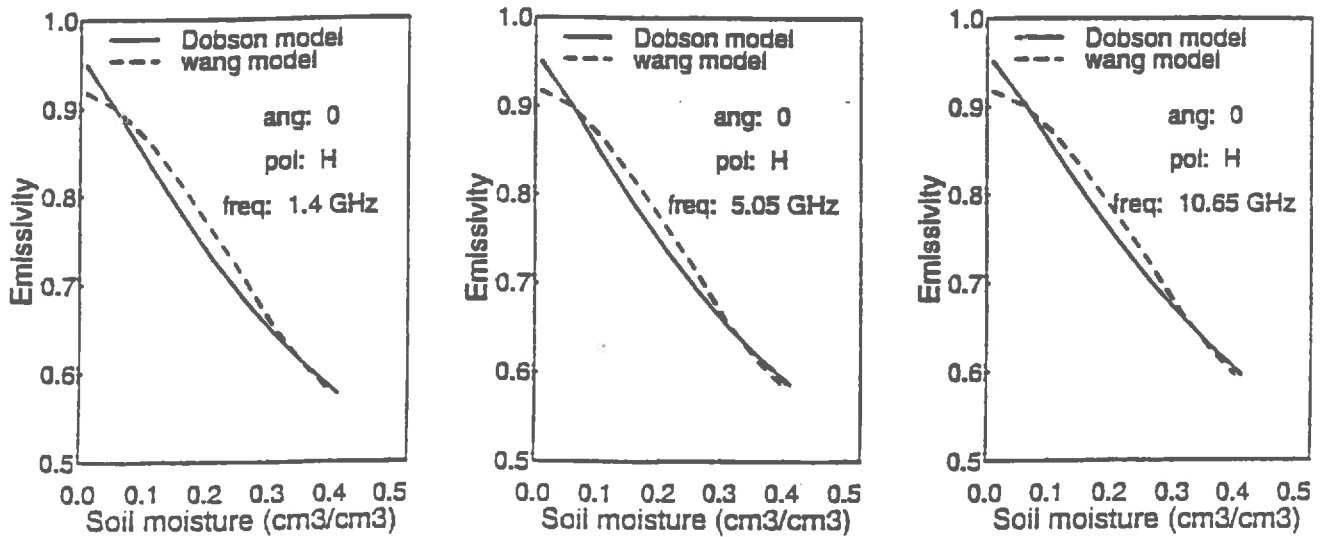
Figure 4.5: Fresnel emissivity calculated using the dielectric values of Wang and Schmugge model and Dobson semi empirical model for silty clay loam soil.

versions of the PORTOS;) radiometer PORTOS 91 and PORTOS 93 (PORTOS 91 was having horn antenna for L and C bands and the different tillage practices, we can notice the remarkable similarity of the relationships obtained from the two fields. It is an encouraging feature for the experimental data quality.

Examples of T_B continuous acquisition are displayed in Paper I (Figure 3 and 4). They show how the soil temperature and moisture vertical profiles affect the evolution of T_B at the different frequencies. The Figure 4 (Paper I) highlights the large amplitude of the T_B diurnal variations, especially at 5.05 and 10.65 GHz.

4.2 Validation of the microwave emission models

4.2.1   Selection of a model to determine soil dielectric constant.

The models of Wang and Schmugge (1980) and the Dobson et al, (1985) described in Appendix A are compared. Though, both dielectric models are based on the mixing principle, different approaches were adopted to define the soil water interaction (bound and bulk water). With the exception of the study reported by Dobson and O'Neill (1987) for sandy soil, no detailed work has been reported on the influence of the different approaches on the emissivity estimation of different soils.

The figure (4.4) shows the results of both dielectric models that are applied to calculate the dielectric constant of sandy soil and silty clay loam soil.   A general trend that can be observed is that Wang and Schmugge model dielectric values are always lower than Dobson model results except for very high and low soil moisture conditions. The dielectric constant of sandy soil predicted by both models are comparable at all frequencies. In case of silty clay loam soil, both real and imaginary parts of dielectric constant show larger difference compared to that in sandy soil. In order to see the effect of the difference in the model result on emissivity calculation, we calculated the corresponding emissivity for the silty clay loam soil. Figure (4.5) shows the emissivity calculated using the Fresnel model for the horizontal polarization. The emissivity values observed for silty clay loam soil differs at the intermediate moisture, where the mean difference in emissivity is about 0.02.   The 0.02 difference in emissivity can lead to an error in T_B of about 6 K at an effective temperature of 300K.
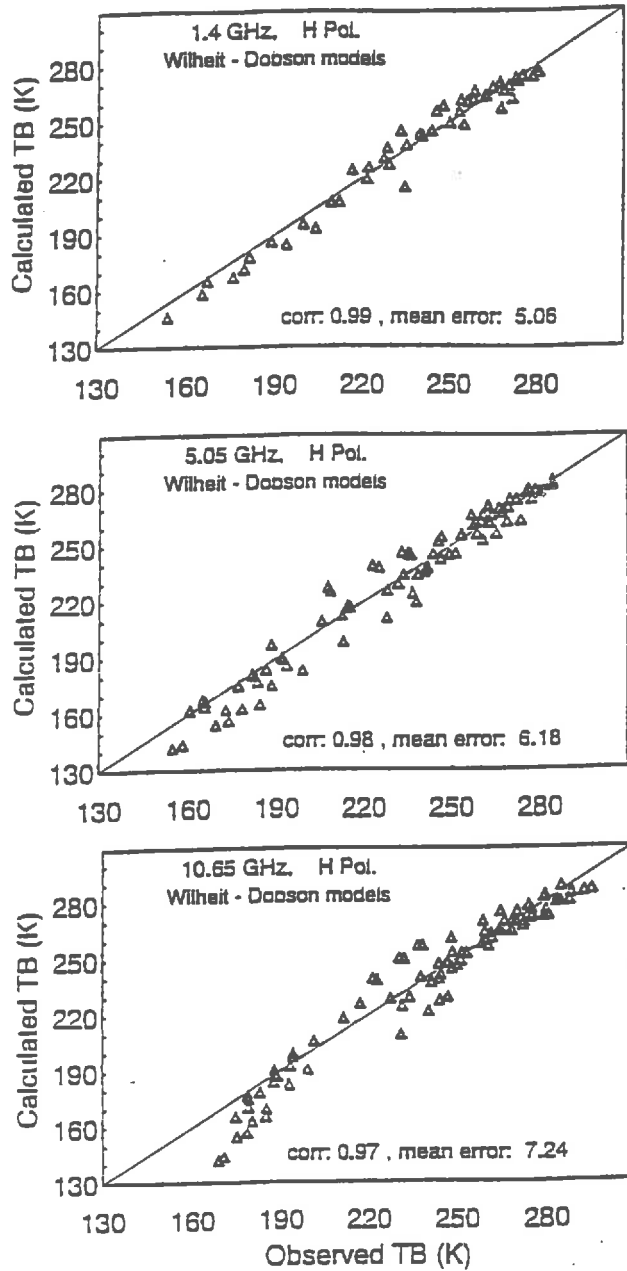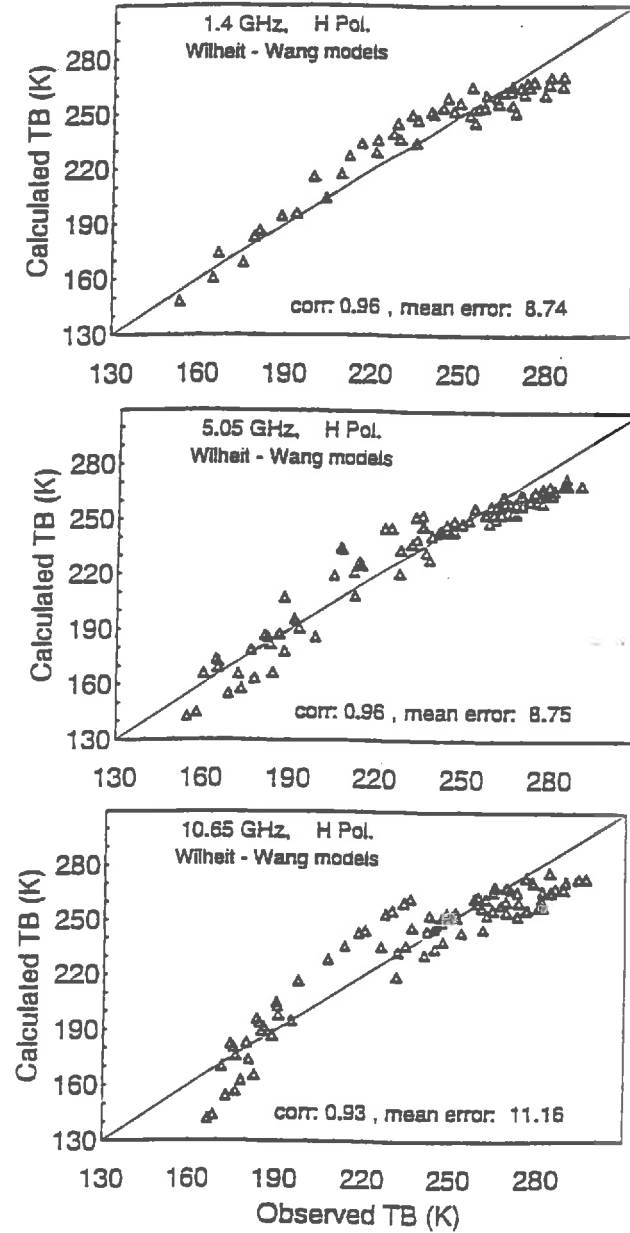
Figure 4.6: Validation of (a) Dobson's Semi-empirical model and (b) Wang and Schmugge model. The dielectric constant obtained by the two models are used in emission models to simulate the theoretical T_B and then correlated against PORTOS - 1993 T_B data.

Table: 4.1 Statistical results of the regression between computed and experimental T_B for the SI surface condition.

WITH WILHEIT MODEL (A)

Frequency (GHz)	Dobson dielectric model				Wang & Schmugge model			
	origin (K)	slope (K)	r^2	std. error	origin (K)	slope (K)	r^2	std. error
1.4 h	-13.2	1.05	0.99	5.06	33.6	0.86	0.96	8.74
1.4 v	32.2	0.89	0.97	10.48	60.1	0.8	0.88	16.56
5.05 h	-14.4	1.06	0.98	6.18	20.2	0.91	0.96	8.75
5.05 v	-25.8	1.10	0.98	5.73	8.0	0.97	0.96	6.87
10.65 h	-18.4	1.07	0.97	7.24	28.4	0.87	0.93	11.16
10.65 v	-11.5	1.05	0.97	6.25	13.8	0.95	0.95	7.99

WITH BURKE MODEL (B)

Frequency (GHz)	Dobson dielectric model				Wang & Schmugge model			
	origin (K)	slope (K)	r^2	std. error	origin (K)	slope (K)	r^2	std. error
1.4 h	-6.6	1.04	0.93	11.77	30.5	0.87	0.9	13.74
1.4 v	10.4	1.0	0.86	17.55	38.7	0.89	0.82	19.05
5.05 h	-10.0	1.06	0.97	8.36	26.3	0.9	0.94	11.13
5.05 v	-24.4	1.11	0.97	7.64	11.9	0.96	0.94	8.67
10.65 h	-16.6	1.06	0.97	7.33	-16.6	1.06	0.97	7.33
10.65 v	-10.6	1.05	0.97	6.62	14.7	0.94	0.95	8.07

WITH FRESNEL MODEL (C)

Frequency (GHz)	Dobson dielectric model				Wang & Schmugge model			
	origin (K)	slope (K)	r^2	std. error	origin (K)	slope (K)	r^2	std. error
1.4 h	16.4	0.93	0.97	6.4	21.6	0.91	0.97	6.92
1.4 v	24.0	0.94	0.96	10.08	24.0	0.94	0.96	10.09
5.05 h	-3.2	1.02	0.98	6.01	-2.4	1.02	0.98	5.96
5.05 v	-14.0	1.07	0.98	6.19	-11.8	1.06	0.98	6.48
10.65 h	-5.2	1.01	0.98	5.69	4.9	0.97	0.98	6.14
10.65 v	4.1	0.99	0.98	5.41	-5.0	1.02	0.98	4.84

The difference observed between the emissivity for silty clay loam soil when using the two models of soil dielectric constant prompted us to compare their results against experimental results before selecting one of them for further studies. Since we had not the equipment to measure the soil dielectric constant, we made the comparison of the T_B calculated by using both dielectric models in different microwave emission models against experimental T_B data collected in the PORTOS - 93 campaign. The T_B was simulated using Wilheit model, Burke model and Fresnel relation. The results of the comparison made using Wang and Schmugge model and Dobson model in Wilheit model at 1.4, 5.05 and 10.65 GHz and horizontal polarization is shown in the figures (4.6 a and b). The table 4.1 presents the summary of the result for both polarization with three emission models i.e. the Fresnel, the Burke and the Wilheit model. The T_B obtained by using the Dobson dielectric model in Wilheit model and Burke model present the best correlation with the PORTOS data for all frequencies and both polarization. Moreover, the mean error observed between the simulated and measured T_B data is less in the case of Dobson model. At 1.4 GHz, the difference observed between the two models was larger than the difference observed with other two frequencies. Based on these results, we selected the Dobson model for the subsequent simulations of T_B by the emission models.

The temperature of the near surface soil layer undergoes large variation of about 30°C during the day - night cycle and season to season as we have seen in both experimental and simulation studies. The effect of this temperature difference on the dielectric constant and hence the emissivity calculations were studied. The figure (4.7) shows the variation of dielectric constant of silty clay loam soil as a function of soil temperature and the corresponding emissivity at soil moisture 0.3 cm^3cm^{-3}. Overall, the temperature effect on the real part of the dielectric constant is found to be negligible. Only very small variation in soil emissivity is observed at 1.4 GHz. The emissivity variations stay within a range of about 0.005 for a temperature variation of 15 to 35C. Thus we can make the conclusion that the temperature effect on the dielectric constant is negligible in case of our experimental conditions.

4.2.2   Estimation of the error in the comparison between simulated data by the microwave emission models and the experimental measurements

Before making the validation of the emission models by comparing their results against the experimental data, we must have to quantify the different errors that affect the comparison.
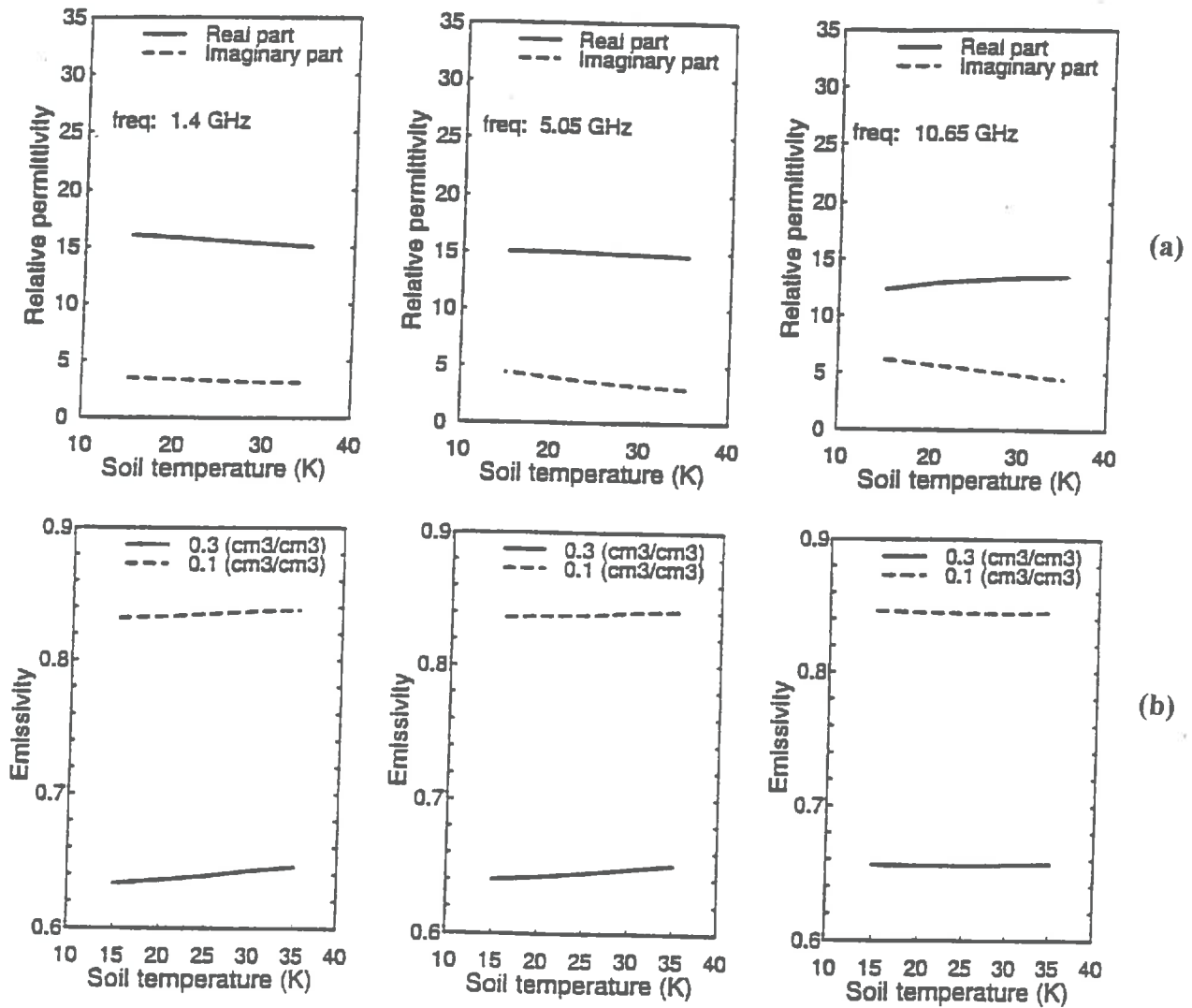
Figure 4.7: The temperature effect (a) on soil dielectric constant and (b) the corresponding emissivity variation.

From such an error analysis, we can define a range of T_B within which it is impossible to invalidate the model. The errors have two origins :

i) the experimental errors, which come from both the radiometric and ground measurements;

ii) the errors associated to the implementation of the emission model. The sources of error in the implementation of the microwave emission model from layered media are :

-description of the layered soil medium (layer thickness, the depth of the soil considered hereafter referred to as the total depth).

-error due to the methodology adopted for the reconstruction of soil moisture and temperature profiles.

A detailed description on the methodology used to estimate the error that affect the model-experiment comparison is presented in Paper I.

With the Wilheit (see Paper I), we arrived to the conclusion that a difference of 25K between simulated and experimental T_B can be explained by the combination of experimental errors and those due to the description of the layered media used in the Wilheit model. The value of 25K is obtained after determining optimal layer thickness (<0.01 cm) and total depth (>8.5 cm). We also find that a linear interpolation to determine the soil moisture profile is far better than using an exponential relationship fitted to the experimental data, as done usually.

Similar results are obtained with the Burke model. The layer thickness should be lower than 0.01 cm, whereas the soil total depth should be larger than 5, 4, 2 cm for L, C and X band frequencies respectively. To infer the soil moisture profile from an experimental profile, both linear interpolation and exponential fitting were considered. Both methods lead to a similar result in T_B estimation. No significant difference in the soil temperature estimation was observed by using both fitting methods. The method used to retrieve the soil moisture profile observed has a weaker influence in the Burke model than in the Wilheit model. This is explained by the following property of the Burke model : the soil moisture and temperature profiles are only involved in estimation of the effective temperature. Indeed, we can show that the soil moisture profile does not affect the calculation of the soil emissivity, which only depends on the soil moisture of the first layer. Such a property was already underlined by Schmugge and Choudhury (1981). A summary of the different error sources is given in Table 4.2. This table is similar to Table 3 in Paper I given for the Wilheit model.
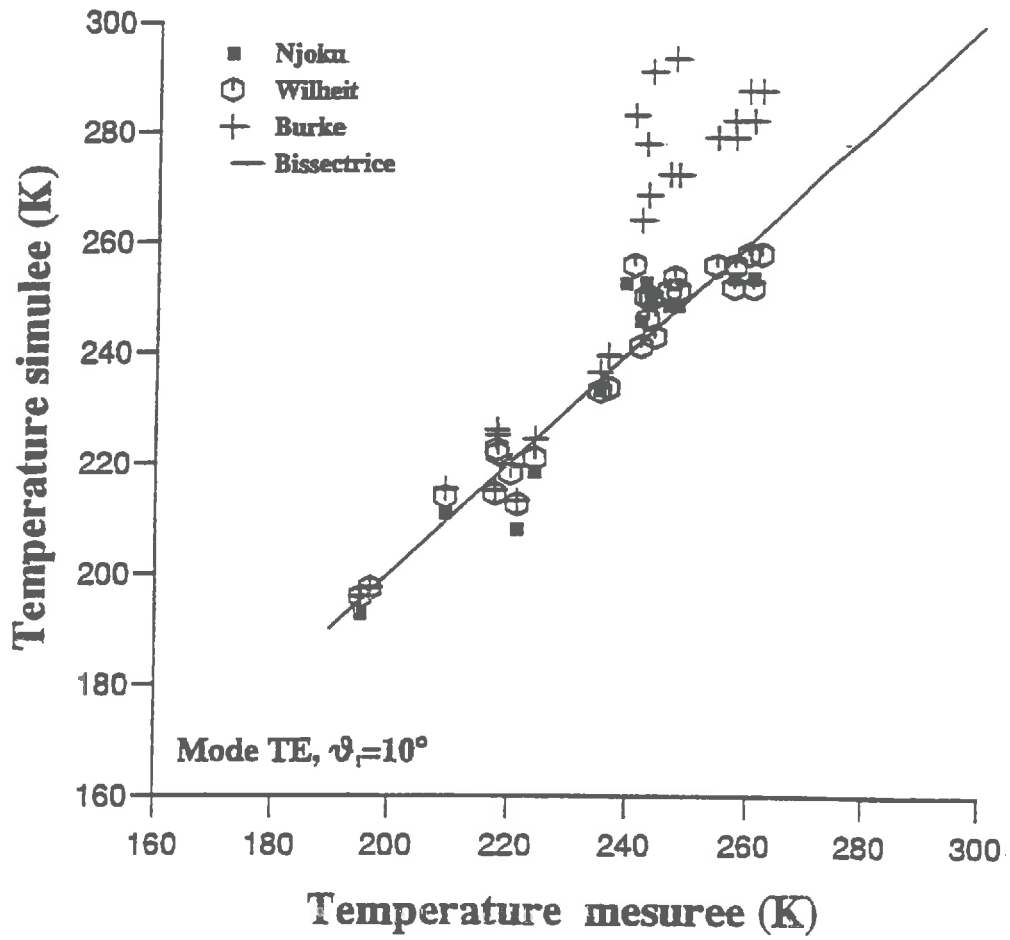
Figure 4.8: Comparison of the measured T_B collected with the SMb surface condition and the computed T_B by the Njoku, the Wilheit model and the Burke models. The comparison is done at 1.4 GHz, in H - polarization and 10° incident angle.

If we add all the error terms, we get a very large error of about 30 K. This means it would be very difficult to provide a reliable evaluation of the model performance by a simple comparison against experimental data.

Table 4.2 : Total error estimation in the validation of the Burke model. The errors in the implementation of the model and radiometric data collection are presented separately.

Error origin	Error in T_B (K)		
	1.4 GHz	5.05 GHz	10.65 GHz
Implementation of the Burke model			
Layer thickness (0.01 cm)	0.3	0.3	0.3
Total soil depth (8.5 cm)	0.4	0.1	0.1
Soil moisture profile (linear Int.)	5.8	2.4	5.7
Soil temperature profile	0.5	0.5	0.5
total	7.0	3.3	6.6
Experimental errors			
ground soil moisture measurements	14	14	14
radiometer	7.5	2	2

A similar analysis was done by Costes (1994) for the Njoku model. She arrived to the conclusion that the layer thickness need to be lower than 0.1 cm and the total depth should be higher than 15, 5 and 2.5 cm at 1, 5 and 10 GHz, respectively. Unfortunately, she didn't make an error analysis as presented previously. However, we can expect similar conclusions to that given from the error analysis of the Burke and Wilheit models.

4.2.3 Validation of the microwave emission model

4.2.3.1 Validation and comparison of the emission from layered media

The comparison between experimental and simulated T_B was done for the three emission models from layered media (Njoku, Wilheit and Burke models) in the case of the SMb field. These results were obtained in the frame of a collaborative work carried out with Florence Costes and J. Lemorton, CERT- ONERA/DERMO Toulouse, France. Results in Figure 4.8

and Table 4.3 shows the comparison between simulated and observed T_B at L-band, H polarization and 10° angle of incidence. Two important conclusions can be drawn from this Figure (4.8):

- there are only a small difference between the two coherent models. It confirms earlier results (Schmugge and Choudhury, 1981). In the following analysis, we selected the Wilheit model which is easier and faster to implement. The difference between observed and simulated T_B is always lower than the total error determine in Paper I (Table 3). Therefore, the coherent models are validated or at least not invalidated.

Table 4.3 : Results of the regression between observed and simulated T_B by the Njoku (N) and Wilheit (W) models in the case of the SMb surface condition.

Angle & model	L band H pol.	origin (K)	slope (K)	r^2	L band V Pol.	Angle & model	origin (K)	slope (K)	r^2
10° N		-19.2	1.09	0.90		10° N	0.0	1.0	0.92
W		- 2.2	1.0	0.93		W	14.6	0.93	0.95
20° N		-18.6	1.08	0.92		20° N	3.5	0.99	0.92
W		-3.1	1.01	0.94		W	18.3	0.92	0.93
30° N		-25.5	1.11	0.91		30° N	6.35	0.99	0.91
W		-8.1	1.02	0.93		W	21.8	0.92	0.94
Angle & model	C band H pol.	origin (K)	slope (K)	r^2	C band V Pol.	Angle & model	origin (K)	slope (K)	r^2
10° N		5.9	1.0	0.92		10° N	1.5	1.0	0.94
W		4.1	1.0	0.95		W	3.6	1.0	0.96
20° N		5.16	0.99	0.93		20° N	0.68	1.01	0.94
W		3.0	1.01	0.95		W	1.9	1.01	0.96
30° N		-2.22	1.03	0.93		30° N	-0.37	1.02	0.94
W		-4.3	1.04	0.96		W	-2.1	1.03	0.95

- the coherent models are far better than the Burke model, especially in dry condition. The results of the SMb experiment are confirmed by the results obtained later with the SM surface condition (Table 4.1). Better results would have been obtained with the Burke model by changing the layer thickness of the first layer, since it determines the soil emissivity. However, such a fitting is inconsistent with the interest of an emission model from layered which should not require any fitting operation.
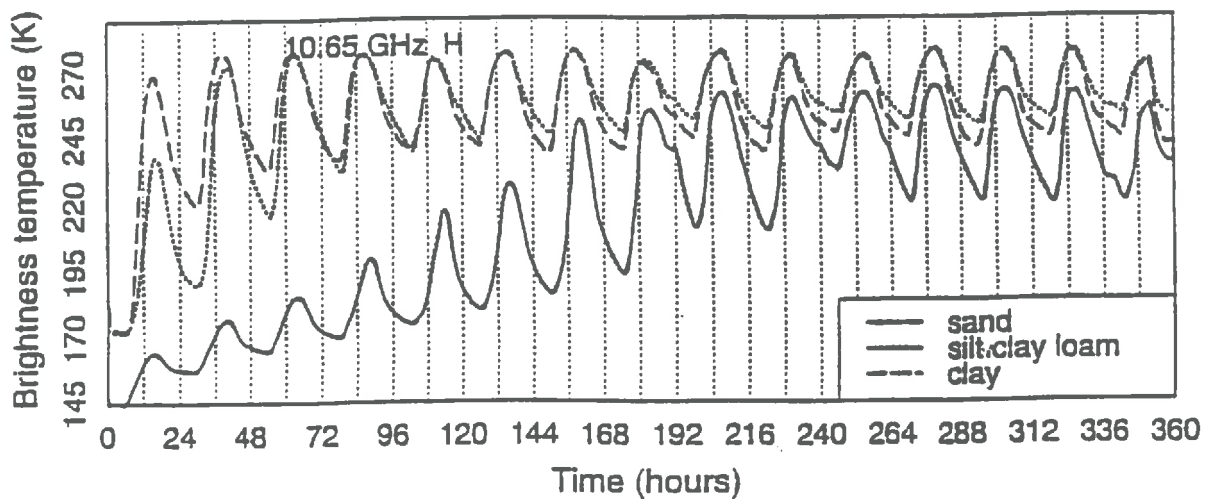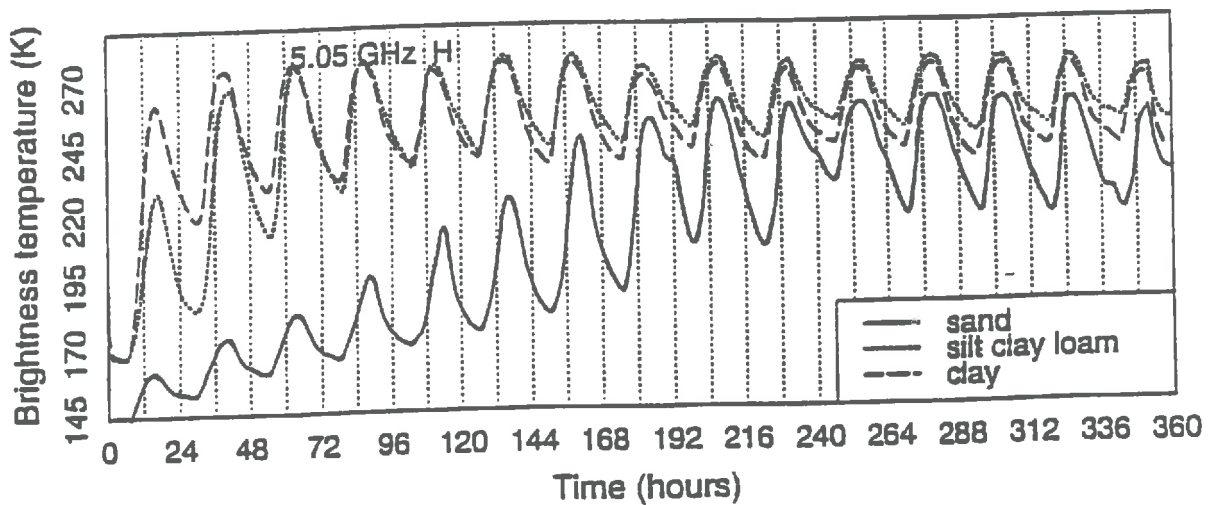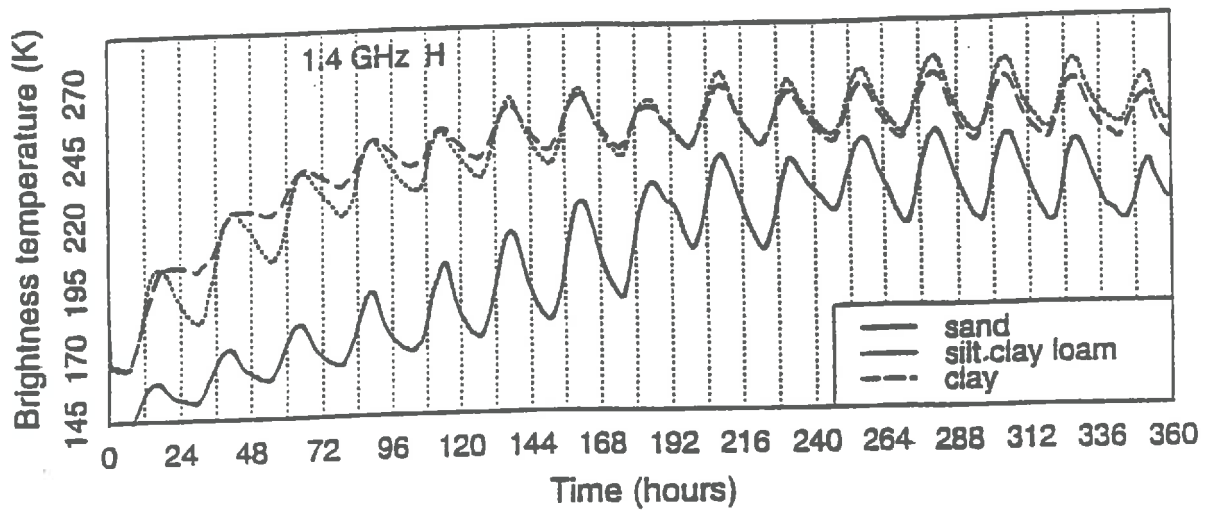
Figure 4.9: Diurnal evolution of T_B (20° incident angle) at 1.4, 5.05 and 10.65 GHz for sandy soil, silty clay loam soil, and clay soils. The T_B were simulated by running the Wilheit model with the outputs of the mechanistic model of soil heat and mass flows.
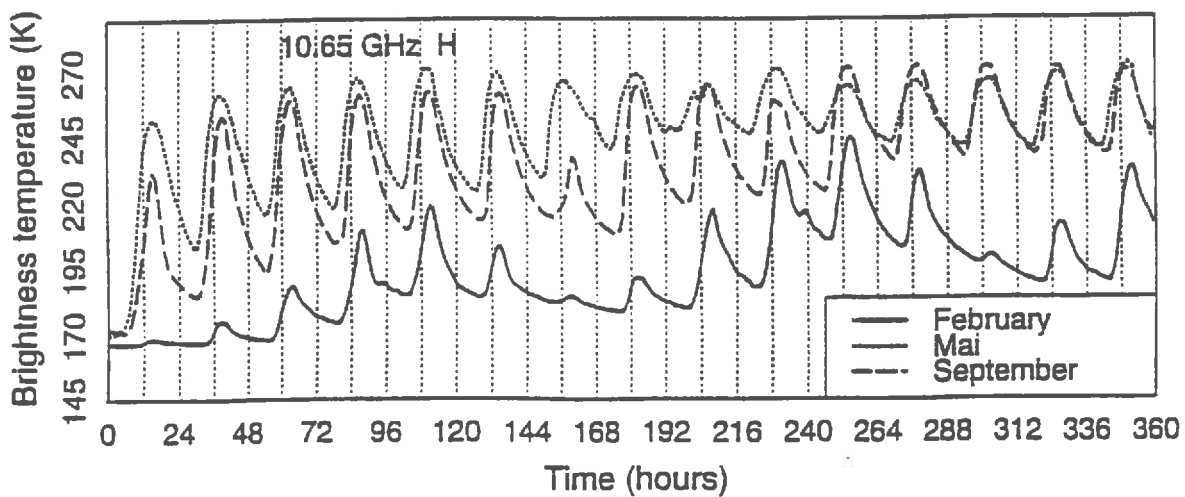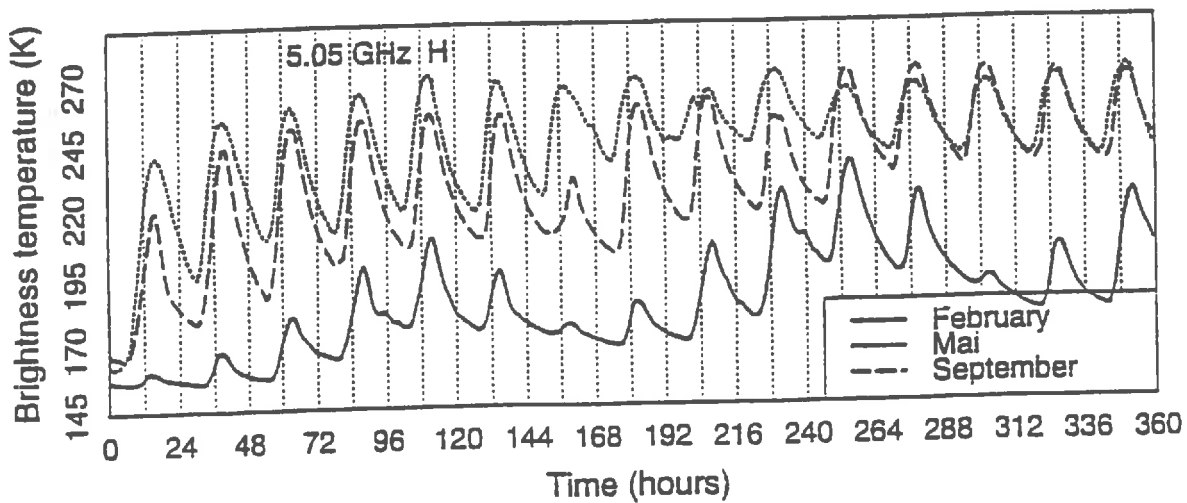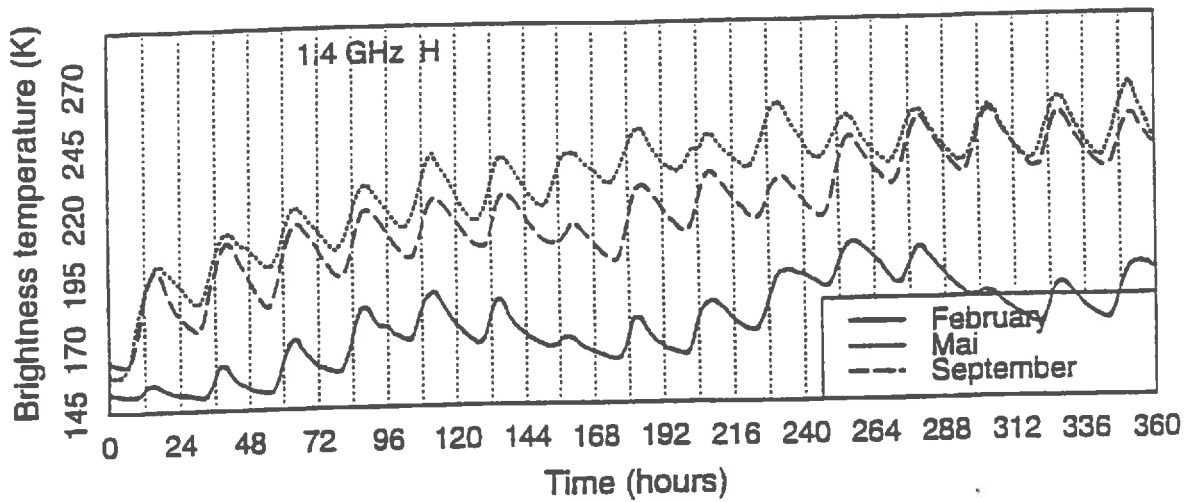
Figure 4.10: Diurnal evolution of T_B (20° incident angle) of silty clay loam soil for of the months of February, May and September. The T_B were simulated by running the Wilheit model with the outputs of the mechanistic model of soil heat and mass flows.

4.2.3.2 Comparison between Fresnel and Wilheit model

The aim of this comparison is to evaluate the benefit we can get when a soil profile is considered instead of describing the soil as a single layer (Fresnel model). The comparison is presented in Paper I. We show that the Wilheit model is better than the Fresnel model at L band. For higher frequencies, results of the Fresnel model, implemented with a fitted sampling depth, are comparable to those obtained with the Wilheit model. We also show that the field of validity of the sampling depth has a limited temporal field of validity.

4.3. T_B simulation by combining the Wilheit model to the mechanistic model

The diurnal evolution of soil moisture and temperature in different soils and climatic conditions simulated by mechanistic model of soil heat and mass flows were used to simulate the diurnal brightness temperature at 1.4, 5.05 and 10.65 GHz frequencies by the Wilheit model. The figure (4.9) shows the evolution of T_B in different soils simulated for the warm (July) climatic conditions at three frequencies. We can see from the figure that:
- the T_B variation in silty clay loam soil and clay soil are comparable when the soil reaches dry surface condition.
- the T_B of sandy soil differs largely from the T_B of other two soils. It is the consequence of the drying patterns, which lead to very different soil moisture profiles near the surface with the sandy soil than with the other two soils.
- as the frequency increases, the amplitude of the T_B variation within the day increases. This is a consequence of the sampling depth which decrease with the radiation frequency. The amplitude of the soil moisture diurnal cycle is the highest near the surface (Chanzy, 1991) and therefore, the T_B at the highest frequencies is more sensitive to the soil surface conditions.

The figure (4.10) shows the diurnal variation of T_B of the silty clay loam soil for three different climatic conditions. There is a large difference between the T_B variation in the warm (May) and cold (February) climatic conditions.

The above figures(4.9 and 4.10) show the influences of the soil hydrodynamic properties and climatic conditions on the microwave emission. The moisture gradients near the soil surface lead to different multifrequency signature which could be used to infer the soil
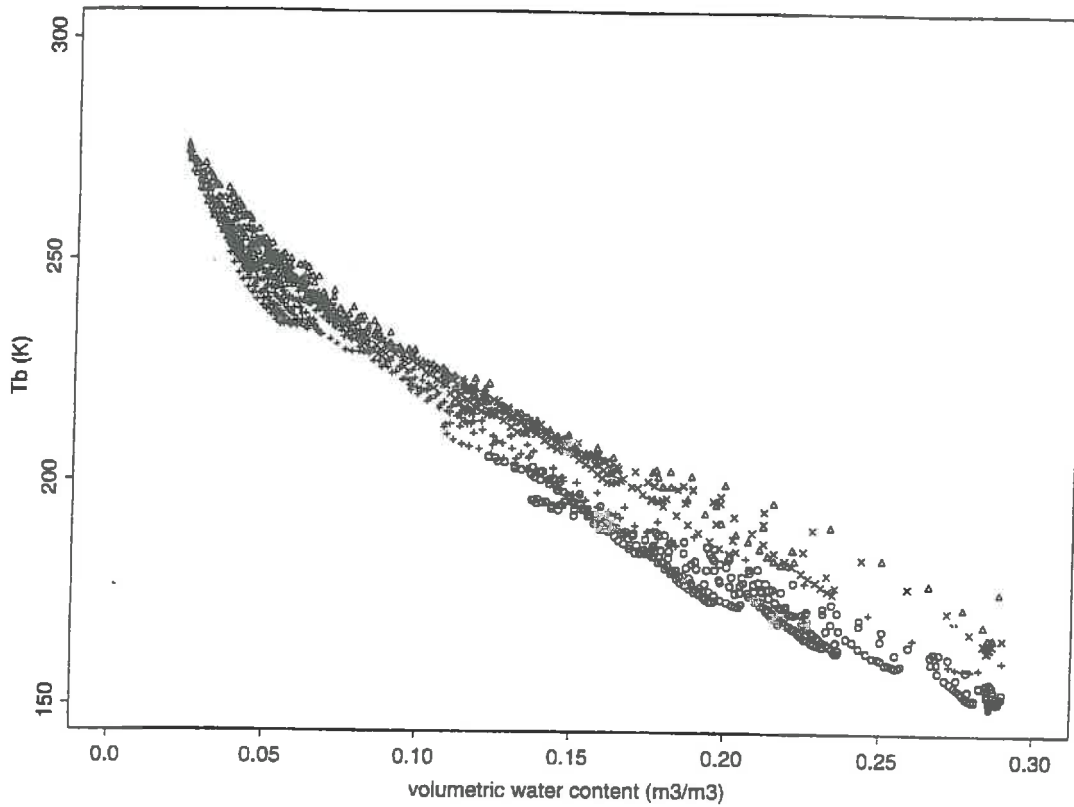
Figure 4.11: Soil moisture - T_B relationship. The T_B are simulated by running the Wilheit model with the outputs of the mechanistic model of soil heat and mass flows. The T_B simulated for silty clay loam soil (variability of moisture and temperature profiles due to different climate and soil types are taken into account)
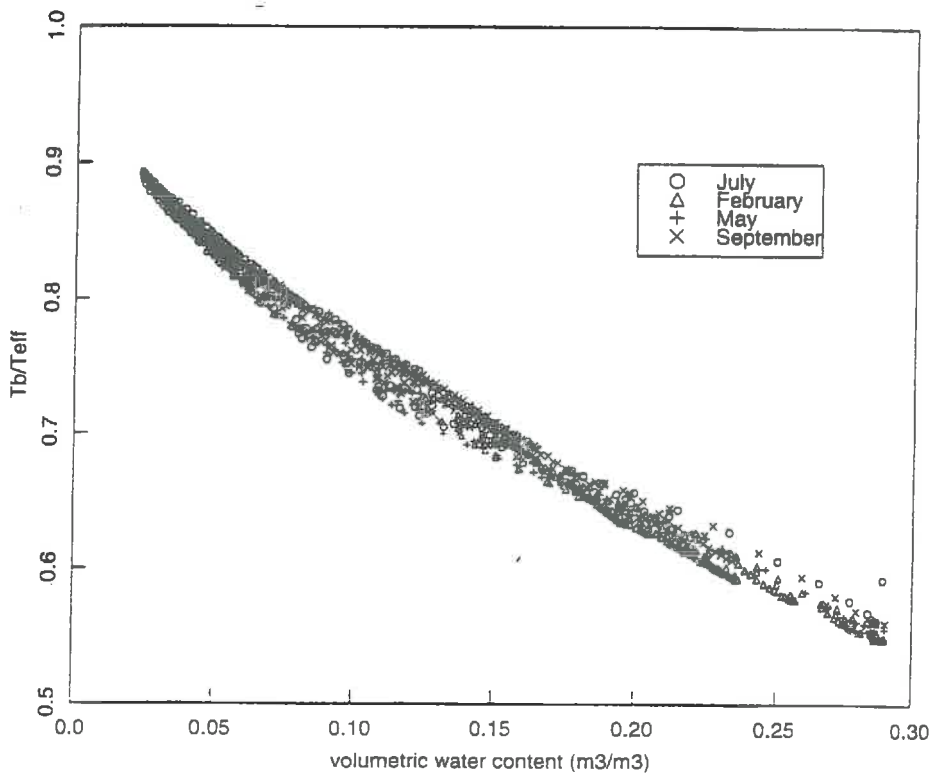
Figure 4.12: Same as 4.15 but with T_B/T_e.

moisture gradients near the soil surface. Such an information would be useful to investigate soil hydraulic properties. These points should be studied in a future endeavor.

4.4. Impact of the soil moisture and temperature profile variability on the soil moisture estimation

We assume here that the soil moisture is determined in a single layer either by inverting the Fresnel model or establishing a relationship between the soil moisture and T_B. In Figure (4.11) we pooled together the results of the simulations obtained for the silty clay loam soil. The Figure exhibits a scattering of the points which affect the soil moisture accuracy. Indeed, for a given T_B, there is a range of possible soil moisture which extent reach 0.10 m^3/m^3. Such a scattering is explained by the influence of the soil temperature and the soil moisture profile (See Paper I). The scattering can be strongly reduced by accounting for the effective temperature (Figure (4.12) and Figure (10) of Paper I). The latter result justified the study on the effective temperature modeling presented in Paper II.

CHAPTER 5

PRESENTATION OF PUBLICATIONS

5.1   PRESENTATION OF PUBLICATION - I

Soil Moisture and Temperature Profile Effects on Microwave Emission at Low Frequencies

Suresh Raju,* André Chanzy,* Jean-Pierre Wigneron,**
Jean-Christophe Calvet,† Yann Kerr,‡ and Laurent Laguerre‡

Soil moisture and temperature vertical profiles vary quickly during the day and may have a significant influence on the soil microwave emission. The objective of this work is to quantify such an influence and the consequences in soil moisture estimation from microwave radiometric information. The analysis is based on experimental data collected by the ground-based PORTOS radiometer at 1.4, 5.05, and 10.65 GHz and data simulated by a coherent model of microwave emission from layered media [Wilheit model (1978)]. In order to simulate diurnal variations of the brightness temperature (T_B), the Wilheit model is coupled to a mechanistic model of heat and water flows in the soil. The Wilheit model is validated on experimental data and its performances for estimating T_B are compared to those of a simpler approach based on a description of the soil media as a single layer (Fresnel model). When the depth of this single layer (hereafter referred to as the sampling depth) is determined to fit the experimental data, similar accuracy in T_B estimation is found with both the Wilheit and Fresnel models. The soil microwave emission is found to be strongly affected by the diurnal variations of soil moisture and temperature profiles. Consequently, the T_B sensitivity to soil moisture and temperature profiles has an influence on the estimation, from microwave observations, of the surface soil moisture in a surface layer with a fixed depth (θ_s): the accuracy of θ_s retrievals and the optimal sampling depth depends both on the variation in soil moisture and temperature profile shape.

*INRA, Science du sol, Domaine St Paul, France
**INRA, Bioclimatologie, Domaine St. Paul, Avignon, France
*Météo-France / CNRM, Toulouse, France
‡LERTS / CESBIO, Toulouse, France

Address correspondence to Dr. Andre Chanzy, INRA, Station de Science du Sol, Domaine Saint-Paul, Site Agroparc. 84914 Avignon, Cedex 9, France.

INTRODUCTION

Surface soil moisture is a key parameter for hydrological, meteorological, and agricultural studies. For these studies, the temporal evolution of the soil moisture is an important feature that needs to be tracked daily or even several times a day. It is now well established that microwave emission from the land surface involves several parameters that include the soil moisture and temperature, the surface roughness, and the vegetation through its water content and structure. The estimation of surface soil moisture from passive microwave observations has already been widely studied over the past two decades and the main results were reported by Jackson and Schmugge (1989). From these studies, penetration of the microwave radiation in the soil is shown as an important property for understanding the soil contribution to the microwave emission from the land surface (Burke et al., 1979, Newton et al., 1982, Njoku and O'Neill, 1982, Wang, 1987). Using a theoretical approach, Njoku and Kong (1977) have shown the influence of soil moisture in the thickness variations of the soil layer that contributes significantly to the microwave emission. Practically, the surface soil moisture is often derived from the microwave brightness temperature (T_B) by inverting microwave emission models (Wang, 1987, Wigneron et al., 1993) or by establishing a direct relationship between T_B and the soil moisture (Wang et al., 1983, Schmugge et al., 1994, Chanzy et al., 1995). To account for the microwave penetration depth in soils, soil moisture and temperature are averaged within a surface soil layer. The thickness of this layer (hereafter referred to as the sampling depth) is generally considered as constant for the whole range of soil moisture conditions. In this paper, θ_s represents the soil moisture in this soil layer. Although there is now a general agreement about the order of magnitude of the microwave sampling depth (Jackson and Schmugge, 1989),

its magnitude is often obtained empirically. Moreover, the field of validity of a given sampling depth is only discussed in relation to the frequency. But the influence of soil moisture and temperature vertical profiles on the soil microwave emission or on the penetration depth is seldom analyzed. These profiles are known to vary strongly during the day and from one soil to another (Chanzy and Bruckler, 1993). At the present time, however, we do not know in which proportion the variations in soil moisture and temperature profiles affect the accuracy of the θ_r retrievals. This should be investigated prior to analyzing radiometric observations made on large areas with heterogeneous soils or acquired at different times of the day. In order to maximize diurnal variations of soil moisture and temperature profiles, only bare soils are considered in this study.

As a first approach, the influence of the soil moisture and temperature vertical profiles on T_B is discussed from experimental data. The T_B measurements were collected by the ground-based radiometer PORTOS and the study focuses on its three lower frequencies (1.4, 5.05, and 10.65 GHz). The experimental errors obtained on both ground and microwave measurements were too large to identify clearly the influence of soil moisture and soil temperature profile shape on T_B. Therefore, the analysis is pursued with physically based microwave emission models.

Among the existing physical models of soil microwave emission, radiative transfer models in layered media are well suited for examining the influence of soil moisture and temperature vertical profiles on T_B. The radiative transfer models could be divided between the coherent models of Njoku and Kong (1977) and Wilheit (1978), and noncoherent model (Burke et al., 1979) approaches. In the noncoherent Burke model, soil moisture profile contributes only to the effective temperature calculation, whereas the soil emissivity is solely determined by the moisture content in the surface layer (Schmugge and Choudhury, 1981). Therefore, the Burke model does not allow proper analysis of the influence of soil moisture profile variations on T_B. Results of the two coherent models (Njoku and Kong, 1977; Wilheit 1978) were compared by Schmugge and Choudhury (1981) and Costes et al. (1994). They found a good agreement between the results of both models. Consequently, the Wilheit model, which is simpler, is selected in the following study. In previous studies, the Wilheit model results were found to be in agreement with experimental observations (Wang, 1987; Laguerre et al., 1994). Nevertheless, the improvement brought by a layered representation of the soil in comparison to simpler approaches based on a single layer, that is, the Fresnel model based on the Fresnel reflectivity calculation, needs to be analyzed.

In this study, the validity of the Wilheit model is examined and its performances are compared to that of the Fresnel model. In order to provide diurnal variations of the T_B, the Wilheit model is coupled to a mechanistic model of soil heat and mass flows (Chanzy and Bruckler, 1993), which simulates the temporal evolution of the soil moisture and temperature profiles with a short time interval (several minutes). Based on these simulations of T_B, we then analyze the influence of the soil moisture and temperature profiles on soil moisture estimation from microwave observations.

THEORY

Microwave Emission Models

Two soil microwave emission models are implemented in this study. The Fresnel model (Schmugge and Choudhury, 1981) is the simplest. It is based only on the reflection at the air–soil interface and ignores all the reflections within the soil medium. Assuming that the air–soil boundary is a plane and that the atmospheric contributions are negligible, T_B at an angle of incidence I and polarization p is given by:

$$T_B(I,p) = [1 - \Gamma(I,p)] \cdot T_{soil} \qquad (1)$$

where $\Gamma(I,p)$ is the Fresnel specular reflectivity and T_{soil} is the soil temperature. To compute $\Gamma(I,p)$, the dielectric constant of the soil medium is calculated with the semi-empirical model presented by Dobson et al. (1985). To compute T_B by the Fresnel model, T_{soil} and θ_r are averaged in the top layers over the sampling depth.

In the Wilheit model, the soil is described as a layered dielectric medium. Each layer is characterized by its dielectric constant and temperature, which are assumed to be homogeneous within the layer. The following assumptions are made in the Wilheit model: (1) the soil is a semi-infinite medium with a smooth air-soil boundary, (2) boundaries between the layers are planar and parallel, and (3) each layer is in thermal equilibrium. Similar to the Fresnel model, the soil dielectric constant is also estimated here with the Dobson et al. semi-empirical model. The energy contribution of each layer to the total soil microwave emission is determined by the absorption of a coherent electromagnetic wave, which propagates through the layer. Under thermal equilibrium conditions, each layer emits the same energy as it absorbs. Applying the Rayleigh–Jeans approximation to Plank's law, T_B can be written as:

$$T_B = \sum_{i=1}^{N} f_i \cdot T_i \qquad (2)$$

where T_i is the temperature of the ith layer, f_i is the fraction of energy absorbed by the ith layer with regard to the energy of the incident wave, and N is the number of layers. To determine f_i, the electric field is calculated at each boundary by solving Maxwell's equations for a coherent electromagnetic wave propagating through the layered soil medium. Then, the electromagnetic energy

is calculated at the top and bottom of each layer by using the Poynting theorem. The effective radiating temperature (T_{eff}) of the soil medium could be calculated by the Wilheit model with the following equation:

$$T_{eff} = \frac{\sum_{i=1}^{N} T_i \cdot f_i}{\sum_{i=1}^{N} f_i} \qquad (3)$$

Soil Heat and Water Flows Mechanistic Model

Simulations of the evolution of the soil moisture and temperature profiles are performed with a mechanistic model based on the theory of heat and water flows in unsaturated and nonisothermal soils (Chanzy and Bruckler, 1993). It is based on the Philip and De Vries (1957) partial differential equations reduced to the case of vertical flows. These equations are solved by a Galerkin finite element method. The soil is divided in 100 linear elements over the top 80 cm. The element dimensions vary from 0.01 cm near the surface to 2 cm. At the surface, the boundary conditions are obtained by solving the energy balance using climatic data (air temperature and vapor pressure and wind velocity at a height of 2 meters, short-wave incoming solar radiation). This mechanistic model simulates the evolution of water content and temperature profiles under given climatic conditions with a time interval that never exceeds 600 sec. These profiles are then used as inputs in the microwave emission models.

DATA ACQUISITION

Test Site

The experimental studies were carried out at the test site of INRA Montfavet, France, during June 16th–July 6th 1993 [Day of the year (DOY) 167 to 187]. The study area is the Mediterranean climatic zone, which is characterized by dry and warm weather during the experimental period. An experimental plot of 40 m by 20 m was tilled by a rotary digging machine in order to obtain small clods. Then, the field was rolled twice with a road roller to make the soil surface very smooth. The soil is a silty clay loam with 11% sand, 61.7% silt, and 27.2% clay. The field, initially dry, was wetted by two irrigations of 10 mm on DOY 173 and 179, and by two rainfalls of 13 and 23.5 mm on DOY 173 and 181, respectively.

Radiometric Measurements

The microwave observations were made with the CNES (Centre National d'Etudes Spatiales) radiometer PORTOS. It is a multifrequency and dual-polarization system operating at 1.4, 5.05, 10.65, 23.8, 36.5, and 90 GHz in Dicke mode (Grosjean and Sand, 1994). The 3

dB and the 20 dB beam width are approximately 12.5° and 30°, respectively. The radiometer measures T_B in both polarizations simultaneously, except for the 1.4 GHz channel, which requires a manual rotation of the parabolic antenna. This manipulation induces a delay between H and V measurements, which never exceeded 2 hours. The system was attached to a crane boom at a height of 20 m. The radiometer was coupled to a mechanical system for varying the angle of incidence from 0 to 40°. By moving the crane along a rail, the T_B measurements were centered on the same target for all incidence angles. The whole radiometer is thermally regulated with an accuracy of 1°K. The 1.4 GHz antenna is mounted apart from the radiometer and placed at the air temperature, however.

The radiometer absolute calibration was performed regularly throughout the experimental period. Cold targets were obtained by pointing the radiometer on a calm water surface. Eccosorb slabs (emissivity very close to 1) were placed in front of the antennas at ambient temperature for the high T_B calibration points (Grosjean and Sand, 1994). In the range of the measured soil T_B [160–300 K] the accuracy of the radiometer is estimated to ± 7.5 K, ± 2 K and ± 2 K at 1.4, 5.05, and 10.65 GHz, respectively (accuracy values correspond to two residual standard deviations of the linear regression between the calibration target T_B and PORTOS measurements). The loss in accuracy observed at 1.4 GHz in comparison to the other frequencies is partly explained by the lack of thermal regulation at 1.4 GHz. Moreover, external sources of electromagnetic radiations seem to increase the noise of the radiometric measurements at 1.4 GHz during some periods.

Microwave observations were made daily in all radiometric configurations. In order to track the diurnal variations of T_B, several continuous acquisitions of measurements were collected during periods limited to 4 hours due to the data system storage capacity. During the continuous acquisitions, the radiometer was set to a given configuration and the measurements were averaged over a period of 60 seconds.

Ground Measurements

Soil temperature was automatically measured with platinum resistance temperature probes. Ten probes were installed in the soil medium at different depths from very near the surface to 25 cm. The soil temperature was measured continuously and averaged every 10 minutes. In addition, a thermal infrared radiometer (8–14 μm) was kept along with the PORTOS system to measure the surface temperature during the radiometric measurements.

Soil moisture vertical profile was measured gravimetrically. The soil samples were taken in the following layers (3 to 5 replications): 0–0.5, 0–1, 1–2, 2–3, 3–4, 4–
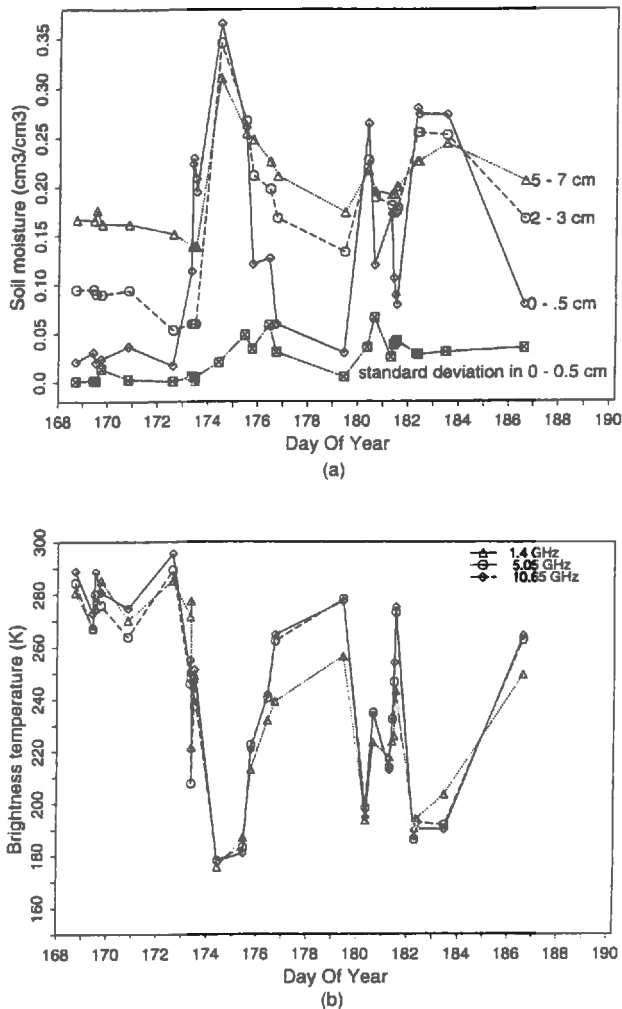
Figure 1. Evolution during the experiment of (a) the soil moisture in 0–0.5, 2–3, and 5–7 cm layers measured; (b) the T_B measured by H polarization and at a 20° angle of incidence.

Figure 2. Diurnal soil moisture evolution in silty clay loam soil at 0.25-, 2.5-, and 6-cm depths simulated by the mechanistic model of soil heat and mass flows.

5, 5–7 and 7–10 cm just before or after the radiometric measurements. In the case of continuous sequences, soil moisture profiles were measured several times. Vertical profiles of the dry bulk density were measured by a transmission gamma ray probe (Bertuzzi et al., 1987). The dry bulk density of the experimental plot was equal to 1.440 g cm^{-3} in the top 4 cm, which decreased to 1.350 g cm^{-3} at 10 cm. Volumetric water content was then computed from the gravimetric and the soil dry bulk density observations. The volumetric soil moisture in 0–0.5, 2–3, and 5–7 cm layers during the period of experiment is shown in Figure 1 a. It shows that a wide range of soil moisture has been covered during the experiment. In medium wet conditions, there are large gradients in soil moisture within the 0–3 cm layer. In Figure 1 b. the evolution of the T_B is consistent with soil moisture variations. Observations at 5.05 and 10.65 GHz are similar, whereas T_B at 1.4 GHz differs signifi-

cantly to the higher frequencies during the drying sequences.

Surface roughness parameters were measured by a noncontact laser profilometer (Bertuzzi et al., 1990). The results of the measurements showed that standard deviation in surface height (s) was 0.24 cm and correlation length (l) was 16.2 cm. According to the Rayleigh criterion (Ulaby et al., 1982), the surface is smooth for all the frequencies considered in this study.

Simulations with the Mechanistic Model of Soil Heat and Mass Flows

Simulations of soil temperature and moisture profiles were performed with the aim of being close to the experimental conditions. Therefore, the mechanistic model of soil heat and mass flows was run with soil hydrodynamic properties, which were calibrated on data collected during a previous experiment (1988) on the same experimental plot (Chanzy and Bruckler, 1993). Among the climatic input data set, we selected the one that is representative of the experimental period presented in this paper. A 20-day drying period was then simulated by the mechanistic model. Figure 2 displays the temporal evolution of the simulated soil moisture profiles. The figure clearly shows the diurnal cycling of the soil water content, which is important in the top 2.5 cm.

INFLUENCE OF SOIL MOISTURE AND TEMPERATURE VERTICAL PROFILES ON T_B: EXPERIMENTAL RESULTS

To show the importance of soil moisture and temperature profiles on T_B in this section we present two continuous acquisitions of T_B collected by PORTOS for two different days.
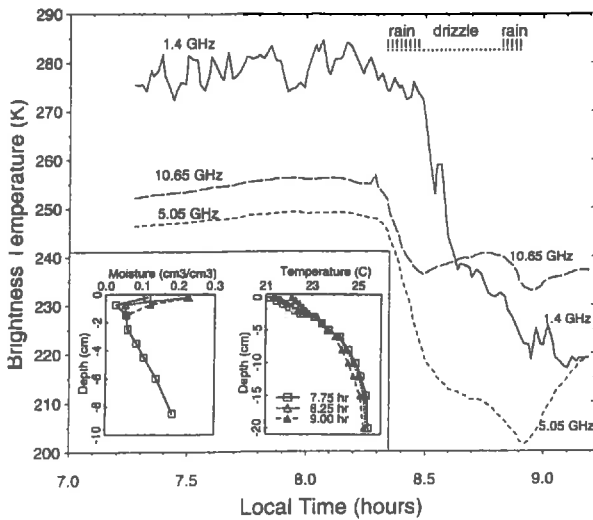
Figure 3. T_B evolution before and during a rainfall event at 1.4, 5.05, and 10.65 GHz (H polarization , 20°, DOY 173).

Figure 4. T_B evolution at 1.4, 5.05, and 10.65 GHz (H polarization, 20°) from morning to early afternoon, 40 hours after the last irrigation (DOY 181).

Experimental Evolution of T_B during a Small Rain

The first PORTOS continuous acquisition was done during a period of brief rainfall on the morning of DOY 173 (Figure 3). The soil was dry at the beginning of the measurements. A first shower started around 08:15 and continued for about 15 minutes. Then the intensity of the rain slowed and the soil was slightly wetted by a drizzle until 08:45. A second shower occurred and stopped completely around 09:00. The total amount of precipitation was less than 2 mm. The soil moisture profiles displayed in Figure 3 vary quickly during the rain in the top 2 cm soil layer while the soil temperature is homogeneous within the top soil layers and almost constant with time. Therefore, these experimental conditions highlight the influence of the soil moisture profiles on T_B.

In Figure 3, the 1.4 GHz measurements present fluctuations that are likely due to an external microwave emitter, as mentioned previously in the description of radiometric measurements. Nevertheless, the general level of the 1.4 GHz T_B is found to be in agreement with the T_B–θ_s relationship established with our measurements and a soil moisture averaged in the top 2 centimeters. Prior to the rainfall, the T_B are lower at high frequency (5.05 and 10.65 GHz) than at 1.4 GHz. This T_B variation with frequency is explained by the moisture of the 0–0.5 cm soil layer, which was the only one moistened by the dew. The decrease in T_B begins concurrently with the rain (Figure 3) at 5.05 and 10.65 GHz, whereas the decrease in T_B is delayed for about 10 minutes at 1.4 GHz. Such a delay and the high T_B obtained at 1.4 GHz prior to the rain show that a very thin wet layer does not influence T_B significantly at 1.4 GHz. After the first shower, the T_B at 10.65 GHz in-

creases while it continues to decrease at the lower frequencies. The increase in T_B at 10.65 GHz is confirmed by PORTOS higher frequencies measurements (23.8, 36.5, 90 GHz) and indicates that the infiltration flow at the soil surface is higher than rain intensity during the drizzle period. Therefore, the decrease in T_B of about 15 and 30 K (Figure 3) at 5.05 and 10.65 GHz, respectively, is above all the consequence of the water redistribution in the surface soil layers, rather than the increase in soil moisture.
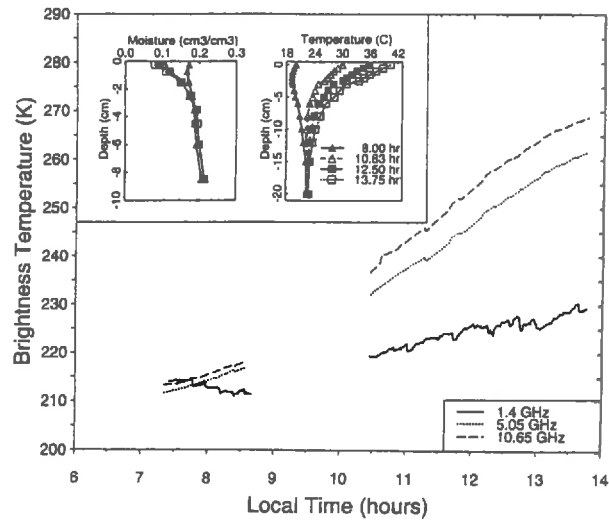
Diurnal Evolution of T_B during the Drying Period

We have selected a morning drying sequence when both soil temperature and moisture profiles vary quickly. Measurements were done on DOY 181, 40 hours after the last irrigation. In the early morning soil moisture and temperature profiles are rather homogenous, resulting from the previous night's redistribution of heat and water in the soil (Figure 4). Under the effects of evaporation and surface heating, soil moisture and temperature profiles move quickly toward steep gradients near the surface. Concurrently, microwave radiometric measurements were performed during a 6-hour period. In Figure 4, the T_B increases very quickly at 10.65 and 5.05 GHz. At 10.65 GHz, the range in T_B represents about 50% of the total range measured during the whole experiment, which covered contrasting soil moisture conditions (Figure 1). Consistent with Njoku and O'Neill's (1982) experimental results, T_B variations at 1.4 GHz are weaker due to a deeper penetration of the microwave radiation at this frequency. The very strong variation in T_B in Figure 4, observed during only a part of the diurnal cycle, demonstrates the major influence the diurnal variations

of soil moisture and temperature profiles on T_B. With the aim of estimating θ_s, we have to quantify how such diurnal variations of the soil surface conditions affect the accuracy in the soil moisture retrievals. This will be investigated in subsequent sections by using the Wilheit model, which will be validated against experimental results.

IMPLEMENTATION AND VALIDATION OF THE EMISSION MODELS

Implementation of Microwave Emission Models and Error Analysis

Before comparing the results of the microwave emission models to the measurements, we have to quantify the different errors that affect this comparison. With the Fresnel model implemented with an adequate sampling depth, only experimental errors on the ground characterization and on the microwave measurements need to be accounted for. With the Wilheit model, the description of the layered soil media should also be considered. As a matter of fact, the following three properties can affect the results of the Wilheit model: (1) the soil layer thickness, (2) the total soil depth defined here as the thickness of the layered soil medium, and (3) the method required to estimate the moisture and temperature in each layer from a limited amount of observations. These properties need therefore to be optimized in order to minimize the errors associated with the description of the layered soil system.

In this section, the implementation of the Wilheit model is analyzed with soil moisture and temperature profiles simulated by the mechanistic model of soil heat and mass flows. The use of simulated profiles is justified by their good vertical resolution of the temperature and moisture. Nine moisture profiles covering contrasting moisture conditions were selected with their corresponding temperature profiles (Figures 5a,b). For each soil moisture profile we have defined as reference the T_B computed by the Wilheit model with:

- a layer thickness of 0.001 cm;
- a total soil depth of 40 cm;
- soil moisture and temperature profiles obtained by linear interpolation from a detailed description of the soil (24 levels from the surface to 40 cm).

We will now evaluate how a degradation in the soil description can degrade the Wilheit model's results.

Layer Thickness

The T_B are calculated using the Wilheit model for different layer thicknesses varying from 0.001 cm to 2.5 cm and at different frequencies. The T_B are computed for the nine soil profiles given in Figure 5. The difference in T_B between the computed T_B and the reference

(a)

(b)
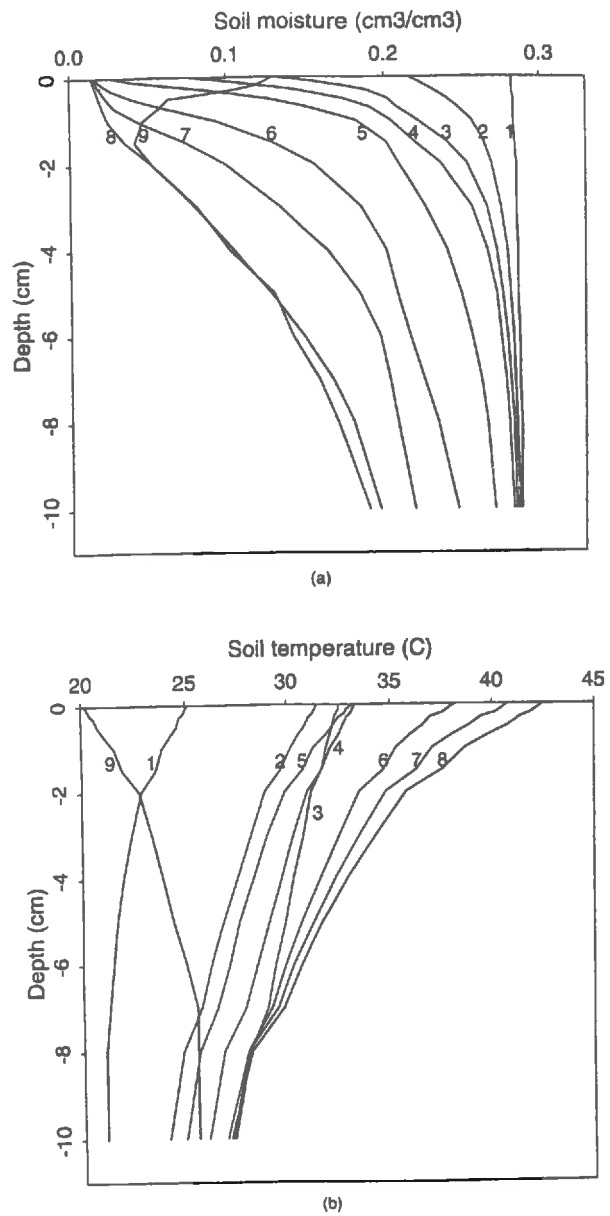
Figure 5. (a) Soil moisture and (b) temperature profiles selected from the outputs of the mechanistic model of soil heat and mass flows. These profiles are used in the sensitivity analysis of the Wilheit model to the description of the soil as a layered media.

T_B is determined for every layer thickness and soil profile. The maximum difference obtained among the nine soil profile cases is plotted against the layer thickness in Figure 6. If the layer thickness is larger than 0.1 cm, the computed T_B differs significantly (> 5 K) than the reference T_B computed with very thin layers. Such a result points out the very strong sensitivity of the Wilheit model to the layer thickness. This sensitivity is partly explained by the high soil moisture gradients
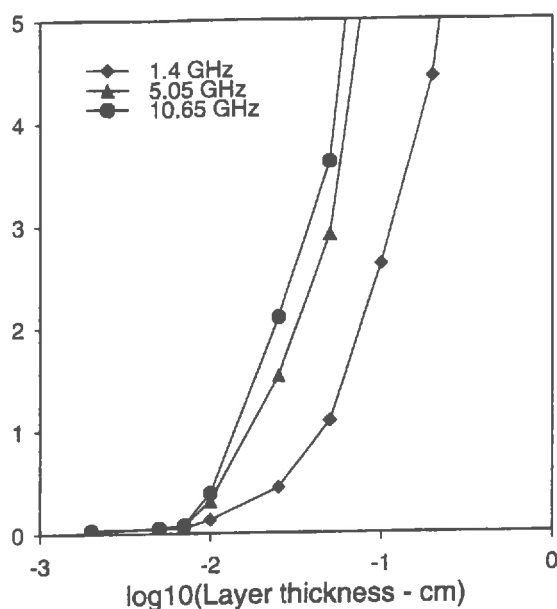
Figure 6. Predicted error in T_B simulated by the Wilheit model induced by the layer thickness. The difference in T_B calculated between the reference T_B and the T_B computed · a given layer thickness. Maximum differences are ob-ned among the results of the nine soil profiles (Figure 5). ie results are obtained in H polarization and with a 20° gle of incidence.

;ar the soil surface, which are responsible for the rong variations of the average soil moisture in the top il layer. Results in Figure 6 also show that the layer iickness should not exceed 0.01 cm if simulated T_B iould not differ from reference T_B by more than 1 K. layer thickness of 0.01 cm is then used for the subse-uent calculations with the Wilheit model.

nil Total Depth
he minimum total soil depth required to compute an stimation of T_B, which is not influenced by deeper yers, is important for establishing the field sampling rotocol. Quantitative assessment of the influence of tal soil depth is presented in Table 1. It is obtained

able 1. Minimum Total Soil Depth (cm) with Which ie Simulated T_B does not present a Difference ;reater than 1 K in Comparison to the Referenced T_B imulated with a Total Soil Depth of 40 cm

Profile number (Fig. 5)	Frequency (GHz)		
	1.4	5.05	10.65
2	2	0.5	0.2
8	5	4	0.2
Average (profile 1–9)	3.45	1.22	0.41

T_B is simulated by the Wilheit model in H polarization and for 20° ingle of incidence.

by comparing results obtained on the nine soil moisture profiles (Figure 5) with different total soil depths (from 0.25 cm to 40 cm) to the reference T_B. The depths reported in Table 1 correspond to a threshold below which the soil contribution to the total T_B does not influence T_B to more than 1 K. Such a depth threshold is close to the penetration depth concept. Therefore, our results are consistent with the theory that predicts a penetration depth between λ and $\lambda / 10$ (Wang, 1987). In terms of ground-sampling strategy, soil moisture and temperature should be observed at least within the top 5, 4, and 2 cm soil layers to validate the Wilheit model at 1.4, 5.05, and 10.65 GHz, respectively. In our experimental study, we measured the soil moisture in the top 10 cm. With a total depth of 10 cm, the T_B computed by the Wilheit model never differs by more than 0.5 K from the reference T_B.

Characterization of the Soil Layers
There is a gap between the layer thickness chosen to implement the radiative transfer models and the thickness of the layer we are able to sample for moisture measurements. Therefore, we must calculate in each soil layer the moisture and the temperature from a limited number of measurements. This task is usually performed by fitting an exponential function to the measurements done at different depths in the soil (Schmugge and Choudhury, 1981). The profile shape given by the exponential function may be a strong hypothesis to describe the soil moisture and temperature in some situations like a moisture profile after a small rain or a temperature profile in the early morning. Moreover, such methods may lead to unrealistic extrapolation near the soil surface where the gradients are generally very strong. Because the weight of the near-surface water content in the T_B calculation is high, we have to examine carefully how the water content at the soil surface (θ_0) can be related to measurements collected for the 0–0.5 cm layer. From the average soil moisture of the top 5-mm layer ($\theta_{0-0.5}$), θ_0 is inferred using a relationship established on a large set of soil moisture profiles simulated by the mechanistic model of soil heat and mass flow for a silty clay loam soil (Chanzy and Bruckler, 1993). The average soil moisture values in the different layers (0–0.5, 0–1, 1–2, 2–3, 3–4, 4–5, 5–7, 7–10 cm) according to the field sampling condition are extracted from the simulated profiles (Figure 5). To reproduce the continuous soil moisture profile from the extracted point values, two options are compared. It is computed either by a linear interpolation between the observations (Option 1) or an exponential fitting to the observations (Option 2). Differences between the T_B computed according to each option and the reference T_B are calculated to quantify the error associated to the method for retrieving the soil moisture profile. The error is found to be randomly scattered

Table 2. Error in T_B (Computed by the Wilheit Model) Induced by the Interpolation Method Used to Characterize the Soil Moisture Profile

Interpolation Method	*1.4 GHz* *Mean / Max (K)*	*5.05 GHz* *Mean / Max (K)*	*10.65 GHz* *Mean / Max (K)*
Linear interpol.	1.49 / 2.57	3.1 / 8.3	0.8 / 2.4
Exponential fit.	4.42 / 11.1	5.1 / 10.1	2.6 / 5.6

The results were obtained from the nine simulated profiles (Fig. 5) at an angle of incidence of 20° and in H polarization.

with both methods and results are summarized in Table 2. It shows that the error can be higher than 10 K. Linear interpolation appears to be much better than exponential fitting, especially at 1.4 GHz. Linear interpolation and exponential fitting to determine soil temperature profiles were also analyzed and both led to similar results. In addition to this source of error, we also considered the accuracy ($\pm$ 0.5 cm) in the temperature probe depth. Both sources of error led to the total error in T_B calculation of lower than 0.5 K based on the nine temperatures profiles displayed in Figure 5.

Implementation of the Microwave Emission Models and Resulting Errors

Wilheit model results presented in the following sections were obtained by using a 0.01-cm layer thickness and an 8.5-cm total depth, which corresponds to the center of the deepest sampling layer. Soil moisture profiles were calculated according to Option 1, whereas temperature profiles were estimated by fitting an exponential function to the experimental data. The different error sources that can affect the comparison between observed and simulated T_B by the microwave emission models (Wilheit and Fresnel) are quantified in Table 3. Errors associated to the implementation of the Wilheit model are established as previously by comparing the calculated T_B for the nine soil profiles (Figure 5) to the reference T_B. Experimental errors were determined from the maximum standard deviation obtained on soil

moisture measurements (Figure 1a) and from PORTOS accuracy. We did not consider the error associated with the dielectric constant determination. Nevertheless, this error term would support the following conclusions. The sum of all errors reported in this table would represent an unrealistic case. Nevertheless, in this table the most striking feature is the very large range of acceptable T_B computed by the emission models with ground measurements when they are compared to the microwave measurements.

Validation and Comparison of the Microwave Emission Models

The T_B simulated by the Wilheit model are plotted against the measurements collected during the whole experiment in H polarization and with incidence angles of 20°, 30°, and 40° (Figure 7). Below 10°, the measurements are contaminated by the reflection of the antennas. Therefore we have neglected the small incidence angles for the evaluation of the microwave emission models. The predictions of T_B by the Wilheit model are satisfactory when error analysis summarized in Table 3 is accounted for. Thus, there is no reason to reject the Wilheit model statistically. Best results are obtained at 1.4 GHz frequency, which have the deepest penetration depth. It can be noticed in Figure 7 that the simulated T_B are lower than the measurements in wet condition at

Table 3. List of the Error Contributions that affect the Comparisons between T_B simulated by the Wilheit or Fresnel Models and those observed by a Radiometer

Error origin	*Error in T_B (K)*		
	1.4 GHz	*5.05 GHz*	*10.65 GHz*
Implementation of the emission model (Wilheit model only)			
Layer thickness (0.01 cm)	0.13	0.33	0.39
Total soil depth (8.5 cm)	0.5	0.05	0.02
Soil moisture profile (linear Int.)	2.57	8.27	2.4
Soil temperature profile	0.5	0.5	0.5
Total	3.7	9.15	3.31
Experimental errors (Wilheit and Fresnel models)			
Ground soil moisture measurements	14	14	14
Radiometer	7.5	2	2

Errors are given either by the maximum error encountered with the 9 soil profiles (Fig. 5) for the errors associated with the model implementation, or by two standard deviations for experimental errors.
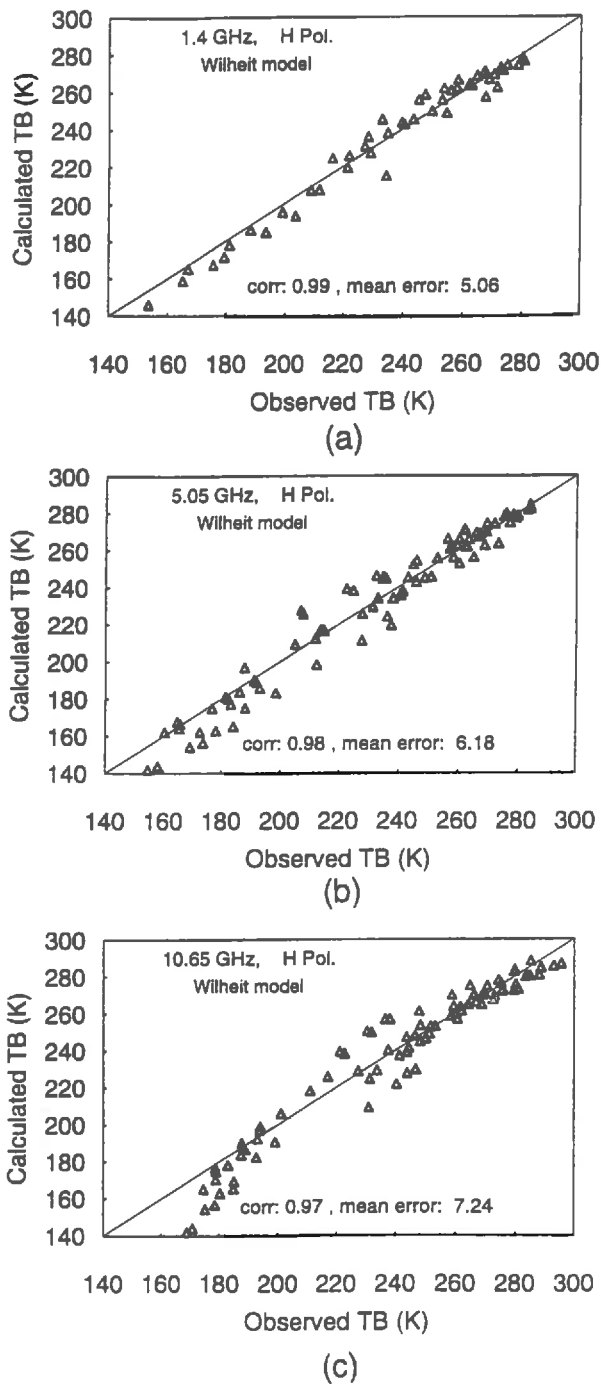
Figure 7. Simulated T_B by the Wilheit emission model versus observed T_B measured by PORTOS at (a) 1.4, (b) 5.05, and (c) 10.65 GHz. Incidence angles of 20°, 30°, and 40° are selected in the comparison.

all frequencies. Errors in the estimation of the dielectric constant from the soil moisture modeled by the Dobson semi-empirical model could be one explanation of such underestimations.

Comparison of the estimation performances of both the Wilheit and Fresnel models are reported in Table 4. With the Fresnel model, the sampling depths that lead to the best comparisons between simulated and measured T_B in both polarizations are 2.5, 1, and 0.5 cm at 1.4, 5.05 and 10.65 GHz, respectively. These sampling depths are consistent with Wang's (1987) conclusions. When the sampling depth is set to the best value, the improvement brought by a multilayer approach is only significant at 1.4 GHz in H polarization. The value of using the Wilheit model becomes less evident with increasing frequency. Moreover, better simulation results are obtained with the Fresnel model at 10.65 GHz. It must be reminded that the results presented in Table 4 are obtained from the experimental data that were mostly collected during the 10 A.M.–4 P.M. period. Therefore, Table 4 shows the daily variations of the soil microwave emission could be estimated with the Fresnel model implemented with an adequate sampling depth. This conclusion may be revised with the estimation of the diurnal variations in T_B, however, which will be analyzed in the next sections.

SIMULATION OF T_B DIURNAL VARIATIONS

Comparison of Wilheit and Fresnel Microwave Emission Models

Hourly T_B were computed by the Fresnel and Wilheit models using the soil temperature and moisture profiles simulated by the mechanistic model of soil heat and mass flows. The Fresnel model was run with the previously defined optimal sampling depths. Only results at 1.4 and 10.65 GHz are displayed in Figure 8. Results obtained at 5.05 GHz, however, which will not be displayed in this paper, present an intermediate case between 1.4 and 10.65 GHz. At 10.65 GHz, the results of both models are similar. Conversely, the predicted T_B by the Wilheit and Fresnel models at 1.4 GHz are only in good agreement in the warming period of the day, whereas they differ from one another by 5 to 15 K from the mid-afternoon to the early morning. Moreover, when the soil gets dried, the diurnal amplitude in T_B simulated by the Wilheit model is smaller and the maximum in T_B appears 1–2 hours later than with the Fresnel model. Analysis of the results presented in Figure 8 leads to the following conclusions:

1. At 10.65 GHz, the Wilheit and Fresnel model results are similar whatever the time of the day. This indicates that there is no significant advantage at this frequency of using an emission model based on soil described as a layered media.
2. At low frequency, that is, 1.4 GHz, results of the Wilheit model differ from those simulated by the Fresnel model during some period of the day.

Table 4. Results of the Linear Regression between Simulated and Measured T_B in Horizontal (H-Pol) or Vertical (V-Pol) Polarizations with Angles of Incidence of 20°-, 30°-, and 40°

Frequency (GHz)	Model	Slope (K/K) H-Pol	Slope (K/K) V-Pol	Origin (K) H-Pol	Origin (K) V-Pol	Prediction error (K) H-Pol	Prediction error (K) V-Pol
1.4	Wilheit	1.05	0.89	−13.2	32.2	5.06	10.48
	F-0.5	1.05	1.07	−5.2	−3.02	12.22	14.42
	F-2.5	0.90	0.91	21.2	30.0	6.58	9.52
	F-5.0	0.77	0.77	44.9	57.7	14.58	9.97
5.05	Wilheit	1.06	1.10	−14.4	−25.8	6.18	5.73
	F-0.5	1.02	1.07	−3.2	−14.0	6.01	6.19
	F-1.0	0.96	0.99	10.4	3.6	5.76	5.68
	F-2.5	0.83	0.87	34.8	32.3	9.26	7.55
10.65	Wilheit	1.07	1.05	−18.4	−11.5	7.24	6.25
	F-0.5	1.01	0.99	−5.2	3.2	5.69	5.45
	F-1.0	0.94	0.93	8.6	18.5	7.2	5.63
	F-2.5	0.82	0.82	32.3	42.5	12.06	8.09

F-d corresponds to the Fresnel model implemented with a sampling depth of d cm. The prediction error is given by the average of absolute difference between the observed and calculated T_B.

Therefore, by this theoretical approach it can be shown that significant differences in T_B are obtained when the whole soil moisture and temperature profiles are accounted for, instead of considering the soil as a single layer. The curves displayed in Figure 8 indicate that it would be interesting to compare the performances of the two presented emission models with complete diurnal cycle of measured T_B. The amplitude of the T_B diurnal variations and/or the hour of the daily maximum in T_B can be interesting criteria to validate the microwave emission models. Such criteria are less affected by the measurement errors than a validation based on a classical comparison between observed and calculated T_B. Unfortunately, our radiometric continuous acquisitions were not long enough to use these validation criteria for comparing the performance of the Fresnel and Wilheit models.

3. At 1.4 GHz, both the Wilheit and Fresnel models provide similar results between approximately 10 A.M. and 4 P.M. (Figure 8). Most of the PORTOS measurements, which were used to fit the soil sampling depth for the Fresnel model, were collected during this period of the day. The same period of the day is then selected to determine sampling depth from the Wilheit model simulations. Best fit between Fresnel and Wilheit results are obtained with a sampling depth of 2.0 cm, which is close to the depth of 2.5 cm obtained from the experimental data. This points out the relevancy of the Wilheit model and its ability to simulate the soil microwave emission. Figure 9 illustrates the influence of the sampling depth on T_B computed by the Fresnel model. They are plotted against the T_B simulated by the Wilheit model. Three sampling depths (0.5, 2.0,

and 5 cm) and two periods of the day (10 A.M.–4 P.M. and 0–6 A.M.) are considered. For each period of the day, we have selected the simulated T_B corresponding to soil moisture and temperature profiles of the considered period. For the 10 A.M.–4 P.M. period, results from the Fresnel and Wilheit models are in good agreement with a sampling depth of 2.0 cm. whereas a 0.5-cm sampling depth is optimal for the night period between 0 and 6 A.M.. The sampling depth appears in Figure 9 to be an important parameter of the Fresnel model. The field of validity of the sampling depth is limited to a period of several hours on a given day, however. Variations in sampling depth are likely due to the varying shape of the soil moisture and temperature profiles in the top layers during the day. This means that all factors that influence these profiles, that is, the soil hydrodynamic and thermal properties or the intensity of the climatic demand (Chanzy and Bruckler, 1993), can also influence the sampling depth.

SOIL MOISTURE AND TEMPERATURE PROFILE INFLUENCES ON SOIL MOISTURE ESTIMATION

For operational applications involving microwave radiometry, soil moisture is generally estimated within a single layer by inverting a simple model of soil microwave emission (i.e., from Fresnel or regression models). In the previous sections, soil microwave emission is shown to be dependent on the soil moisture and temperature profiles. This means that for a given θ_s, there is a range of possible T_B values. Therefore, when the soil is considered as a single layer, the accuracy in the soil moisture retrieval depends on the extent of this range of possible T_B. Based on the hourly T_B simulated by the
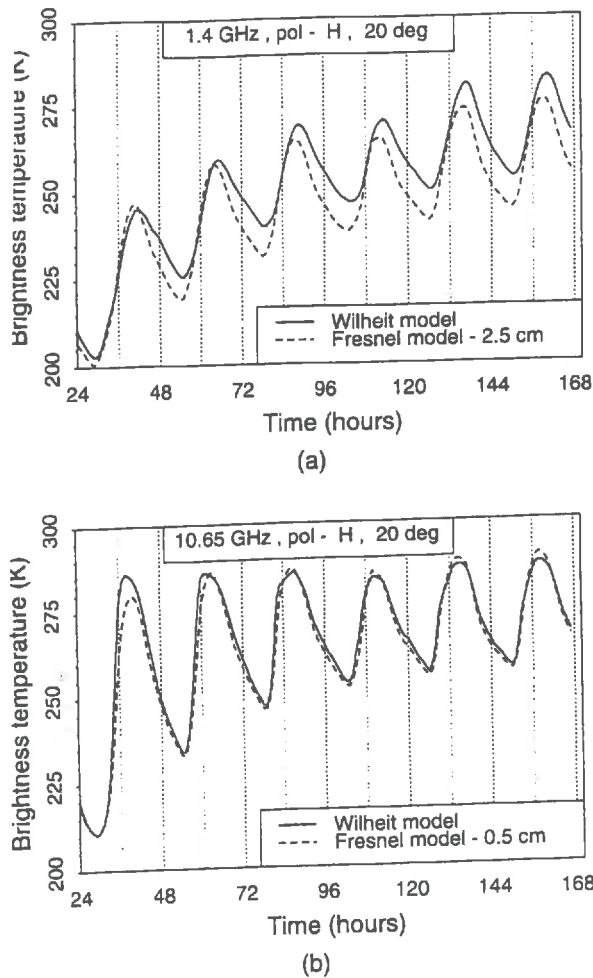
Figure 8. Diurnal evolution of T_B predicted by Wilheit and Fresnel models with a 20° angle of incidence, in H polarization, at (a) 1.4 GHz, and (b) 10.65 GHz. Fresnel model is implemented with 2.5- and 0.5-cm sampling depth at 1.4 and 10.65 GHz, respectively.

Figure 9. Relationships between the T_B simulated by the Fresnel model and those computed by the Wilheit model (1.4 GHz, H polarization, 20°). Fresnel model is implemented with a sampling depth of (a,d) 0.5 cm, (b,e) 2.0 cm, and (c,f) 5.0 cm. The simulated T_B are selected in the following periods of the day: 10 A.M.–4 P.M. (a,b,c) and 0–6 A.M. (d,e,f).

Wilheit model with the outputs of the mechanistic model of soil heat and mass flows (Figure 2), the accuracy in moisture estimation is quantified in Figure 10. The range of ε_s, defined here as $\varepsilon_s = T_B / T_{soil}$, obtained for a given θ_s (in fact within a range of $\theta_s \pm 0.005$ cm³/cm³) is determined for different soil moisture conditions. Because the sensitivity of the ε_s–θ_s relationship is around 1 cm³/cm³ in case smooth bare soil [determined on our experimental results, which confirm results given in Jackson and Schmugge (1989)] the range of ε_s corresponds to the errors in θ_s estimation. Such errors are plotted in Figure 10 at 1.4 GHz and with sampling depth of 2.5 cm. To account for the improvements in θ_s estimation, when the soil temperature is known, we have considered different approaches according to the information available on the soil temperature, such as

(1) $T_{soil} = 300$ K when there is no information on the soil temperature; (2) $T_{soil} = T_{surf}$ where T_{surf} is the soil surface infrared temperature when infrared observations are available at the time of the microwave measurement; or (3) $T_{soil} = T_{eff}$ (Equation 3) when the soil temperature profile is well described.

Best results are obtained when ε_s is calculated with T_{eff}. The soil moisture error for a given average θ_s reaches 0.025 cm³/cm³ in medium wet conditions. This is an estimation of the loss in θ_s accuracy, which is only related to the variation of soil moisture profile shape. When T_{eff} is replaced by T_s, the additional loss in θ_s accuracy is about 0.01 cm³/cm³. This term corresponds to the soil temperature profile effect. Finally, when the soil temperature is neglected we can expect an error in the θ_s determination, which can reach 0.06 cm³/cm³ in dry conditions. θ_s retrievals from observations at 5.05 and 10.65 GHz were found to be more influenced by soil moisture and temperature profile shape. When θ_s is directly related to T_B (the soil moisture profile and the soil temperature are neglected), the error in θ_s reaches 0.10 cm³/cm³ in dry condition.

CONCLUSIONS

The soil microwave emission is strongly affected by the diurnal variation of soil moisture and temperature. For
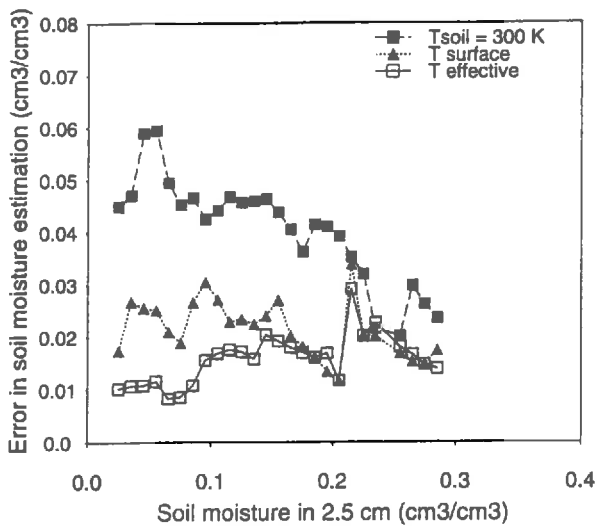
Figure 10. Errors in the estimation of the average soil moisture within the top 2.5-cm layer due to the variations of soil moisture and temperature profiles shape. The figure is based on hourly simulated T_B by the Wilheit model at 1.4 GHz, H polarization, and 20°.

instance, when the soil dries, the magnitude of the diurnal amplitude in T_B may be higher than 50% of the total range of T_B encountered with smooth bare soils. Consequently, it is shown that for a given T_B, there is a range of possible soil moisture values when averaged within a fixed soil layer (θ_s). At 1.4 GHz, when the diurnal cycle is accounted for, the expected loss in soil moisture accuracy is 0.025 cm^3/cm^3 due to the soil moisture profile shape and 0.01 cm^3/cm^3 due to the temperature profile. The accuracy in θ_s retrievals is still further degraded if the soil temperature is not accounted for, particularly in dry conditions. Another important consequence of the soil-moisture profile's influence on soil microwave emission is shown experimentally when a dry soil is slightly wetted at the soil surface either after the dew or at the beginning of a rainfall. In such conditions, the T_B are strongly affected by the thin wet layer at 5.05 and 10.65 GHz, whereas the wet layer is not seen at 1.4 GHz. If such results are confirmed by further experiments, we can foresee the difficulties of monitoring soil moisture evolution from night or early morning microwave observations at 5.05 and 10.65 GHz, which are sensitive to the dew.

The optimal sampling depth to implement the Fresnel model has a temporal field of validity that is limited to data collected during a given period of the day. For example, a sampling depth established for data collected during an afternoon period should not be applied to data collected during the night. Such a limitation in the field of validity of the sampling depth is another way to illustrate the consequence of the moisture and temperature profiles on the soil microwave emission. All the factors that contribute to modifying the moisture or temperature profiles will affect the sampling depth. It can be influenced by the surface soil hydrodynamic properties, which govern the water content gradients in the top layers (Chanzy and Bruckler, 1993). Conversely, for soils covered by vegetation, the soil moisture and temperature gradients are reduced by the shadowing of leaves. Therefore, the profile effect on the soil microwave emission is expected to be less important in this case.

Wilheit and Fresnel model performances are compared with the same set of experimental data. Considering the measurement errors of the ground and microwave observations, both models are statistically valid. When the Fresnel model is implemented with its optimal sampling depth, it offers performances in T_B estimations similar to the Wilheit model. The large error in T_B associated with the implementation of microwave emission models can explain the difficulty in evaluating the improvement in T_B estimation brought by a multi-layer approach in comparison to a single-layer approach. However, hourly simulations of T_B by both models exhibit some differences. Therefore, instead of validating the models by observed / simulated data analysis, we can evaluate the models on the temporal patterns of the T_B, such as the time of maximum T_B or the diurnal relative amplitude between frequencies. Such patterns could be powerful criteria to compare different models.

REFERENCES

Bertuzzi, P., Bruckler, L., Gabilly, Y., and Gaudu, J. C. (1987), Calibration and error analysis of gamma-ray probe for the in-situ measurement of dry bulk density, *Soil Sci.* 144:425–436.

Bertuzzi, P., Caussignac, J. M., Stengel, P., Morel, G., Lorendeau, J. Y., and Pelloux, G. (1990), An automated non-contact laser profile meter for measuring soil roughness in-situ, *Soil Sci.* 143:169–178.

Burke, W. J., Schmugge, T. J., and Paris, J. F. (1979), Comparison of 2.8- and 21-cm microwave radiometer observations over soils with emission model calculations, *J. Geophys. Res.* 84:287–294.

Chanzy, A., and Bruckler, L. (1993), Significance of soil moisture with respect to daily bare soil evaporation, *Water Resour. Res.* 29:1113–1125.

Chanzy, A., Schmugge, T. J., Calvet, J. C., Kerr, Y., Van Oevelen, P., Grosjean, O., and Wang, J. R. (1995), Surface

observations from airborne microwave radiometers in HAPEX-Sahel, *J. Hydrol.* (in press).

Costes, F., Raju, S., Chanzy, A., Chenerie, I., and Lemorton, J. (1994), Microwave radiometry on bare soils: Comparison of various emission models of layered media with measurements, *Proc. Geosci. Remote Sensing Symp. (IGARSS 94)*; vol. III, IEEE, Seabrooke, TX, pp. 1579–1581.

Dobson, M. C., Ulaby, F. T., Hallikainen, M. T., and El Rayes, M. A. (1985), Microwave dielectric behavior of wet soils - Part II, Dielectric mixing models, *IEEE Trans. Geosci. Remote Sens.* 23:35–46.

Grosjean, O., and Sand, A. (1994), Etalonnage du radiometre hyperfrequence portos et methode de correction de mesures, *Proc. 6th Internat. Symp. Physical Measurements Signatures Remote Sens.*, CNES, Paris, pp. 513–518.

Jackson, T. J., and Schmugge, T. J. (1989), Passive microwave remote sensing system for soil moisture: Some supporting research, *IEEE Trans. Geosci. Remote Sens.* 27:225–235.

Laguerre, L., Ragu, S., Chanzy, A., Kerr, Y. H., Calvet, J. C., and Wigneron, J. P. (1994), Physical modeling of microwave emission from bare soils. Inter comparison of models and ground data, *Proc. 6th Internat. Symp. Physical Measurements Signatures Remote Sens.*, CNES, Paris, pp. 527–534.

Newton, R. W., Black, Q. R., Makanvand, S., Blanchard, A. J., and Jean, B. R. (1982), Soil moisture information and thermal microwave emission, *IEEE Trans. Geosci. Remote Sens.* GE-20(3):275–281.

Njoku, E. G., and Kong, J. A. (1977), Theory for passive microwave sensing of near surface soil moisture, *J. Geophys. Res.* 82:3108–3118.

Njoku, E. G., and O'Neill, P. E. (1982), Multifrequency microwave radiometer measurements of soil moisture, *IEEE Trans. Geosci. Remote Sens.* 20:468–475.

Philip, J. R., De Vries, D. A. (1957), Moisture movements in porous materials under temperature gradients, *Trans. Ann. Geophys. Union* 38:222–232.

Schmugge, T. J., and Choudhury, B. J. (1981), A comparison of radiative transfer models for predicting the microwave emission from soils, *Radio Sci.* 16:927–938.

Schmugge, T. J., Jackson, T. J., Kustas, W. P., Roberts, R., Parry, R., Goodrich, D., et al. (1994), PBMR observations of surface soil moisture in Monsoon 90. *Water Resour. Res.* 30:1321–1327.

Ulaby, F. T., Moore, R. K., and Funk, A. K. (1982), Microwave remote sensing, active and passive, in Vol. II: Radar Remote Sensing and Surface Scattering and Emission Theory, Addison Wesley.

Wang, J. R., O'Neill, P. G., Jackson, T. J., and Engman, E. T. (1983), Multifrequency measurements of the effects of soil moisture, soil texture, and surface roughness, *IEEE Trans. Geosci. Remote Sens.* 21(1):44–51.

Wang, J. R. (1987), Microwave emission from smooth bare fields and soil moisture sampling depth, *IEEE Trans. Geosci. Remote Sens.* 25:616–622.

Wigneron, J. P., Kerr, Y., Chanzy, A., and Jin, Y. Q. (1993), Inversion of surface parameters from passive microwave measurements over a soybean field, *Remote Sens. Environ.* 46:1–25.

Wilheit, T. T. (1978), Radiative transfer in a plane stratified dielectric, *IEEE Trans. Geosci. Electron.* 16:138–143.

5.2   **PRESENTATION OF PUBLICATION - II**

ESTIMATION OF SOIL MICROWAVE EFFECTIVE TEMPERATURE AT L AND C BANDS

A. Chanzy (1)*, Suresh Raju (1), JP Wigneron (2)

(1) INRA; Unité de Science du Sol, Domaine Saint Paul, Site Agroparc, 84914 Avignon Cédex 9, France.
(2) INRA; Unité de bioclimatologie, Domaine Saint Paul, Site Agroparc, 84914 Avignon Cédex 9, France.

* Corresponding author. Tel : (33) 90 31 61 29, Fax : (33) 90 31 62 44, E-mail : achanzy@avignon.inra.fr

ABSTRACT

The soil microwave effective temperature (T_e) is an important parameter, which improves the accuracy of the soil surface moisture derived from low frequency microwave radiometric observations. A new semi empirical model of T_e at L- and C-bands is proposed. The model is based on the following inputs: the air temperature (T_a), a deep soil temperature (T_d) and the microwave brightness temperature measured at X band ($\lambda \cong 3cm$) and V polarization (T_{BXV}). Unlike to other approaches based on the surface temperature (T_s), the proposed model can be implemented without being dependent on the clear sky conditions required to measure T_s whith a spaceborne infrared radiometer. However, the proposed model may also use T_s, when available. The model was designed from a large data set simulated by a physical model for a smooth bare soil. The model of T_e was then successfully validated with experimental data acquired during a ground based experiment with the multifrequency PORTOS radiometer. This model designed from smooth soil data, was successfully tested on a rough bare soil using experimental data.

I. INTRODUCTION

It has been shown during the past two decades that microwave radiometry is a suitable method for estimating soil surface moisture [1]. In the microwave spectral domain, frequencies lower than 10 GHz present several interesting properties. The small atmospheric contribution to the brightness temperature (T_B) observed from space is an advantage to record the multitemporal series of observations required for hydrological or climatic applications. Moreover, Chanzy and Bruckler [2] have stressed the importance of the low microwave frequencies to infer soil evaporation from soil surface moisture. They have shown that soil evaporation can be accurately estimated, if soil moisture is determined within a surface layer of at least two centimeter depth. This is only possible at L- and C-bands. Several airborne sensors currently operate at L-band [3], [4], [5], however the lowest frequency of the future spaceborne Multifrequency Imaging Microwave Radiometer (MIMR), will be at C-band. The present paper is therefore limited to these frequency bands, which are expected to be widely used in the future.

In the microwave frequency domain, the energy emitted by the soil is proportional to the thermodynamic temperature (Raleigh Jeans' approximation). The microwave brightness temperature can be written as :

$$T_B = e \cdot T_e \tag{1}$$

where e is the soil emissivity and T_e the effective soil temperature. Soil surface moisture can be derived from T_B, due to the soil emissivity dependence on soil moisture. To infer the soil moisture from T_B, it is therefore necessary to estimate T_e (see equation 1). For instance, we have found from data covering diurnal variations of soil moisture and temperature during a dry

summer period [6], that the errors in soil moisture estimation are reduced by 0.05 m^3/m^3, when T_e is accounted for.

T_e can be computed precisely from soil moisture and temperature vertical profiles. However, such profiles are difficult to assess from remote sensing and in situ measurements are only collected at a few locations. To overcome this difficulty, different estimations of T_e can be used. The rougher estimate is to set T_e equal to a prescribed temperature, which is assumed to be representative of the studied area at a given period [7]. Such an estimate is merely a way to normalize T_B. When thermal infrared observations are available, T_e can be estimated by the surface temperature (T_s) [8]-[10]. Nevertheless, Choudhury et al. [11] have shown a poor relationship between T_e and T_s at frequencies lower than 10 GHz. They proposed a simple model of T_e based on T_s and a deep soil temperature (T_d). This model (hereafter referred to as Choudhury's model) is probably the most tractable model for estimating T_e at low frequency. The Choudhury's model was successfully validated on a wide range of moisture and temperature profile conditions, but only with one soil. Moreover, the model, based on T_s, is dependent on the availability of infrared observations, which are only possible under clear sky conditions when using spaceborne sensors. The availability of infrared observations is thus limited in many areas of the world.

In this paper we propose a new model for estimating T_e which can be implemented when T_s is not available. Hence, other temperature measurements are used to compute T_e i.e. the air temperature (T_a), a deep soil temperature (T_d) and a measurement of T_B. With the latter the choice of the frequency is important. To infer information about soil temperature from a microwave observation, we need a microwave measurement configuration that both maximizes the soil emissivity and minimizes its temporal variations. To reach these requirements, the small penetration depth of the microwave radiations at a high frequency is an interesting property. Indeed, during a drying sequence, the soil moisture near the surface (<0.5 cm) decreases

quickly down to a constant moisture content, whereas drying is more gradual in a deeper layer (>1cm) [2]. Thus, during a drying sequence, the soil emissivity reaches its maximum value more quickly at high frequency. The X-band is then chosen as being the highest microwave frequency which remains slightly disturbed by the atmosphere. Furthermore, several airborne radiometers and MIMR operate at X-band [9]-[10]. To maximize the emissivity, vertical polarization (V) is selected. The proposed model of T_e is then based on four temperatures: T_a, T_B at X band and V polarization (T_{BXV}), T_d and T_s, when the latter is available.

II. PARAMETRIC EQUATIONS

From the radiative transfer theory, T_e can be expressed as :

$$T_e = \frac{1}{\cos(I)} \int_{-\infty}^{0} T(z) \cdot \alpha(z) \cdot \exp[-\int_{z}^{0} \alpha(z') / \cos(I) \cdot dz'] dz \tag{2}$$

where $T(z)$ is the soil temperature at depth z and I the angle of incidence. $\alpha(z)$ is the attenuation coefficient related to the soil dielectric properties by the following approximation:

$$\alpha(z) \cong \frac{4\pi}{\lambda} \varepsilon''(z) / (2\sqrt{\varepsilon'(z)}) \tag{3}$$

where λ is the wavelength and $\varepsilon'(z)$ and $\varepsilon''(z)$ are the real and imaginary parts of the soil dielectric constant. The integral in equation (2) can be written in the following form :

$$T_e = \int_{-\infty}^{0} T(z) \cdot g(z) \cdot dz \tag{4}$$

where $g(z)$ is defined as :

$$g(z) = \alpha(z) / \cos(I) \cdot \exp[-\int_{z}^{0} \alpha(z') / \cos(I) \cdot dz'] \tag{5}$$

The function g(z) is a temperature weighting function which represents the contribution of each soil layer to the total effective temperature T_e. The integral of $[g(z) \cdot dz]$ from 0 to $+\infty$ is equal to 1. In this study, we propose a model of both $T(z)$ and $g(z)$ based on T_d, T_a, T_{BXV} and T_s, when the measurement of T_s is available. The integral in equation (4) could be then calculated from the estimates of $T(z)$ and $g(z)$.

III. DATA COLLECTION

To propose a model of T_e, which is as general as possible, we needed a data set covering different soil and climate conditions. We have shown in [6] that such a data set could be simulated by combining a soil heat and mass flow mechanistic model [2] with the soil microwave emission model developed by Wilheit [12] for smooth bare soils. The soil heat and mass flow model simulates the hourly variation of the soil moisture and temperature vertical profiles under various conditions of climate and soil hydraulic and thermal properties. The so simulated profiles are then used to compute T_B with the Wilheit model. With such combination of models, the hourly variations of T_B can be simulated from a sequence of climatic data, a description of the soil physical properties (dielectric and transfer properties) and initial conditions of soil moisture and soil temperature. In this study, four climatic sequences of 20 days (hereafter referred to as « February », « May », « July » and « September ») covering the different seasons of the year in a Mediterranean area [13] and three soils were selected [2]. The soils presented contrasted texture composition and hydrodynamic properties. The « Loam » (10.5% clay and 38.8% sand) and the « Clay » (47.4% clay and 12.5% sand) had the highest and the lowest soil hydraulic conductivity, respectively. The « Silty Clay Loam (SCL) » (27.2% of clay, 11% of sand) wass intermediate, which was representative of the experimental field where the PORTOS radiometric measurements were taken, as described below. The

simulations were all initialized under the same soil water potential conditions (water potential = 1 meter). The influence of the soil texture on the soil dielectric properties was accounted for, in this study, through the Dobson et al. semi empirical model [14].

Experimental data were used to assess the accuracy of T_e estimated by the proposed model. The data were collected during a field experiment in Avignon, France [6]. Microwave data were measured with the PORTOS multifrequency (1.4, 5.05, 10.65, 23.8, 36.5 and 90 GHz) and dual polarized radiometer which was mounted under a crane boom at a height of 20 m. Data from two bare fields were used in this study. The fields differed by their surface roughness. The roughness was measured with a laser profilometer [19] which operated along 2-meter transects. Roughness parameters were averaged from five transects. The first field (SM) was characterized by a RMS height of 2mm and a correlation length of 162 mm, and can therefore be considered as smooth for all PORTOS frequencies. The other field (SR) was rougher with a RMS height of 8 mm and a correlation length of 23 mm.

The measurements were collected in May and June 1993 during periods of 10 to 20 days for each field. These periods were long enough to scan a wide range of soil moisture conditions. Soil moisture and temperature vertical profiles were measured, concurrently to each PORTOS acquisition sequence.

Spaceborne microwave radiometers (SMMR, SSMI or MIMR) operates at a high angle of incidence (>50°). Therefore, the study was limited to data acquired at 40°, which was the highest angle of incidence available during the Avignon 1993 experiment.

IV- DESCRIPTION OF THE PROPOSED MODEL OF T_e

The $T(z)$ and $g(z)$ functions are studied separately in the following sections. Each function was designed to be implemented from the available temperature measurements that are T_a, T_d, T_{BXV}

and T_s. Then, the integral given in Equation 4 is computed from the surface ($z=0$) to the depth $z=z_d$ corresponding to T_d. The depth z_d is chosen large enough to neglect the deeper layer contribution to T_e.

A. Estimation of the soil temperature vertical profile T(z)

We present in this section the method used to retrieve the soil temperature profiles. We explain how the temperature profiles are computed from the available soil temperature information. To retrieve the temperature profile, we have to clarify how T_a or T_{BXV} are related to the soil temperature. Since the microwave radiations penetrate the soil media, the effective temperature at X band for V polarization (T_{BXV}/e_{XV}) is representative of the temperature in the first top centimeters of the soil. Similarly, the soil surface temperature resulting from the surface energy balance is rarely equal to T_a. The depth z, where $T(z)=T_a$, is generally below the soil surface. Consequently, the soil temperature derived from either T_a or T_{BXV} corresponds to a subsurface temperature hereafter referred to as T_{sub}. We then define the significance of T_{sub} and the relationships between T_{sub} and T_a or T_{BXV} more precisely.

Representation of the soil temperature profile. The soil temperature vertical profiles are estimated from T_s, T_{sub} and T_d. T_s is derived from thermal infrared measurements and is representative of the soil temperature at the surface, that is $z=0$. For T_d, we obtained in a preliminary study that z_d should be higher or equal to 20 cm. As a matter of facts, T_e does not vary by more than 0.01 K when the soil layers below 20 cm are considered to compute the integral in Equation 2. The depth for z_d is hereafter set to 50 cm. T_{sub} is analyzed in the next section. We only assume here, that T_{sub} corresponds to the soil temperature at a depth which is located between the surface and z_d.

Two cases are considered for the modeling of soil temperature profiles.

* When T_s is available, temperature profiles are estimated using T_s, T_d and T_{sub} which represent the soil at the depth $z=0$ (surface), $z=z_{sub1}$ and $z=z_d$, respectively (Figure 1). The following exponential function is fitted to these three temperature points :

$$T(z)=T_d + (T_s-T_d) \cdot e^{(A^*z)} \tag{6}$$

where A is the fitted parameter. The function written in Equation 6 is monotonic. Therefore, it cannot be applied properly to all temperature profile conditions (for instance, when there are both positive and negative temperature gradients in the soil). Consequently, if T_{sub} is an extremum among the three temperatures, or if $|T_s-T_{sub}| > 0.5 \cdot |T_{sub}-T_d|$ (to avoid convergence problems in fitting the A parameter, Eq. 6), a linear interpolation is preferred (Figure 1).

* When T_s is not available, the soil temperature is assumed to be constant and equal to T_{sub} in a surface layer whose thickness (z_{sub2}) is determined further (Figure 1). Below, $T(z)$ is given by a linear interpolation from the bottom of this surface layer (z_{sub2}) to z_d.

T_{sub} is a crucial variable in all cases. In the next section, we establish how T_{sub} is inferred from T_a and T_{BXV} and we determine the depths z_{sub1} and z_{sub2} for the temperature profile description.

Definition and determination of T_{sub}. To infer a soil temperature from a measurement of T_{BXV}, it is necessary to know the soil emissivity. Figure 2 shows the variations of the soil emissivity at X-band and V polarization, starting from wet conditions and drying out. The data were simulated by the Wilheit model coupled to the mechanistic model of heat and mass flows in soil [6] for the three soils and under the same climatic conditions. The diurnal variations in emissivity result from the diurnal damping-desiccation cycle, which mainly affects the top soil first centimeters [2]. The evolution of the soil emissivity is also strongly influenced by the soil properties (Figure 2). The much lower emissivity of the loamy soil is attributed to its hydraulic properties. Indeed, the lower initial emissivity is the consequence of a higher water retention of

the loam soil under the water potential initial condition used for all the simulations. The slow increase in emissivity results from a higher hydraulic conductivity: water losses by evaporation near the soil surface are then almost balanced by the upwards soil water flow. The decreasing rate in surface soil moisture is thus reduced for the loam soil.

Figure 2 shows that the microwave emissivity e_{XV} reaches a plateau during the afternoon after two days for the SCL and the Clay, and eight days for the loam. The e_{XV} plateau corresponds to periods when the soil surface is very dry. For this reason, the soil moisture cannot decrease significantly, even under warm and dry climatic conditions. The level of the plateau is constant from one day to another and only small differences are observed between the different soils. Therefore, dry conditions appear to be the most favorable to estimate T_{sub} from T_{BXV}, since e_{XV} can be reasonably estimated by a prescribed value during the plateau periods. Consequently, T_{sub} is defined as the X-band soil effective temperature under dry conditions. According to the results shown in Figure 2, an emissivity of 0.965 is assumed to be representative of the different soils (it varies actually between 0.95 and 0.974). From Equation 1, we can write $T_{sub}=T_{BXV}/0.965$. In wet conditions, soil evaporation is not limited by the water availability. The temperature in the surface layer is then close to the air temperature, whereas it is no more representative of top soil temperature in dry conditions. Therefore, T_{sub} is equal to T_a in wet conditions.

We just showed that T_a and T_{BXV} are complementary for estimating T_{sub}, according to the soil moisture conditions. To take advantage of this complementarity, a threshold between wet and dry conditions has to be defined. We suggest to use the T_{BXV}/T_a ratio as a wetness indicator of the soil surface, since this ratio approximates e_{XV}, which depends on the surface soil moisture. We saw that T_{sub} represents either the soil temperature at z_{sub1} [$T(z_{sub1})$] or the average temperature in the $0-z_{sub2}$ layer [$T(0-z_{sub2})$](Figure 2). To determine z_{sub1}, z_{sub2} and the wetness threshold, we computed the errors defined by $E_1=|T_{sub}-T_{soil}(z_{sub1})|$ and $E_2=|T_{sub}-T_{soil}(0-z_{sub2})|$ for

all the simulated data sets, where $T_{soil}(z)$ is the soil temperature reference given by the mechanistic model of heat and mass flows and where T_{sub} is given by T_a or $T_{BXV}/0.965$. Then, the computed error terms E_1 and E_2 were splitted into groups according to the soil surface wetness conditions identified by the T_{BXV}/T_a ratio. Finally, E_1 and E_2 were averaged within each group. Results shown in Figure 3 are obtained for 4 classes of T_{BXV}/T_a and different depths for z_{sub1} and z_{sub2}. In wet conditions, when $T_{BXV}/T_a<0.94$, the error is the lowest if T_{sub} is estimated from T_a (note that the error for $T_{sub}=T_{BXV}/0.965$ is too high to be plotted in Figure 3). Conversely, in dry conditions when $T_{BXV}/T_a>0.98$, the best estimate of T_{sub} is $T_{BXV}/0.965$. When comparing the results obtained with the [0.94-0.96[and [0.96-0.98[classes of T_{BXV}/T_a (Figure 3), a threshold of $T_{BXV}/T_a=0.96$ is the best value to separate the dry and wet soil surface conditions. Considering the minimum errors given in Figure 3, we suggest the following depths for z_{sub1} and z_{sub2} to define T_{sub} :

if $T_{BXV}/T_a>0.96$ $\qquad$ $T_{sub}=T_{BXV}/0.965$ $\qquad$ and $z_{sub1}=1$ cm, $z_{sub2}=2$ cm $\qquad$ (7a)

if $T_{BXV}/T_a\leq0.96$ $\qquad$ $T_{sub}=T_a$ $\qquad$ and $Z_{sub1}=2$ cm, $z_{sub2}=4$ cm $\qquad$ (7b)

The Equations 7a and b were applied for all the simulated data. Results are shown in Figure 4 where the estimated T_{sub} is plotted against the actual T_{sub} computed from the temperature profiles simulated by the mechanistic model of soil heat and mass flows. Figure 4 is limited to the case with $T_{sub}=T(z_{sub1})$. Similar results are obtained when T_{sub} corresponds to $T(0-z_{sub2})$. In Figure 4, both estimators of T_{sub}, under dry and wet conditions, give good results with a mean error of prediction (defined as E_1) equal to 1.7 C.

B. Estimation of the g(z) function

The g(z) function can be computed theoretically from soil moisture and temperature profiles (Eq. 3 and 5). Examples of g(z) functions are given in Figures 5 a-f. The functions are selected

to show the effects of soil moisture, soil type and frequency on g(z). In Figures 5 a-f, Day 1 corresponds to the wettest soil condition, while Day 15 is the driest day. The curves in Figures 5 a-f have two different shapes, which are similar to those obtained by Njoku and Kong [15]. The curves are either exponential from the surface to z_d (curve of type 1) or first start by a peak and then decrease exponentially (curve of type 2). The increase in g(z) near the surface can be explained by the strong soil moisture gradients when the soil is drying. Indeed, g(z) (Eq. 5) is the product of two terms: the attenuation term $\alpha(z)$, which increases with soil moisture and an exponential term, which decreases with both soil moisture and depth. Thus, for a drying soil with a moisture increasing with depth, the increase in $\alpha(z)$ is partially or fully balanced by the decreasing trend of the exponential term. Consequently, the curve of type 2 mainly concerns dry soils whith a strong moisture gradient near the surface.

For a given soil, the value of g(z) near the surface increases as the soil wetness conditions and frequency increase (Figure 5 a-f). The g(z) functions are also affected by the soil type, that influences the magnitude of g(z) near the surface and the peak amplitude. For instance, the g(z) peaks are less pronounced with the loam soil since the moisture gradients of this soil are smaller. Soil texture also affects the g(z) function through the dependence of $\alpha(z)$ on the soil dielectric properties.

From the analysis of Figures 5 a-f, we propose a simple model to estimate g(z) which accounts for the effects of soil moisture, soil texture and frequency.

   * The curve of type 1 corresponds to wet soils with small moisture gradients. As for the retrieval of the soil temperature profile, the moisture conditions are considered as wet, when $T_{BXV}/T_a \leq 0.96$. The g(z) function is expressed by an exponential function (Figure 6), whose integral from z=0 to $+\infty$ is equal to 1 :

$$g(z) = g(0) \cdot \exp[-g(0) \cdot z] \tag{8}$$

where $g(0)$ is the value of $g(z)$ at the soil surface, and z is the depth given positively. The determination of $g(0)$ will be discussed further.

     * The curve of type 2 is applied for dry conditions when $T_{BXV}/T_a > 0.96$. The peak is represented by a parabolic function whereas an exponential function describes the decreasing portion of $g(z)$ (Figure 6). The parabolic function is determined from $g(0)$, the peak magnitude (g_m) and the peak location (z_m). The link between the parabolic and the exponential functions is set arbitrarily at a depth of $z=2z_m$. Considering that the integral of $g(z)$ from $z=0$ to $+\infty$ must be equal to 1, we obtain the following equations for $g(z)$:

if $z \leq 2 \cdot z_m$:

$$g(z) = a_2 \cdot z^2 + a_1 \cdot z + a_0 \tag{9}$$

with

$$a_0 = g(0) \tag{10a}$$

$$a_1 = -2 \cdot [g(0) - g_m]/z_m \tag{10b}$$

$$a_2 = [g(0) - g_m]/z_m^2 \tag{10c}$$

if $z > 2 \cdot z_m$:

$$g(z) = g(0) \cdot \exp[b \cdot (z - 2 \cdot z_m)] \tag{11}$$

where

$$b = \frac{g(0)}{(\int_0^{2 \cdot z_m} g(z) \cdot dz) - 1} = \frac{g(0)}{8/3 \cdot a_2 \cdot z_m^3 + 2 \cdot a_1 \cdot z_m^2 + 2 \cdot a_0 \cdot z_m - 1} \tag{11a}$$

It should be noticed from Equations 8 to 11 that the $g(z)$ model is based on three parameters ($g(0)$, g_m and z_m) which have to be determined.

From Equation 5, $g(0)$ is equal to $\alpha(0)$ which is a function of the soil surface dielectric constant (Eq. 3). To estimate $g(0)$, the following relationship is then proposed :

$$g(0) = C_c \cdot Clay\% + C_s \cdot Sand\% + C_m \, T_{BXV}/T_a + C_0 \tag{12}$$

where Clay% and Sand% are the clay and sand soil fractions (%) to account for the influence of soil texture on the soil dielectric constant. The term T_{BXV}/T_a is an approximation of the soil emissivity. It is introduced into Eq. 12 to account for the soil moisture influence on $g(0)$. C_c, C_s, C_m and C_0 are four empirical coefficients determined from the simulated data sets. We computed T_{BXV} and $g(0)$ from the soil moisture and temperature profiles simulated for the silty clay loam. To enlarge the range of soil textures, the soil dielectric constant was computed from these profiles using five different soil textures. The following soil properties (Sand%, Clay%, Dry bulk density) were used : (10,50,1), (10, 30, 1.2), (20,10, 1.27), (50,10, 1.45) and (30, 30, 1.25). The coefficients C_c, C_s, C_m and C_0 are obtained from a linear regression and results are given in Table I. In this Table, the dry ($T_{BXV}/T_a>0.96$) and wet cases ($T_{BXV}/T_a \leq 0.96$) are separated with two sets of coefficients for each frequency. In Figure 7, the theoretical $g(0)$ is plotted against the $g(0)$ estimated with Eq. 12. The Figure shows that $g(0)$ varies within a large range of values at L-band. These variations are well reproduced by Eq. 12. At C-band, the range in $g(0)$ variations is larger and Eq. 12 still provides a good estimate of $g(0)$ [the mean error is equal to 3.70 and the correlation coefficient (r^2) is equal to 0.96].

The T_e computed by Equations 4, 6-11 has been found to be less sensitive to z_m and $\Delta g = g_m - g(0)$ than to $g(0)$. Moreover, z_m and Δg cannot be defined analytically as $g(0)$ [$g(0) = \alpha(0)$] and the dependence of z_m or Δg under soil wetness conditions is not clear. Therefore, z_m and Δg are set to prescribed values. The best values have been found to be $z_m = 0.5$ cm and $\Delta g = 2$ at both L and C-bands.

V- RESULTS: VALIDATION OF THE PROPOSED MODEL AND CONSEQUENCES FOR SOIL MOISTURE ESTIMATIONS.

The estimations of T_e given by the proposed model (Eqs. 4, 7-12) are compared to the theoretical results (Eqs. 2 and 3) in Figure 8 and Table II. Results with the SCL simulations are plotted in Figures 7a,b,e,f to show the ability of the simple model to estimate T_e through the year (« February », « May », « July » and « September » climate sequences are gathered in the Figures). The estimation of T_e are also evaluated against the experimental set of data collected in the SM smooth field (Fig. 8c,d,g,h). The theoretical T_e for the experimental data set were computed using the measured profiles of soil water content and temperature and the proposed model of T_e was implemented with measured inputs (T_{BXV}, T_a, T_s, T_d). From both simulated and experimental sets of data, the value of T_e estimated by the proposed model are in good agreement with the theoretical values (Fig. 8, Table II). In Figures 8d,h and to some extent in Figure 8c, estimations of T_e by the proposed model present a bias of about 2K. A more thorough analysis of the data has shown that the bias is explained by an underestimation of T_{sub} in the conditions of the experiment. We have to keep in mind that only one set of values for z_{sub1}, z_{sub2} and e_{XV} values is proposed to represent a wide range of soil types, soil moisture and climatic conditions. The range of conditions of the experiment is much smaller and therefore, z_{sub1}, z_{sub2} and e_{XV} are not necessarily optimal for the experimental conditions. However, the magnitude of the average errors is low whatever the data set considered in the study (Table II). The average error is always lower than 10% of the range of values for T_e. The comparison between the two versions of the proposed model, i.e. with T_s and without T_s, shows that the benefit given by the measurement of T_s is not very important. In fact, for the estimation of T_e, the gain in accuracy given by the T_s measurement is lower than 1.5 K (Table II).

We recall that soil surface moisture is one of the main geophysical parameters, which is expected to be derived from microwave radiometry at low frequencies. The estimation of T_e should improve the accuracy in soil moisture retrieval. To evaluate the improvement given by the knowledge of T_e, the scattering of the relationship between soil moisture and T_B/T_e is quantified in Figures 9a-b. To quantify such a scattering, we gathered for a given soil emissivity (in fact within a range of ±0.005) the corresponding surface soil moisture. Then, the extent of the range of these selected soil moistures is plotted against the soil emissivity (Figure 9). The ranges of soil moisture, which are indicative of the accuracy of soil moisture retrieval, were computed using the SCL simulated data set. Three modes of emissivity calculation are compared in Figures 7a-b : 1) $e=T_B/300$ when T_e is not available; 2) $e=T_B/T_e$ with T_e computed using Eqs. 2 and 3; 3) $e=T_B/T_e$ with T_e computed using the proposed model without T_s. The aim of the comparison is to evaluate what we win if T_e is estimated by the proposed model instead of using a prescribed value (300K) and what we lose by using an estimation of T_e instead of its theoretical value.

The importance of the improvement in soil moisture accuracy, obtained when T_e is known, depends on the radiometer configuration. The smallest improvement is obtained at L-band for a horizontal polarization (Figure 9a). However, the improvement in soil moisture estimation is significant in the wet region (volumetric water content > 0.15 m^3/m^3) where all the climatic conditions are represented. In these wetness conditions, the soil moisture estimation error is cut in half. The best improvement in soil moisture accuracy is obtained at C-band and for vertical polarization (Figure 9b) since the soil emissivity is higher than with the other studied radiometric configurations. The high level in emissivity enhances the influence of the soil temperature on the soil microwave emission.

The soil moisture accuracy does not significantly decrease, when T_e is estimated by the proposed model implemented without T_s, instead of using the theoretical T_e (Figure 9a-b). The

residual error in soil moisture estimation, when T_e is accounted for, has been shown to be the consequence of the variations in vertical soil moisture profile shapes [6].

As far as the experimental set of data obtained for the smooth soil SM is concerned, the improvement for soil moisture estimation brought by the estimation of T_e is not significant (results not shown). This can be explained by both the weight of measurement errors and the moderate range of soil temperature conditions encountered during the experiment.

VI DISCUSSION

The encouraging results given in the previous sections are, however, limited to smooth bare soils when every model input is known exactly. The interest of the proposed model will depend on its low sensitivity to the error on the model inputs and its field of validity, which needs to be at least extended to rough soils.

A) Sensitivity of the model to the errors on input data

The sensitivity of the proposed model is quantified by applying an error ΔT to one of the model inputs (T_d, T_a, T_s or T_{BXV}). The resulting $T_e(\Delta T)$ is then compared to T_e computed by the proposed model with exact inputs. $\Delta T_e = |(T_e(\Delta T) - T_e)|$ is computed for the whole set of data simulated for the three soils with the « July » climatic sequence. Results are summarized in Table III, where the average ΔT_e is given for each input variable.

In Table III, the proposed model appears to be the most sensitive to T_{sub} inferred from either T_a or T_{BXV}, whatever the model version used (with or without T_s). Such a high sensitivity to T_{sub} highlights the importance of introducing T_{sub}, which is the main innovation of the proposed model. Hopefully, the errors on T_a and T_{BXV} are expected to be smaller than those for T_d or T_s. T_d can be estimated from the climatic history of the surface observed. Nevertheless, accurate

estimate of T_d cannot be derived from climate observations without accounting for the soil thermal properties, which are difficult to map over large areas. The estimation of T_s with a thermal infrared radiometer requires knowledge of the surface infrared emissivity and the atmospheric contribution in the infrared wavelength region. Even with the recent progress in this field, errors of several K will likely affect the measurement of T_s, especially in the case of bare soils. Conversely, T_a can be fairly well estimated by combining the measurements of the meteorological network and climatic models, and T_{BXV} is only slightly influenced by the atmospheric conditions. Indeed, the atmospheric contributions to the microwave radiations received by a spaceborne radiometer lead to write T_B as following :

$$T_B = \tau \cdot [eT_e + (1-e) \cdot T_{SKY}] + T_{atm} \qquad \qquad 13)$$

where τ is the atmospheric transmission factor, e the surface emissivity, T_{SKY} the sky microwave brightness temperature corresponding to the downward radiations and T_{atm} is the upward contribution from the atmosphere between the surface and the radiometer. If it is placed onboard satellite, $T_{SKY} \cong T_{atm}$ at 10.65 GHz. The computed T_{SKY} of the whole Avignon 93 experiment [16] varied from 6 to 11K at 10.65 GHz and 40°. Assuming that τ is equal to 0.98 and 0.965 (τ values are given in Ulaby *et al.* [20]) for T_{SKY} equal to 6 and 11 K, respectively. The apparent T_B observed from space would be 289.92 and 289.70 K for a surface emissivity of 0.965 and a temperature of 300K. These apparent T_B are very close to the value 289.5 K (300/0.965) obtained when the effects of the atmosphere are neglected. This analysis thus demonstrates the weak influence of the atmosphere on T_{BXV}.

Finally, the errors on T_e estimation (Table III) due to the input error propagation are in the same order than that presented in Table II for the simulated data, which corresponds to the error due to the proposed model simplifications. Moreover, the error propagation is not too critical for implementing the proposed model, since the most sensitive input variables (T_{BXV} and T_a) are easier to obtain accurately than T_d and T_s

B) Effects of soil roughness

To apply the proposed model to rougher soils, we have to consider the following question : to which extent are the $g(z)$ and $T(z)$ functions affected by changes in surface conditions? The increase in soil roughness is generally due to tillage practices, when soils are prepared for seeding. By breaking the continuity between the clods and soil aggregates, such practices lead to a decrease in soil heat and water conductivity within the tilled soil layer. Consequently, soil moisture and temperature gradients tend to be stronger near the soil surface. We discussed above the influence of the soil moisture gradients on the $g(z)$ function, namely the magnitude of the $g(z)$ peak near the surface. In the proposed model, the peak is parameterized by two parameters z_m and $\Delta g = (g_m - g_0)$ (Eqs. 10 and 11), which are set to constant average values established from the simulated sets of data. These values are representative of a wide range of soil moisture gradients, due to the very different soil hydraulic properties and the wide range of climatic conditions used for the simulations. Therefore, the soil moisture gradients of rough soils are likely to fall in the range of the profiles taken for determining z_m and Δg.

How the proposed model accounts for changes in soil temperature profiles remains an open question. Difficulties in the acquisition of T_a, T_d and T_s do not depend on the surface roughness, whereas the relationship between T_{BXV} and T_{sub} could change with the surface conditions. For rough soils, we have to check the validity of an emissivity of 0.965 to infer T_{sub} from T_{BXV}. According to published results [17-18], the emissivity of dry soils is slightly affected by the surface roughness. Therefore, the use of a single emissivity for the different soil roughness conditions seems to be a reasonable assumption. This assumption is confirmed experimentally in Figure 10. In this plot the T_e estimated by the proposed model is plotted against the theoretical T_e in the case of the medium rough field SR, which had a RMS height of 8 mm and a correlation length of 23 mm. In this figure, the performance in T_e estimation with

the proposed model appears to be even better than those obtained experimentally with the smooth field SM. The proposed model was validated for a medium rough field. However, the validity of the proposed model for roughness conditions has to be further investigated for rougher soils.

VII CONCLUSIONS

A new model to estimate the soil microwave effective temperature (T_e) is proposed. Conversely to the Choudhury's model [11], which was the only simple model available to estimate T_e, the proposed model can be implemented without measuring the soil surface temperature (T_s). The main innovation of the proposed model stands in the soil subsurface temperature (T_{sub}) inferred from either the air temperature (T_a) in wet conditions or the microwave brightness temperature at X-band, V polarization and with 40° angle of incidence (T_{BXV}) in dry conditions. When $T_{BXV}/T_a > 0.96$, we have shown that T_{BXV} can provide an estimate of the soil temperature in the vicinity of the soil surface. Beyond the goal of this paper, such a result can be accounted for in studies that deal with the surface temperature estimation using microwave radiometry.

In the proposed model, several parameters need to be established. In order to make the use of the model as general as possible, we propose a set of parameters which was established on a wide range of soil and climate conditions. However, some parameters can be easily updated. For instance, the use of the actual soil emissivity at X-band (instead of using 0.965) of the studied area and/or the actual soil dielectric properties (instead of using Eq. 12) should improve the estimation of T_e.

Very rough soils and soils covered by vegetation were not investigated in this study. They have to be studied in a future endeavor in order to propose a more general method to estimate T_e suitable for all surface conditions.

ACKNOWLEDGEMENTS

REFERENCES

[1] Jackson, T.J. and T.J Schmugge, "Passive microwave remote sensing system for soil moisture: Some supporting research", *IEEE Trans. Geosci. Remote Sensing.* vol. 27, pp. 225 - 235. 1989.

[2] Chanzy, A. and L. Bruckler, "Significance of soil moisture with respect to daily bare soil evaporation", *Water Resour. Res.*, vol 29, pp 1113 - 1125, 1993.

[3] Schmugge, T., Jackson, T.J., Kustas, W.P. and J.R. Wang, "Passive microwave remote sensing of soil moisture: results from HAPEX, FIFE and MONSOON 90", *ISPRS J Photogramm. Remote Sensing*, vol 47, pp. 127-143, 1992

[4] Jackson, T.J., Le Vine, D.M., Griffis, A.J., Goodrich D.C., Schmugge, T.J., Swift, C.T. and P.O' Neill, "Soil moisture and rainfall estimation over a semiarid environment with the ESTAR microwave radiometer", *IEEE Trans. Geosci. Remote Sensing*, vol. 31, pp. 836-841, 1993

[5] Pampaloni, P., Paloscia, S., Chiarantini, L., Coppo, P., Gagliani, S. and G. Luzi, "Sampling depth of soil moisture content by radiometric measurement at 21 cm wavelength: some experimental results", *Int. J. Remote Sensing*, vol 11, no. 6, pp. 1085-1092, 1990.

[6] Suresh Raju, Chanzy, A., Wigneron, J.P.; Calvet J.C., Kerr, Y and L. Laguerre, "Soil moisture and temperature profile effect on microwave emission at low frequencies", accepted in *Remote Sensing of Environ.*, vol 54, no 1, pp. 85-97, 1995.

[7] Schmugge T.J., O'Neill, P.E. and J.R. Wang, "Passive microwave soil moisture research", *IEEE Trans. Geosci. Remote Sensing*, vol 24, no 1, pp. 12-22, 1986.

[8] Schmugge T.J., Wang, J.R. and G Asrar, "Results from the pushbroom microwave radiometer flights over the Konza prairie in 1985", *IEEE Trans. Geosci. Remote Sensing*, vol 26, no. 5, pp. 590-596, 1985.

[9] Paloscia, S., Pampaloni P., Chiarantini, L., Coppo, P., Gagliani, S. and G. Luzi, "Multifrequency passive microwave remote sensing of soil moisture and roughness", *Int. J. Remote Sensing*, vol 14, no 3, pp. 467-483, 1993.

[10] Chanzy, A., Schmugge, T.J., Calvet, .C., Kerr, Y., Van Oevelen, P., Grosjean O. and J.R. Wang, "Surface observations from airborne microwave radiometers in HAPEX-Sahel", *J. of hydrology*, accepted, 1996.

[11] Choudhury, B.J., Schmugge, T.J. and T. Mo, "A parameterization of effective soil temperature for microwave emission", *J Geophys. Res.*, vol 84, pp. 287-294, 1982.

[12] Wilheit, T.T., "Radiative transfer in a plane stratified dielectric", *IEEE Trans. Geosci. Electron.*, vol 16, pp. 138-143, 1978.

[13] Chanzy, A., Bruckler, L. and A. Perrier, "Soil evaporation monitoring: a possible synergism of microwave and infrared remote sensing", *J. of hydrology*, vol 165, pp. 235-259, 1995.

[14] Dobson, M.C., Ulaby, F.T., Hallikainen, M.T. and M.A. El Reyes, "Microwave dielectric behavior of wet soil - Part II: Dielectric mixing models", *IEEE Trans. Geosci. Remote Sens.*, vol 23, pp. 35-46, 1985

[15] Njoku, E.G. and J.A. Kong, "Theory for the passive microwave remote sensing of near surface soil moisture", *J. Geophys. Res.*, vol 82, pp. 3108-3118, 1977.

[16] Calvet, J.C., Wigneron, J.P., Chanzy, A., Suresh Raju and L. Laguerre, "Microwave dielectric properties of Silt-Loam at high frequencies", *IEEE Trans. Geosci. Remote Sens.*, vol 33, no 3, pp. 634-642, 1995.

[17] Newton, R.W. and J.W. Rouse, "Microwave radiometer measurements of soil moisture content", *IEEE Trans. Antennas and Propag.*, Vol. 28, pp. 680-686, 1980.

[18] Wang, J.R., O'Neill, P.E., Jackson, T.J., and T.E. Engman, "Multifrequency measurements of the effects of soil moisture, soil texture and surface roughness", *IEEE Trans. Geosci. Remote Sens.*, vol 21, pp. 44-51, 1983.

[19] Bertuzzi, P., Caussignac, J.M., Stengel, P., Morel, G., Lorendeau, J.Y. and G. Pelloux, "An automated non contact laser profile meter for measuring soil roughness in-situ", *Soil Sci.*, vol 143, pp. 169-178, 1990.

[20] Ulaby, F.T., Moore, R.K. and A.K. Fung, "Microwave remote sensing, vol III, from theory to applications", Artech House, Dedhal, MA., 1986.

CAPTION OF THE FIGURES

Figure 1 : Schematic representation of the retrieved soil temperature profiles for the different temperature profile schemes of the proposed model.

Figure 2 : Hourly variation of the soil emissivity during the day at 10.65 GHz, Vertical polarization and with a 40° angle of incidence. The data are simulated, for the « July » climatic sequence, by combining the Wilheit model of bare soil emission [12] and a mechanistic model of soil heat and mass flows.

Figure 3 : Mean error of prediction of T_{sub} estimated from either T_a or T_{BXV}. The error is computed by class of T_{BXV}/T_a and for different soil depths. In a) T_{sub} is the soil temperature at z_{sub1}; in b) T_{sub} is the average temperature from the surface ($z=0$) to $z=z_{sub2}$.

Figure 4 : Comparison between T_{sub} estimated by Equations 7 and T_{sub} simulated by the mechanistic model of soil heat and mass flows. T_{sub} corresponds to the soil temperature at a depth of z_{sub1}.

Figure 5 : Theoretical g(z) functions computed with Equation 5. The soil moisture and temperature profiles are simulated by the mechanistic model of soil heat and mass flows.

Figure 6 : g(z) function estimated by the proposed model and comparison with theoretical g(z) computed from Eq. 5.

Figure 7 : Comparison of the actual g(0) (Eq. 5) and the estimated g(0) (Eq. 12). The comparison is made with the simulated data used to fit C_s, C_c, C_m and C_0 (Eq 12, Table I).

Figure 8 : Comparison between T_e estimated by the proposed model (with T_s or without T_s) and the theoretical T_e computed by Eq. 5. Figures a-d and Figures e-h correspond to the L-band and C-band, respectively. Figures a,b,e,f present the results from the simulated data set on the silty clay loam soil and with the four climatic sequences. Figures c,d,g,h present the experimental results for the smooth bare soil (SM).

Figure 9 : Accuracy of soil moisture retreived from T_B plotted versus the soil emissivity. The accuracy is given by the extent of the soil moisture range that gives the same emissivity. The range of soil moistures was established on the data sets simulated with the silty clay loam soil and the four climate sequences. Soil moisture is the average in the 0-2 cm and 0-1 cm layer when retrieved from L-band (a) and C-band (b), observations, respectively.

Figure 10 : Comparison between T_e estimated at 1.4 GHz by the proposed model (without T_s) and the theoretical T_e computed by Eq. 5 in the case of the medium rough bare field (SR).

TABLE I
FITTED VALUES OF EQUATION 12 PARAMETERS AND STATISTICAL RESULTS FOR THE ESTIMATIONS OF G(0).

	C_s	C_c	C_m	C_0	r^2	residual standard deviation
L-band - dry condition	-0.1487	0.1528	-159.80	170.92	0.83	2.4
L-Band - wet condition	-0.-2660	0.2331	-43.60	60.95	0.96	1.9
C-Band - dry condition	-0.2023	0.2432	-332.93	348.07	0.84	3.9
C-Band - wet condition	-0.3286	0.3269	-355.01	372.30	0.97	5.8

The values are fitted on the simulated set of data. r^2 and the residual standard deviation were computed from the comparison between g(0) and its estimation from Equation 12.

TABLE II
COMPARISON BETWEEN T_E ESTIMATED BY THE PROPOSED MODELS
AND THE THEORETICAL T_E (EQS. 2 AND 3).

	With T_s		Without T_s	
	Mean Error (K)	r^2	Mean Error (K)	r^2
L-Band				
Loam	1.6	0.79	1.6	0.85
SCL	1.5	0.97	2.0	0.95
Clay	1.3	0.93	2.6	0.94
Experiment	1.8	0.89	2.2	0.88
C Band				
Loam	2.0	0.86	2.1	0.86
SCL	1.5	0.98	2.3	0.95
Clay	1.1	0.96	2.3	0.95
Experiment	1.6	0.90	2.2	0.87

The mean error was determined with the absolute value of the difference between the estimated and the theoretical T_e. r^2 is the correlation coefficient.

TABLE III
SENSITIVITY OF THE PROPOSED MODEL TO THE INPUT ERRORS.

Input Temperature Considered	ΔT (K)	Averaged ΔT_e	
		Simple Model (With T_s)	Simple Model (Without Ts)
T_d	+2	0.44	0.13
T_d	+4	1.06	0.25
T_d	+6	1.51	0.38
T_a	+2	1.04	1.28
T_a	+4	2.16	2.72
T_a	+6	3.47	4.28
T_s	+2	1.04	0.00
T_s	+4	1.51	0.00
T_s	+6	2.02	0.00
T_{BXV}	+2	1.68	1.42
T_{BXV}	+4	3.42	2.98
T_{BXV}	+6	5.00	4.65

The averaged ΔT_e is obtained from the simulated data sets including the three soils. ΔT_e is defined as the absolute value of $T_e(\Delta T) - T_e$.

figure 1

figure 2

figure 3

Estimated Tsub (C)

figure 4

Tsub=Tbxv/0.965
Tsub=Ta

Regression results
slope = 0.93
intercept = 2.2
R2 = 0.96
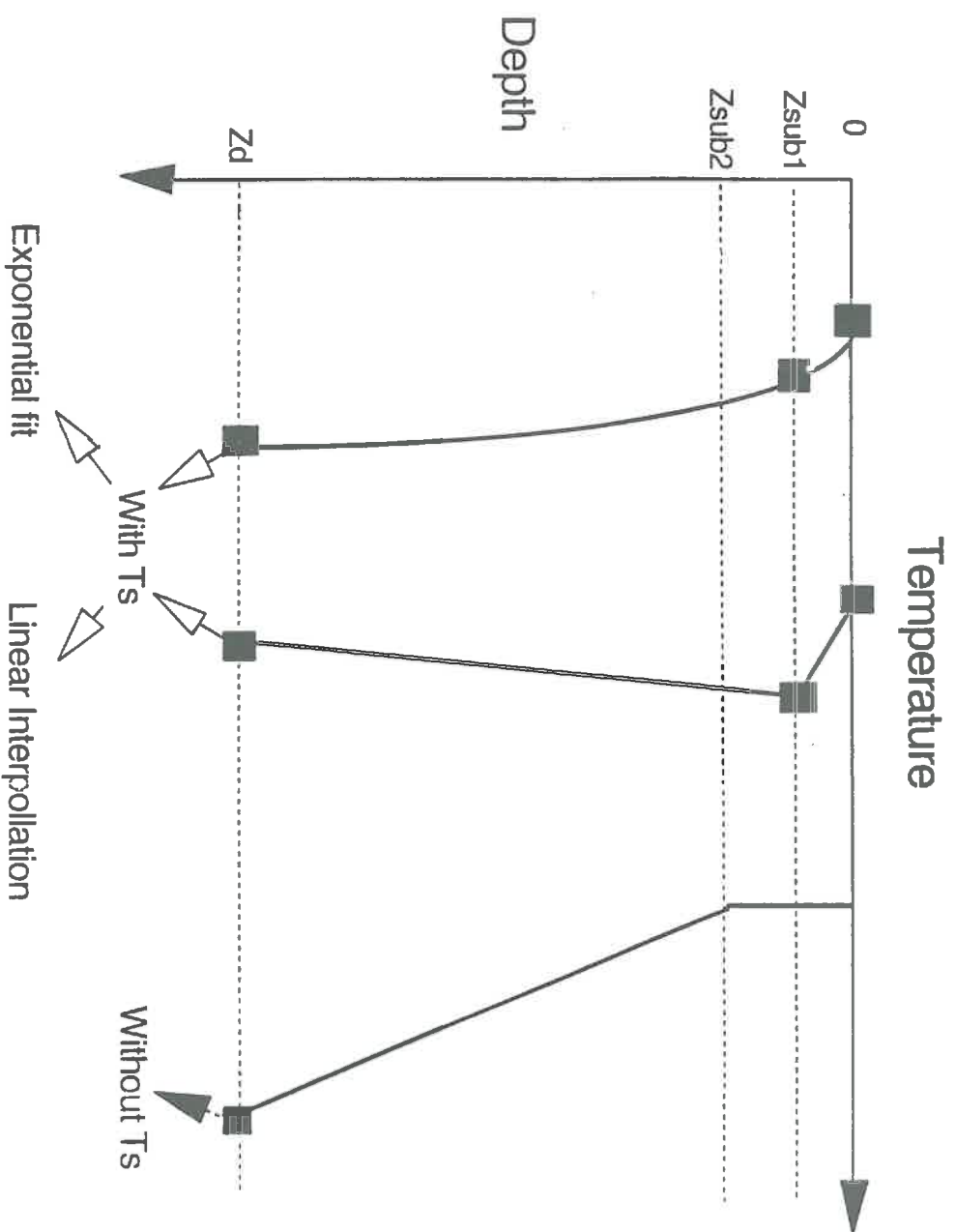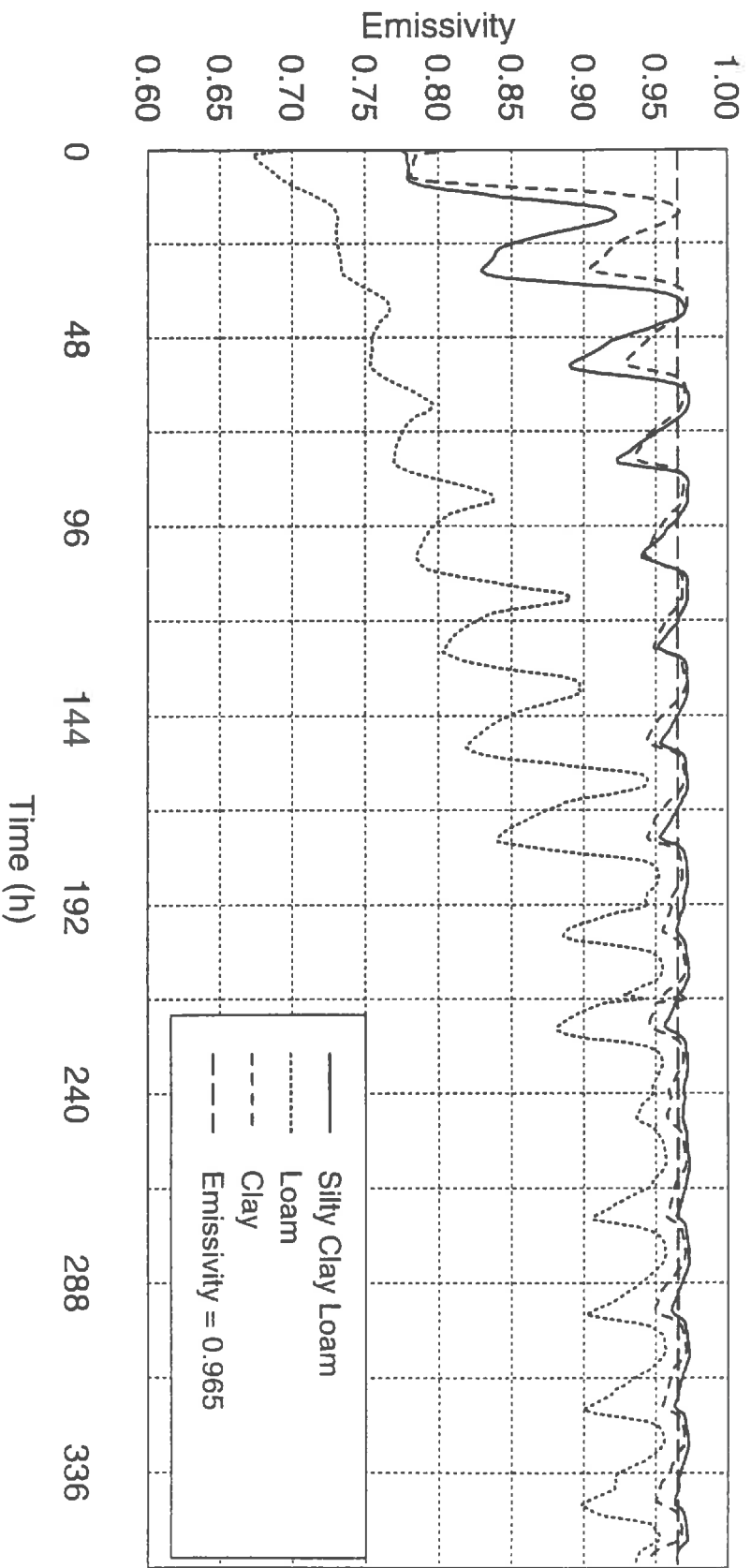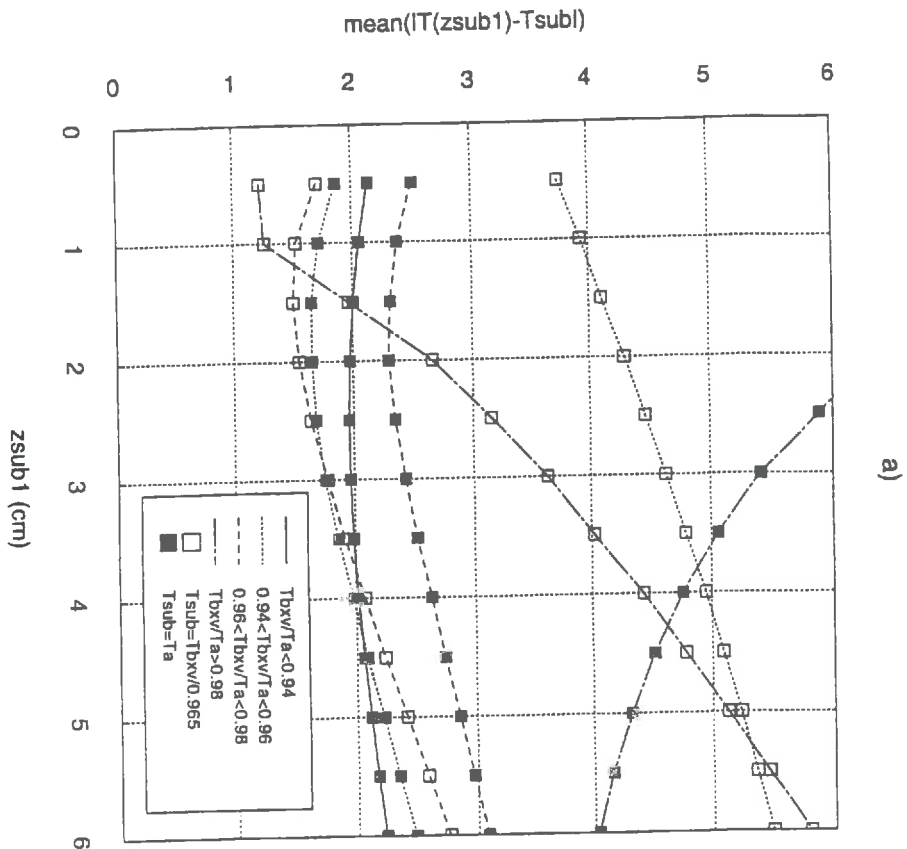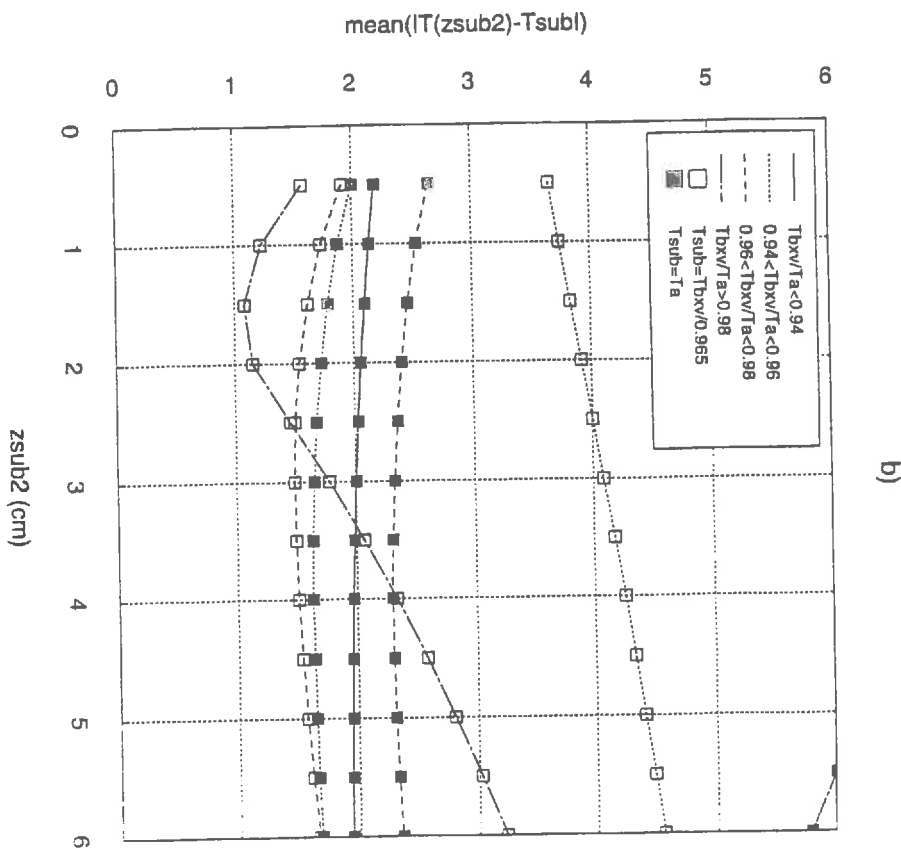
figure 5

figure 6

figure 7

Estimated g0

Actual g0

Tbxv/Ta>0.96 (Dry)
Tbxv/Ta<0.96 (Wet)

mean error = 1.8
r2 = 0.85
L-band
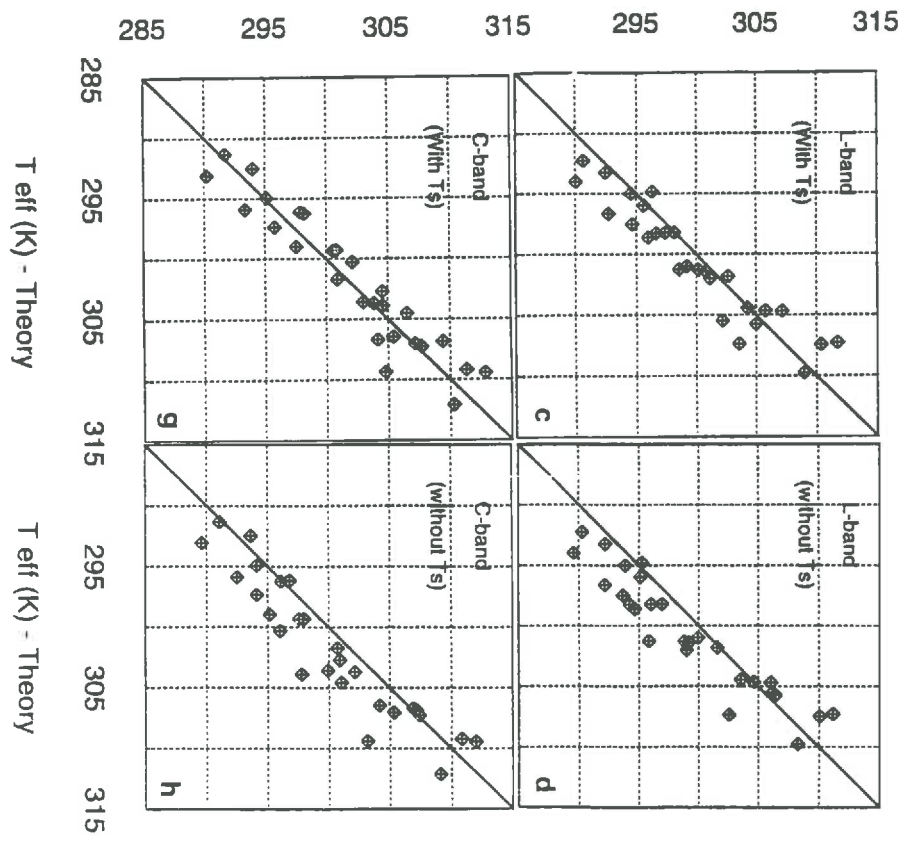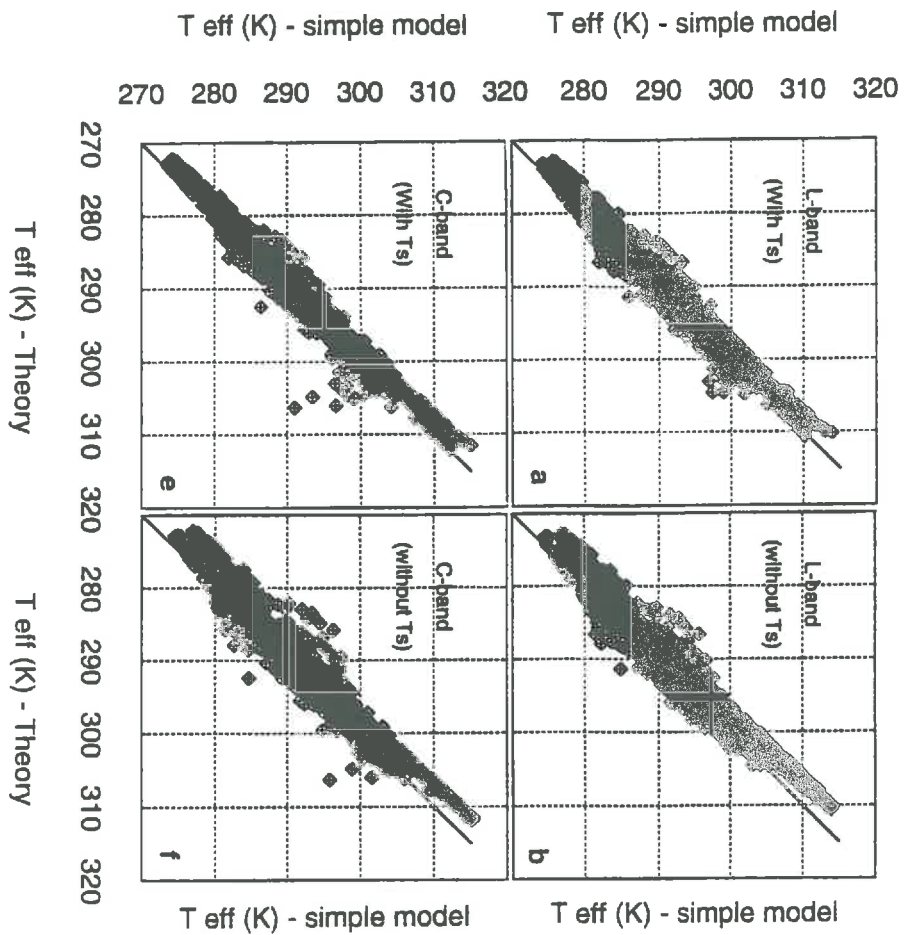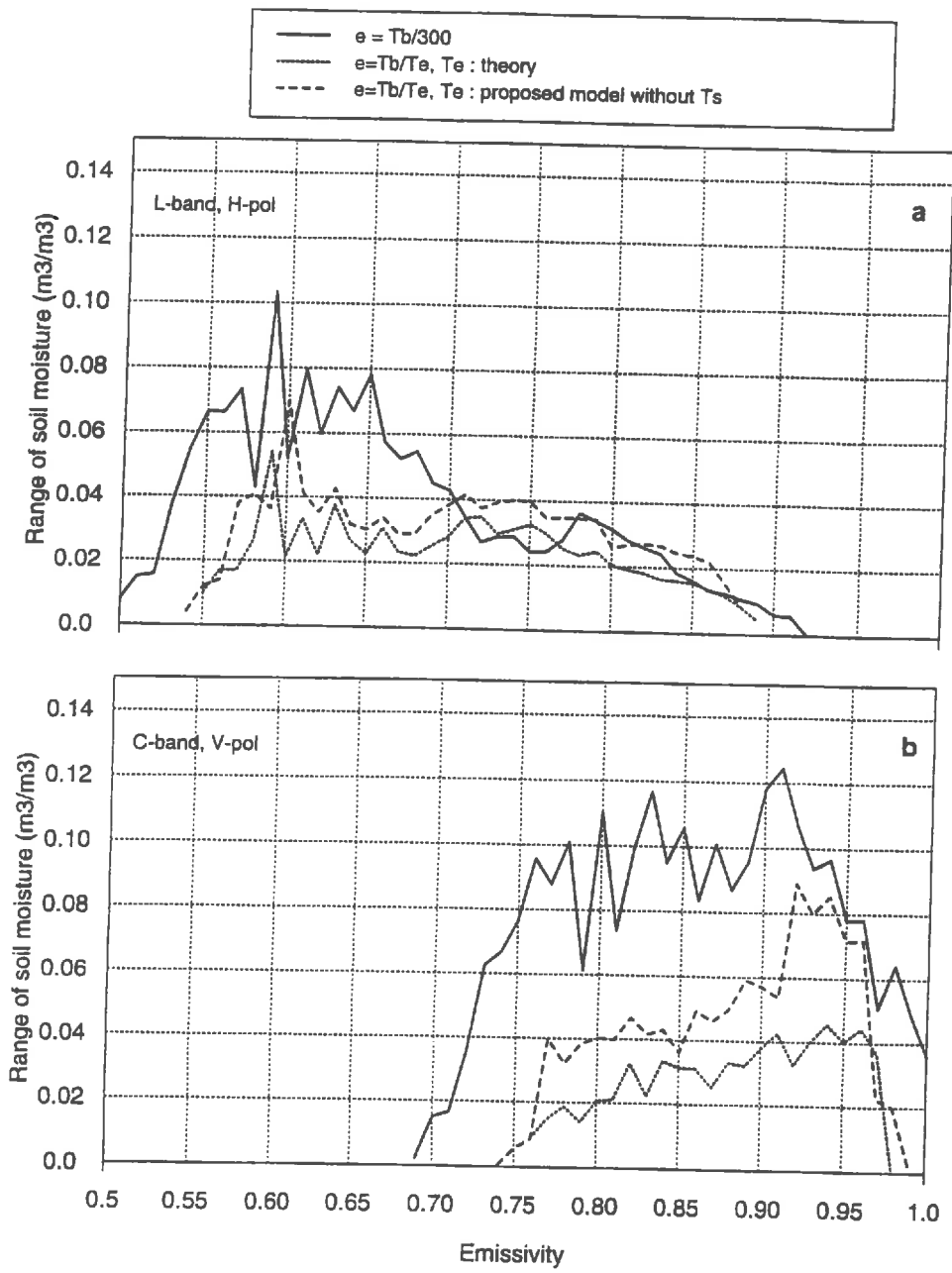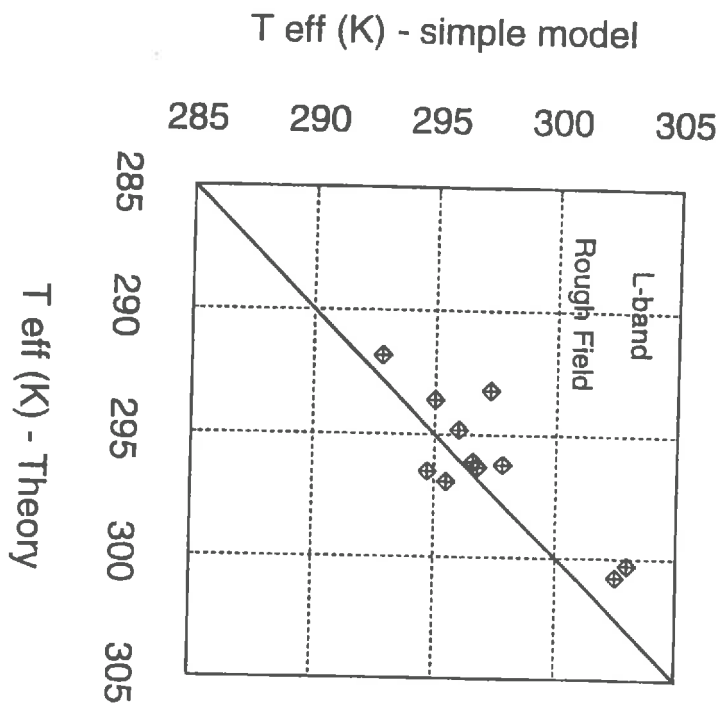
figure 8

figure 9

figure 10

GENERAL CONCLUSIONS

General Conclusions

In this study, microwave emission models from layered media were evaluated against experimental data. We confirm that the both coherent models (the Njoku model and the Wilheit model), give similar results. Conversely, the results of the coherent models differed significantly to those given by the incoherent model (Burke model) in dry condition. With the Burke model, the surface layer strongly influences the results. To obtain reasonable results, we have to fit the layer thickness of the surface layer. This is in contradiction with the interest of emission models from layered media that should be implemented without fitting any parameter. Consequently, we chose the Wilheit model and it was coupled to a mechanistic model of soil heat and mass flows. The mechanistic model simulates the evolution of the soil moisture and temperature profiles, which are then used as inputs in the Wilheit model. This coupling allowed the simulation of diurnal T_B evolution. We analyzed the diurnal T_B evolution to study:

* the influence of the soil moisture and temperature on the soil microwave emission;

* the influence of the climatic conditions on the "T_B - surface soil moisture relationship" to account for the diurnal and seasonal cycles in soil moisture and temperature profiles.

* the influence of the soil hydraulic and dielectric properties on the "T_B - surface soil moisture" relationship.

We estimated the total error which can be encountered in the comparison between layered model and experimental data. Through this error analysis, we can also estimate the optimum model parameters that are necessary to tune the layered model 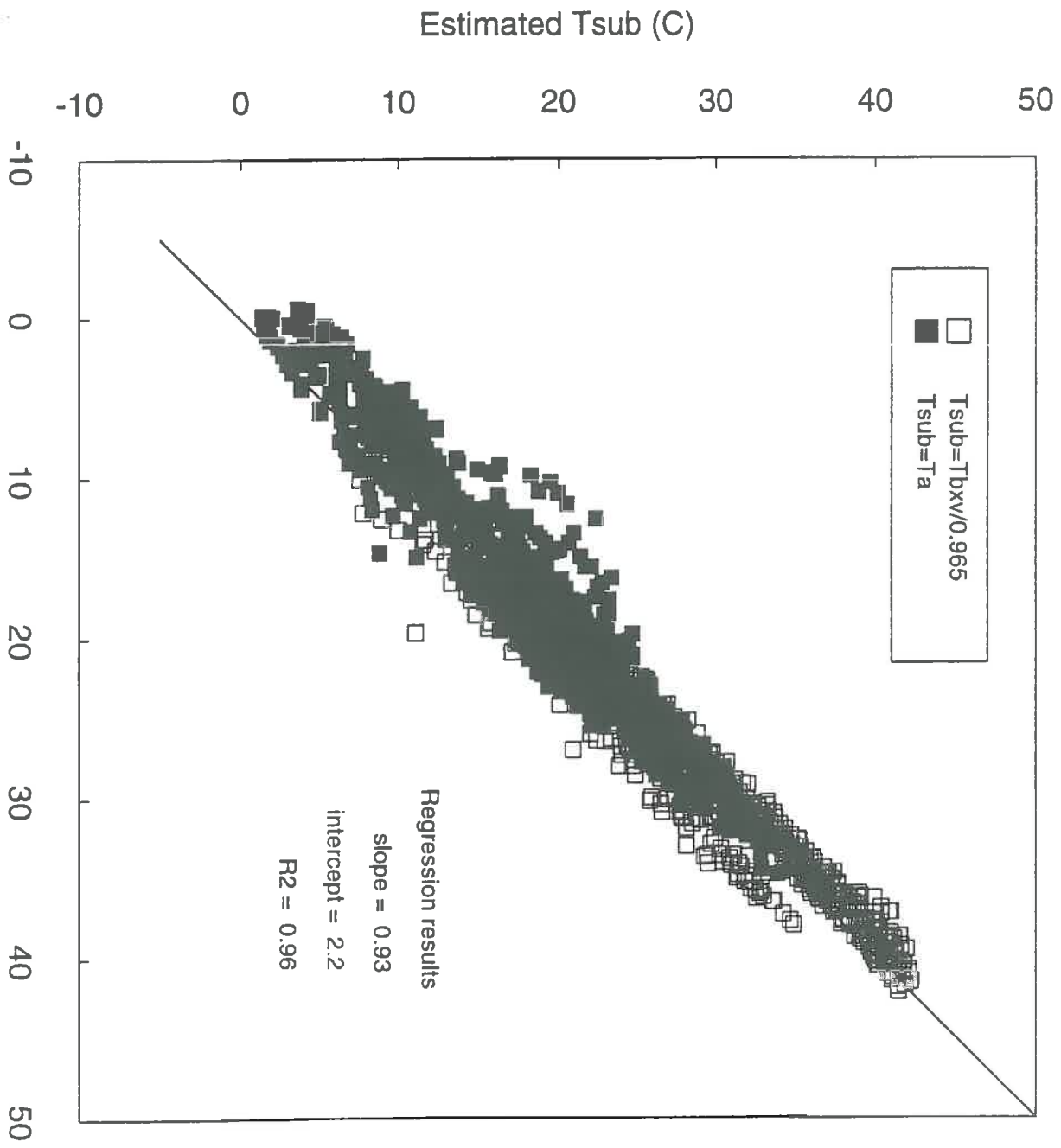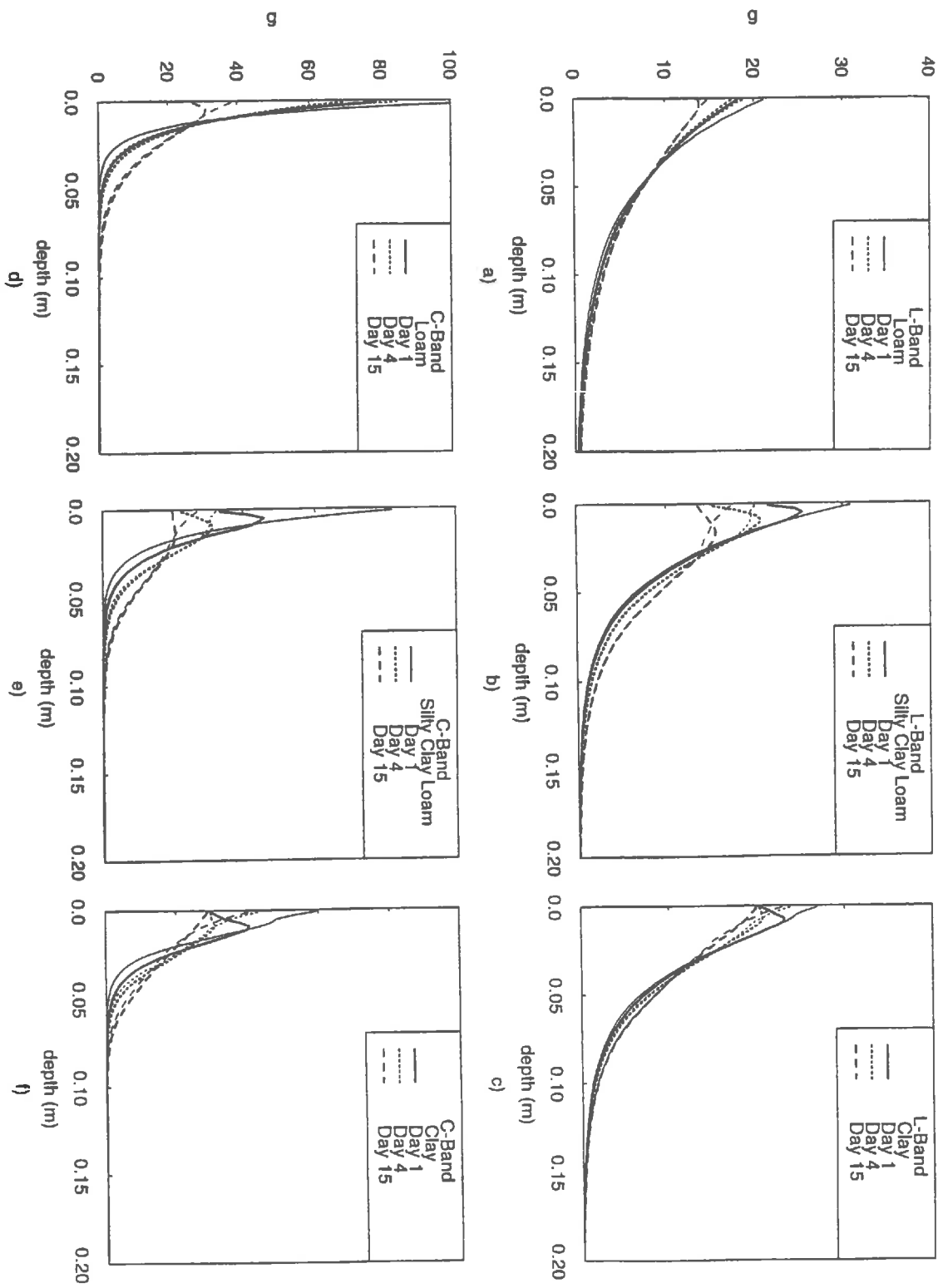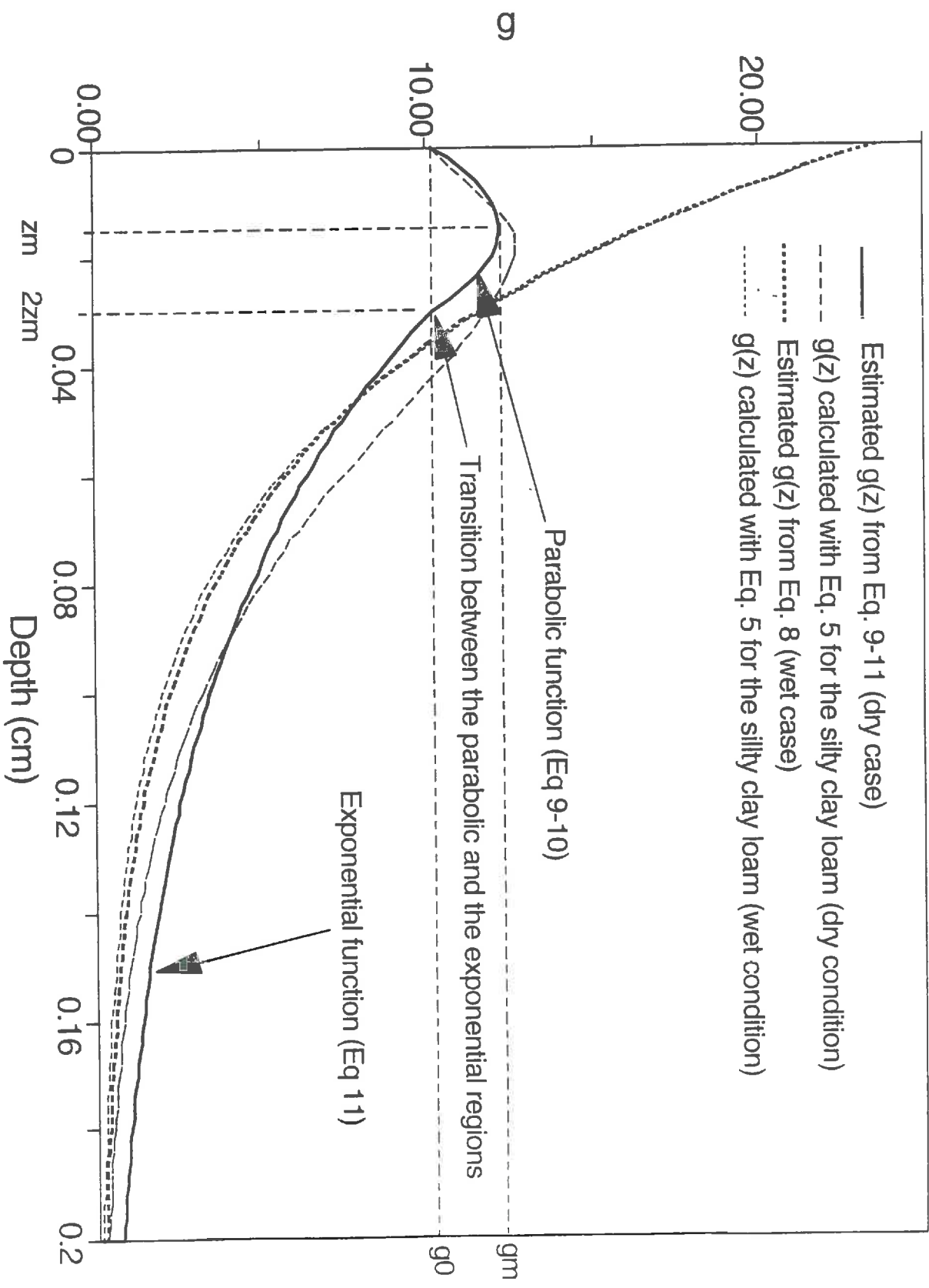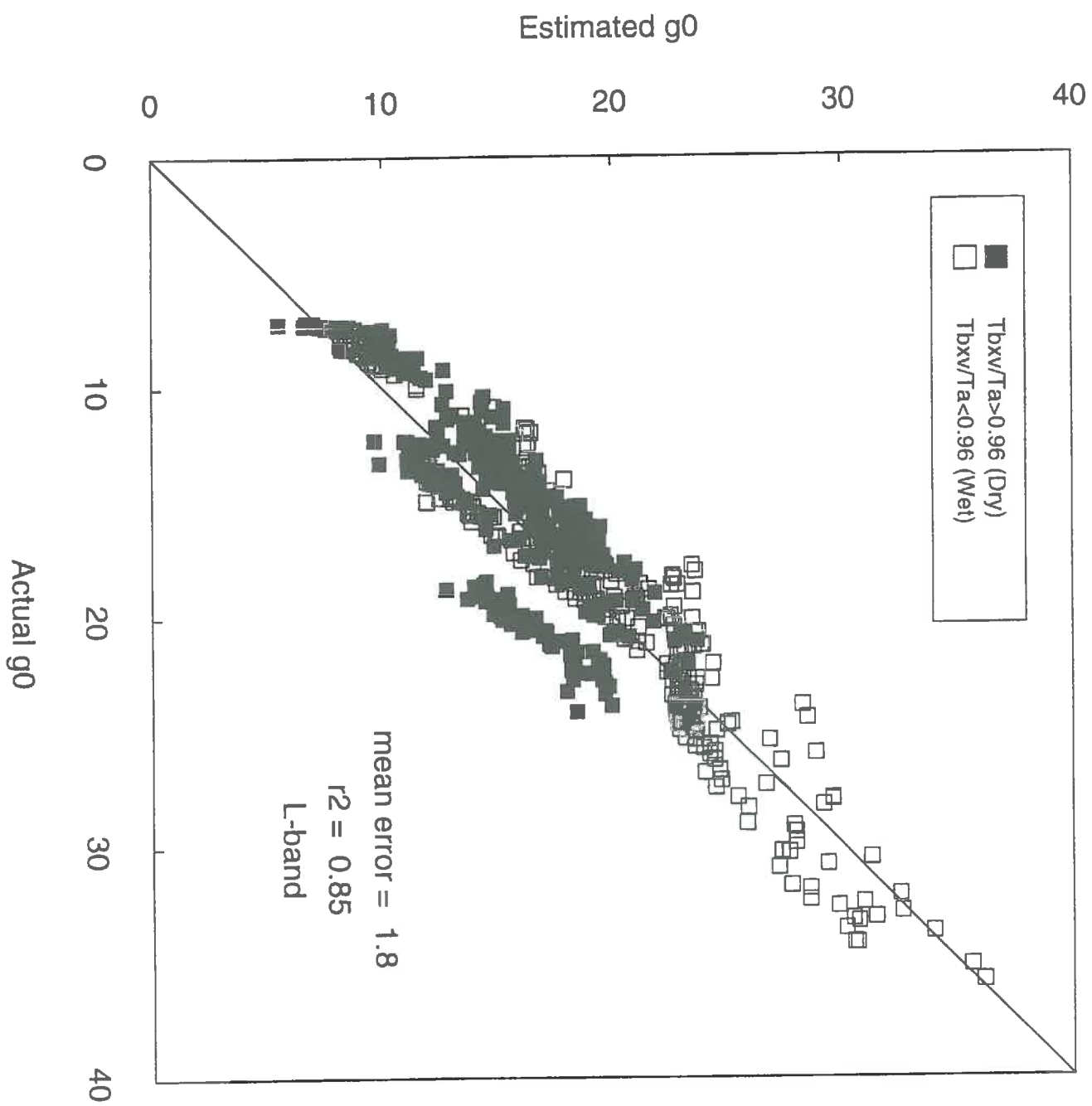for accurate result. Since the error affects the comparison between the model and experimental results is very large, it is difficult to discriminate the models by their accuracy. However, the diurnal evolution of the soil microwave emission simulated by the Wilheit and the Fresnel models are different. The differences affect the amplitude of the diurnal variation of T_B and the time of day which corresponds to the daily maximum T_B. This features can be further used as criteria to compare the performances of several models

The interest of using a multilayer model instead of a single layer model (Fresnel model) was studied. When the sampling depth for the single layer model was optimized, the benefit brought by the multilayer approach was significant at 1.4 GHz only. At this frequency we got better results with the Wilheit model than with the Fresnel model.

We observed in our study that the shape of the moisture and temperature profiles influences considerably the microwave emission (about 30K). As a consequence, the error in the estimation of the soil moisture within the sampling depth reaches 0.06m3/m3, if we do not take into account the effect of soil moisture and temperature profiles. This error is considerably reduced when the effective temperature is accounted for. An other consequence of the soil moisture and temperature profile effects is the field of validity of the sampling depth used to run a single layer emission model. This field of validity is limited in time. For instance at L band, the sampling depth obtained with afternoon observations is significantly different to that obtained with data collected during the night. It is possible that soil moisture and temperature profile obtained under different climatic condition or with different soil would lead to different values of sampling depth. One of the possible ways is to incorporate the sampling depth information that may be extracted by combining observations at different frequencies to account for the moisture profile.

We propose a new semi-empirical model to estimate the effective temperature in L and C bands. It is based on the use of microwave radiometric data or easily available data. The model inputs are the air temperature, the T_B of X band in vertical polarization and the temperature of the deeper depth soil (50 cm). The main innovation of the proposed model stands in the possibility of implementing it without measuring the surface temperature which is important to compute the effective temperature when needed. The model was designed with smooth bare soils and its application to rougher fields is encouraging. However, the roughness effect on the soil effective temperature estimation by the proposed model should be thoroughly investigated in a future endehavour. As far as vegeteted surface are concerned, we have to study the impact of the vegetation on the surface emissivity at X-band which is a key step to retrieve the soil temperature.

REFERENCES

Bard A. (1974), 'Non-linear parameter estimation',Academic, San Diego, Calif.

Barton I. J. (1978), 'A case study of microwave radiometer measurements over bare and vegetated surfaces', *J. Geophys. Res.* Vol. 83, pp 3515 - 3517.

Basharinov, A. Y., and A. M. Shutko, (1975), 'Simulation studies of the SHF radiation characteristics of soil under moist conditions', *NASA Tech. Trans.* TTF - 16, Greenbelt, MD.

Beckman P.(1968), 'The depolarization of electromagnetic waves', *Golem, Boulder, Colo.*

Bertuzzi P., L. Bruckler, Y. Gabilly, and J. C. Gaudu (1987), 'Calibration and error analysis of gamma-ray probe for the in-situ measurement of dry bulk density', *Soil science*, Vol. 144, No 6, pp 425 - 436.

Bertuzzi P., M. Caussignac, P. Stengel, J. Y. Lorendeau, and Pelloux (1990), 'An automated non contact laser profile meter for measuring soil roughness in-situ', *Soil Science*, Vol. 149, No 3, pp 169 - 178.

Bernard R., P. Martin, J. L. Thony, M. Vauclin, and D. Vidal Madjar (1982), 'C band radar for determining surface soil moisture', *Remote Sens. Environ.* Vol. 12, pp 189 - 200.

Birchak J. R., C. G. Gardner, J. E. Hipp and J. M. Victor (1974), 'High dielectric constant microwave probes for sensing soil moisture', *Proc. IEEE* Vol. 62(1), pp 93 - 98.

Bruckler L., H. Witono and P. Stengel (1988), 'Near surface estimation from microwave measurements', *Remote Sens.. Environ.* Vol. 26, pp 101 - 121.

Burke W. J., T. Schmugge, and J. F. Paris (1979), 'Comparison of 2.8 and 21 cm microwave radiometer observations over soils with emission model calculations', *J. Geophys. Res.* 84, pp 287 - 294.

Calvet J. C, J. P. Wigneron, E. Mougin, Y. H. Kerr and J. L. Brito (1993), 'Plant water content and temperature of the Amazon forest from satellite microwave radiometry', *IEEE Trans. Geosci. Remote Sensing.*, GE 32, pp 397 - 408.

Calvet J. C, J. P. Wigneron, A. Chanzy, S. Raju and L Laguerre (1995), ' Microwave dielectric properties of a silt - loam at high frequencies', *IEEE Trans. Geosci. and Remote sensing.* GE - 33, pp 634 - 642.

Camillo P. J. and T. J. Schmugge (1984), 'Correlating rainfall with remote sensed microwave radiation using physically based models', *IEEE Trans. Geosci. Remote Sensing*, GE-22, pp 415 - 423.

Chandrasekhar S. (1960), 'Radiative Transfer', *Dover Publications*, Inc., New York.

Chanzy A. (1991), 'Modelisation simplifiee de l'evaporation d'un sol nu utilisant l'humidite et la temperature de surface accessibles par teledetection', *Ph.D. Thesis, Institut National Agronomique*, Paris - Grignon, France.

Chanzy A and L. Bruckler (1993), ' Significance of soil surface moisture with respect to daily bare soil evaporation', *Water Resour. Res.*, Vol. 29, pp 1113 - 1125.

Chanzy A. and W. P. Kustas (1994), 'Evaporation monitoring over land surface using microwave radiometry', *ESA/NASA Int. Workshop*, B. J. Choudhury, Y. H. Kerr, E. G. Njoku and P. Pampaloni (Eds), pp 531 - 550.

Chanzy A., D. Haboudane, J. P. Wigneron, J. C. Calvet and O. Grosjean (1994), 'Radiometrie micro-onde sur divers types de couverts vegetaux: influence de l'humidite du sol', *ISPRS 6th International Symp. Physical measurements and signatures in remote sensing*, France.

Chanzy A, T. J. Schmugge, J. C. calvet, Y. H. Kerr, P. Van Oevelen, O. Grosjean and J. R. Wang (1995), 'Airborne microwave radiometry on a semi arid area during HAPEX-SAHEL', *J. Hydrology*, (in press)

Choudhury B. J., T. J. Schmugge, A. Chang, and R. W. Newton (1979), 'Effect of surface roughness on the microwave emission from the soils', *J. Geophys. Res.* Vol. 99., pp 5699 - 5706

Choudhury B. J., T. J. Schmugge, and T. Mo (1982), 'A parameterization of effective soil temperature for Microwave emission', *J. Geophys. Res.* 87., pp 1301 - 1304.

Choudhury B. J. (1990), 'Monitoring arids land using AVHRR -observed visible reflectance and SMMR - 37 GHz polarization difference', *Int. J. Remote Sens.* Vol. 11(10), pp 1949 - 1956.

Choudhury B. J., and J. R. Wang (1990), 'Simulated and observed 37 GHz emission over Africa', *Int. J. Remote Sens.* Vol. 11, pp 1837 - 1868.

Choudhury B. J. (1993), 'Reflectivities of selected land surface types at 19 and 37 GHz from SSM/I observations', *Remote Sens. Environ.* Vol. 46, pp 1- 17.

Chouhan N., D. Le Vine, and R. Lang (1994), 'Use of discrete scatter model to predict active and passive microwave sensor response to corn: comparison of theory and data', *IEEE Trans. Geosci. Remote Sensing*, GE-32, pp 416 - 426.

Costes F. (1994), Contribution à l'étude des signatures actives et passives micro-ondes des sols nus. Application à la télédétection. *Thèse de doctorat de l'Université Paul Sabatier*, Toulouse, France, 215p.

Costes F, S. Raju, A. Chanzy, I. Chenerie and J. Lemorton (1994), 'Microwave radiometry on bare soils: Comparison of various emission models of layered media with measurements', *Proce. IGARSS'94, California Institute of Technology*, Pasadena, California, USA.

De Loor G. P. (1968), 'Dielectric properties of heterogeneous mixtures containing water', *J. Microwave Power*, Vol. 3, pp 67 - 73.

Dobson, M. C. and F. T. Ulaby (1981), 'Microwave backscattering dependence on surface roughness, soil moisture, and soil texture: part III- Soil tension', *IEEE Trans. Geosci. Remote Sensing*, GE-19, pp 51 - 61.

Dobson M. C., F. Kouyate and F. T. Ulaby (1984), ' A reexamination of soil textural effects on microwave emission and backscattering', *IEEE Trans. Geosci. Remote Sensing*, GE-22(6), pp 530 - 536.

Dobson M. C., F. T. Ulaby, M. T. Hallikainen and M. A. El Rayes (1985), 'Microwave dielectric behavior of wet soils - Part II, Dielectric mixing models', *IEEE Trans. Geosci. Remote Sensing*, GE - 23, pp 35 - 46.

England A. W, J. F. Galantowicz and M. S. Schretter (1992), ' The radio brightness thermal inertia measure of soil moisture', *IEEE Trans. Geosci. Remote Sensing*, GE - 30, pp 132 - 139.

Entekhabi. D., Nakamura H., and E. G. Njoku, (1994), ' Solving the inverse problem for soil moisture by sequential assimilation of multifrequency remotely sensed observations', *IEEE Trans. Geosci. and Remote sensing*. GE - 32(2), pp 438 - 448.

Fung, A. K. and H. J. Eom (1981), Emission from a Rayleigh surface with irregular boundaries', *J. Quant. Spectrosc. Radiat. Transfer*. Vol. 26, pp 397 - 409.

Grosjean O. and A Sand (1993), 'Etalonnage du radimetre hyperfrequence PORTOS et methode de correction du mesures', *ISPRS 6th International Symp. Physical measurements and signatures in remote sensing*, France, 1994.

Hallikainen M. T., F. T. Ulaby, M. C. Dobson, M. El-Rayes and L. K. Wu (1985), 'Microwave dielectric behavior of wet soil - Part I: Empirical models and experimental observations', *IEEE Trans. Geosci. and Remote sensing*. GE - 23, pp 25 - 34.

Ijjas G. and Y. S. Rao (1992), 'Passive microwave remote sensing of soil moisture from aircraft in Hungary', *Int. J. Remote Sensing*, Vol. 13, pp 471 - 479.

Ishimaru A., J. N. Hwang, and J. S. Chen (1992), 'Remote sensing of rough surface parameters using artificial neural network techniques', *Proce. IGARSS'92, Houston*, Texas, pp 1072.

Jackson T. J., T. J. Schmugge and J. R. Wang (1982), 'Passive microwave sensing of soil moisture under vegetation canopies'. *Water Resour. Res*. Vol. 18, pp 1137 - 1142.

Jackson T. J, and P. E. O'Neill (1986a), 'Temporal observations of surface soil moisture using a passive microwave sensor', *Remote Sens. of Environ.* Vol. 21, pp 281 - 296.

Jackson T. J. and P. E. O'Neill (1986b), 'Microwave dielectric model for aggregate soils', *IEEE Trans. Geosci. Remote Sensing*, GE-24, pp 920-929.

Jackson T. J. and P. E. O'Neill (1987), 'Salinity effect on the microwave emission of soils', *IEEE Trans. Geosci. and Remote Sensing*, GE-25, pp 214 - 220.

Jackson T. J. and T. J. Schmugge (1989), 'Passive microwave remote sensing system for soil moisture: some supporting research', *IEEE Trans. Geosci. Remote Sensing*, GE-27, pp 225 - 235.

Jackson T. J. and T. J. Schmugge (1991), ' Vegetation effects on the microwave emission of soils', *Remote Sens. Environ.* Vol. 36, pp 203 - 212.

Jackson T. J., D. M. Le Vin, C. T. Swift and T. J. Schmugge (1993), 'Large area mapping of soil moisture using the ESTAR passive microwave radiometer', *ISPRS 6th International Symp. Physical measurements and signatures in Remote Sensing,* France, 1994.

Karam M. A., A. K. Fung, Lang R. H. and N. S. Chouhan (1992), 'A microwave scattering model for layered vegetation', *IEEE Trans. Geosci. Remote Sensing.* GE-30, pp 767 - 784.

Kerr, Y. H. and E. G. Njoku, (1990), 'A semiempirical model for interpreting microwave emission from semiarid land surface as seen from space', *IEEE Trans. Geosci. Remote Sens.* GE-28, pp 384 - 393.

Kerr Y. H. and E. G. Njoku (1993), ' On the use of passive microwaves at 37 GHz in remote sensing of vegetation', *Int. J. Remote Sens.* Vol. 14(10), pp 1931 - 1943.

Kerr Y. H. and J. P. Wigneron (1993), 'Vegetation models and observations - A review', *ESA NASA International workshop on Passive microwave Remote Sensing Research related to Land - Atmosphere Interactions,* 11 - 15 January, 1993, St. Lary, France.

Kirdiashev K. P., A. A. Chukhlantsev and A. M. Shutko (1979), 'Microwave radiation of the earth's surface in the presence of vegetation cover', *Radiotekhnika*, Vol. 24, pp 256 - 264 - Also NASA.Tech.Trans TM - 75469.

Kobayashi. T. and H. Hirosawa (1985), 'Measurement of radar backsactter from rough soil surface using linear and circular polarization', *Int. J. Remote Sens.* Vol. 6(13), pp 345 - 352.

Kraus J. D. (1966), 'Radio astronomy', *McGrow - Hill*, New York, Chapter 3.

Laguerre L. Suresh Raju, A. Chanzy, Y. H. Kerr, J. C. Calvet and J. P. Wigneron (1994), 'Physical modeling of microwave emission from bare soils - Inter comparison of models and ground data', *ISPRS 6th International Symp. Physical measurements and signatures in remote sensing*, France, 1994.

Laguerre L. (1995), 'Influence de la rugosité de surface en radiométrie micro-onde des sols nus: Modélisation et expérimention', *Thèse de Doctorat de l'Institut National Polytechnique de Toulouse*, France.

Lambert B. M. and M. J. McFarland (1987), 'Land surface temperature estimation over the northern Great Plains using dual polarized passive microwave data from the Nimbus 7', *summer meeting ASAE, Baltimore*, MD, ASAE paper, 87-4041,. 23 pp.

Le Vine D. M., S.Ruf, A. B. Tanner (1988), 'Interferometric synthetic apperture microwave radiometry for remote sensing of the earth', *IEEE Trans. Geosci. Remote Sensing*, GE 26(2).

Lundien J. R. (1971), 'Terrain analysis by electromagnetic means', U.S. Army Engineer waterways experiment station, *Vicksburg*, MS, Tech. Rep. 3-727.

McFarland M. J, R. L. Miller and C. M. U. Neale (1990), 'Land surface temperature derived from the SSM/I passive microwave brightness temperature', *IEEE Trans. Geosci. Remote Sensing*. GE-28(5), pp 839 - 845.

Mo T. and T.J Schmugge (1987)," A parameterization of the effect of surface roughness on microwave emission", *IEEE Trans. Geosci. Remote Sensing*, 25(4): 481-486.

Newton R. W. (1977), 'Microwave remote sensing and its applications to soil moisture detection', *Tech. Rep. RSC-81, Remote sensing center, Texas Univ.*, College station, TX.

Newton R. W. and J. W. Rouse, Jr. (1980), 'Microwave radiometer measurements of soil moisture content', *IEEE Trans. Antennas and Propag.* AP-28, pp 680 - 686.

Newton R. W, Q. R. Black, S. Makanvand, A. J. Blanchard and B. R. Jean (1982), 'Soil moisture information and Thermal microwave emission', *IEEE Trans. Geosci. Remote sensing*. GE - 20, pp 275 - 281.

Njoku E. G and J. A. Kong (1977), 'Theory of passive microwave sensing of near surface soil moisture', *J. Geophys. Res.* Vol. 82, pp 3108 - 3118.

Njoku E. G. and P. E. O'Neill (1982), ' Multifrequency microwave radiometer measurements of soil moisture', *IEEE Trans. Geosci. Remote Sensing*. GE-20, pp 468 - 475.

Njoku E. G. (1992), 'Land surface signatures using spaceborne microwave radiometry', Specialist meeting on Microwave radiometry and remote sensing appilcations, *Boulder, CO*, 14 - 16 January.

Palocia S. and P. Pampaloni (1992), 'Microwave vegetation indexes for detecting biomass and water condition of agricultural crops', *Remote Sens. Environ.* Vol. 40, pp 15 - 26.

Pampaloni P. and S. Paloscia (1986), ' Microwave emission and plant water content: a comparison between field measurements and theory', *IEEE Trans. Geosci. Remote Sensing*. GE-24, pp 900 - 905.

Peake W. H. (1959), 'Interaction of electromagnetic waves with some natural surfaces', *IEEE Trans. antennas Propagat.* Vol. AP-7: pp 324 - 325.

Philip J. R. and D. A. de Vireos (1957), 'Moisture movements in porous materials under temperature gradients', *Eos Trans.* Vol. 38, pp 222 - 232.

Prevot L, R Bernard, O. Taconet, D. Vidal-Madjar, and J. L. Thony (1984), 'Evaporation from a bare soil evaluated using a soil water transfer model and remotely sensed surface soil moisture data', *Water Res. Res..* Vol. 20, pp 311 - 316.

Reutov E. A. and A. M. Shutko (1992),' Estimation of the depth to a shallow water-table using microwave radiometry', *Int. J. Remote Sens.* 13, pp 2223 - 2232.

Rouse J. W. (1983), 'Comments on the effects of texture on microwave emission from soils', *IEEE Trans. Geosci. Remote Sensing*. GE-21, pp 508 - 511.

Saatchi S.S., E.G. Njoku and U. Wegmuller (1994), "Synergism of active and passive microwave data for estimating bare soil surface moisture", Passive Microwave Remote Sensing of Land and Atmosphere Interactions, 205-224, Editors : Choudhury B.J., Y.H. Kerr, E.G. Njoku, P.Pampaloni.

Schanda (1986), 'Physical fundamentals of remote sensing'. *Spinger-Verlag*, Berlin, Heidelberg,187.

Schmugge T. J., P. Gloersen, T. T. Wilheit and F. Geiger (1974), 'Remote sensing of soil moisture with microwave radiometers', *J. Geophys. Res.*, Vol. 79(2), pp 317 - 323.

Schmugge T. J. (1980), 'Effect of texture on microwave emission from soils', *IEEE Trans. Geosci. Remote Sensing*. GE-18(4), pp 353 - 361.

Schmugge T. J, and B. J. Choudhury (1981), 'Comparison of radiative transfer models for predicting the microwave emission from soils', *Radio Science*, Vol. 16, pp 927 - 938,

Schmugge T. J.,(1983), ' Remote sensing of soil moisture: Recent advances', *IEEE Trans. Geosci. Remote Sensing*, GE 21(3), pp. 336 - 344.

Schmugge T. J., P. E. O'Neill and J. R. Wang (1986), ' Passive microwave soil moisture research', *IEEE Trans. Geosci. Remote Sensing*. GE-24, pp 12 - 22.

Schmugge T. and T. J. Jackson (1994), 'Mapping surface soil moisture with microwave radiometers', *Meteorol. Atmos. Phys.* Vol. 54, pp 213 - 223.

Shutko, A. M. (1982), 'Microwave radiometry of lands under natural and artificial moisturing', *IEEE Trans. Geosci. Remote Sensing*, GE-20, pp 18 - 26.

Smith, E. A. (1982), 'Centimeter and millimeter wave attenuation and brightness temperature due to atmospheric oxygen and water vapor', Radio Sci. 17, pp 1455 - 1464.

Smith, E. A. (1986), 'The structure of the Arabian heat low. Part 1: Surface energy budget', *Mon. Weather Rev.* Vol. 114. pp 1067 - 1083.

Stogryn A. (1970), 'The brightness temperature of a vertically structured medium', *Radio Science*, Vol. 5(12), pp 1397 - 1406.

Stogryn A. (1971), 'Equations for calculating the dielectric constant of saline water', *IEEE Trans. Microwave Theory Tech.*, MIT 19, pp 733 - 736.

Theis S. W., B. J. Blanchard and R. W. Newton (1984), 'Utilization of vegetation indices to improve microwave soil moisture estimates over agricultural lands', *IEEE Trans. Geosci. Remote Sensing*, GE-22(6), pp 490 - 496.

Theis S. W., Blanchard B. J. and Blanchard A. J. (1986), 'Utilization of active microwave roughness measurements to improve passive microwave soil moisture estimates over bare soils', *IEEE Trans. Geosci. Remote Sensing*, GE-24(3), pp 334 - 339.

Tsang L. and J. A. Kong (1981), 'Scattering of electromagnetic waves from random media with strong permittivity fluctuations', *Radio Sci.* Vol. 16, pp 303 - 320.

Tsang L and R. W. Newton (1982) 'Microwave emission from soils with rough surfaces' *J. Geophys.* Res. 87, pp 9017-9024.

Tsang L. (1991), 'Polarimetric passive microwave remote sensing of random discrete scatters and rough surface', *J. Electr. Waves and Appl.* Vol. 5, pp 41 - 57.

Ulaby F. T., P. P. Batlivala and M. C. Dobson (1978), 'Microwave backscatter dependence on surface roughness, soil moisture and soil texture: PartI-Bare Soil', *IEEE Trans. Geosci. Remote Sensing*. GE-16, pp 286 - 295.

Ulaby F. T., R. K. Moore and A. K. Fung (1981 - 1986), 'Microwave remote sensing - Active and Passive', *Addison - Wesley Publishing company*, 1981 - 82 Vol. I, II; Artech House, Vol. III. 1986.

Ulaby F. T., M Razani and M. C. Dobson (1983), ' Effects of vegetation cover on the microwave radiometric sensitivity to soil moisture', *IEEE Trans. Geosci. Remote Sensing*, GE-21, pp 51 - 61.

Viswanadham Y., L. C. B. Molin, A. O. Manzy, et al. (1990), 'Micro meteorological measurements in Amazon forest during GTE-ABLE 2A mission', *J. Geophys. Res.* Vol. 95, pp 13669 - 13682.

Vyas A. D, A. J. Trivedi, O. P. N. Calla, S. S. Rana, S. B. Sharma and A. B. Vora (1990), 'Experimental data for separation of vegetation and soil and estimation of soil moisture using passive microwaves', *Int. J. Remote Sens.* Vol. 11, pp 1421 - 1438.

Waters J. W., (1976), 'Absorption and emission of Microwave radiation by atmospheric gases, in methods of experimental physics' (M.L Meeks, ed.*) Ch.12, Part B, Radio Astronomy Academic Press*, New York, Section2.3.

Wang J. R., T. Schmugge and D. Williams (1978), 'Dielectric constants of soil at microwave frequencies - II', *NASA Tech.* Pap. 1238.

Wang J. R. and T. J. Schmugge (1980), 'An empirical model for the complex dielectric permittivity of soils as function of water content', *IEEE Trans. Geosci. Remote sensing*, GE - 18, pp 288 - 295.

Wang J. R., J. C. Shiue and J. E. McMurtrey (1980), 'Microwave remote sensing of soil moisture content over bare and vegetated field', *Geophys. Res.* Lett. Vol. 7, pp 801 - 804.

Wang J. R., and B. J. Choudhury (1981), 'Remote sensing of soil moisture content over bare field at 1.4 GHz frequency', *J. Geophys. Res.*, Vol. 86, No. C6, pp 5277 - 5282.

Wang J. R. (1983), 'Passive microwave sensing of soil moisture content: the effects of soil bulk density and surface roughness', *Remote Sens. Environ.* Vol. 13, pp 329 - 344.

Wang J. R, P. O'Neill, T. J. Jackson and E. T. Engman (1983), 'Multifrequency measurements of the effects of soil moisture, soil texture, and surface roughness', *IEEE Trans. Geosci. Remote. sensing*, GE - 21, pp 44 - 50.

Wang J. R (1987), 'Microwave emission from smooth bare fields and soil moisture sampling depth', *IEEE Trans. Geosci. Remote sensing*, GE - 25, pp 616 - 622.

Wang J. R., E. T. Engman, T. J. Schmugge, T. Mo and J. C. Shiue (1987), 'the effects of soil moisture, surface roughness and vegetation on L - band emission and backscatter', *IEEE Trans. Geosci. Remote Sensing*, GE - 25, pp 825 - 833.

Wegmuller U (1993), 'Signature research for crop classification by active and passive microwaves', *Int. J. Remote Sens.* Vol. 14, pp 871 - 883.

Wigneron, J. P (1993), 'Modélisation de l'émission micr-onde d'un couvert végétal - Mise en relation de la mesure hyperfréquence passive avec les échanges énergétiques et hydriques d'une culture de soja' *Ph.D. Thesis, Université Paul Sabatier*, Toulouse, France.

Wigneron, J. P, J. C. Calvet, Y. H. Kerr, A. Chanzy, and A. Lopes (1993 A), ' Microwave emission of vegetation: Sensitivity to leaf characteristics', *IEEE Trans. Geosci. Remote sensing*, GE - 31, pp 716 - 726.

Wigneron, J. P, Y. H. Kerr, A. Chanzy, and Y. Q. Jin. (1993 B), 'Inversion of surface parameters from passive microwave remote measurements over a soybean field', *Remote Sens. Environ.* Vol. 46, pp 61 - 72.

Wigneron, J. P, Y. H. Kerr, F. Biard and N. Bruguier (1994A), 'Vegetation models used to retrieve geophysical parameters from passive microwave measurements', *ISPRS 6th International Symp. Physical measurements and signatures in remote sensing*, France.

Wigneron, J. P, J. C. Calvet, and A. Chanzy (1994B), 'A composite Discrete-Continuous approach to model microwave emission of vegetation canopy', *IEEE Trans. Geosci. Remote Sensing*, Vol. 33, pp 201 - 211.

Wigneron, J. P, Calvet, J. C, Chanzy A., Grosjean O., and Laguerre L. (1995), 'A composite discrete - continuous approach to model the microwave emission of vegetation', *IEEE Trans. Geosci. Remote Sensing*, GE-33, pp 201 - 210.

Wilheit T. T. (1978), 'Radiative transfer in plane stratified dielectric', *IEEE Trans. Geosci. Electron.* GE - 16, pp 138 - 143.

Witono H and L. Bruckler (1989), 'Use of remotely sensed soil moisture content as boundary conditions in soil - atmosphere water transport modeling, 1, Field validation of a water flow model', *Water Resour. Res.* Vol. 25, pp 2423 - 2435.

Zotova E and A. Geller (1985), ' Soil moisture content estimation by radar survey data during the sowing campaign', *Int. J. Remote Sens.* Vol. 6, pp 353 - 364.

Appendix - A

DIELECTRIC MODELS

As we have seen in part1 (3.4) the wet soil medium is a mixture of soil particles, air voids and liquid water. The liquid water is the major contributor of dielectric constant of soil mixture. The water in the soil is divided into bound water and bulk water. The dielectric models are developed based on mixing of the dielectric of the constituents. The results of a number of laboratory measurements of soil dielectric constant for different soil texture (Lundien 1971; Newton 1977; Wang et al. 1978; Hallikainen et al. 1985) are used to develop and verify the dielectric models. Two of the more sophisticated and reliable of these models are those developed by Wang and Schmugge (1980) and Dobson et al. (1985). Conceptually both models are the same but they differ in the treatment of bound water and free water. Wang and Schmugge (1980) considered a soil texture (via wilting point) dependent parameter called transition point to separate the bound water and free water in the soil medium. While Dobson et. al. (1985) directly related the specific surface area of soil particle to the bound water. Here we present the some of the dielectric models.

1. Wang and Schmugge model

Wang and Schmugge (1980) modeled the dielectric constant of wet soil by using the dielectric mixing equation which considers the dielectric contributions of soil, air, and water. They proposed a soil texture (via wilting point) dependent parameter called transition point (θ_t) to separate the bound water and free water in the soil medium. When the value of wilting point (θ_p) is not available they proposed an empirical relationship to estimate (θ_t) :

$$(\theta_t) = 0.49 \cdot \theta_p + 0.165 \tag{1}$$

and

$$\theta_p = 0.06774 - 0.064 * S + 0.478 * C\% \quad (cm^3 cm^{-3}) \tag{2}$$

- $S /$ is the fraction of sand
- $C /$ is the fraction of clay

Wang and Schmugge (1980) assumed that for volumetric water content (θ) below the θ_t, water molecules near to soil solids behave like ice and consequently, the dielectric constant of ice is used in the mixing model. And when θ is greater than θ_t the water dielectric constant is used. Thus two separate dielectric models for soil water mixture for θ below θ_t and θ above θ_t were proposed as follow

1) When $\theta \leq \theta_t$

$$\varepsilon = \theta\varepsilon_x + (p_r - \theta)\varepsilon_a + (1 - p_r)\varepsilon_s \tag{3}$$

$$\text{with } \varepsilon_x = \varepsilon_i + (\varepsilon_w - \varepsilon_i)\frac{\theta}{\theta_t} \cdot \gamma \tag{4}$$

2) While $\theta > \theta_t$

$$\varepsilon = \theta_t\varepsilon_x + (\theta - \theta_t)\varepsilon_a + (p_r - \theta)\varepsilon_a + (1 - p_r)\varepsilon_s \tag{5}$$

$$\text{with } \varepsilon_x = \varepsilon_i + (\varepsilon_w - \varepsilon_i)\gamma$$

Where
- ε is the dielectric constant of soil (ratio)
- p_r is the porosity (ratio)
- ε_a is the air dielectric constant (ratio)
- ε_s is the soil solid dielectric constant (ratio)
- ε_w is the water dielectric constant (ratio)
- ε_i is the ice dielectric constant (ratio)
- θ is the water contents ($cm^3 cm^{-3}$)
- ε_x stands for the dielectric constant of the initially absorbed water.
- γ is a fitted parameter for equation (4) and (5) and is related to θ p.

For the imaginary part of dielectric constant at low frequencies, it is necessary to add a conductivity loss term and the total dielectric loss, ε''_t:

$$\varepsilon''_t = \varepsilon'' + 60\lambda\sigma \tag{6}$$

or

$$\varepsilon''_t = \varepsilon'' + A\theta^2 \tag{7}$$

Where
- σ is the ionic conductivity ($S\ m^{-1}$)

2

- λ is the wavelength (m)

- A is the fitted parameter which was varying for 0 to 26 for different soil types they used in their study at 1.4 GHz. However, in case of low conductivity, the variations of A from 0 to 26 do not make significant change in the T_B estimation (~1 K) (Wang and Schmugge 1980). The porosity of a dry soil is defined as:

$$p_r = 1 - \frac{\rho_b}{\rho_s} \tag{8}$$

Where
- ρ_b is the dry bulk density

- ρ_s is the density of solid rock.

The advantages of the Wang and Schmugge model are that all of the required input data are easily available for most situations. It explains most of the phenomena observed in laboratory dielectric measurements. However, the drawback of this approach is that it is empirical and does not consider firmly established theories on structural effects the on soil mixture.

2. Dobson's dielectric models

2.1 Physical model

The Physical dielectric model developed by Dobson et al. (1985) is dependent upon measurable characteristics only and requires no adjustable parameter to fit experimentally measured data. The pore size distribution calculated from particle size distribution determines the bound water and free water volume fractions. This model treats the soil water system as a host medium of dry soil solids containing randomly distributed and oriented disc-shaped inclusions of bound water, bulk water and air. The final expression of the physical model is obtained by following the approach used by De Loor (1968).

The expression of Dobson's physical model:

$$\varepsilon_0 = \frac{3\varepsilon_s + 2V_{fw}\left(\varepsilon_{fw} - \varepsilon_s\right) + 2V_{bw}\left(\varepsilon_{bw} - \varepsilon_s\right) + 2V_a\left(\varepsilon_a - \varepsilon_s\right)}{3 + V_{fw}\left(\frac{\varepsilon_s}{\varepsilon_{fw}} - 1\right) + V_{bw}\left(\frac{\varepsilon_s}{\varepsilon_{bw}} - 1\right) + V_a\left(\frac{\varepsilon_s}{\varepsilon_a} - 1\right)} \tag{9}$$

- V stands for the volume fraction and the subscripts
  - fw for free water
  - bw for bound water
- ε_{bw} dielectric constant of bound water (ratio)
- ε_{fw} is dielectric constant of free water, (ratio)
- ε_s is soil solid dielectric constant ~ (4.7 -i0),
- ε_a is the air dielectric constant ~ (1.0 - i0),

The ε_{fw} is obtained from the modified Debye's equation which accounts for the conductivity loss also:

$$\varepsilon_{fw} = \varepsilon_{w\infty} + \frac{\varepsilon_{w0} - \varepsilon_{w\infty}}{1 + i2\pi f\tau_w} + i\frac{\sigma_\theta}{2\pi\varepsilon_0 f} \tag{10}$$

σ_θ is the effective conductivity of water in $(S.m^{-1})$ whose formulation is given by Dobson et al (1995).

This model provided an excellent agreement with experimental data in the validation study which shows the ability of the model to define the soil water system properly (Dobson et al. 1985). But the drawback of this model is that many of the input parameters are not easily available. As a result Dobson et al. (1985) presented a more simple and convenient empirical expression. We presented the semi-empirical model in the following.

2.2 Semi-empirical model

The semi-empirical model is the modified form of Birchak mixing model (Birchak et al.1974) based upon refractive volumetric mixing applicable to wet soil. The final expression for the semi-empirical model is:

$$\varepsilon^u = 1 + \frac{\rho_b}{\rho_s}\left(\varepsilon_s^u - 1\right) + \theta^\beta \varepsilon_{fw}^u - \theta \tag{11}$$

where
- u is a constant shape factor equal to 0.65
- β is a soil texture dependent empirical parameter:

$$\beta = 1.09 - 0.11*S + 0.18*C \tag{12}$$

4

In the above equation (12) all other terms are defined. The dielectric constant of free water is calculated at a given frequency and temperature using a modified Debye's equation:

$$\varepsilon_\theta = \varepsilon_{w\infty} + \frac{\varepsilon_{w0} - \varepsilon_{w\infty}}{1 + i2\pi f \tau_w} + i \frac{\sigma_{eff}}{2\pi\varepsilon_0 f} \frac{\rho_s - \rho_b}{\rho_s \theta} \tag{13}$$

In the above equation all terms except the effective conductivity σ_{eff} are presented in the section (3). σ_{eff} is related to soil physical properties as given below:

$$\sigma_{eff} = -1.645 + 1.939\rho_b - 0.02013 \cdot S \cdot 100 + 0.01594 \cdot C \cdot 100 \tag{14}$$

Where S and C are the fractions of sand and clay respectively.

In the validation of semi-empirical model, it was reported by Dobson et al. (1985) that the model has a tendency to overestimate ε at low moisture contents and under estimate the ε at high moisture contents. However, the error observed is very small with a mean of -0.142 and -0.136 and a standard deviation about 2.248 and 0.4 for ε' and ε'' respectively over wide range of soil moisture and frequencies (Dobson et al. 1985).

The input parameters require to calculate the ε by using either Dobson's semi-empirical model or Wang and Schmugge model are fraction of sand, clay, dry bulk density, specific density, soil salinity and volumetric water content. It should be noted that both the above models (Dobson's Physical model and Semi-empirical model) are valid in the approximate frequency domaine of 1.0 to 18 GHz.

3   Dielectric constant of water

The dielectric constant of water (ε_{fw}) in the microwave frequency has the average value of about (85, -i11) is a function of frequency, temperature and salinity. First we discuss dielectric constant of pure water which is only a function of temperature and frequency.

The frequency dependence of the dielectric constant of pure water (ε_{fw}) is given by Debye's equation (Stogryn (1975)):

$$\varepsilon_{fw} = \varepsilon_{w\infty} + \frac{\varepsilon_{w0} - \varepsilon_{w\infty}}{1 + i2\pi f\tau_w} \qquad (15)$$

- ε_{w0} is the static dielectric constant of the pure water (ratio)
- $\varepsilon_{w\infty}$ is the high-frequency limit of ε_{fw} (ratio)
- τ_w is the relaxation time of pure water, (s)
- f is the frequency (Hz)

In addition to their dependency on frequency, ε is also temperature (T) and salinity (S$_l$) dependent because ε_{w0} and τ_w are functions of T and S$_l$. At first we will see the temperature effect of pure water.

The relaxation time of pure water ε_{fw} as function of T (Stogryn (1975)):

$$\tau_w(T) = (1.1109 \cdot 10^{-10} - 3.824 \cdot 10^{-12}T + 6.938 \cdot 10^{-14}T^2 + -5.096 \cdot 10^{-16}T^3)/2\pi \quad (16)$$

A related term used in the literature is relaxation frequency:

$$f_0 = \frac{2\pi}{\tau} \qquad (Hz) \qquad (17)$$

The relaxation frequency of water lies in the microwave region ($f_0 \sim$ 17 GHz at 20°c).

The static dielectric constant of pure water (Stogryn (1975)):

$$\varepsilon_{w0}(T) = 88.045 - 0.4147T + 6.295 \cdot 10^{-4}T^2 + 1.075 \cdot 10^{-5}T^3 \qquad (18)$$

Salinity effect on water dielectric constant

The water with dissolved salt is called saline water. The salinity S$_l$ of a solution indicates the quantity of salt dissolved in the saline water. S$_l$ is expressed in parts per thousand (°/oo) on weight basis. The presence of salinity in the water changes ε_{w0} and τ_w of the pure water and adds ionic conductivity loss factor σ_i. The dielectric constant of saline water (Ulaby et al. 1986)):

$$\varepsilon_{fw} = \varepsilon_{w\infty} + \frac{\varepsilon_{w0} - \varepsilon_{w\infty}}{1 + i2\pi f\tau_w} + i\frac{\sigma_i}{2\pi\varepsilon_0 f} \qquad (19)$$

Where
- σ_i is the ionic conductivity
- ε_0 is the dielectric constant of air (8.854 10^{-12} Fm^{-1})

6

The static dielectric constant is modified into (Stogryn (1975)):

$$\varepsilon_{w0}(T,S_1) = \varepsilon_{wo}(T,0) \cdot a(T,S_1) \tag{20}$$

Where

$$\varepsilon_{wo}(T,0) = 87.134 - 1.949 \cdot 10^{-1}T - 1 \cdot 276 \cdot 10^{-2}T^2 + 2.491 \cdot 10^{-4}T^3 \tag{21}$$

and

$$a(T,S_1) = 1.0 + 1.613 \cdot 10^{-5}T \cdot S_1 - 3.656 \cdot 10^{-3}S_1 + 3.21 \cdot 10^{-5}S_1^2 - 4.232 \cdot 10^{-7}S_1^3 \tag{22}$$

The above equation is valid for $4 < S_1 > 35$‰, (Ulaby et al. 1986)

The relaxation time is modified into

$$\tau_w(T,S_1) = \tau_w(T,0) \cdot b(T,S_1) \quad \text{(Ulaby et al. 1986)} \tag{23}$$

Where

$\tau_w(T,0)$ is the relaxation time of pure water (s)

and

$$b(T,S_1) = 1.0 + 2.282 \cdot 10^{-5}T \cdot S_1 - 7.638 \cdot 10^{-4}S_1 - 7.760 \cdot 10^{-6} \cdot S_1^2 + 1.105 \cdot 10^{-8}S_1^3 \tag{24}$$

The above equation is valid for $0 < T < 40°C$ and $0 < S_1\ 157$‰ (Ulaby et al. 1986).

The additional parameter is the ionic conductivity. For saline water, Stogryn (1971) presented the expression:

$$\sigma_i(T,S_1) = \sigma_i(25,S_1)e^{-\phi} \tag{25}$$

Where

$\sigma_i(25,S_1)$ is the ionic conductivity of the saline water at 25°C:

$$\sigma_i(25,S_1) = S_1[0.18252 - 1.4619 \cdot 10^{-3}S_1 + 2.093 \cdot 10^{-5}S_1^2 - 1.282 \cdot 10^{-7}S_1^3] \tag{26}$$

And the function ϕ depends on S_1 and $\Delta = 25 - T$:

$$\phi = \Delta[2.033 \cdot 10^{-2} + 1.266 \cdot 10^{-4}\Delta + 2.464 \cdot 10^{-6}\Delta^2 - \\ S\ (1.849 \cdot 10^{-5} - 2.551 \cdot 10^{-7}\Delta + 2.551 \cdot 10^{-8}\Delta^2)] \tag{27}$$

The above sets of equation is valid for $0 < S < 40$ ‰

The solution extracted from the saturated soil water mixture (from agricultural field) has the salinity less than 1 °/oo which has negligible influence on soil dielectric constant for the frequencies above 4.0 GHz (Dobson et al. 1985).

Appendix II:

Njoku and Kong Model

In order to find the source current and electric field values, we have a pair of Maxwell's equations that relate the current source (J), electric field (E) and magnetic field (H):

$$\nabla \times E = -i\omega\mu H \qquad (1)$$

and

$$\nabla \times H = i\omega(\varepsilon E - J) \qquad (2)$$

Where
- E is the electric field (V m^{-1})
- H is the magnetic field (A m^{-1})
- J is the source current (A)
- ω angular frequency (rad s^{-1})
- ε permittivity (farad m^{-1})
- μ is permeability (henry m^{-1})

From the manipulation of above two equations:

$$\nabla \times \nabla \times E - k^2 E = i\omega\mu J \qquad (3)$$

The above equation has a formal solution using the Green's function

$$E(r,\omega) = i\omega\mu \int_V G_0(r,r') \cdot J(r')d^3r' \qquad (4)$$

Where
- G$_0$(r,r) is the green's function

In case of a multilayer stratified medium, we have to find the electric field value for every layer:

$$E_j(r,\omega) = i\omega\mu \int_V G_{0j}(r,r') \cdot J_j(r')d^3r' \qquad (5)$$

Where
- j represents the layer number

The estimation of J is done by using fluctuation and dissipation theorem (Stogryn, 1970):

$$\left\langle J_j(r,\omega) \cdot J_j(r,\omega)^* \right\rangle = \frac{4}{\pi}\omega\varepsilon_j'' k_B T_j I\delta(\omega-\omega')\delta(r-r') \tag{6}$$

Where
- * represents the complex conjugate
- T_j is the temperature of the layer (K)
- ε_j is the imaginary part of complex permittivity of the layer (ratio)
- k_B is the Boltzmann's constant($1.3.10^{-23}$ Joule K^{-1})
- I is the unit dyadic function
- $I\delta(r-r')$ represents the point source

Stogryn (1970) presented the expression for the intensity of thermal radiation with polarization p and at an angular frequency ω:

$$I^P(k,\omega) = \frac{c\varepsilon_0}{2}\int_0^\infty d\omega'\int_0^\infty k^2 dk\int_{-\infty}^{+\infty}d^3k'$$
$$\left\{\left(\hat{p}\cdot\left\langle E(k,\omega)E^*(k',\omega')\right\rangle\cdot\hat{p}\right)\exp i\left((k-k')\cdot r - i(\omega-\omega')t\right)\right\} \tag{7}$$

Where
- * represents the complex conjugate
- $I^P(k,\omega)$ is the intensity of the radiation at an angular frequency ω (W $Sr^{-1}m^{-2}Hz$)
- k is the wave vector with magnetite of $2\pi/\lambda$ (m^{-1})
- E is the electric field strength (V m^{-1})

From the Rayleigh Jean's approximation to Plank's blackbody radiation law, the intensity of microwave radiation emitted by a blackbody at a temperature T:

$$I^P = \frac{k_B}{(2\pi)^3}\left(\frac{\omega}{c}\right)^2 T \tag{8}$$

Since the blackbody temperature (T) is same as the brightness temperature T_B:

$$T_B(k,\omega) = \frac{(2\pi)^3}{k_B}\left(\frac{c}{\omega}\right)^2 I^P(k,\omega) \quad (K) \tag{9}$$

Considering the above equations (5) and (9) we have the expression for T_B:

$$T_B^P(k,\omega) = \frac{(2\pi)^3}{k_B}\left(\frac{c}{\omega}\right)^2 \frac{c\varepsilon_0}{2} \int_0^\infty d\omega' \int_0^\infty k^2 dk \int_{-\infty}^{+\infty} d^3k'$$

$$\left\{\left(\hat{p}\cdot\left\langle E(k,\omega)E^*(k',\omega')\right\rangle\cdot\hat{p}\right)\exp i\left((k-k')\cdot r - i(\omega-\omega')t\right)\right\} \tag{10}$$

In case of a stratified soil medium with *n* number of layers, the above equation provides the T_B value in each layer. All radiations are then summed up in a coherent way in order to get the total intensity of the radiation emitted by the soil medium and then the brightness temperature. The final expression for brightness temperature:

For horizontal polarization:

$$T_{Bh}(\Theta) = k^2 \cos(\Theta) \sum_{j=1}^n \frac{\varepsilon_j'' T_j}{\varepsilon_0 |k_z|^2} \left\{ \frac{\left|A_j \exp\left(k_{jz}'' dz_j\right)\right|^2}{2k_{jz}''} \cdot \left\{1 - \exp\left[2k_{jz}''\left(d_{j-1} - d_j\right)\right]\right\} - \right.$$

$$\frac{\left|B_j \exp\left(-k_{jz}'' dz_j\right)\right|^2}{2k_{jz}''} \cdot \left\{1 - \exp\left[-2k_{jz}''\left(d_{j-1} - d_j\right)\right]\right\} +$$

$$\frac{\left[A_j \exp(-ik_{jz}' d_j)\right]\left[B_j \exp\left(ik_{jz}' d_j\right)\right]^*}{2ik_{jz}'} \cdot \left\{1 - \exp\left[-2ik_{jz}'\left(d_{j-1} - d_j\right)\right]\right\} +$$

$$\left.\frac{\left[A_j \exp(-ik_{jz}' d_j)\right]^* \left[B_j \exp\left(ik_{jz}' d_j\right)\right]}{2k_{jz}'} \cdot \left\{1 - \exp\left[2ik_{jz}'\left(d_{j-1} - d_j\right)\right]\right\}\right\} +$$

$$k^3 \cos(\Theta) \frac{1}{|k_z|^2} \frac{|\Gamma_h|^2}{2k_{(n+1)z}''} \exp\left(-2k_{(n+1)z}'' dz_n\right) \cdot \frac{\varepsilon_{n+1}'' T_{n+1}}{\varepsilon_0} \tag{11}$$

For vertical polarization:

$$T_{Bv}(\Theta) = k^2 \cos(\Theta) \sum_{j=1}^n \frac{\varepsilon_j'' T_j}{\varepsilon_0 |k_z|^2} \left\{ \frac{\left|C_j \exp\left(k_{jz}'' dz_j\right)\right|^2}{2k_{jz}''} \cdot \left\{1 - \exp\left[2k_{jz}''\left(dz_{j-1} - dz_j\right)\right]\right\} - \right.$$

$$\frac{\left|D_j \exp\left(k_{jz}'' dz_j\right)\right|^2}{2k_{jz}''} \cdot \left\{1 - \exp\left[-2k_{jz}''\left(dz_{j-1} - dz_j\right)\right]\right\} +$$

$$\frac{\left[C_j \exp(-ik'_{jz} d_j)\right]\left[D_j \exp(ik'_{jz} d_j)\right]^*}{2ik'_{jz}} \cdot \left\{1 - \exp\left[-2ik'_{jz}\left(d_{j-1} - d_j\right)\right]\right\} +$$

$$\frac{\left[C_j \exp(-ik'_{jz} d_j)\right]^*\left[D_j \exp(ik'_{jz} d_j)\right]}{2ik'_{jz}} \cdot \left\{1 - \exp\left[2ik'_{jz}\left(d_{j-1} - d_j\right)\right]\right\}\right\} +$$

$$k^2 \cos(\Theta) \frac{1}{|k_z|^2} \frac{|\Gamma_v|^2}{2k''_{(n+1)}} \exp\left(-2k''_{(n+1)z} dz_n\right) \cdot \frac{\varepsilon''_{n+1} T_{n+1}}{\varepsilon_0} \tag{12}$$

Where

- j refers the layer number
- A_j and B_j are the wave amplitude for horizontal polarization
- C_j and D_j are the wave amplitude for vertical polarization
- Γ_p is the reflectivity for the polarization p, (p= h or v)(ratio)
- d is the layer thickness (m)

The values of A_j, B_j, C_j and D_j are presented by Kong(1975).

This method permits the estimation of microwave emission from a soil medium whose soil moisture and temperature has large variation with depth.

Titre Français

Influence des profils verticaux d'humidité et de température sur l'émission micro-onde d'un sol nu : conséquence sur l'estimation de la teneur en eau du sol.

Résumé Français :

Nous étudions l'influence des profils hydrique et thermique sur l'émission micro-onde de sol. Pour cela, nous avons validé plusieurs modèles d'émission micro-onde (à 1.4, 5.05 et 10.65 GHz) par un milieu stratifié. Les données expérimentales ont été recueillies en milieu contrôlé sur le site expérimental d'Avignon avec le radiomètre PORTOS du CNES. Un bilan des erreurs affectant la comparaison modèle expérience montre qu'une telle comparaison est difficile à réaliser finement. Nous établissons néanmoins que les modèles cohérents donnent de meilleurs résultats que les modèles incohérents et que la prise en compte des profils hydriques et thermique n'apporte un gain de précision qu'à 1.4 GHz. Nous avons ensuite couplé le modèle cohérent de Wilheit à un modèle mécaniste de transferts couplés d'eau et de chaleur dans le sol pour simuler les variations horaires de l'émission micro-onde dans une large gamme de situations. A partir des données expérimentales et simulées, on montre que les variations diurnes et saisonnières des profils hydrique et thermique affectent significativement l'estimation de la teneur en eau du sol, lorsque celle-ci est déterminée dans une couche de sol d'épaisseur fixée. Nous avons ainsi mis au point un modèle d'estimation de la température effective micro-onde du sol.

Mots clés : Télédétection, micro-onde, modélisation, humidité, sol, température, Radiométrie

Title in English

Influence of soil moisture and temperature vertical profiles on the soil microwave emission : consequence on soil moisture estimation.

Resume

The influence of soil moisture and temperature vertical profiles on the soil microwave emission is investigated. Three emission models, which described the soil as a layered media, were validated at 1.4, 5.05 and 10.65 GHz. The experimental results were collected on the Avignon INRA test site using the ground based PORTOS radiometer (CNES). An error analysis has shown that an accurate comparison between experimental data and model results is difficult since the error that may affect this comparison can be very large. However, we have shown that the coherent models are better than the incoherent model. Then we have combined a coherent model to a mechanistic model of soil heat and mass flows in order to simulate the hourly variations of the brightness temperature. From the experimental and simulated data, we have shown that the seasonal and diurnal variations of the soil moisture and temperature profiles affect the soil moisture estimation from microwave radiometry when estimated in a soil layer with a constant depth. To account for the temperature profile, we have developed a new model for the soil microwave effective temperature.

Key word: Remote sensing, microwave, modelization, soil, moisture, temperature